

In the Zone: the Effects of Soil Pipes and Dunes on Hyporheic and Riparian Zone  
Hydraulics and Biogeochemistry

William Seth Lotts, Sr., P.E.

Dissertation submitted to the faculty of the Virginia Polytechnic Institute and State  
University in partial fulfillment of the requirements for the degree of

Doctor of Philosophy

In

Civil Engineering

Erich T. Hester, Chair

Mark A. Widdowson

Kyle B. Strom

Durelle T. Scott

May 4, 2022

Blacksburg, Virginia

Keywords: Hyporheic zones, riparian zones, preferential flow, floodplains, nitrate  
attenuation, groundwater modeling, surface water modeling

# **In the Zone: the Effects of Soil Pipes and Dunes on Hyporheic and Riparian Zone Hydraulics and Biogeochemistry**

William Seth Lotts, Sr.

## **ABSTRACT**

Streams and rivers are a vital part of our ecosystem. They are imperiled by human ecological activities such as urbanization, industrialization, and agriculture which discharge excess nitrate and other pollutants into our waterways. Here, this dissertation seeks to understand the physical and biogeochemical processes which attenuate pollutants in stream corridors. The focus is hyporheic zones which form the interface between surface water and groundwater below and adjacent to stream channels, and riparian zones which form the interface between channels and adjacent uplands, both of which can attenuate pollutants. In this context, soil-pipes can dominate subsurface hydraulics. This research first employed MODFLOW and MT3D-USGS to model transient hyporheic hydraulics and nitrate transport in a length of riparian/riverbank soil to probe the effects of soil pipes on hydraulics and denitrification due to peak flow events in the channel. Findings showed that inserting just one soil pipe 1.5 m in length caused a ~75% increase in both hyporheic exchange and denitrification. A rough upscaling showed soil pipes could remove up to ~3% of nitrate along a 1-km reach. Next, the ability of soil pipes to bypass the often championed ability of riparian buffers to remove nitrate migrating from uplands to the channel was evaluated. This effort also employed MODFLOW and MT3D-USGS to simulated hydraulics and nitrate removal along a length of riparian soil. Findings showed that soil pipes increased flow of nitrate to the banks by five orders of magnitude in some cases. We posited a non-dimension parameter which governs when nitrate bypass is significant. In addition to soil pipes, dune bedforms can also enhance hyporheic exchange, primarily in the stream/riverbed. Again employing MODFLOW but now pairing with the transport code SEAM3D to simulate microbially-mediated aerobic metabolism of dissolved organic carbon and dissolved oxygen, the combined effects of dune translation and microbial growth and death were explored. Major findings include that neglecting microbial growth can lead to inaccurate modeling of biogeochemistry, and that aerobic metabolism increased with celerity. The results herein bolster knowledge of natural pollutant attenuation in stream and river corridors, and have implications for pollutant mitigation strategy and stream credit allocation.

# **In the Zone: the Effects of Soil Pipes and Dunes on Hyporheic and Riparian Zone Hydraulics and Biogeochemistry**

William Seth Lotts, Sr.

## **GENERAL AUDIENCE ABSTRACT**

Streams are a vital part of our ecosystem. They are imperiled by human ecological activities such as urbanization, industrialization, and agriculture which discharge nitrate and other pollutants into our waterways. Here, this dissertation seeks to understand the physical and biological processes which attenuate pollutants. The hyporheic zone is the interface between surface water and groundwater below the bed and adjacent to stream banks, and can attenuate pollutants. Transient peak flow events such as a storm or snow melt raise the stream water levels, causing the water pressure in the stream channel to temporarily outweigh the water pressure in the soil pore spaces adjacent to the stream channel. This drives water into the banks subjecting it to pollutant attenuation processes. Soil pipes (long cylindrical void spaces created by decayed plant roots) are prevalent along stream banks, and they dominate subsurface hydraulics. This dissertation implemented a numerical study on a chunk of riparian soil to probe the effects of soil pipes on hydraulics and denitrification. Findings showed that inserting just one – 1.5 m soil pipe caused a ~75% increase in both water flow volume into the bank and nitrate removal. Riparian buffers are the vegetated strips adjacent to stream channels and have long been championed as stalwarts of pollutant removal. Soil pipes undermine this by acting as a bypass mechanism. A numerical study was again performed on a chunk of riparian soil to quantify the effects soil pipes on riparian bypass of nitrate. Findings showed that soil pipes increased flow of nitrate to the banks by five orders of magnitude in some cases. This means that a buffer enhancement strip with fine roots that prevent the formation of soil pipes should be installed along riparian buffers. In addition to soil pipes, dune bedforms can increase flowrate of water into the hyporheic zone. This dissertation modeled the combined effects of dune translation and microbial growth and death. Major findings include that neglecting microbial growth can lead to inaccurate modeling of biogeochemistry, and that biodegradation increases with increased dune velocity. The results herein bolster knowledge on natural pollutant attenuation in streams, and have implications in terms of pollutant mitigation strategy and stream credit allocation.

## **DEDICATION**

This dissertation is dedicated to my beloved wife and Brittany Brienne Lotts, who followed me off the ledge of a cliff of financial uncertainty for me to pursue this passion. Brittany left a prestigious corporate job to follow me around for 7 years in the Army before coming to Virginia Tech to work on my Ph.D. She has borne the brunt of raising our four children, and has run the household while I have buried my head in my studies.

## ACKNOWLEDGEMENTS

Thank you to the National Science Foundation, the Department of Energy, the Sussman Foundation, and the Via Fellowship for funding this research. Without these organizations I could not have completed the degree.

I would like to thank my advisor Erich T. Hester, for blessing me with this opportunity to merge two of my passions (math and environmental engineering), and earn a living conducting numerical modeling for five years. He was accommodating and understanding about my Reserve duty, and other humanitarian endeavors, and suffered through my floral, verbose, Herman Melville-style manuscripts. He bestowed valuable career advice, teaching me to focus on the most important things, communicate more concisely and not always be buried in details. I'd like to also acknowledge Kyle Strom, who was never too busy to entertain my questions or listen to me pontificate about the matters of computational fluid dynamics, Python, or open channel flow.

I would like to acknowledge Eduardo Mendez for his assistance with troubleshooting the binary formatting issues in Fortran. Without his assistance, I may be still figuring out how to convert .UCN files into .CON files. I would also like to acknowledge Brandon Dillon and Katherine Santizo – who offered excellent company in our treks to the American Geophysical Union conference. A special thank you to Michael Calfe as well for helping me hand-drill soil pipes in the side of Strouble's creek.

I am forever indebted to my wife for following me on this journey. She held our household together while I focused on my work. She raised our kids, and kept everything going these last five year. My best friend Peter Cho and my dad and mom who have also bolstered me with emotional support through this process.

Finally, I'd like to thank my pastor Jim Krouscas for his spiritual counseling through these five years, and I'd like to thank Christ for being a source of hope in dark, uncertain times.

## TABLE OF CONTENTS

<b>ABSTRACT</b> .....	ii
<b>GENERAL AUDIENCE ABSTRACT</b> .....	iii
<b>DEDICATION</b> .....	iv
<b>ACKNOWLEDGEMENTS</b> .....	v
<b>TABLE OF CONTENTS</b> .....	vi
<b>ATTRIBUTION</b> .....	x
<b>CHAPTER 1: Watch your ecotone! Physical and biogeochemical processes within two critical ecotones in stream and river ecosystems</b> .....	1
<i>1.1 The Importance of Streams and Rivers and Pollution Mitigation Therein</i> .....	1
<i>1.2 Two Key Ecotones: the Hyporheic Zone and the Riparian Zone</i> .....	3
<i>1.3 Preferential Flow and Its Effect on Hyporheic Zones and Riparian Zones</i> .....	5
<i>1.4 Dynamics of Bedforms and Microbes and Their Effect on Hyporheic Hydraulics and Biogeochemistry</i> .....	7
<i>1.5 Summary and Organization of Dissertation</i> .....	10
<b>REFERENCES</b> .....	11
<b>CHAPTER 2: Filling the void: the effect of streambank soil pipes on transient hyporheic exchange during a peak flow event</b> .....	24
<b>KEY POINTS</b> .....	24
<b>ABSTRACT</b> .....	24
<b>2.1 INTRODUCTION</b> .....	25
<b>2.2 METHODS</b> .....	27
<i>2.2.1 Modeling Overview and Governing Equations for Soil Matrix</i> .....	27
<i>2.2.2 Model Domain and Boundary Conditions</i> .....	27
<i>2.2.3 Governing Equations for Soil Pipes</i> .....	29
<i>2.2.4 CFP Model Reliability</i> .....	30
<i>2.2.5 Calculating Hyporheic Volume</i> .....	31
<i>2.2.6 Sensitivity Analysis and Parameter Values</i> .....	32
<b>2.3 RESULTS</b> .....	35
<b>2.4 DISCUSSION AND FURTHER ANALYSIS</b> .....	38
<i>2.4.1 Soil Pipe Preferential Flow Processes in Streambanks</i> .....	38
<i>2.4.2 Controls on Soil Pipe Preferential Flow in Streambanks</i> .....	39
<i>2.4.3 Model Limitations and Future Studies</i> .....	44
<i>2.4.4 Practical Application</i> .....	44
<b>2.5 CONCLUSIONS</b> .....	45
<b>ACKNOWLEDGEMENTS</b> .....	45
<b>REFERENCES</b> .....	45
<b>CHAPTER 3: Pipe dreams: the effects of stream bank soil pipes on hyporheic denitrification caused by a peak flow event</b> .....	54
<b>KEY POINTS</b> .....	54
<b>ABSTRACT</b> .....	54
<b>3.1 INTRODUCTION</b> .....	55
<b>3.2 METHODS</b> .....	57

3.2.1 Streambank Scale Analysis.....	57
3.2.1.1 Hydraulics.....	57
3.2.1.2 Nitrate Transport and Reaction.....	59
3.2.1.3 Parameter Selection and Sensitivity Analysis.....	60
3.2.1.4 Boundary Conditions.....	62
3.2.1.5 Residence Time Calculation.....	64
3.2.2 Stream Corridor Scale Analysis.....	64
<b>3.3 RESULTS.....</b>	<b>66</b>
3.3.1 Effect of Soil Pipe and Soil Matrix Parameters at Streambank Scale.....	66
3.3.2 Effect of Transport Parameters at Streambank Scale.....	68
3.3.3 Effect of Channel Width and Slope at Stream Corridor Scale.....	69
<b>3.4. DISCUSSION.....</b>	<b>72</b>
3.4.1 How Soil Pipes Alter Hyporheic Flowpaths and Hence Denitrification.....	72
3.4.1.1 Adjacent Soil Pipes Constrain Lateral Extent of Nitrate Plumes.....	72
3.4.1.2 Soil Pipe Groupings Create Transverse Head Gradients that Push Nitrate Back into the Matrix.....	73
3.4.1.3 High Dispersivity Enhances Nitrate Storage on “Potentiometric Shelves”.....	75
3.4.1.4 Soil Pipes Being Situated Above Baseflow Leads to Stranded Nitrate Plumes.....	75
3.4.2 Relative Importance of Transport and Reaction Processes.....	77
3.4.3 Scientific Impact and Practical Application.....	79
3.4.4 Model Limitations and Future Study.....	79
<b>3.5 CONCLUSIONS.....</b>	<b>81</b>
<b>ACKNOWLEDGEMENTS.....</b>	<b>82</b>
<b>REFERENCES.....</b>	<b>82</b>

<b>CHAPTER 4: Take it to the bank: A numerical examination of the effects of soil pipes on bypass of riparian buffer nitrate removal capacity.....</b>	<b>89</b>
<b>ABSTRACT.....</b>	<b>89</b>
<b>4.1. INTRODUCTION.....</b>	<b>90</b>
<b>4.2. METHODS.....</b>	<b>91</b>
4.2.1 Hydraulics; Governing Equations and Boundary Conditions.....	91
4.2.2 Nitrate Transport; Governing Equations and Boundary Conditions.....	93
4.2.3 Parameter Selection and Sensitivity Analysis.....	95
4.2.4 Particle Tracking and Residence Time Calculation.....	98
<b>4.3. RESULTS.....</b>	<b>99</b>
4.3.1 Sensitivity Analyses of Soil Pipe and Matrix Physicochemical Parameters.....	99
4.3.2 Comparison with Gravel Veins.....	103
<b>4.4 DISCUSSION.....</b>	<b>104</b>
4.4.1 Significance of Normalized Concentration, Residence Time, Damköhler Number, and Normalized Riparian Flowrate on Riparian Bypass.....	104
4.4.2 Scientific Impact and Practical Application.....	109
4.4.3 Model Limitations and Future Study.....	109
<b>4.5 CONCLUSIONS.....</b>	<b>110</b>
<b>ACKNOWLEDGEMENT.....</b>	<b>111</b>

<b>REFERENCES</b> .....	112
<b>CHAPTER 5: “Lost in dune translation: the effects of microbial growth dynamics on hyporheic biogeochemistry underneath moving dunes”</b> .....	117
<b>KEY POINTS</b> .....	117
<b>ABSTRACT</b> .....	117
<b>5.1 INTRODUCTION</b> .....	118
<b>5.2 METHODS</b> .....	121
5.2.1 <i>Surface Water Domain</i> .....	121
5.2.2 <i>Bedload and Celerity</i> .....	123
5.2.3 <i>Groundwater Hydraulic Equations</i> .....	124
5.2.4 <i>Reactive Transport and Microbial Growth/Death Equations</i> .....	125
5.2.5 <i>Sensitivity Analysis</i> .....	126
5.2.6 <i>Benchmarking</i> .....	129
5.2.6.1 <i>Approach</i> .....	129
5.2.6.2 <i>Benchmarking Results</i> .....	130
<b>5.3 RESULTS</b> .....	131
5.3.1 <i>Surface Water Results</i> .....	131
5.3.2 <i>Groundwater Results</i> .....	132
5.3.2.1 <i>Effect of Channel Velocity and Depth</i> .....	132
5.3.2.2 <i>Effects of Channel DOC/DO Concentration and Groundwater Upwelling Rate</i> .....	136
<b>5.4 DISCUSSION</b> .....	138
5.4.1 <i>Effects of Increasing Celerity on Biomass and DOC Dynamics</i> .....	138
5.4.2 <i>Relative Importance of Celerity Versus Pore Water Velocity</i> .....	140
5.4.3 <i>Scientific Contribution and Practical Application</i> .....	141
5.4.4 <i>Limitations and Future Study</i> .....	142
<b>5.5 CONCLUSIONS</b> .....	143
<b>ACKNOWLEDGEMENTS</b> .....	144
<b>REFERENCES</b> .....	144
<b>CHAPTER 6: Conclusion</b> .....	152
6.1 <i>Summary of Research Work</i> .....	152
6.2 <i>Engineering Significance and Implication</i> .....	155
6.3 <i>Future Work</i> .....	158
<b>REFERENCES</b> .....	160
<b>APPENDIX A: Soil Pipe GPR Experiments</b> .....	163
<b>REFERENCES</b> .....	164
<b>APPENDIX B: Supporting information for CHAPTER 2: Filling the Void: the Effect of Riverbank Soil Pipes on Transient Hyporheic Exchange During a Peak Flow Event</b> .....	165
<i>B1: A discussion of the numerical methods and limitations</i> .....	165
<i>B1.1 Why the numerical method struggled with soil pipe diameters of 0.5 – 1 cm</i> .....	165
<i>B1.2 Why did we change the diameter if it converged for the length and soil pipe density study?</i> .....	171

<i>B2: Amplitude and Peak</i> .....	173
<i>B3: Comparison of Pipe Flow vs. Matrix Flow</i> .....	174
<i>B4: Head Contour Maps at different Ks</i> .....	174
<b>REFERENCES</b> .....	174

<b>APPENDIX C: Supporting Information for CHAPTER 3: Pipe dreams: the effects of stream bank soil pipes on hyporheic denitrification caused by a peak flow event</b> .....	176
<i>C1 Supplemental Methods</i> .....	176
<i>C1.1 Growing Boundary Condition</i> .....	176
<i>C1.2 Effect of Use of First Order Kinetics and Neglecting Aerobic Respiration</i> .....	177
<i>C2 Supplemental Results</i> .....	178
<i>C2.1 Effect of Use of First Order Kinetics and Neglecting Aerobic Respiration</i> .....	179
<i>C2.2 Denitrification vs. Reactive Transport Parameters</i> .....	180
<i>C2.3 Whole Stream Removal for <math>K = 1 \times 10^{-6}</math> m/s, <math>\rho = 5</math></i> .....	181
<i>C3 Error of the Stair-Step Boundary Condition</i> .....	181
<i>C4 Animation Notes</i> .....	182
<b>REFERENCES</b> .....	182

<b>APPENDIX D: Python code for residence time calculation, implicit solving of Manning’s equation in CHAPTER 3</b> .....	184
--	-----

<b>APPENDIX E: Python code for residence time calculation, and conservation of mass in the soil pipe for CHAPTER 4</b> .....	187
--	-----

<b>APPENDIX F: Supporting Information for CHAPTER 5: “Lost in dune translation: the effects of microbial growth dynamics on hyporheic biogeochemistry underneath moving dunes”</b> .....	189
<i>F1 Quasi-periodic Boundary Condition</i> .....	189
<i>F2 Results for Dissolved Oxygen</i> .....	189
<i>F3 Temporal Biomass Curves</i> .....	191
<i>F4 Varying Celerity Apart from Stream Hydrodynamics</i> .....	192
<b>REFERENCES</b> .....	194

<b>APPENDIX G: Python code for celerity calculation</b> .....	195
---	-----

## ATTRIBUTION

The contributions of the authors of the manuscripts presented in this dissertation are summarized below.

**William Seth Lotts, Sr., P.E., Ph.D. Candidate**

The Charles E. Via, Jr. Department of Civil and Environmental Engineering  
Virginia Polytechnic Institute and State University. Blacksburg, VA, 24061

*Lead author of Chapters 2, 3, 4 and 5. Participated in development of research design (objectives, methods, hypotheses). Performed all numerical modeling set up, troubleshooting, and simulation. Created, prepared, edited, and prepared manuscript text and figures for review and submission to peer reviewed journals.*

**Erich T. Hester, Ph.D., P.E. Associate Professor**

The Charles E. Via, Jr. Department of Civil and Environmental Engineering  
Virginia Polytechnic Institute and State University. Blacksburg, VA, 24061

*Coauthor of Chapters 2, 3, 4, and 5. Participated in development of research design (objectives, methods, hypotheses). Offered quality control and assurance at each phase of manuscript development. Reviewed, revised, edited, and provided significant contributions to the manuscripts. Principle investigator on grants that funded the research.*

**Kyle B. Strom, Ph.D. Associate Professor**

The Charles E. Via, Jr. Department of Civil and Environmental Engineering  
Virginia Polytechnic Institute and State University. Blacksburg, VA, 24061

*Coauthor of Chapter 5. Participated in development of research design (objectives, methods, hypotheses). Offered quality control and assurance at each phase of manuscript development. Lead on sediment transport methodology in Chapter 5.*

**Mark A. Widdowson, Ph.D., P.E. Professor**

The Charles E. Via, Jr. Department of Civil and Environmental Engineering  
Virginia Polytechnic Institute and State University. Blacksburg, VA, 24061

*Coauthor of Chapter 5. Participated in development of research design (objectives, methods, hypotheses). Offered quality control and assurance at each phase of manuscript development. Lead on biogeochemical modeling methodology in Chapter 5.*

## **CHAPTER 1: Watch your ecotone! Physical and biogeochemical processes within two critical ecotones in stream and river ecosystems.**

### *1.1 The Importance of Streams and Rivers and Pollution Mitigation Therein*

Streams and rivers play a vital role in society, providing drinking water, recreation, food sources, as well as acting as a hotbed for biodiversity and a key component of ecological systems. In the United States, surface waters provide roughly 70% of drinking water (Dieter et al., 2018). Furthermore, in 2006, 357,403 total miles of streams nationwide sourced public drinking water systems of which 207,476 miles (58%) were headwater streams. In 2006, over 117 million people relied on headwater streams for drinking water (USEPA, 2006). Presently in Virginia, there are 4,435 community water systems sourced from surface water which collectively service 6,788,891 people (USEPA, 2021). Streams, rivers, and lakes allow opportunities for recreational activities such as fishing, tubing, canoeing, boating, jet skis, and swimming (Waters, 1973). In 2016, 30.1 million Americans took 322 million freshwater fishing trips, spending 383 million days, amassing \$29.9 billion worth of expenditures for trips and equipment for freshwater fish for the year (U.S. Department of the Interior, 2018). More important than providing activities for fishermen, streams and rivers (and also lakes) are home for 963 species of freshwater fish in the contiguous United States (Froese and Pauly, 2021), as well as hundreds of species of macro-invertebrates (Wurtz, 1955) to include caddisflies, beetles, mayflies, gastropods, frog tadpoles, limpets, and benthic organisms (Cummins and Klug, 1979; Hart, 1981). Streams and rivers also provide critical food sources for surrounding terrestrial organisms including birds which serve as pollinators (Nakano and Murakami, 2001), terrestrial invertebrates which serve as both pollinators and soil aerators (Ramey and Richardson, 2017), turtles (McGaugh and Janzen, 2008), frogs, and mammals (New, 2020). Floodplains along rivers are low lying flat areas adjacent to the channel whose high level of spatial and temporal heterogeneity engenders abounding species-richness (Ward et al., 1999). This biodiversity effectuated by streams and rivers helps regulate and support critical ecological services such as aesthetic beauty, water quality and quantity, and regulation of disease vectors and pests (Balvanera et al., 2006). Given that streams play such a crucial role in our ecosystems and society, it is important to understand biogeochemical phenomenon which mitigate or exacerbate stream pollution.

There are many kinds of harmful pollutants in streams and rivers today: metals (Clements et al., 2000; Fuller and Harvey, 2000; Neiva et al., 2019), pharmaceuticals (Nieto-Juarez et al., 2021; Peng et al., 2008; Wiegel et al., 2004), microplastics (Frei et al., 2019; Klein et al., 2015; Yonkos et al., 2014), pesticides (Climent et al., 2019; Climent et al., 2018; Knillmann et al., 2018; Rizzi et al., 2019), excess phosphorus (Carpenter et al., 1998; McDowell et al., 2009; Royer et al., 2006), and excess total nitrogen (nitrate, nitrite, ammonia, and organic nitrogen) (McDowell et al., 2009; Paerl et al., 2016; Royer et al., 2006). Each pollutant has a wide array of negative impacts on the fauna and flora in stream and river systems. For example, heavy metals cause brain defects, gill defects, and mortality in *caltacalta* fish (Bose Jagannath et al., 2013), and they cause increased mortality and reduced reproduction in benthic macroinvertebrates (Hickey and Clements, 1998). Pharmaceuticals (diclofenac) can cause adverse effects with

crustaceans and fish (Nieto-Juarez et al., 2021). Further, some antibiotics foster the emergence of multiple antibiotic resistance genes or strains of bacteria (Nieto-Juarez et al., 2021). Microplastics have a myriad of negative toxicological effects on many different types of freshwater aquatic species (Anbumani and Kakkar, 2018) such as decreased body length, reproduction impairment, significant reduction in survival (laboratory nematodes), and intestinal damage (laboratory zebrafish; Lei et al., 2018); altered distal intestines of seabass (Peda et al., 2016); altered mortality of goby fish (Oliveira et al., 2013); and altered immune response in Medaka fish (Rochman et al., 2013). Organochlorine pesticides cause generalized edema, organ hyperemia, severe emaciation, gross deformities, pneumonia, pulmonary edema, and atelectasis in American alligator embryos and hatchlings in northcentral Florida (Sepulveda et al., 2006). Excess phosphorus is a main contributor to eutrophication, and excess nitrogen is another (USGS, 1996). This cocktail of pollutants is an existential problem in our streams and rivers, and threatens the ecosystems and hampers their functions and services. Understanding how to reduce or remove any of these pollutants is an important research topic, but we focus here on excess nitrogen.

Although nitrogen in proper quantities is essential to plant and animal nutrition, such as nitrate stimulating plant growth (Crawford, 1995), excess nitrogen causes a multitude of negative consequences for the environment. Excess nitrogen causes eutrophication worldwide (Bergstrom et al., 2018; Boesch et al., 2001; Dalu et al., 2019; Dodds, 2006; Dodds et al., 2009; Kemp et al., 2005; Le Moal et al., 2019; Liu et al., 2019; Liu et al., 2015; Nguyen et al., 2019; Sinha et al., 2017) and hence dead zones in streams, rivers, lakes, estuaries and coastal seas, with attendant economic consequences (Boyer et al., 2006; Carpenter et al., 1998; Galloway et al., 2008; Gruber and Galloway, 2008; Howarth et al., 2002; Mosier et al., 2002). Symptomatic of eutrophication, excess nitrogen leads to an over-abundance of nuisance algae (McDowell et al., 2009) which then die off with decomposers subsequently using up all the dissolved oxygen which in turn kills other aquatic organisms. In this way, nitrate (an oxygenated inorganic species of nitrogen,  $\text{NO}_3^-$ ) emanating from streams and rivers contributes to hypoxia in the Gulf of Mexico (Rabalais et al., 2002). Although solving the problem of excess nitrogen has remained a focus for the academic and scientific communities (National Academy of Engineering, 2008), little progress has been made in many parts of the USA despite much effort to reduce loading (Oelsner and Stets, 2019). For example, Jones et al. (2018) examined the impact of livestock manure on streams, and clearly demonstrated that nitrate is still very prevalent in the Midwest. Vilmin et al. (2018) showed nitrate to be a significant component of total nitrogen load in fresh surface waters in highly populated areas impacted by agriculture. Nitrate has other harmful effects other than those associated with eutrophication, for example, methemoglobinemia in infant humans (Miodovnik, 2009). Nitrate can also be metabolized by certain species of bacteria into nitroso compounds, which have been shown to be carcinogenic in more than 40 animal species including birds, reptiles, fish, and mammals such as humans (Hill, 1999). Nitrate poisoning from contaminated plants or drinking water can cause sudden death, sudden miscarriage, cyanosis, brown mucus membranes, brown discoloration of the blood, abdominal pain, ataxia, muscle tremor, severe dyspnea, and fatigue in cattle (Vermunt and Visser, 1987). Thus, although nitrate at low levels is innocuous and required for life, nitrate can be a significant problem at high levels. Fortunately, there are two transition zones or “ecotones” within stream and river ecosystems which have

shown considerable natural capacity to attenuate nitrate, the hyporheic zone and the riparian zone.

### *1.2 Two Key Ecotones: the Hyporheic Zone and the Riparian Zone*

The hyporheic zone is the interface between surface water and groundwater (Bencala, 2000; Lawrence et al., 2013; Triska et al., 1989; White, 1993; Winter et al., 1998), and has many beneficial functions, including removing nitrate. There are many different ways to define the hyporheic zone. Some authors have defined the hyporheic zone in terms of the prevalence of epigeal vs. hypogean organisms (White, 1993). There are also physicochemical definitions, which examine the prevalence of ions, isotopes, and levels of electrical conductivity in the stream water and groundwater, and define the hyporheic zone as the zone which has a mixture of the two compositions. For example, Triska et al. (1989) defined the hyporheic zone as the zone which contains less than 98 percent but greater than 10 percent advected channel water. In other words, water that exhibits between 10 percent and 98 percent of the surface water composition in terms of some physicochemical parameter, such as electrical conductivity, isotope concentration, or ion concentration. As mentioned above, White (1993) defined the hyporheic zone “as the saturated interstitial areas beneath the stream bed and into the stream banks that contain some proportion of channel water or that have been altered by channel water infiltration.” The hyporheic zone serves as an epicenter for biodiversity and biogeochemical reactions and serves as an ecotone between stream channels, floodplains and groundwater (McClain et al., 2003; Stanford and Ward, 1988). The hyporheic zone can filter out contaminants via sorption and biodegradation (Brunke and Gonser, 1997; Moser et al., 2003; Winter et al., 1998). It also cycles nutrients and minerals between biota in the channel and banks (Brunke and Gonser, 1997; Hester and Gooseff, 2011; Stanford and Ward, 1993; Triska et al., 1989; Winter et al., 1998). Water from the stream brings oxygen to micro-organisms in the subsurface. Harmful contaminants sorb onto the soil or sediment matrix and denitrification often occurs (Hester et al., 2018; Hester et al., 2016), and water goes back into the stream cleaner and loaded with minerals that benefit the stream biota. For example, while sorption mechanisms attenuate excess solutes (Bencala et al., 1984), shallow groundwater can also be a source of Ca, Cl, K, Mg, Na, Mn, Fe, and dissolved organic carbon (DOC) for biota in streams and rivers (Hoagland et al., 2017) all of which are necessary to sustain life. Dissolved oxygen (DO) travels in the interstices in the hyporheic zone and supplies the aerobic bacteria who then expel CO<sub>2</sub>, which is then used by autotrophs (Brunke and Gonser, 1997). Further, the hyporheic zone can also regulate pH (Brunke and Gonser, 1997), and be a source or sink for heat, thereby helping to regulate stream temperatures (Arrigoni et al., 2008; Burkholder et al., 2008; Hester et al., 2009). Considering all the benefits of hyporheic zones and hyporheic exchange, it is important to understand the various methods by which hyporheic exchange occurs.

There are several different mechanisms by which hyporheic exchange occurs. There is turbulence and fluid momentum which carry water through the interstices at the stream bed and banks and to shallow layers below the surface, particularly in streams where coarse grains dominate (Nagaoka and Ohgaki, 1990). There is hyporheic exchange due to hydrostatic differences due to instream structures (Hester and Doyle, 2008); due to pressure differentials

caused by form drag of bed forms (Elliott and Brooks, 1997b) which includes dunes and ripples (Janssen et al., 2012; Zheng et al., 2019); due to hydraulic head difference caused by large scale changes in slope of the lateral cross-sections of the catchment perpendicular to the stream (Toth, 1963); due to upwelling at large scales due to periodic bedrock outcrops constraining alluvial aquifers (Hiscock and Grischek, 2002); due to hydraulic head differences caused by stream sinuosity (Cardenas, 2009); due to hydraulic head differences along the reach from a variety of spatial scales (Poole et al., 2008); and also due to transient peak flow events (Sawyer et al., 2009).

The steady-state unidirectional hyporheic flow that occurs under steady/state hydraulics with instream structures, bed forms, dunes, ripples and spatial heterogeneities in hydraulic head has been called “gill model” exchange, and the transient out-and-back hyporheic flow caused from hydraulic gradient reversals due to temporal fluctuations in stage height has been called “lung model” exchange (Sawyer et al., 2009). Lung model exchange benefits organisms in the stream (Allen and Vaughn, 2009; DiStefano et al., 2009) and improves water quality (Anderson et al., 2011; Gu et al., 2012). Gill model exchange may offer some of the same benefits, but often occurs in localized areas as opposed to lung model exchange which occurs over much larger spatial scales (Gu et al., 2012). Furthermore, the hot moments (short periods of time that exhibit disproportionately high reaction rates) created by episodic fluctuations characteristic in lung model exchange effectuate carbon and nitrogen cycling (McClain et al., 2003). Sawyer et al. (2009) examined the impact of dam-induced surface water stage fluctuations on lung model exchange, and showed that lung model exchange had greater lateral extent than gill model exchange. Gerecht et al. (2011) characterized the spatial extent and timing of lung model exchange using temperature probes. Schmadel et al. (2016) examined riparian groundwater head dynamics and fluxes caused by the interaction of sinusoidal boundary conditions on both the channel and hillslope sides. Under settings favorable to denitrification – high amounts of labile organic carbon, anoxic conditions, and in the presence of denitrifying bacteria – lung model exchange has the potential to act as a significant nitrate sink. In providing this function, hyporheic zones are similar to riparian zones, which we discuss next.

Riparian zones are the vegetated margins of stream and river channels which serve as connective tissue between aquatic and terrestrial systems, and provide many ecosystem services including nitrate removal. Riparian zones include the vegetation, soil layer, unsaturated zone and saturated groundwater beneath. Floodplains are low lying flat sections of the riparian zone created from sediment moved by channel flows during regular flood inundations and supporting diverse ecosystems (Huggenberger et al., 1998; Meyer and Edwards, 1990; Smock et al., 1992). They are ecotones between terrestrial and aquatic biota (Thoms, 2003), where groundwater exchange cycles nutrients between the two (Jung et al., 2004). Floodplains filter out nitrate and other nutrients from upstream and adjacent uplands (Connolly et al., 2015; Winter et al., 1998), provide habitat for diverse species, and mitigate floods and erosion (Winter et al., 1998). Riparian buffers are a subset of riparian zones that filter our pollutants coming from adjacent human-dominated uplands (Dosskey, 1997). Riparian buffers protect from bank erosion, enhancing geomorphic stability. They trap sediment-bound contaminants at the surface and attenuate reactive contaminants (e.g., nitrates) in groundwater from anthropogenic sources such

as farms, commercial areas, and industrial parks (Fennessy and Cronk, 1997; Mayer and Canfield, 2018; Osborne and Kovacic, 1993; Stutter et al., 2019; Turunen et al., 2019). Although there are other mechanisms that can reduce nitrate concentrations in water flowing from uplands to channel (i.e. vegetation uptake and dilution (Hill, 2019)), denitrification in groundwater is the primary removal mechanism in riparian zones (Hill, 1996; Hill, 2019).

Several studies have demonstrated the effectiveness of riparian buffers on nitrate removal to be variable. For example, Fennessy and Cronk (1997) concluded that a riparian buffer zone of 20 to 30 m width can remove up to 100% of incoming nitrate. Mayer and Canfield (2018) found that some narrow buffers (up to 25 meters) proved effective, but buffers wider than 50 meters consistently removed excess nitrogen. Osborne and Kovacic (1993) found that both forested and grass riparian buffers reduced nitrate-N concentrations in shallow groundwater (up to 90% reduction). By contrast, McKergow et al. (2003) and Turunen et al. (2019) showed more inconclusive results for removing nitrogen and phosphorus, indicating that there are cases where riparian buffers are not as effective. One of the causes of variation in riparian effectiveness is variation in soil properties. For example, Gold et al. (2001) observed that high nitrate removal was restricted to hydric soils. Varying depths of hydrologic flow paths may cause variations in dilution in groundwater inflow to streams and therefore cause variations in mitigation of nitrate and other pollutants (Hill, 2019). A physical phenomenon called preferential flow is one such mechanism which undermines riparian buffer effectiveness.

### *1.3 Preferential Flow and Its Effect on Hyporheic Zones and Riparian Zones*

Hendrickx et al. (2001) defined preferential flow as the phenomenon where “water moves faster and with increased quantity at certain locations in the vadose zone than at others as a consequence of irregular flow pattern.” This definition can be extended to all water flow in the subsurface not just in the unsaturated zone. There are a number of mechanisms which cause water to move faster in one area than another: water repellency, fingered flow, funnel flow, heterogeneities, and macropores and soil pipes. Water repellency refers to the repelling of water via molecular forces caused by various polarized substances in the soil matrix such as exudates from biota microbes, fungi, roots, and earthworms, (Morales et al., 2010), or simply different soil grain textures (Blackwell, 2000; McHale et al., 2005). Fingered flow stems from hydrodynamic instability due to certain values of a parameter called the perturbation characteristic critical value, which relates capillary forces, gravitational forces, and hydrostatic forces (Hillel, 1987; Philip, 1975; Rezanezhad et al., 2006; Selker et al., 1996). In particular, fingered flow occurs when the driving forces such as hydrostatic and gravitational forces dominate the capillary forces (Rezanezhad et al., 2006), analogous to the way turbulent flow develops in pipes when the inertial forces dominate the viscous forces. The capillary forces tend to stabilize the front analogous to the viscous forces, and the driving forces seem to foment instability analogous to inertial forces. In pore spaces which exhibit these ratios of forces, water will coalesce into fingers as it breaks through the capillary forces. This happens in coarse soils (even in homogeneous, uniform soils) as pores become big enough where gravity forces are large compared to capillary forces. Another common example of fingered flow is how water on a windshield will coalesce into beads on the surface of the glass until the bead gathers enough

inertia overcomes the surface tension forces and flows down the windshield in fingers. Funnel flow occurs in the unsaturated zone at an interface between two different soil layers of disparate pore sizes, wherein there is an outcrop of coarse layer amidst a fine layer. Since significant pressure is required to push moisture into the larger pores from the smaller pores, the water will flow around the coarse layer despite its large pores. Water is compressed against the side edge of the coarse layer and is constricted as it flows around the edge of the coarse layer (Steenhuis et al., 2002; Walter et al., 2000). The faster-moving water then advances ahead of the other portions of the wetted front. Water repellency, fingered flow, and funnel flow refer mostly to percolation through the top layer of agricultural soil.

Another type of preferential flow more pertinent to riparian aquifers are heterogeneities, such as gravel bars, gravel veins, patches of coarse sediment, and other forms of geologic heterogeneity (Fleckenstein et al., 2006; Kalbus et al., 2009; Laube et al., 2018; Pryshlak et al., 2015). Finally, there are macropores and soil pipes, open conduits formed from decayed roots, burrowing fauna, desiccation, and internal erosion (Beven and Germann, 1982; 2013; Jones, 2010; Sidle et al., 2001; Uchida et al., 2001). The former are usually vertically oriented and slightly smaller ( $0.5 \mu\text{m} - 0.5 \text{ cm}$ ), whereas the latter are often more horizontal and significantly bigger ( $1 \text{ mm} - 0.3 \text{ m}$ ). Soil pipes have been shown to be nearly ubiquitous along stream banks (McEwen and Hester, 2019; Menichino et al., 2015), and therefore may play a large role in riparian/floodplain groundwater hydraulics.

The general consensus in the literature is that preferential flow, including through soil pipes, has a profound effect on the groundwater hydrology of hillslopes and floodplains, to include riparian zones and the hyporheic zone. Many studies show soil pipes are the primary conveyance of precipitation to the stream in a hillslope setting (Mosley, 1982; Wilson et al., 2017; Wilson et al., 1990; Wilson et al., 2016). Macropores and soil pipes have been shown to account for up to 50% of inflow to streams during storms (Jones, 2010). In an attempt to account for all the variation in runoff and streamflow, Sidle et al. (2001) showed that significant contributions would have to come from soil pipe networks. Wilson et al. (1990) showed that 71% of precipitation on a hill-slope sub-catchment entered the stream through soil pipes. Fleckenstein et al. (2006); Kalbus et al. (2009); Laube et al. (2018) and Pryshlak et al. (2015) have all quantified effects of heterogeneity such as gravel veins and similar areas of higher matrix hydraulic conductivity on near-channel flow and found similar effects. Preferential flow paths can also undermine the benefits of riparian buffers, a phenomenon which has been documented by numerous studies (Allaire et al., 2015; Angier and McCarty, 2008; Angier et al., 2001; Angier et al., 2005; Ashby et al., 1998; Bohlke and Denver, 1995; Bohlke et al., 2007; Burt et al., 1999; Devito et al., 2000; Fox et al., 2011; Hanson et al., 1994; Heeren et al., 2010; Hill et al., 2000; McCarty et al., 2007; O'Driscoll and DeWalle, 2010; Orozco-Lopez et al., 2018; Smethurst et al., 2014; Williams et al., 2014). In particular, macropores and soil pipes short circuit hydrologic flow between an agricultural catchment and the stream, allowing pesticides and fertilizers to circumvent the soil matrix and associated attenuation processes (Bernatek-Jakiel et al., 2017). Effluent from soil pipes and macropores can contribute more than half the total nitrate load to channels (Bohlke et al., 2007). While the ability of preferential flow paths to undermine riparian buffers has been established, the effects of soil pipe configuration and

characteristics on pollutant transport and reaction (e.g., nitrate transport and denitrification) have not been quantified (Allaire et al., 2015). **To our knowledge, no prior studies have rigorously quantified the impact of soil pipes and other preferential flow paths on bypass of nitrate and other pollutants in riparian zones.** Soil pipes and other preferential flow can also strongly affect hydraulics and exchange processes of hyporheic zones.

Several studies have demonstrated how preferential flow, including through soil pipes, has strongly influenced hyporheic exchange processes. For example, Cardenas et al. (2004) modeled the effects of sediment heterogeneity and therefore preferential flow on hyporheic exchange and contaminant transport, but did not consider soil pipes. Similarly, Zhou et al. (2014) showed that in heterogeneous river beds, 70% of the total hyporheic exchange occurred across 30% of the channel boundary with the higher hydraulic conductivity portion dominating. Due to their frequency along stream and river banks, it is important to factor in the effects of soil pipes when modeling hyporheic hydraulics. Jones and Cottrell (2007); McEwen and Hester (2019); Menichino et al. (2015) have shown that soil pipes are common along stream banks in many regions. Heeren et al. (2010) and Fox et al. (2011) conducted tracer tests on preferential flow paths including soil pipes, but did not isolate their effects from those of gravel veins. Some studies focused specifically on the effects of soil pipes on hyporheic exchange. For example, Menichino et al. (2015); Zhou et al. (2016) reported a slight increase in transient storage from soil pipes, but did not quantify the hyporheic exchange component. Furthermore, thermal imaging from Briggs et al. (2016) demonstrated the dominance of soil pipes on hyporheic hydraulics by showing substantial unidirectional inflow into a stream from a 2.5 cm diameter soil pipe along the stream bank in contrast with a lack of visible soil matrix inflow. Menichino et al. (2014) showed that an open soil pipe in a meander bend had 29 to 550 times greater hydraulic conductivity and 9 to 21% faster transport velocities than a partially plugged soil pipe. Finally, in another field study, Menichino and Hester (2015) showed that streambank soil with pipes was more hydraulically connected to stream stage than that without pipes, demonstrating that pipes can significantly affect lung model exchange. **But as with bypass of nitrate by riparian zones, we are unaware of previous work that conducted a rigorous, quantitative analysis of the impact of soil pipes on lung model hyporheic exchange caused by a peak flow event.** Withal, soil pipes do have a considerable influence on hyporheic zone hydraulics, as do other geomorphic structures, such as bedforms – namely dunes and ripples.

#### *1.4 Dynamics of Bedforms and Microbes and Their Effect on Hyporheic Hydraulics and Biogeochemistry*

Channel bedforms can have a significant impact on subsurface hydraulics and biogeochemistry, benefitting subsurface biota with sources of dissolved organic carbon and oxygen (DOC and DO respectively). The ratio of the Froude number ( $Fr$ ) and parameter “ $j$ ” governs which type of bedform will form (Kennedy, 1969). The “ $j$ ” parameter is the amount by which the local sediment-transport rate lags behind the local water velocity at the mean level of the bed, normalized by flow depth. Depending on the  $Fr/j$  ratio, the system will form (ranking from lowest to highest  $Fr/j$  ratio) ripples, dunes, a flat bed, downstream moving antidunes, stationary antidunes, or upstream moving antidunes (Kennedy, 1969). Ripples and dunes are

distinct as dunes will form at higher Froude numbers and have minimum lengths which are far greater than the maximum length of ripples (Kennedy, 1969).

Water of streams and rivers flows over these dunes and other bedforms and creates velocity and pressure variations along a longitudinal cross-section of the dune, subsequently resulting in form drag. This is analogous to the way air flowing over an airfoil creates lift for an airplane. In short, high pressure forms on the stoss (upstream) side of the dune creating downwelling (water flowing from the stream down into the aquifer) in this area, whereas low pressure forms on the lee side of the dune and near the dune cap creating upwelling (the opposite of downwelling). Hyporheic flow cells within the sediment, which connect the high and low pressure areas form inverted arches underneath the surface (Figure 1.1, bottom right). The flow cells and their concomitant biogeochemical activity has been thoroughly examined with the assumption of fixed dunes through modeling and field studies (Bardini et al., 2012; Cardenas and Wilson, 2007a; b; Elliott and Brooks, 1997a; b; Fox et al., 2014; Hester et al., 2013; 2014; Janssen et al., 2012; Marzadri et al., 2016). Studies such as Elliott and Brooks (1997a) and Elliott and Brooks (1997b) confirmed the formation of these hyporheic flow cells over stationary dunes in both laboratory and in theory. The relative significance of “pumping” (hyporheic exchange due to form drag) and “turnover” (“exchange due to a moving dune”) was unknown for in-situ rivers and streams, and the fact that “pumping” was confirmed through laboratory experiments (Elliott and Brooks, 1997a) made the parsimonious fixed dune assumption appealing. DOC and DO coming from the stream via these flow cells forming underneath fixed dunes are thought to benefit the aerobic microbes and burrowing invertebrates in the subsurface (Boulton et al., 1998; Findlay et al., 1993; Stelzer et al., 2014; Stern et al., 2017). Aerobic biofilms in the interstices serve as an excellent food source for the hyporheos, which includes many types of crustaceans, segmented worms, flatworms, rotifers, water mites, and juvenile stages of aquatic insects (Boulton et al., 1998). Thus, these processes are important to the sustainment of the food web and therefore the entire stream and river ecosystem.

While hyporheic flow cells underneath dunes benefit the subsurface biota, many ripples and dunes do not remain stationary. Dune translation occurs as a result of flowing stream/river water scouring the sediment on the stoss side and depositing it on the lee side (Elliott and Brooks, 1997b). In order for scouring to occur, particles must be able to be entrained from the bed. Although there have been many disparate methods to quantify criteria for entrainment, all methods generally involve the bed shear stress being high relative to that needed to move the particular grain size. For example, van Rijn (1984) and Coleman and Melville (1994) both posited different sets of deterministic equations which calculate bed shear stress and bedload transport rate where the equations are valid after the bed shear stress rises above a critical level. Contrastively, Papanicolaou et al. (2002) proposed a stochastic method for determining the probability of a particle being entrained based on hydrodynamic forces (which are proportional to bed shear stress). How much greater the bed shear is than the critical stress will determine the dune’s celerity, or the velocity at which the dune translates (Coleman and Melville, 1994). There may be a small subset of hydrodynamic conditions which will satisfy  $Fr/j$  ratio discussed above yet fail to achieve bed particle entrainment; however, many hydrodynamics conditions impel dune translation.

There are a few different ways to model dune translation. It is possible to model the force balance physics at a granular level with a two-phase (solid/liquid phase) Navier-Stokes scheme with two Euler-type domains, and update the solid/liquid interface with each time step (Zhao and Fernando, 2007). It is also possible to implement a Lagrangian approach to calculate a force balance on individual particles and track their movement (Charru et al., 2016). These approaches are computationally very intensive, and are not tractable to use for more than one case. For example, just one simulation without any transport on a mesoscale domain in Zhao and Fernando (2007) took 260 hours. Further, in Charru et al. (2016) the domain size is only 20, 20, and 10 times the grain size in the  $x$ ,  $y$ , and  $z$  directions, respectively, with temporal scales in the hours. By contrast, for computational tractability, several studies used a moving frame of reference, where the domain's grid moves at the speed of the bedform celerity (Ahmerkamp et al., 2015; Kessler et al., 2015; Zheng et al., 2019). In the case of mobile bedforms, the flow cell underneath the dune behaves much differently; instead of a flow cell arching from the high pressure to the low pressure area of the dunes, the water simply flows in a straight line from the lee to the stoss side (Zheng et al., 2019).

Moreover, in addition to accounting for dynamics of bedforms, dynamics of biomass may be important when modeling biogeochemical phenomenon. The microbial metabolic activity in subsurface environments (such as flow cells underneath dunes) leads to the expansion or contraction (i.e. growth and/or death) of microbial biomass in groundwater over time (Widdowson et al., 1988). Extensive sampling in field study Lowell et al. (2009) has confirmed the spatial heterogeneity of microbial communities in the hyporheic zone, and linked areas of dense microbial population to increased consumption of  $(\text{NO}_3)^-$  and DOC. Most prior studies simulating hyporheic biogeochemical reactions such as Hester et al. (2014) and Zarnetske et al. (2012) assumed constant concentration of microbial biomass in the pore space, and thus did not account for growth and death dynamics of the microbial colonies. Recent modeling study Chowdhury et al. (2020) and recent laboratory flume study Cook et al. (2020) demonstrated how microbial growth and death led to bio-clogging and significantly decreased hyporheic exchange underscoring the importance of microbial growth dynamics in modeling biogeochemistry in the subsurface. Finally, Monterroso (2021) recently explored the effects of many parameters such as stream DOC/DO ratio, and the surface water/groundwater head ratio of upwelling on microbial growth and death dynamics and ultimately DOC/DO consumption rates. However, **no one has yet evaluated the combined effects of dune translation and microbial growth dynamics on hyporheic biogeochemistry.**

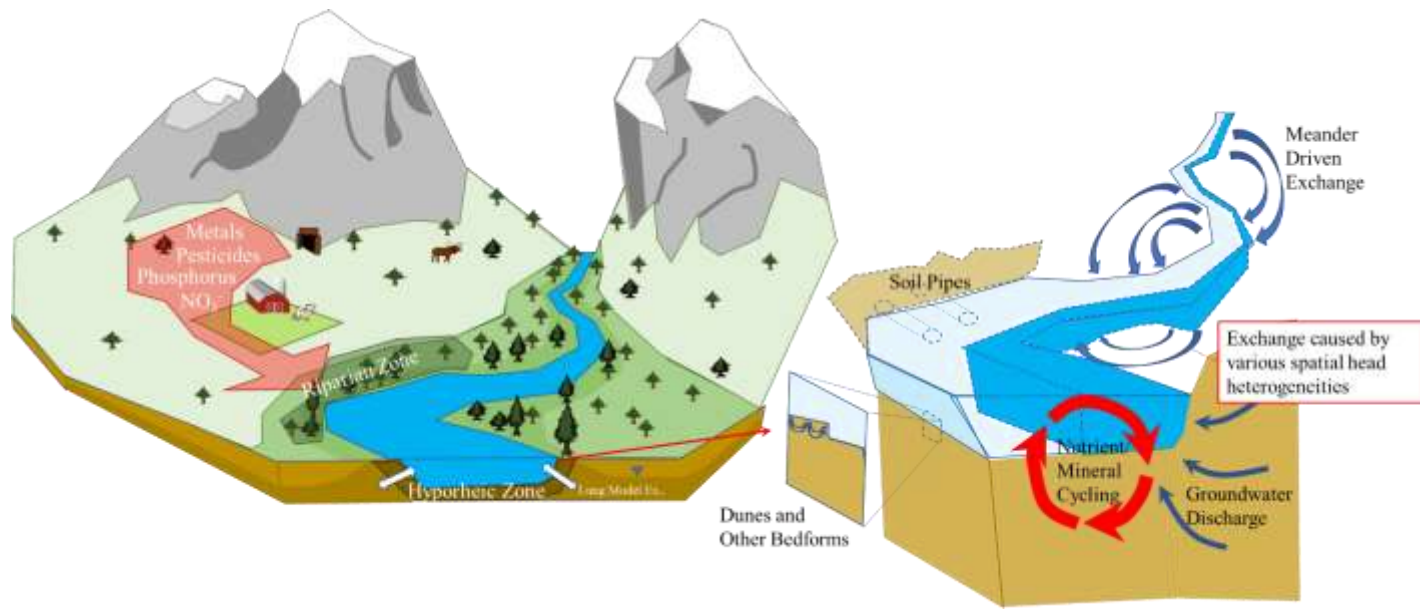


**Figure 1.1 Summary schematic of the key ecotones and hydraulic processes in stream and river ecosystems.**

### *1.5 Summary and Organization of Dissertation*

In summary, streams and rivers are acutely important to ecosystems, and they are imperiled by different pollutants, including excess nitrate. The riparian zone and hyporheic zone have many beneficial functions, including pollutant removal. However, that removal can be substantially enhanced or reduced by the presence of preferential flow, including through soil pipes. In addition to soil pipes, dunes are also geomorphic features that can affect hyporheic zone flow and biogeochemistry. When modeling flow and contaminant transport beneath dunes, it is important to account for both sediment movement and microbial growth dynamics. This dissertation presents a series of studies of the mitigating properties of stream and river ecotones, particularly the effects of soil pipes and dunes. We address three main knowledge gaps, particularly that prior studies have not (1) rigorously quantified soil pipe impacts on hyporheic hydraulics or contaminant transport, (2) rigorously quantified soil pipe impacts on riparian bypass of nitrate, and (3) examined the effects of dune translation in conjunction with microbial growth dynamics on biogeochemistry beneath dunes. These knowledge gaps lead to the following research questions:

**(1a)** How much do the presence and characteristics of soil pipes (e.g., density, length, diameter, and height above baseflow water surface elevation) affect lung model hyporheic hydraulics and contaminant transport in a riverbank during a peak flow event?

**(1b)** How do soil matrix parameters (porosity, hydraulic conductivity) and reactive transport parameters (first order reaction rate) combine with the effects of soil pipes to affect lung model hyporheic hydraulics and contaminant transport?

**(2)** How much do the combination of soil pipe, soil matrix, and reactive transport parameters affect bypass of nitrate past riparian buffer zones?

(3) What effect does microbial growth play in hyporheic biogeochemistry in systems with translating dunes?

The remainder of the dissertation is organized as follows.

**Chapter 2**, entitled “Filling the void: the effect of stream bank soil pipes on transient hyporheic exchange during a peak flow events” answers the hydraulic components of Questions 1a and 1b.

**Chapter 3**, entitled “Pipe dreams: The effects of stream bank soil pipes on hyporheic denitrification caused by a peak flow event” addresses the contaminant transport components of Questions 1a and 1b.

**Chapter 4**, entitled “Take it to the bank: A numerical examination of the effects of soil pipes on bypass of riparian buffer nitrate removal capacity” answers Question 2.

**Chapter 5**, entitled “Lost in dune translation: the effects of microbial growth dynamics on hyporheic biogeochemistry underneath moving dunes” answers Question 3.

**Chapter 6**, then discusses the collective scientific impact and practical application of all our findings.

## References

- Ahmerkamp, S., Winter, C., Janssen, F., Kuypers, M. and Holtappels, M. 2015. The impact of bedform migration on benthic oxygen fluxes. *Journal of Geophysical Research-Biogeosciences*, published online.
- Allaire, S.E., Sylvain, C., Lange, S.F., Theriault, G. and Lafrance, P. 2015. Potential Efficiency of Riparian Vegetated Buffer Strips in Intercepting Soluble Compounds in the Presence of Subsurface Preferential Flows. *Plos One* 10(7).
- Allen, D.C. and Vaughn, C.C. 2009. Burrowing behavior of freshwater mussels in experimentally manipulated communities. *Journal of the North American Benthological Society* 28(1), 93-100.
- Anbumani, S. and Kakkar, P. 2018. Ecotoxicological effects of microplastics on biota: a review. *Environmental Science and Pollution Research* 25, 14373-14396.
- Anderson, W.P., Storniolo, R.E. and Rice, J.S. 2011. Bank thermal storage as a sink of temperature surges in urbanized streams. *Journal of Hydrology* 409(1-2), 525-537.
- Angier, J.T. and McCarty, G.W. 2008. Variations in base-flow nitrate flux in a first-order stream and riparian zone. *Journal of the American Water Resources Association* 44(2), 367-380.
- Angier, J.T., McCarty, G.W., Gish, T.J. and Daughtry, C.S.T. 2001. Impact of a first-order riparian zone on nitrogen removal and export from an agricultural ecosystem. *TheScientificWorldJOURNAL* 1(Cited Dec 18, 2001), 642-651.
- Angier, J.T., McCarty, G.W. and Prestegard, K.L. 2005. Hydrology of a first-order riparian zone and stream, mid-Atlantic coastal plain, Maryland. *Journal of Hydrology* 309(1-4), 149-166.

- Arrigoni, A.S., Poole, G.C., Mertes, L.A.K., O'Daniel, S.J., Woessner, W.W. and Thomas, S.A. 2008. Buffered, lagged, or cooled? Disentangling hyporheic influences on temperature cycles in stream channels. *Water Resour Res* 44, W09418.
- Ashby, J.A., Bowden, W.B. and Murdoch, P.S. 1998. Controls on denitrification in riparian soils in headwater catchments of a hardwood forest in the Catskill mountains, USA. *Soil Biology & Biochemistry* 30(7), 853-864.
- Balvanera, P., Pfisterer, A.B., Buchmann, N., Jing-Shen, H., Nakashizuka, T., Raffaelli, D. and Schmid, B. 2006. Quantifying the evidence for biodiversity effects on ecosystem functioning and services. *Ecology Letters* 9, 1146-1156.
- Bardini, L., Boano, F., Cardenas, M.B., Revelli, R. and Ridolfi, L. 2012. Nutrient cycling in bedform induced hyporheic zones. *Geochimica Et Cosmochimica Acta* 84, 47-61.
- Bencala, K.E. 2000. Hyporheic zone hydrological processes. *Hydrological Processes* 14(15), 2797-2798.
- Bencala, K.E., Kennedy, V.C., Zellweger, G.W., Jackman, A.P. and Avanzino, R.J. 1984. Interactions of solutes and streambed sediment. 1. An experimental-analysis of cation and anion transport in a mountain stream. *Water Resources Research* 20(12), 1797-1803.
- Bergstrom, L., Karlsson, M., Bergstrom, U. and Pihl, L. 2018. Relative impact of fishing and eutrophication on coastal fish assessed by comparing a no-take area with an environmental gradient. *Ambio* 48, 565-579.
- Bernatek-Jakiel, A., Vannoppen, W. and Poesen, J. 2017. Assessment of grass root effects on soil piping in sandy soils using the pinhole test. *Geomorphology* 295, 563-571.
- Beven, K. and Germann, P. 1982. Macropores and water-flow in soils. *Water Resour Res* 18(5), 1311-1325.
- Beven, K. and Germann, P. 2013. Macropores and water flow in soils revisited. *Water Resour Res* 49(6), 3071-3092.
- Blackwell, P.S. 2000. Management of water repellency in Australia, and risks associated with preferential flow, pesticide concentration and leaching. *Journal of Hydrology* 231, 384-395.
- Boesch, D.F., Brinsfield, R.B. and Magnien, R.E. 2001. Chesapeake Bay eutrophication: Scientific understanding, ecosystem restoration, and challenges for agriculture. *Journal of Environmental Quality* 30(2), 303-320.
- Bohlke, J.K. and Denver, J.M. 1995. Combined use of groundwater dating, chemical, and isotopic analyses to resolve the history and fate of nitrate contamination in 2 agricultural watersheds, Atlantic coastal-plain, Maryland. *Water Resources Research* 31(9), 2319-2339.
- Bohlke, J.K., O'Connell, M.E. and Prestegard, K.L. 2007. Ground water stratification and delivery of nitrate to an incised stream under varying flow conditions. *Journal of Environmental Quality* 36(3), 664-680.
- Bose Jagannath, M.T., Ilavazhahan, M., Tamilselvi, R. and Viswanathan, M. 2013. Effect of heavy metals on the histopathology of gills and brain of fresh water fish *Calta catla*. *Biomedical & Pharmacology Journal* 6(1), 99-105.
- Boulton, A.J., Findlay, S., Marmonier, P., Stanley, E.H. and Valett, H.M. 1998. The functional significance of the hyporheic zone in streams and rivers. *Annual Review of Ecology and Systematics* 29, 59-81.

- Boyer, E.W., Howarth, R.W., Galloway, J.N., Dentener, F.J., Green, P.A. and Vorosmarty, C.J. 2006. Riverine nitrogen export from the continents to the coasts. *Global Biogeochemical Cycles* 20(1).
- Briggs, M.A., Hare, D.K., Boutt, D.F., Davenport, G. and Lane, J.W. 2016. Thermal infrared video details multiscale groundwater discharge to surface water through macropores and peat pipes. *Hydrological Processes* 30(14), 2510-2511.
- Brunke, M. and Gonser, T. 1997. The ecological significance of exchange processes between rivers and groundwater. *Freshwater Biology* 37(1), 1-33.
- Burkholder, B.K., Grant, G.E., Haggerty, R., Khangaonkar, T. and Wampler, P.J. 2008. Influence of hyporheic flow and geomorphology on temperature of a large, gravel-bed river, Clackamas River, Oregon, USA. *Hydrological Processes* 22(7), 941-953.
- Burt, T.P., Matchett, L.S., Goulding, K.W.T., Webster, C.P. and Haycock, N.E. 1999. Denitrification in riparian buffer zones: the role of floodplain hydrology. *Hydrological Processes* 13(10), 1451-1463.
- Cardenas, M.B. 2009. A model for lateral hyporheic flow based on valley slope and channel sinuosity. *Water Resour Res* 45, W01501.
- Cardenas, M.B. and Wilson, J.L. 2007a. Dunes, turbulent eddies, and interfacial exchange with permeable sediments. *Water Resources Research* 43(8), W08412.
- Cardenas, M.B. and Wilson, J.L. 2007b. Hydrodynamics of coupled flow above and below a sediment-water interface with triangular bedforms. *Advances in Water Resources* 30(3), 301-313.
- Cardenas, M.B., Wilson, J.L. and Zlotnik, V.A. 2004. Impact of heterogeneity, bed forms, and stream curvature on subchannel hyporheic exchange. *Water Resour Res* 40(8), W08307.
- Carpenter, S.R., Caraco, N.F., Correll, D.L., Howarth, R.W., Sharpley, A.N. and Smith, V.H. 1998. Nonpoint pollution of surface waters with phosphorus and nitrogen. *Ecological Applications* 8(3), 559-568.
- Charru, F., Bouteloup, J., Bonometti, T. and Lacaze, L. 2016. Sediment transport and bedforms: a numerical study of two-phase viscous shear flow. *Meccanica* 51, 3055-3065.
- Chowdhury, R.S., Zarnetske, J., Phanikumar, M.S., Briggs, M.A., Day-Lewis, F. and Singha, K. 2020. Formation criteria for hyporheic anoxic microzones: assessing interactions of hydraulics, nutrients, and biofilms. *Water Resources Research* 56, 1-15.
- Clements, W.H., Carlisle, D.M., Lazorchak, J.M. and Johnson, P.C. 2000. Heavy metals structure benthic communities in Colorado mountain streams. *Ecological Applications* 10(2), 626-638.
- Climont, M.J., Herrero-Hernández, E., Sánchez-Martín, M.J., Rodríguez-Cruz, M.S., Pedreros, P. and Urrutia, R. 2019. Residues of pesticides and some metabolites in dissolved and particulate phase in surface stream water of Cachapoal River basin, central Chile. *Environmental Pollution* 251, 90-101.
- Climont, M.J., Sanchez-Martin, M.J., Rodriguez-Cruz, M.S., Pedreros, P., Urrutia, R. and Herrero-Hernandez, E. 2018. Determination of Pesticides in River Surface Waters of Central Chile Using Spe-Gc-Ms Multi-Residue Method. *Journal of the Chilean Chemical Society* 63(2), 4023-4031.
- Coleman, S.E. and Melville, B.W. 1994. Bed-form development. *Journal of Hydraulic Engineering-Asce* 120(5), 544-560.

- Connolly, N.M., Pearson, R.G., Loong, D., Maughan, M. and Brodie, J. 2015. Water quality variation along streams with similar agricultural development but contrasting riparian vegetation. *Agriculture Ecosystems & Environment* 213, 11-20.
- Cook, S., Price, O., King, A., Finnegan, C., van Egmond, R., Schafer, H., Pearson, J.M., Abolfathi, S. and Bending, G.D. 2020. Bedform characteristics and biofilm community development interact to modify hyporheic exchange. *Science of the Total Environment* 749, 1-12.
- Crawford, N.M. 1995. Nitrate: nutrient and signal for plant growth. *American Society of Plant Physiologists* 7, 859-868.
- Cummins, K.W. and Klug, M.J. 1979. Feeding Ecology of Stream Invertebrates. *Annual Review of Ecology and Systematics* 10, 147-172.
- Dalu, T., Wasserman, R.J., Magoro, M.L., Froneman, W.P. and Weyl, O.L.F. 2019. River nutrient water and sediment measurements inform on nutrient retention, with implications for eutrophication. *Science of the Total Environment* 684, 296-302.
- Devito, K.J., Fitzgerald, D., Hill, A.R. and Aravena, R. 2000. Nitrate dynamics in relation to lithology and hydrologic flow path in a river riparian zone. *Journal of Environmental Quality* 29(4), 1075-1084.
- Dieter, C.A., Maupin, M.A., Caldwell, R.R., Harris, M.A., Ivahnenko, T.I., Lovelace, J.K., Barber, N.L. and Linsey, K.S. 2018. Estimated use of water in the United States in 2015, p. 65 p., Reston, VA.
- DiStefano, R.J., Magoulick, D.D., Imhoff, E.M. and Larson, E.R. 2009. Imperiled crayfishes use hyporheic zone during seasonal drying of an intermittent stream. *Journal of the North American Benthological Society* 28(1), 142-152.
- Dodds, W.K. 2006. Eutrophication and trophic state in rivers and streams. *Limnology and Oceanography* 51(1), 671-680.
- Dodds, W.K., Bouska, W.W., Eitzmann, J.L., Pilger, T.J., Pitts, K.L., Riley, A.J., Schloesser, J.T. and Thornbrugh, D.J. 2009. Eutrophication of US Freshwaters: Analysis of Potential Economic Damages. *Environmental Science & Technology* 43(1), 12-19.
- Dosskey, M.S., Dick, Isenhardt, Tom 1997. Riparian Buffers for Agriculture Land. *Agroforestry Notes*, USDA Forest Service.
- Elliott, A.H. and Brooks, N.H. 1997a. Transfer of nonsorbing solutes to a streambed with bed forms: Laboratory experiments. *Water Resources Research* 33(1), 137-151.
- Elliott, A.H. and Brooks, N.H. 1997b. Transfer of nonsorbing solutes to a streambed with bed forms: Theory. *Water Resour Res* 33(1), 123-136.
- Fennessy, M.S. and Cronk, J.K. 1997. The effectiveness and restoration potential of riparian ecotones for the management of nonpoint source pollution, particularly nitrate. *Critical Reviews in Environmental Science and Technology* 27(4), 285-317.
- Findlay, S., Strayer, D., Goumbala, C. and Gould, K. 1993. Metabolism of streamwater dissolved organic-carbon in the shallow hyporheic zone *Limnology and Oceanography* 38(7), 1493-1499.
- Fleckenstein, J.H., Niswonger, R.G. and Fogg, G.E. 2006. River-aquifer interactions, geologic heterogeneity, and low-flow management. *Ground Water* 44(6), 837-852.
- Fox, A., Boano, F. and Arnon, S. 2014. Impact of losing and gaining streamflow conditions on hyporheic exchange fluxes induced by dune-shaped bed forms. *Water Resources Research* 50(3), 1895-1907.

- Fox, G.A., Heeren, D.M., Miller, R.B., Mittelstet, A.R. and Storm, D.E. 2011. Flow and transport experiments for a streambank seep originating from a preferential flow pathway. *Journal of Hydrology* 403(3-4), 360-366.
- Frei, S., Piehl, S., Gilfedder, B.S., Loder, M.G.J., Krutzke, J., Wilhelm, L. and Laforsch, C. 2019. Occurrence of microplastics in the hyporheic zone of rivers. *Scientific Reports* 9, 1-10.
- Froese, R. and Pauly, D. 2021 FishBase, World Wide Web publication, [https://www.fishbase.in/Country/CountryChecklist.php?c\\_code=840&vhabitat=fresh&cs\\_ub\\_code=&cpresence=present](https://www.fishbase.in/Country/CountryChecklist.php?c_code=840&vhabitat=fresh&cs_ub_code=&cpresence=present), accessed on February 25, 2022.
- Fuller, C.C. and Harvey, J.W. 2000. Reactive uptake of trace metals in the hyporheic zone of a mining-contaminated stream, Pinal Creek, Arizona. *Environmental Science & Technology* 34(7), 1150-1155.
- Galloway, J.N., Townsend, A.R., Erisman, J.W., Bekunda, M., Cai, Z.C., Freney, J.R., Martinelli, L.A., Seitzinger, S.P. and Sutton, M.A. 2008. Transformation of the nitrogen cycle: Recent trends, questions, and potential solutions. *Science* 320(5878), 889-892.
- Gerecht, K.E., Cardenas, M.B., Guswa, A.J., Sawyer, A.H., Nowinski, J.D. and Swanson, T.E. 2011. Dynamics of hyporheic flow and heat transport across a bed-to-bank continuum in a large regulated river. *Water Resour Res* 47.
- Gold, A.J., Groffman, P.M., Addy, K., Kellogg, D.Q., Stolt, M. and Rosenblatt, A.E. 2001. Landscape attributes as controls on ground water nitrate removal capacity of riparian zones. *Journal of the American Water Resources Association* 37(6), 1457-1464.
- Gruber, N. and Galloway, J.N. 2008. An Earth-system perspective of the global nitrogen cycle. *Nature* 451(7176), 293-296.
- Gu, C.H., Anderson, W. and Maggi, F. 2012. Riparian biogeochemical hot moments induced by stream fluctuations. *Water Resour Res* 48.
- Hanson, G.C., Groffman, P.M. and Gold, A.J. 1994. Denitrification in riparian wetlands receiving high and low groundwater nitrate inputs. *Journal of Environmental Quality* 23(5), 917-922.
- Hart, D. 1981. Foraging and Resource Patchiness: Field Experiments with a Grazing Stream Insect. *Oikos* 37(1), 46-52.
- Heeren, D.M., Miller, R.B., Fox, G.A., Storm, D.E., Halihan, T. and Penn, C.J. 2010. Preferential flow effects on subsurface contaminant transport in alluvial floodplains. *Transactions of the ASABE* 53(1), 127-136.
- Hendrickx, J.M.H., Flury, M., Xx and Xx (2001) Uniform and preferential flow mechanisms in the vadose zone.
- Hester, E.T., Brooks, K.E. and Scott, D.T. 2018. Comparing reach scale hyporheic exchange and denitrification induced by instream restoration structures and natural streambed morphology. *Ecological Engineering* 115, 105-121.
- Hester, E.T. and Doyle, M.W. 2008. In-stream geomorphic structures as drivers of hyporheic exchange. *Water Resour Res* 44(3), W03417.
- Hester, E.T., Doyle, M.W. and Poole, G.C. 2009. The influence of in-stream structures on summer water temperatures via induced hyporheic exchange. *Limnology and Oceanography* 54(1), 355-367.
- Hester, E.T. and Gooseff, M.N. (2011) Stream Restoration in Dynamic Fluvial Systems: Scientific Approaches, Analyses, and Tools. Simon, A., Bennett, S.J. and Castro, J.M. (eds), American Geophysical Union, Washington, DC.

- Hester, E.T., Hammond, B. and Scott, D.T. 2016. Effects of inset floodplains and hyporheic exchange induced by in-stream structures on nitrate removal in a headwater stream. *Ecological Engineering* 97, 452-464.
- Hester, E.T., Young, K.I. and Widdowson, M.A. 2013. Mixing of surface and groundwater induced by riverbed dunes: implications for hyporheic zone definitions and pollutant reactions. *Water Resources Research* 49, 5221-5237.
- Hester, E.T., Young, K.I. and Widdowson, M.A. 2014. Controls on mixing-dependent denitrification in hyporheic zones induced by riverbed dunes: A steady state modeling study. *Water Resources Research* 50(11), 9048-9066.
- Hickey, C.W. and Clements, W.H. 1998. Effects of heavy metals on benthic macroinvertebrate communities in New Zealand streams. *Environmental Toxicology and Chemistry* 17(11), 2338-2346.
- Hill, A.R. 1996. Nitrate removal in stream riparian zones. *Journal of Environmental Quality* 25(4), 743-755.
- Hill, A.R. 2019. Groundwater nitrate removal in riparian buffer zones: a review of research progress in the past 20 years. *Biogeochemistry* 143, 347-369.
- Hill, A.R., Devito, K.J., Campagnolo, S. and Sanmugas, K. 2000. Subsurface denitrification in a forest riparian zone: Interactions between hydrology and supplies of nitrate and organic carbon. *Biogeochemistry* 51(2), 193-223.
- Hill, M.J. 1999. Invited commentary, Nitrate toxicity: myth or reality? *British Journal of Nutrition* 81, 343-344.
- Hillel, D. 1987. Unstable Flow in Layered Soils - a Review. *Hydrological Processes* 1(2), 143-147.
- Hiscock, K.M. and Grischek, T. 2002. Attenuation of groundwater pollution by bank filtration. *Journal of Hydrology* 266(3-4), 139-144.
- Hoagland, B., Russo, T.A., Gu, X., Hill, L., Kaye, J., Forsythe, B. and Brantley, S.L. 2017. Hyporheic zone influence on concentration-discharge relationships in a headwater sandstone stream. *Water Resources Research* 53, 4643-4667.
- Howarth, R.W., Boyer, E.W., Pabich, W.J. and Galloway, J.N. 2002. Nitrogen use in the United States from 1961-2000 and potential future trends. *AMBIO: A Journal of the Human Environment* 31(2), 88-96.
- Huggenberger, P., Hoehn, E., Beschta, R. and Woessner, W. 1998. Abiotic aspects of channels and floodplains in riparian ecology. *Freshwater Biology* 40(3), 407-425.
- Janssen, F., Cardenas, M.B., Sawyer, A.H., Dammrich, T., Krietsch, J. and de Beer, D. 2012. A comparative experimental and multiphysics computational fluid dynamics study of coupled surface-subsurface flow in bed forms. *Water Resources Research* 48, 1-16.
- Jones, C.S., C.W., D., Hraby, C.E., Schilling, K.E. and Wolter, C.F. 2018. Livestock manure driving stream nitrate. *AMBIO- A Journal of the Human Environment*.
- Jones, J.A.A. 2010. Soil piping and catchment response. *Hydrological Processes* 24(12), 1548-1566.
- Jones, J.A.A. and Cottrell, C.I. 2007. Long-term changes in stream bank soil pipes and the effects of afforestation. *Journal of Geophysical Research-Earth Surface* 112(F1).
- Jung, M., Burt, T.P. and Bates, P.D. 2004. Toward a conceptual model of floodplain water table response. *Water Resour Res* 40(12).

- Kalbus, E., Schmidt, C., Molson, J.W., Reinstorf, F. and Schirmer, M. 2009. Influence of aquifer and streambed heterogeneity on the distribution of groundwater discharge. *Hydrology and Earth System Sciences* 13(1), 69-77.
- Kemp, W.M., Boynton, W.R., Adolf, J.E., Boesch, D.F., Boicourt, W.C., Brush, G., Cornwell, J.C., Fisher, T.R., Glibert, P.M., Hagy, J.D., Harding, L.W., Houde, E.D., Kimmel, D.G., Miller, W.D., Newell, R.I.E., Roman, M.R., Smith, E.M. and Stevenson, J.C. 2005. Eutrophication of Chesapeake Bay: historical trends and ecological interactions. *Marine Ecology Progress Series* 303, 1-29.
- Kennedy, J.F. 1969. The formation of sediment ripples, dunes, and antidunes. *Annual Review of Fluid Mechanics* 1, 147-168.
- Kessler, A.J., Cardenas, M.B. and Cook, P.L.M. 2015. The negligible effect of bed form migration on denitrification in hyporheic zones of permeable sediments. *Journal of Geophysical Research-Biogeosciences* 120(3), 538-548.
- Klein, S., Worch, E. and Knepper, T.P. 2015. Occurrence and Spatial Distribution of Microplastics in River Shore Sediments of the Rhine-Main Area in Germany. *Environmental Science & Technology* 49, 6070-6076.
- Knillmann, S., Orlinskiy, P., Kaske, O., Foit, K. and Liess, M. 2018. Indication of pesticide effects and recolonization in streams. *Science of the Total Environment* 630, 1619-1627.
- Laube, G., Schmidt, C. and Fleckenstein, J.H. 2018. The systematic effect of streambed conductivity heterogeneity on hyporheic flux and residence time. *Advances in Water Resources* 122, 60-69.
- Lawrence, J.E., Skold, M.E., Hussain, F.A., Silverman, D.R., Resh, V.H., Sedlak, D.L., Luthy, R.G. and McCray, J.E. 2013. Hyporheic Zone in Urban Streams: A Review and Opportunities for Enhancing Water Quality and Improving Aquatic Habitat by Active Management. *Environmental Engineering Science* 30(8), 480-501.
- Le Moal, M., Gascuel-Oudou, C., Menesguen, A., Souchon, Y., Etrillard, C., Levain, A., Moatar, F., Pannard, A., Souchu, P., Lefebvre, A. and Pinay, G. 2019. Eutrophication: A new wine in an old bottle? *Science of the Total Environment* 651, 1-11.
- Lei, L., Wu, S., Lu, S., Liu, M., Song, Y., Fu, Z., Shi, H., Raley-Susman, K.M. and He, D. 2018. Microplastic particles cause intestinal damage and other adverse effects in zebrafish *Danio rerio* and nematode *Caenorhabditis elegans*. *Science of the Total Environment* 619-620, 1-8.
- Liu, D., Duan, H., Yu, S., Shen, M. and Xue, K. 2019. Human-induced eutrophication dominates the bio-optical compositions of suspended particles in shallow lakes: Implications for remote sensing. *Science of the Total Environment* 667, 112-123.
- Liu, T.K., Chen, P. and Chen, H.Y. 2015. Comprehensive assessment of coastal eutrophication in Taiwan and its implications for management strategy. *Marine Pollution Bulletin* 97(1-2), 440-450.
- Lowell, J.L., Gordon, N., Engstrom, D., Stanford, J.A., Holben, W.E. and Gannon, J.E. 2009. Habitat Heterogeneity and Associated Microbial Community Structure in a Small-Scale Floodplain Hyporheic Flow Path. *Microbial Ecology* 58(3), 611-620.
- Marzadri, A., Tonina, D., Bellin, A. and Valli, A. 2016. Mixing interfaces, fluxes, residence times and redox conditions of the hyporheic zones induced by dune-like bedforms and ambient groundwater flow. *Advances in Water Resources* 88, 139-151.
- Mayer, P.M. and Canfield, T. 2018. Effectiveness of riparian buffers for managing nitrogen. National Risk Management Research Laboratory, Groundwater and Ecosystems

- Restoration Research, United State Environmental Protection Agency. Downloaded November 11, 2018.
- McCarty, G.W., Mookherji, S. and Angier, J.T. 2007. Characterization of denitrification activity in zones of groundwater exfiltration within a riparian wetland ecosystem. *Biology and Fertility of Soils* 43(6), 691-698.
- McClain, M.E., Boyer, E.W., Dent, C.L., Gergel, S.E., Grimm, N.B., Groffman, P.M., Hart, S.C., Harvey, J.W., Johnston, C.A., Mayorga, E., McDowell, W.H. and Pinay, G. 2003. Biogeochemical hot spots and hot moments at the interface of terrestrial and aquatic ecosystems. *Ecosystems* 6(4), 301-312.
- McDowell, R.W., Larned, S.T. and Houlbrooke, D.J. 2009. Nitrogen and phosphorus in New Zealand streams and rivers: Control and impact of eutrophication and the influence of land managment. *New Zealand Journal of Marine and Freshwater Research* 43(4), 985-995.
- McEwen, A.M. and Hester, E.T. 2019. Abundance, distribution, and geometry of naturally occurring macropores and soil pipes in stream banks. *Freshwater Science*, In review.
- McGaugh, S.E. and Janzen, F.J. 2008. The status of apalone atra populations in Cuatro Ciénegas, Coahuila, México: preliminary data. *Chelionian Conservation and Biology* 7(1), 88-95.
- McHale, G., Newton, M.I. and Shirtcliffe, N.J. 2005. Water-repellent soil and its relationship to granularity, surface roughness and hydrophobicity: a materials science view. *European Journal of Soil Science* 56(4), 445-452.
- McKergow, L.A., Weaver, D.M., Prosser, I.P., Grayson, R.B. and Reed, A.E.G. 2003. Before and after riparian management: sediment and nutrient exports from a small agricultural catchment, Western Australia. *Journal of Hydrology* 270(3-4), 253-272.
- Menichino, G.T. and Hester, E.T. 2015. The Effect of Macropores on Bi-Directional Hydrologic Exchange between a Stream Channel and Riparian Groundwater. *Journal of Hydrology* 529(3), 830-842.
- Menichino, G.T., Scott, D.T. and Hester, E.T. 2015. Abundance and dimensions of naturally occurring macropores along stream channels and the effects of artificially constructed large macropores on transient storage. *Freshwater Science* 34(1), 125–138.
- Menichino, G.T., Ward, A.S. and Hester, E.T. 2014. Macropores as preferential flow paths in meander bends. *Hydrological Processes* 28(3), 482-495.
- Meyer, J.L. and Edwards, R.T. 1990. Ecosystem Metabolism and Turnover of Organic-Carbon Along a Blackwater River Continuum. *Ecology* 71(2), 668-677.
- Miodovnik, A. 2009. Biochemistry, Dagnosis, and Treatment of Nitrate Toxicity. *American Medical Association Journal of Ethics* 11, 451-455.
- Monterroso, H. (2021) Sensitivity Analysis in Growth and Death Dynamics for Hyporheic Zone Aerobic Bacteria in Non-Mobile Dunes, Virginia Polytechnic Institute and State University, Blacksburg, Virginia.
- Morales, V.L., Parlange, J.Y. and Steenhuis, T.S. 2010. Are preferential flow paths perpetuated by microbial activity in the soil matrix? A review. *Journal of Hydrology* 393(1-2), 29-36.
- Moser, D.P., Fredrickson, J.K., Geist, D.R., Arntzen, E.V., Peacock, A.D., Li, S.M.W., Spadoni, T. and McKinley, J.P. 2003. Biogeochemical processes and microbial characteristics across groundwater-surface water boundaries of the Hanford Reach of the Columbia River. *Environmental Science & Technology* 37(22), 5127-5134.
- Mosier, A.R., Bleken, M.A., Chaiwanakupt, P., Ellis, E.C., Frenay, J.R., Howarth, R.B., Matson, P.A., Minami, K., Naylor, R., Weeks, K.N. and Zhu, Z.L. 2002. Policy implications of

- human-accelerated nitrogen cycling (Reprinted from Biogeochemistry, vol 52, pg 281-320, 2001). *Biogeochemistry* 57(1), 477-516.
- Mosley, M.P. 1982. Subsurface flow velocities through selected forest soils, South Island, New Zealand. *Journal of Hydrology* 55(1-4), 65-92.
- Nagaoka, H. and Ohgaki, S. 1990. Mass-transfer mechanism in a porous riverbed. *Water Research* 24(4), 417-425.
- Nakano, S. and Murakami, M. 2001. Reciprocal subsidies: dynamic interdependence between terrestrial and aquatic food webs. *PNAS* 98(1), 166-170.
- National Academy of Engineering 2008. Grand Challenges for Engineering.
- Neiva, A.M.R., Carvalho, P.C.S., Antunes, I.M.H.R., Albuquerque, A.C.S., Cunha, P.P. and Henriques, S.B.A. 2019. Assessment of metal and metalloid contamination in the waters and stream sediments around the abandoned uranium mine area from Mortórios, central Portugal. *Journal of Geochemical Exploration* 202, 35-48.
- New, T.R. 2020 *Insect conservation and Australia's Inland Waters*, Springer.
- Nguyen, T.T.N., Nemery, J., Gratiot, N., Strady, E., Tran, V.Q., Nguyen, A.T., Aime, J. and Peyne, A. 2019. Nutrient dynamics and eutrophication assessment in the tropic river system of Saigon - Dongai (southern Vietnam). *Science of the Total Environment* 653, 370-383.
- Nieto-Juarez, J.I., Torres-Palma, R.A., Botero-Coy, A.M. and Hernandez, F. 2021. Pharmaceuticals and environmental risk assessment in municipal wastewater treatment plants and rivers from Peru. *Environment International* 155, 1-11.
- O'Driscoll, M.A. and DeWalle, D.R. 2010. Seeps Regulate Stream Nitrate Concentration in a Forested Appalachian Catchment. *Journal of Environmental Quality* 39(1), 420-431.
- Oelsner, G.P. and Stets, E.G. 2019. Recent trends in nutrient and sediment loading to coastal areas of the conterminous US: Insights and global context. *Science of the Total Environment* 654, 1225-1240.
- Oliveira, M., Ribeiro, A., Hylland, K. and Guihermino, L. 2013. Single and combined effects of microplastics and pyrene on juveniles (0+ group) of the common goby *Pomatoschistus microps* (Teleostei, Gobiidae). *Ecological Indicators* 34, 641-647.
- Orozco-Lopez, E., Munoz-Carpena, R., Gao, B. and Fox, G.A. 2018. Riparian Vadose Zone Preferential Flow: Review of Concepts, Limitations, and Perspectives. *Vadose Zone Journal* 17(1), 20.
- Osborne, L.L. and Kovacic, D.A. 1993. Riparian vegetated buffer strips in water-quality restoration and stream management *Freshwater Biology* 29(2), 243-258.
- Paerl, H.W., Gardner, W.S., Havens, K.E., Joyner, A.R., McCarthy, M.J., Newell, S.E., Qin, B. and Scott, J.T. 2016. Mitigating cyanobacterial harmful algal blooms in aquatic ecosystems impacted by climate change and anthropogenic nutrients. *Harmful Algae* 54, 213-222.
- Papanicolaou, A.N., Diplas, P., Evaggelopoulos, N. and Fotopoulos, S. 2002. Stochastic incipient motion criterion for spheres under various bed packing conditions *Journal of Hydraulic Engineering* 128(4), 369-380.
- Peda, C., Caccamo, L., Fossi, M.C., Gai, F., Andaloro, F., Genovese, L., Romeo, T. and Giulia, M. 2016. Intestinal alterations in European sea bass *Dicentrarchus labrax* (Linnaeus, 1758) exposed to microplastics: Preliminary results. *Environmental Pollution* 212, 251-256.

- Peng, X.Z., Yu, Y.J., Tang, C.M., Tan, J.H., Huang, Q.X. and Wang, Z.D. 2008. Occurrence of steroid estrogens, endocrine-disrupting phenols, and acid pharmaceutical residues in urban riverine water of the Pearl River Delta, South China. *Science of the Total Environment* 397(1-3), 158-166.
- Philip, J.R. 1975. Stability Analysis of Infiltration. *Soil Science Society of America Journal* 39(6), 1042-1049.
- Poole, G.C., O'Daniel, S.J., Jones, K.L., Woessner, W.W., Bernhardt, E.S., Helton, A.M., Stanford, J.A., Boer, B.R. and Beechie, T.J. 2008. Hydrologic spiralling: The role of multiple interactive flow paths in stream ecosystems. *River Research and Applications* 24(7), 1018-1031.
- Pryshlak, T.T., Sawyer, A.H., Stonedahl, S.H. and Soltanian, M.R. 2015. Multiscale hyporheic exchange through strongly heterogeneous sediments. *Water Resour Res* 51(11), 9127-9140.
- Rabalais, N.N., Turner, R.E. and Wiseman, W.J., Jr.; 2002. Gulf of Mexico hypoxia, AKA "The dead zone". *Annual Review of Ecology and Systematics* 33, 235-263.
- Ramey, T.L. and Richardson, J.S. 2017. Terrestrial invertebrates in the riparian zone: mechanisms underlying their unique diversity. *Bioscience* 67(9), 808-819.
- Rezanezhad, F., Vogel, H.J. and Roth, K. 2006. Experimental study of fingered flow through initially dry sand. *Hydrology and Earth System Sciences* 3, 2595-2620.
- Rizzi, C., Finizio, A., Maggi, V. and Villa, S. 2019. Spatial-temporal analysis and risk characterisation of pesticides in Alpine glacial streams. *Environmental Pollution* 248, 659-666.
- Rochman, C.M., Hoh, E., Kurobe, T. and Teh, S.J. 2013. Ingested plastic transfers hazardous chemicals to fish and induces hepatic stress. *Scientific Reports* 3:3263, 1-7.
- Royer, T.V., David, M.B. and Gentry, L.E. 2006. Timing of riverine export of nitrate and phosphorus from agricultural watersheds in Illinois: Implications for reducing nutrient loading to the Mississippi River. *Environmental Science & Technology* 40(13), 4126-4131.
- Sawyer, A.H., Cardenas, M.B., Bomar, A. and Mackey, M. 2009. Impact of dam operations on hyporheic exchange in the riparian zone of a regulated river. *Hydrological Processes* 23(15), 2129-2137.
- Schmadel, N.M., Ward, A.S., Lowry, C.S. and Malzone, J.M. 2016. Hyporheic exchange controlled by dynamic hydrologic boundary conditions. *Geophysical Research Letters* 43(9), 4408-4417.
- Selker, J.S., Steenhuis, T.S. and Parlange, J.Y. 1996. An engineering approach to fingered vadose pollutant transport. *Geoderma* 70(2-4), 197-206.
- Sepulveda, M.S., Del Piero, F., Wiebe, J.J., Rauschenberger, H.R. and Gross, T.S. 2006. Necropsy findings in American alligator late-stage embryos and hatchlings from northcentral Florida lakes contaminated with organochlorine pesticides. *Journal of Wildlife Diseases* 42(1), 56-73.
- Sidele, R.C., Noguchi, S., Tsuboyama, Y. and Laursen, K. 2001. A conceptual model of preferential flow systems in forested hillslopes: evidence of self-organization. *Hydrological Processes* 15(10), 1675-1692.
- Sinha, E., Michalak, A.M. and Balaji, V. 2017. Eutrophication will increase during the 21st century as a result of precipitation changes. *Science* 357(6349), 405-408.

- Smethurst, P.J., Petrone, K.C., Langergraber, G., Baillie, C.C., Worledge, D. and Nash, D. 2014. Nitrate dynamics in a rural headwater catchment: measurements and modelling. *Hydrological Processes* 28(4), 1820-1834.
- Smock, L.A., Gladden, J.E., Riekenberg, J.L., Smith, L.C. and Black, C.R. 1992. Lotic Macroinvertebrate Production in 3 Dimensions - Channel Surface, Hyporheic, and Floodplain Environments. *Ecology* 73(3), 876-886.
- Stanford, J.A. and Ward, J.V. 1988. The Hyporheic Habitat of River Ecosystems. *Nature* 335(6185), 64-66.
- Stanford, J.A. and Ward, J.V. 1993. An ecosystem perspective of alluvial rivers - connectivity and the hyporheic corridor. *Journal of the North American Benthological Society* 12(1), 48-60.
- Steenhuis, T.S., Geohring, L.D., Richards, B.K., Walter, T.M. and Peranginangin, N. 2002. Preferential Flow, <http://soilandwater.bee.cornell.edu/research/pfweb/contacts.htm>.
- Stelzer, R.S., Scott, J.T., Bartsch, L.A. and Parr, T.B. 2014. Particulate organic matter quality influences nitrate retention and denitrification in stream sediments: evidence from a carbon burial experiment. *Biogeochemistry* 119(1-3), 387-402.
- Stern, N., Ginder-Vogel, M., Stegen, J.C., Arntzen, E., Kennedy, D.W., Larget, B.R. and Roden, E.E. 2017. Colonization Habitat Controls Biomass, Composition, and Metabolic Activity of Attached Microbial Communities in the Columbia River Hyporheic Corridor. *Applied and Environmental Microbiology* 83(16).
- Stutter, M., Kronvang, B., Huallachain, D.O. and Rozemeijer, J. 2019. Current Insights into the Effectiveness of Riparian Management, Attainment of Multiple Benefits, and Potential Technical Enhancements. *Journal of Environmental Quality* 48(2), 236-247.
- Thoms, M.C. 2003. Floodplain-river ecosystems: lateral connections and the implications of human interference. *Geomorphology* 56(3-4), 335-349.
- Toth, J. 1963. A theoretical analysis of groundwater flow in small drainage basins. *Journal of Geophysical Research* 68(16), 4795-4812.
- Triska, F.J., Kennedy, V.C., Avanzino, R.J., Zellweger, G.W. and Bencala, K.E. 1989. Retention and Transport of Nutrients in a 3rd-Order Stream in Northwestern California - Hyporheic Processes. *Ecology* 70(6), 1893-1905.
- Turunen, J., Markkula, J., Rajakallio, M. and Aroviita, J. 2019. Riparian forests mitigate harmful ecological effects of agricultural diffuse pollution in medium-sized streams. *Science of the Total Environment* 649, 495-503.
- U.S. Department of the Interior, U.S.F.a.W.S., U.S. Department of Commerce, U.S. Census Bureau 2018 2016 National Survey of Fishing, Hunting, and Wildlife-Associated Recreation.
- Uchida, T., Kosugi, K. and Mizuyama, T. 2001. Effects of pipeflow on hydrological process and its relation to landslide: a review of pipeflow studies in forested headwater catchments. *Hydrological Processes* 15(11), 2151-2174.
- USEPA 2006 Geographic Information Systems Analysis of the Surface Drinking Water Provided by Intermittent, Ephemeral, and Headwater Streams in the U.S., <https://www.epa.gov/cwa-404/geographic-information-systems-analysis-surface-drinking-water-provided-intermittent>.
- USEPA 2021 SDWIS Fed Reporting Services system, USEPA, SDWIS Fed Data Warehouse, [https://sdwis.epa.gov/ords/sfdw\\_pub/f?p=108:200](https://sdwis.epa.gov/ords/sfdw_pub/f?p=108:200), accessed on February 24, 2022.
- USGS 1996 Nutrients in the Nation's Water -- Too Much of a Good Thing?, p. 24 p.

- van Rijn, L.C. 1984. Sediment transport, part I: bed load transport. *Journal of Hydraulic Engineering* 110(10), 1431-1456.
- Vermunt, J. and Visser, R. 1987. Nitrate toxicity in cattle. *New Zealand Veterinary Journal* 35(8), 136-137.
- Vilmin, L., Mogollon, J.M., Beusen, A.H.W. and Bouwman, A.F. 2018. Forms and subannual variability of nitrogen and phosphorus loading to global river networks over the 20th century. *Global and Planetary Change* 163, 67-85.
- Walter, M.T., Kim, J.S., Steenhuis, T.S., Parlange, J.Y., Heilig, A., Braddock, R.D., Selker, J.S. and Boll, J. 2000. Funneled flow mechanisms in a sloping layered soil: Laboratory investigation. *Water Resources Research* 36, 841-849.
- Ward, J.V., Tockner, K. and Schiemer, F. 1999. Biodiversity of floodplain river ecosystems: Ecotones and connectivity. *Regulated Rivers-Research & Management* 15(1-3), 125-139.
- Waters, T.F. (1973) *Streams and Rivers of Minnesota*, University of Minnesota Press.
- White, D.S. 1993. Perspectives on defining and delineating hyporheic zones. *Journal of the North American Benthological Society* 12(1), 61-69.
- Widdowson, M.A., Molz, F.J. and Benefield, L.D. 1988. A numerical transport model for oxygen-based and nitrate-based respiration linked to substrate and nutrient availability in porous-media *Water Resources Research* 24(9), 1553-1565.
- Wiegel, S., Aulinger, A., Brockmeyer, R., Harms, H., Löffler, J., Reincke, H., Schmidt, R., Stachel, B., von Tumpling, W. and Wanke, A. 2004. Pharmaceuticals in the river Elbe and its tributaries. *Chemosphere* 57(2), 107-126.
- Williams, M.R., Buda, A.R., Elliott, H.A., Hamlett, J., Boyer, E.W. and Schmidt, J.P. 2014. Groundwater flow path dynamics and nitrogen transport potential in the riparian zone of an agricultural headwater catchment. *Journal of Hydrology* 511, 870-879.
- Wilson, G., Nieber, J.L., Fox, G.A., Dabney, S.M., Ursic, M. and Rigby, J.R. 2017. Hydrologic connectivity and threshold behavior of hillslopes with fragipans and soil pipe networks. *Hydrological Processes* 31(13), 2477-2496.
- Wilson, G.V., Jardine, P.M., Luxmoore, R.J. and Jones, J.R. 1990. Hydrology of a forested hillslope during storm events. *Geoderma* 46(1-3), 119-138.
- Wilson, G.V., Rigby, J.R., Ursic, M. and Dabney, S.M. 2016. Soil pipe flow tracer experiments: 1. Connectivity and transport characteristics. *Hydrological Processes* 30(8), 1265-1279.
- Winter, T.C., Harvey, J.W., Franke, O.L. and Alley, W.M. 1998 *Ground Water and Surface Water, A Single Resource*, Circular 1139., U.S. Geological Survey, Denver, CO.
- Wurtz, C.B. 1955. Stream Biota and Stream Pollution. *Sewage and Industrial Wastes* 27(11), 1270-1278.
- Yonkos, L.T., Friedel, E.A., Perez-Reyes, A.C., Ghosal, S. and Arthur, C.D. 2014. Microplastics in Four Estuarine Rivers in the Chesapeake Bay, U.S.A. *Environmental Science & Technology* 48, 14195-14202.
- Zarnetske, J.P., Haggerty, R., Wondzell, S.M., Bokil, V.A. and Gonzalez-Pinzon, R. 2012. Coupled transport and reaction kinetics control the nitrate source-sink function of hyporheic zones (vol 48, W11508, 2012). *Water Resources Research* 48.
- Zhao, Z. and Fernando, H.J.S. 2007. Numerical simulation of scour around pipelines using an Euler-Euler coupled two-phase model. *Environmental Fluid Mechanics* 7, 121-142.
- Zheng, L., Cardenas, M.B., Wang, L. and Mohrig, D. 2019. Ripple effects: bed form morphodynamics cascading into hyporheic zone biogeochemistry. *Water Resources Research* 55, 7320-7342.

- Zhou, Y., Wilson, G.V., Fox, G.A., Rigby, J.R. and Dabney, S.M. 2016. Soil pipe flow tracer experiments: 2. Application of a streamflow transient storage zone model. *Hydrological Processes* 30(8), 1280-1291.
- Zhou, Y.Q., Ritzi, R.W., Soltanian, M.R. and Dominic, D.F. 2014. The Influence of Streambed Heterogeneity on Hyporheic Flow in Gravelly Rivers. *Groundwater* 52(2), 206-216.

## **CHAPTER 2: Filling the void: the effect of streambank soil pipes on transient hyporheic exchange during a peak flow event.**

Status: published in *Water Resources Research* on February 7, 2020, reprinted here with permission from Wiley ©2020. American Geophysical Union. All Rights Reserved.

Lotts, W. S., & Hester, E. T. (2020). Filling the void: the effect of stream bank soil pipes on transient hyporheic exchange during a peak flow event. *Water Resources Research*, 56, e2019WR025959. <https://doi.org/10.1029/2019WR025959>.

**Authors:** W. Seth Lotts<sup>1</sup>, Erich T. Hester<sup>1</sup>

<sup>1</sup>Department of Civil and Environmental Engineering, Virginia Tech, Blacksburg, Virginia 24061 USA

**Corresponding Author:** Erich T. Hester, [ehester@vt.edu](mailto:ehester@vt.edu)

### **Key Points:**

- Modelled the effects of soil pipes on hyporheic exchange volume and particle flow paths caused by a 10 hour half-sinusoid peak flow event
- The addition of a single 1.5 m long soil pipe increased hyporheic exchange volume by 73.4%
- Soil pipe length and density had the greatest effect on hyporheic volume

### **Abstract**

The hyporheic zone is the ecotone between channel flow and groundwater which can process nutrients and improve water quality. Transient hyporheic zones occur in the riparian zone (bank storage or “lung model” exchange) during channel stage fluctuations. Recent studies show soil pipes are widespread in streambanks and beneath floodplains, creating highly preferential flow between channel and riparian groundwater such that the traditional Darcy model of flow does not apply. We used MODFLOW with the conduit flow package (CFP) to model a series of streambank soil pipes, and examined soil pipe density (number per m), length, diameter, height above baseflow water surface, connectivity, and matrix hydraulic conductivity on transient particle flow paths and total hyporheic exchange volume (i.e. bank storage) over the course of a peak flow (e.g., storm) event. We found that adding five soil pipes per m more than doubled hyporheic volume. Soil pipe length was the most important control; adding one 1.5-m-long soil pipe caused a 73.4% increase in hyporheic volume. The effect of increasing soil pipe diameter on hyporheic volume leveled off at ~1 cm, as flow limitation switched from pipe flow to pipe-matrix exchange. To validate our approach, we used the model to successfully reproduce trends from field studies. Our results highlight the need to consider soil pipes when modeling, monitoring, or managing bank storage, floodplain connectivity, or hyporheic exchange.

## 2.1. Introduction

Streams are integral to many ecosystems (Cummins and Klug 1979, Huet 1959, Quaglietta et al. 2018), and a key component of the Earth's critical zone (Richter and Mobley 2009). Impacts from climate change (Du et al. 2019, Molina-Navarro et al. 2018, Tang 2019), urbanization (Bell et al. 2012, Coles and Geological Survey (U.S.) 2012, Hassett et al. 2018, O'Driscoll et al. 2010, Waite et al. 2008), agricultural pesticides (Climent et al. 2019, Knillmann et al. 2018, Rizzi et al. 2019, Stehle and Schulz 2015) and fertilizers (Connolly et al. 2015, Jones et al. 2018, King et al. 2016, White et al. 2018) are increasing concerns. As such anthropogenic effects to streams and rivers mount (Liao et al. 2018, Vorosmarty et al. 2010), research on stream functions has grown.

Floodplains along streams benefit ecosystems (Meyer and Edwards 1990, Smock et al. 1992) and promote biodiversity (Huggenberger et al. 1998). They act as ecotones between terrestrial and aquatic biota (Thoms 2003), where groundwater exchange links the two (Jung et al. 2004). Vegetated floodplains and riparian zones play a vital role in managing stream quality by acting as sinks for nitrate and other nutrients (Connolly et al. 2015, Winter et al. 1998), providing unique habitat, reducing erosion, and mitigating floods (Winter et al. 1998).

The hyporheic zone occurs where surface water and groundwater interact beneath and adjacent to streams, including within stream and river banks (Harvey and Wagner 2000, Triska et al. 1989, Winter et al. 1998). Dissolved oxygen, nutrients, microbes, benthic organisms, and salmon eggs from surface water interact with other nutrients and essential minerals from groundwater (Brunke and Gonser 1997, Stanford and Ward 1993). The hyporheic zone can benefit water quality through reactions such as denitrification (Hester and Gooseff 2010, Meghdadi and Javar 2018, Zarnetske et al. 2012). Hyporheic exchange includes both gill model (essentially steady state movement through bed or banks) and lung model (pulsing due to fluctuating surface water stages) types (Sawyer et al. 2009). Lung model exchange, also known as bank storage (Pinder and Sauer 1971), has received less attention, but is beneficial to biota (Allen and Vaughn 2009, DiStefano et al. 2009) and water quality (Anderson et al. 2011, Gu et al. 2012). Sawyer et al. (2009) examined dam-induced surface water stage fluctuations and their effect on lung model exchange. Gerecht et al. (2011) characterized the spatial extent and timing of lung model exchange using temperature probes. Schmadel et al. (2016) examined riparian groundwater head dynamics and fluxes caused by the interaction of sinusoidal boundary conditions on both the channel and hillslope sides.

Preferential flow is widespread in porous media (Anderson et al. 2015), and occurs where water and associated solutes travel significantly faster in a small portion of the aquifer or soil matrix than the rest of the domain. Preferential flow can result from water repellency in dry soils (Blackwell 2000, Morales et al. 2010), random pore-scale variability causing fingered flow (Hillel 1987, Rezanezhad et al. 2006, Selker et al. 1996), flow focusing or funnel flow from heterogeneity in permeability (e.g., gravel veins), and macropores/soil pipes where water moves through small conduits or voids similarly to pipe flow (Pales et al. 2018).

Macropores and soil pipes are one kind of preferential flow path, defined as void spaces that are long in relation to their width (Beven and Germann 1982), where the concept of a 'representative elementary volume' (REV) does not apply (Anderson et al. 2015, Bear 1972, Fitts 2012, Freeze and Cherry 1979). Macropores and soil pipes are formed by burrowing fauna such as moles, gophers, and wombats (1-5 cm); earthworms (2 mm-1 cm) and insects; decaying plant roots; desiccation of clays; chemical weathering of bedrock; freeze-thaw; or internal erosion (Beven and Germann 1982). Macropores and soil pipes are common in floodplain and riparian zone soils and stream and river banks due to the prevalence of burrowing fauna (Allen and Vaughn 2009, Brown and Brown 2011, DiStefano et al. 2009, Shields and Kelly 1997, Stahl et al. 2014, Williams and Hynes 1974, Williams et al. 1974, Wright et al. 2011) and decayed plant roots (Aubertin 1971, Beasley 1976, Gaiser 1952, Mosley 1979, Mosley 1982). Macropores have been studied in many contexts, including formation and mapping in the field (Allaire et al. 2009, Bryan and Jones 1997) and modeling preferential flow (Šimůnek et al. 2003). Macropores and preferential flow paths are often studied in the context of how fertilizers and pesticides (Jarvis 2007, Kladivko et al. 2001, Villholth et al. 2000) microbes (Darnault et al. 2003), and other sorbing pollutants fail to behave according to a Darcy-Richards advection-dispersion framework. The term soil pipe often overlaps significantly with macropores, although the latter often refers to smaller vertical conduits and the former to horizontal conduits, especially larger ones that are created by internal erosion.

Macropores and soil pipes can have substantial hydrologic effects on stream flow, accounting for up to 50% of inflow to streams during storms (Jones 2010). In an attempt to account for all the variation in runoff and streamflow, Sidle et al. (2001) showed that significant contributions would have to come from the soil pipe networks. Wilson et al. (1990) showed that 71% of precipitation on a hill-slope sub-catchment enters the stream through soil pipes. Similarly, Bernatek-Jakiel and Poesen (2018) remarked that pipeflow can account for up to 70% of overall catchment runoff, underscoring the profound hydrologic effects of soil pipes. Macropores and soil pipes short circuit hydrologic flow between an agricultural catchment and the stream, allowing pesticides and fertilizers to circumvent the soil matrix and associated processes (Bernatek-Jakiel et al. 2017).

Many studies quantify effects of heterogeneity such as gravel veins and similar areas of higher-K matrix on near-channel flow (e.g. (Fleckenstein et al. 2006, Kalbus et al. 2009, Laube et al. 2018, Pryshlak et al. 2015)). For example, Cardenas et al. (2004) modeled the effects of sediment heterogeneity and therefore preferential flow on hyporheic exchange and contaminant transport, but did not consider soil pipes. On the other hand, Jones and Cottrell (2007), McEwen and Hester (2019), Menichino et al. (2015) have shown that soil pipes are common along stream banks in many regions. Wilson et al. (2013) numerically modeled flow and internal erosion in soil pipes, but did not examine their effects on hyporheic exchange. Some studies go further and examine effects of preferential flow on hyporheic exchange. For example, Heeren et al. (2010) and Fox et al. (2011) conducted tracer tests on preferential flow paths including soil pipes, but did not isolate their effects from those of gravel veins. Menichino et al. (2015), and Zhou et al. (2016) reported a slight increase in transient storage from soil pipes, but did not quantify the hyporheic exchange component. Briggs et al. (2016) collected thermal imaging video clearly confirming that macropores and peat pipes have a profound impact on surface-groundwater flow

regimes. Menichino et al. (2014) showed that an open soil pipe in a meander bend had 29 to 550 times greater hydraulic conductivity and 9 to 21% faster transport velocities than a partially plugged soil pipe. Finally, in another field study, Menichino and Hester (2015) showed that streambank soil with pipes was more hydraulically connected to stream stage than that without pipes, demonstrating that pipes can significantly affect lung model exchange. Yet controls on such effects, including soil pipe characteristics such as length and size, have not been systematically quantified.

Here, we used numerical modeling to examine the effect of soil pipes on lung model hyporheic exchange in a streambank. In a sensitivity analysis, we explore the effect of soil and soil pipe characteristics such as soil pipe density, diameter, length, matrix hydraulic conductivity, and tortuosity on induced hyporheic exchange/bank storage volume and flow paths.

## 2.2 Methods

### 2.2.1 Modeling Overview and Governing Equations for Soil Matrix

We used a numerical model to quantify how soil pipes in streambanks or riverbanks affect bidirectional exchange across the bank face between the channel and floodplain/riparian groundwater during channel stage fluctuations. We calculated groundwater flow in the soil matrix with the 2-D unconfined, isotropic, groundwater flow (Boussinesq) equation:

$$\frac{\partial}{\partial x} \left( h \frac{\partial h}{\partial x} \right) + \frac{\partial}{\partial y} \left( h \frac{\partial h}{\partial y} \right) + R = \frac{S_y}{K} \frac{\partial h}{\partial t} \quad [2.1]$$

using a finite difference scheme, with a pre-conditioned conjugate solver in MODFLOW (Harbaugh 2005) and the USGS GUI Model Muse (Winston 2014).  $K$  is isotropic hydraulic conductivity (L/T),  $h$  is the potentiometric head (L),  $R$  is volumetric flux per unit volume representing sources and/or sinks of water (T<sup>-1</sup>),  $S_y$  is the specific yield of the porous media (dimensionless), and  $t$  is time (T). While lung model hyporheic exchange can involve unsaturated groundwater flow, saturated flow computations are simpler and sufficiently accurate. For example, Schmadel et al. (2016) used equation (1) to examine the effects of sinusoidal diel fluctuations of stream flow on riparian groundwater. This approach is sufficiently accurate to reproduce hyporheic zone field data, including hydraulics (Lautz and Seigel 2005) and transport (Lin and Medina 2003). Furthermore, Fox and Durnford (2003) compared saturated and unsaturated approaches for modeling groundwater pumping adjacent to a river and found very similar behavior.

### 2.2.2 Model Domain and Boundary Conditions

We used a simplified model to enhance the generality of our results (Hester and Doyle 2008, Hester et al. 2014, Pescimoro et al. 2019, Schmadel et al. 2016). Our model included a single prismatic stream channel as a boundary condition to a rectangular domain of riparian soil (Figure 2.1). The stream channel was modeled as a specified head boundary, in particular half a sinusoidal cycle (Figure 2.1c) to simulate a peak flow event (Schmadel et al. 2016). The

fluctuation amplitude was 0.5 m for our base case, consistent with transient events such as storms (Menichino and Hester 2015), or dam releases (Sawyer et al. 2009). For example, amplitudes for the storm events in Menichino and Hester (2015) range from roughly 0.1 m to roughly 0.9 m with the median being 0.5 m. The fluctuation half period was 10 hr. for our base case, consistent with storm events (Menichino and Hester 2015) and diurnal peaks caused by dam operations (Sawyer et al. 2009) and snowmelt (Loheide and Lundquist 2009, Lundquist and Cayan 2002). We selected a base flow stream depth of 1 m, consistent with a medium-sized river.

The boundary condition opposite the channel boundary was general head to simulate a far-field condition. We did not simulate hydrologic fluctuation in this boundary condition in order to simplify our analysis, consistent with a range of scenarios including dam fluctuations (Francis et al. 2010, Sawyer et al. 2009), precipitation occurring only significantly upstream of the transect (Elder et al. 1988), daily snowmelt (Loheide and Lundquist 2009), daily channel stage fluctuations due to irrigation (Caldwell and Eddy-Miller 2013, Hedefeff and Caldwell 2017), and significant lag time between channel and hillslope peak (Holden and Burt 2002, Jones 1988, Jones and Crane 1984). On the upstream and downstream end of the domain there were no flow boundaries. The domain of interest was a 2 m × 1 m × 2 m subset centered within the larger model (Figure 2.1a). The boundary extended 2.25 m up and down stream past the domain of interest to minimize boundary effects.

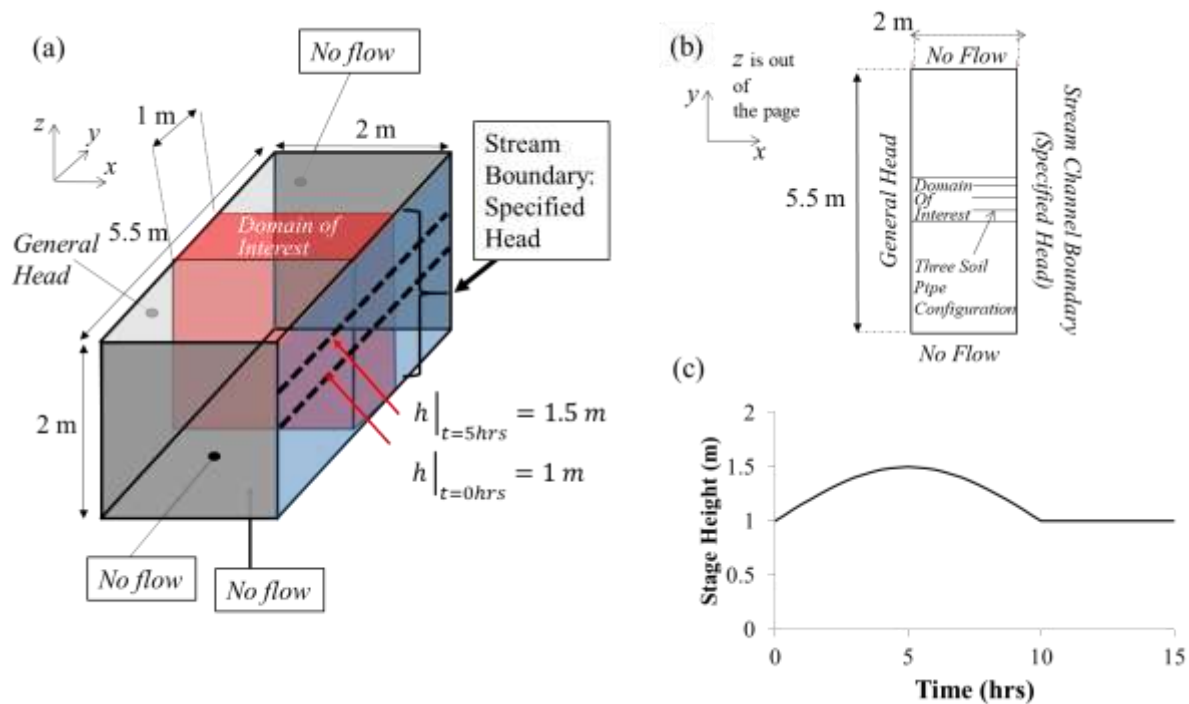


**Figure 2.1: (a) Schematic of riparian groundwater model domain. The  $x$ -direction is perpendicular to the channel, the  $y$ -direction is parallel to the channel, and the  $z$ -direction corresponds to depth. (b) Plan view of the domain, and (c) time-varying stream channel boundary head condition. The soil pipes are open to the channel, i.e. the time-varying specified head boundary shown in (c). Under losing conditions water flows from right to left conditions (channel to riparian groundwater), and the reverse occurs under gaining.**

Model computational cells were  $2 \times 2$  cm in the  $x$  and  $y$  directions, with 275 rows and 100 columns; the model has one layer 2 m thick with time-varying water table. Before subjecting the system to the hydrograph in Figure 2.1, the model was run to steady state with the general head boundary set to 1.2 m above the model bottom (i.e.  $z = 1.2$  m), and the stream channel boundary set to  $z = 1$  m to simulate gaining background conditions. MODPATH version 6 (Pollock 2012) was used to track water parcels (infinitesimal cubes of water), where 400 particles (8 per cell along 50 stream channel boundary cells in the domain of interest) were released 10 minutes into the simulation (after the stream becomes a losing stream) at  $z = 1$  m.

### 2.2.3 Governing Equations for Soil Pipes

Soil pipes were oriented horizontally in one layer, evenly spaced, open to the bank, parallel to each other, and perpendicular to the bank. This simplified parsimonious approach is consistent with the relative lack of information on 3-D spatial layouts of floodplain soil pipes, and our goal to establish relationships between hyporheic volume and pipe parameters. Gormally et al. (2011) is one of the few studies that did map flood plain soil pipes, and found them mostly horizontal.

Soil pipes were modeled in a separate conduit domain using the pipe flow equations [2.2] through [2.4]. The soil pipe boundary condition on the channel end (right most node) was the time-varying specified head in the channel, while the rest of the pipe domain was head-dependent exchange determine by equation [2.5]. We assumed that the soil pipe geometry was static (no internal erosion). In all sensitivity analyses except “height above baseflow channel water surface level”, we assumed full-pipe flow (no partially filled pipes). We assumed the pipes have a roughness height of 1 mm. We simulated flow through the soil pipe(s) using the conduit flow package (CFP) for MODFLOW (Shoemaker et al. 2007). The CFP applies Kirchhoff’s Law (i.e. continuity, Equation 2.2) at each node in each conduit:

$$\sum_{ip=1}^{np} Q_{ip} - Q_{ex} + Q_s = 0 \quad [2.2]$$

where  $\sum_{ip=1}^{np} Q_{ip}$  ( $L^3/T$ ) is the sum of all pipe flows at a node,  $ip$  is a pipe number index, and  $np$  is the number of pipes at a node,  $Q_{ex}$  ( $L^3/T$ ) is flow to or from the matrix, and  $Q_s$  ( $L^3/T$ ) is the change in storage applicable only when the pipe is partially full. The Hagen-Poiseuille equation (equation 2.3) is applied for laminar flow and the Darcy-Weisbach equation (equation 2.4) is applied for turbulent flow to get Kirchhoff’s Law as a function of head:

$$Q_{ip} = - \frac{\pi d_{ip}^4 g (h_{in} - h_{neighbor})}{128 \nu \Delta l_{ip} \tau_{ip}} \quad [2.3]$$

$$Q_{ip} = -\sqrt{\frac{|h_{in}-h_{neighbor}|gd_{ip}^5\pi^2}{2\Delta l_{ip}\tau_{ip}}} \log\left(\frac{2.51\nu}{\sqrt[4]{\frac{2|h_{in}-h_{neighbor}|gd_{ip}^3}{\Delta l_{ip}\tau_{ip}}}} + \frac{k_c}{3.71d_{ip}}\right) \frac{(h_{in}-h_{neighbor})}{|h_{in}-h_{neighbor}|} \quad [2.4]$$

Where  $Q_{ip}$ ,  $d_{ip}$ ,  $\Delta l_{ip}$ ,  $k_c$ , and  $\tau_{ip}$  are the flow rate ( $L^3/T$ ), diameter (L), length (L), roughness height (L), and tortuosity (dimensionless), respectively of the pipe segment at index  $ip$ ;  $h_{in}$  is the head (L) at node index  $in$ , and  $h_{neighbor}$  is the node head (L) at the other end of the pipe segment;  $g$  is the acceleration due to gravity ( $L/T^2$ ), and  $\nu$  is the viscosity ( $L^2/T$ ) of water at 25°C. Transitions from laminar to turbulent flow and from turbulent to laminar are assumed to occur at Reynolds numbers of 4000 and 2000, respectively (see section 5.1 Shoemaker et al. 2007). The resulting system of equations for the heads is solved via the Newton Raphson method. The conduit domain is connected to the soil matrix domain by an exchange term

$$Q_{ex} = \alpha_{i,j}(h_{in} - h_{i,j}) \quad [2.5]$$

Where  $Q_{ex}$  is the volumetric exchange flow rate ( $L^3/T$ ),  $\alpha_{i,j}$  is the conductance ( $L^2/T$ ) at a given node between the pipe and soil matrix at MODFLOW cell  $i,j$ , and  $h_{i,j}$  is the head (L) in the encompassing MODFLOW cell  $i,j$ . Each node in the soil pipe domain corresponds spatially to the center of the MODFLOW (i.e. matrix) cell in which it is located (Shoemaker et al. 2007).

#### 2.2.4 CFP Model Reliability

Most of the studies which use the CFP pertain to karst topography at large scales (Saller et al. 2013, Xu et al. 2015). However, Karay and Hajnal (2015) reproduced laboratory results for a conduit network of diameters 0.8 cm and 3.2 cm, and concluded that the CFP package was a useful tool for modeling conduits and fractures in both karst and non-karst. Further, Gallegos et al. (2013) reproduced laboratory results from a 2 cm diameter conduit network with the CFP more reliably than using high matrix K cells to model the conduits.

To further build confidence in applying the CFP to streambank soil pipes, we used the CFP to simulate the field site in Menichino and Hester (2015). Since the exact soil pipe configuration of Menichino and Hester (2015) is unknown, we used a configuration of five parallel soil pipes and with a matrix K of  $10^{-6}$  m/s. They used riparian wells to monitor propagation of surface water fluctuations into adjacent groundwater in the presence and absence of soil pipes (Figures 2.2a and 2.2b). We ran our model with their channel stage data from a storm event 12 pm on November 12, 2012, to 6 pm November 13, 2012 from Figure 4 of Menichino and Hester (2015) and set the general head boundary condition to produce roughly the same background head gradient as the pre-storm steady state conditions in the field (0.011665 m/m away from the stream channel). The model was able to reproduce roughly the same trend as the field data (Figures 2.2c and 2.2d). The water surface elevations in the two wells closest to the channel with soil pipes (M-A, M-B) show very strong linkage to the channel stage height in both modelled and field graphs, whereas for no soil pipes (NM-A, NM-B) there is a rise in water surface elevation as a result of the storm but with a significant lag and amplitude attenuation. For all four cases, the two farther wells remain relatively invariant. This demonstrates our model's ability to reproduce general trends from the field. Although we could have produced the observation wells more exactly by manipulating the soil pipe and matrix

parameters and spatial layout, it would not have represented the layout at the site. Further, our goal was to establish the model’s ability to reproduce general trends, not calibrate a model for a specific floodplain to make future predictions. Similar comparisons are possible with more general field studies of preferential flow in streambanks. For example, the well fields in Newman and Keim (2013) demonstrated similar lag and amplitude attenuation between the reservoir and monitoring wells.

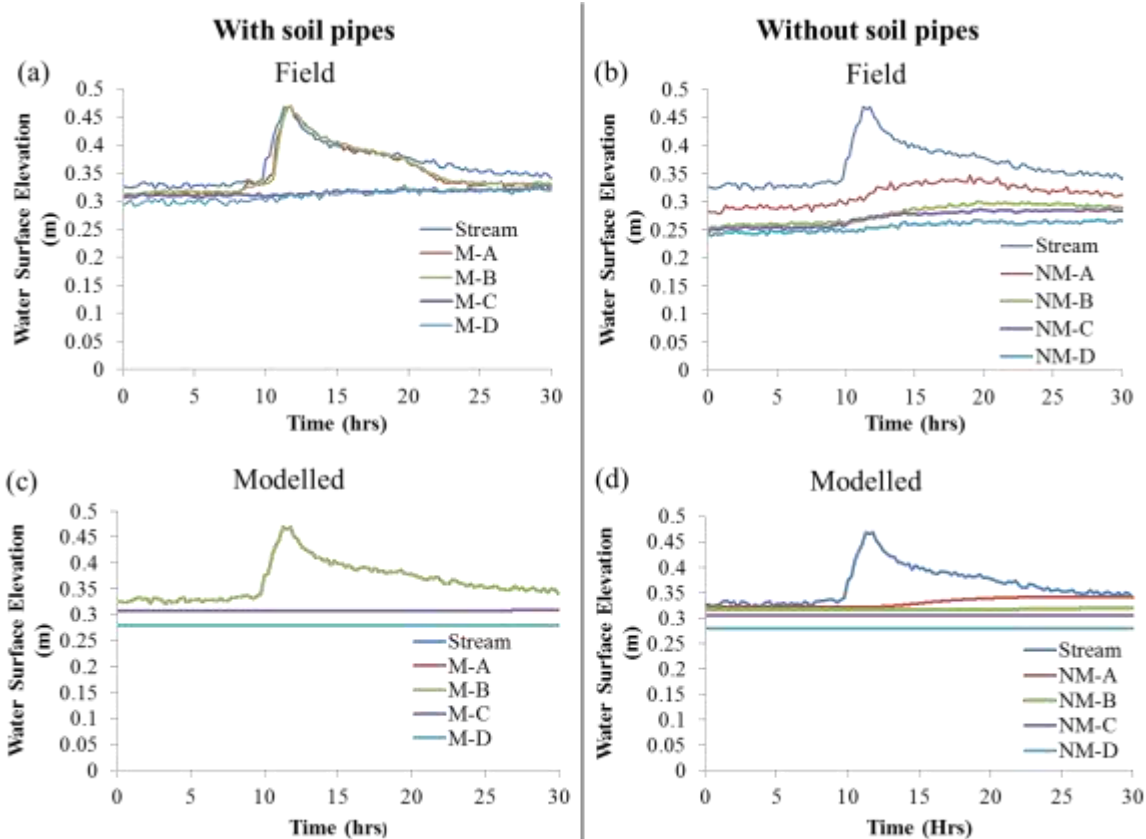


**Figure 2.2: Comparison of field data from Slate Branch (Menichino and Hester 2015) vs. our model simulations using their boundary conditions. There were two transects of wells perpendicular to the channel, one with streambank soil pipes and one without. Wells M-A, M-B, M-C, and M-D were 0.5, 1, 2, and 4 m respectively away from the stream channel at the cross section with soil pipes. Wells NM-A, NM-B, NM-C, NM-D were analogous but without soil pipes. Note that for our model results with soil pipes (panel c), the heads for the two wells closest to the channel (M-A, M-B) are essentially identical with those in the channel, so the lines plot atop one another.**

### 2.2.5 Calculating Hyporheic Volume

For each time step, we recorded the volume of water exchanged between the stream channel boundary and the domain of interest via the Zone Budget post processing package (Figure 2.1). We then summed these for the period when the channel was hydrologically losing. This can be represented mathematically as:

$$V = \int_{\Delta t_{losing}} Q(t)dt \approx \sum_{i=1}^{ntime} Volume \text{ per time step}_i \Delta t_i \quad [2.6]$$

Where,  $V$ ,  $Q(t)$  is the volumetric flow rate,  $\Delta t_{losing}$  is the time period where the system exhibits losing conditions,  $ntime$  is the number of time steps under losing conditions,  $\Delta t_i$  is the length of time step  $i$ . All of the water that flows into the bank will eventually flow back into the channel since the stream is a gaining stream, thus there is no need to conduct Lagrangian techniques. We normalized hyporheic volume by dividing by that without soil pipes ( $V/V_0$ ).

### 2.2.6 Sensitivity Analysis and Parameter Values

We conducted a sensitivity analysis where we individually varied soil pipe density (number of soil pipes per m,  $\rho$ ) within the domain of interest (Figure 2.1), soil pipe length ( $L$ ), soil pipe diameter ( $D$ ),  $K$ , soil pipe height above baseflow channel water level ( $H$ ), soil pipe connectivity ( $\lambda$ ), and soil pipe tortuosity ( $\tau$ ; Table 2.1). For the base case,  $\rho=1$ ,  $L=1$ ,  $D=1.5$  cm,  $K=0.0001$  m/s,  $H= -0.5$  m,  $\lambda = 0$ , and  $\tau_{ip} = 1$ . Note that the diameter was switched to 2 cm from 1.5 cm about half-way through the study because the solver performed better at higher diameters (see section B1 of the supporting information for details). The roughness height,  $k_c$  stayed the same at 1 mm, the wall permeability was set to the matrix  $K$ , and the specific yield stayed the same at 0.32, except for when  $K$  varied. It was then varied based on soil texture (Table 2.2).

We varied soil pipe densities from 0 to 5 per m in increments of 1 based on similar observations in McEwen and Hester (2019), Menichino et al. (2015). We varied soil pipe length from 0 to 1.5 m in 0.25-m increments based on field studies showing streambank lengths to first bend from ~5 cm to ~90 cm (McEwen and Hester 2019, Menichino et al. 2015). These soil pipes undoubtedly extended past the first bend as seen by Gormally et al. (2011), who found true lengths in excess of 4.2 m. We varied pipe diameter up to 4 cm, based on literature median/mean opening heights and widths of 3-4 cm (McEwen and Hester 2019, Menichino et al. 2015). We varied pipe diameter down to 0.0 cm in 0.5 cm increments because soil pipes < 1.0 cm do exist (Uchida et al. 2001).

We varied matrix  $K$  from  $10^{-7}$  m/s to  $10^{-3}$  m/s. This includes ranges of  $K$  commensurate with sandy loam and silt, two soil textures which McEwen and Hester (2019) show to frequently contain soil pipes in floodplains. Bernatek-Jakiel and Poesen (2018) has also shown that soil pipes form prevalently in silty loam and sandy loam in other areas not necessarily under floodplains. The selected  $K$  range also includes coarse and medium sand, where one would expect fewer soil pipes (McEwen and Hester 2019).  $K$  and specific yield typically covary with soil texture, thus during the matrix  $K$  portion of the sensitivity analysis we covaried the two variables (Table 2.2). Currently, there is a dearth of information on specific yield for soils (Crosbie et al. 2019). We used data from the most comprehensive study to link specific yield to soil types, Morris and Johnson (1967), which used the Ground Water Branch, U.S. Geological Survey soil classification system.

**Table 2.1: Summary of simulations.**

Parameter varied	Range; increment	Units	Notes
Soil pipe density, $\rho$	0–5; 1	soil pipes per m	

Soil pipe length, L	0–1.5; 0.25	M	
Soil pipe diameter, D	0, 0.4, 1.05, 1.2, 1.5, 2, 2.5, 3, 3.5, 4 <sup>†</sup>	cm	
Soil matrix hydraulic conductivity, K	10 <sup>-7</sup> , 10 <sup>-6.5</sup> , ..., 10 <sup>-3</sup> <sup>†</sup>	m/s	D=2 cm, S <sub>y</sub> varied simultaneously to match material (Table 2.2)
Soil pipe height above or below baseflow water level, H	-0.5–+0.3; 0.1	m above (+) or below (-) baseflow	D=2 cm
Soil pipe connectivity, intersection/endpoint ratio $\lambda$	0–2; 1/3	Ratio of number of intersections to number of endpoints	D=2 cm
Tortuosity	1-2; 0.25	dimensionless	D=2 cm

<sup>†</sup>a constant interval was not used thus we list each parameter value

**Table 2.2: Covariation of specific yield and hydraulic conductivity via soil texture (Morris and Johnson 1967).**

- Log(K)	Soil Texture	Specific Yield
3	Coarse Sand	0.3
3.5	Coarse Sand	0.3
4	Medium Sand	0.32
4.5	Medium Sand	0.32
5	Fine Sand	0.3
5.5	Silt	0.2
6	Silt	0.2
6.5	Silt	0.2
7	Silt	0.2

We varied soil pipe height above baseflow channel water surface level from -0.5 m to 0.3 m in 0.1 m increments because McEwen and Hester (2019) showed the majority of streambank soil pipes were located less than 0.3 m above baseflow, and Menichino et al. (2015) and McEwen and Hester (2019) showed that 32% and 3.2% of soil pipes were submerged at baseflow, respectively.

We varied soil pipe connectivity. Many studies acknowledge the importance of void space connectivity for flow (Beven and Germann 2013, Menichino and Hester 2015, Menichino et al. 2015, Nieber and Sidle 2010, Sidle et al. 2001, Troch et al. 2009), and there are various

approaches for quantification. For example, Jarvis et al. (2017), Larsbo et al. (2014), Vogel and Kretzschmar (1996) used 2-D or 3-D MRI or X-ray image analyses to determine the probability of connectivity within void space networks. Similarly, Lehmann et al. (2007) viewed the soil domain as a lattice structure of sites connected by bonds of void spaces, quantifying connectivity as bonds per site (i.e. coordination number). These approaches are useful where void space networks are complex and irregular but are unnecessarily cumbersome for the simple conduit networks studied here. By contrast, Luo et al. (2010) reduced macropores in laboratory soil columns into a system of branches and nodes, and quantified connectivity using node density and number of independent paths from one end of the domain to the other. Connectivity increased with the number of nodes and/or the number of paths one could take to get from one end of the column to the other. Inspired conceptually by the Luo approach, but increasing its simplicity and conciseness, we developed the dimensionless ratio ( $\lambda$ ) of intersections ( $N_{intersections}$ , dimensionless) to end points ( $N_{endpoints}$ , dimensionless), which applies well to clearly defined pipes with clear end points and intersections:

$$\lambda = \frac{N_{intersections}}{N_{endpoints}} \quad [2.7]$$

$\lambda$  was varied from 0 to 2 in increments of 1/3. Figure 2.3 shows an example configuration where the  $\lambda = 2$ . We also varied  $\tau$  from 1 to 2 in increments of 0.25, where  $\tau = 2$  corresponds to a very curvy soil pipe. Finally, we varied the peak flow amplitude and duration with little effect (Figure B9).

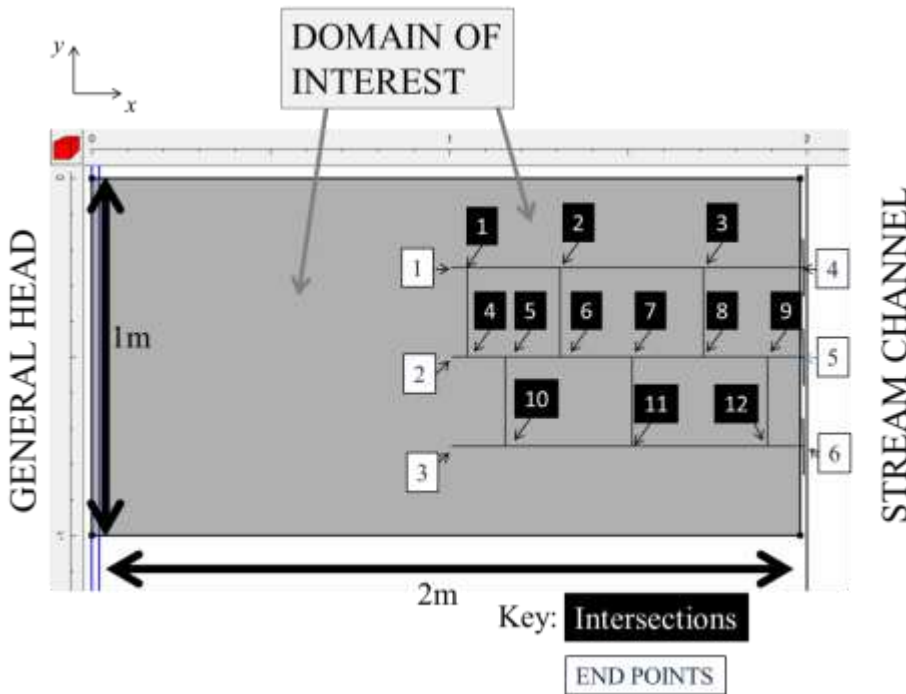


**Figure 2.3: Connectivity: Plan view of domain of interest showing example soil pipe configuration that results in  $\lambda = 2$ . The soil pipes are the black lines on the right half of the domain of interest. Intersections are labeled with black boxes with white lettering, and endpoints are labeled in white boxes with black lettering. The x-direction is perpendicular to the channel, the y-direction is parallel to the channel. Coordinates correspond to spatial distance in m.**

### 2.3 Results

In response to the flood wave in the channel, exchange across the streambank changed from background gaining conditions (Figure 2.4, negative Q) to flow into the bank. Peak inflow corresponded to the highest bankward head gradient (~3 hr.) rather than peak channel stage (~5 hr.) when adjacent riparian groundwater head had also increased, decreasing the gradient. As stream stage lowers, the stream returned to gaining conditions. The sharp corner at t=10 hours resulted from a sharp corner in the hydrograph where it changed from a sinusoid to a constant (Figure 2.1c).

Total hyporheic volume increased approximately linearly as  $\rho$  increased (Figure 2.5a). Adding 5 soil pipes per m more than doubled hyporheic exchange (235% of that without soil pipes). Pipes increased the area over which head gradients drove flow across the streambank, achieving the same effects as if we increased the size of the streambank, as seen by growth in length of the head contours. We discuss particle flow paths in Section 2.4.2.

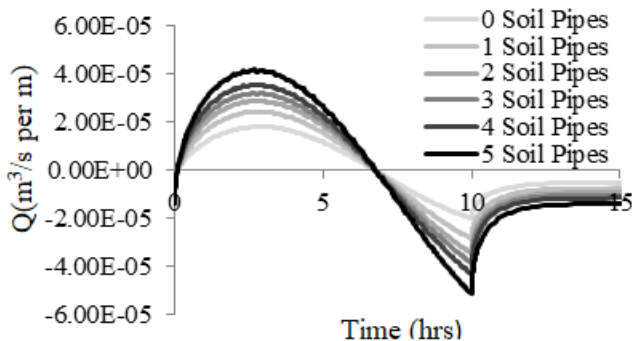


**Figure 2.4: Q (flow across the streambank within domain of interest) vs. t for various soil pipe densities. Negative and positive Q signify gaining and losing conditions, respectively.**

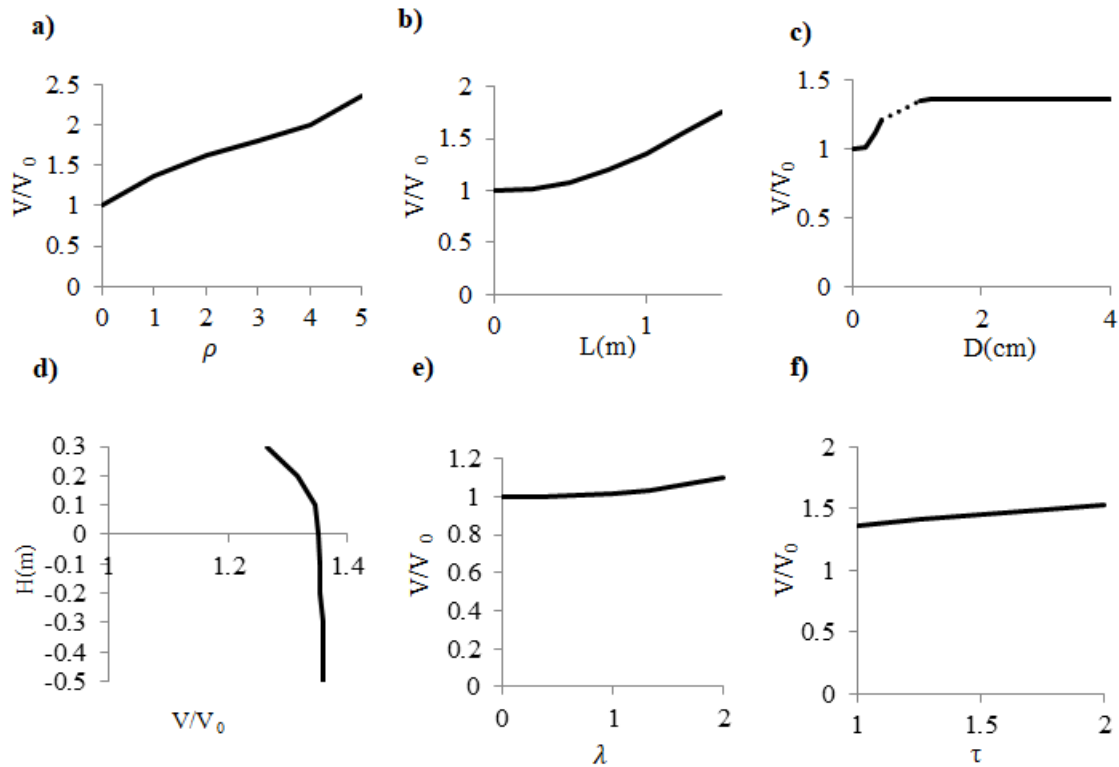


**Figure 2.5:** a) Hyporheic volume (Equation 2.6) normalized to the hyporheic volume of a system without soil pipes (i.e.  $V_0$ ) vs. a) number of soil pipes b) soil pipe length, c) soil pipe diameter (note the Newton-Raphson method had trouble converging in the pipe domain for diameters 0.5 cm-1 cm, see section B1 of Supporting Information for details), d) soil pipe height above base flow water surface elevation (WSEL), and e) soil pipe connectivity,  $\lambda$  (intersection to end point ratio), and f) tortuosity,  $\tau$

As  $L$  increased, hyporheic volume at first did not increase, and then increased by 73.4% from  $L=0.25$  m to 1.5 m (Figure 2.5b). Introduction of pipe flow allowed high head in the channel to protrude into the riparian groundwater at each pipe (Figure 2.6), which increased the length of the head contours in the vicinity, creating the same effect as if we stretched the stream bank into the shape of a Gaussian pulse (see also discussion section). This protrusion increased with pipe length, but only above a minimum pipe length of  $\sim 0.3$ - $0.4$  m, below which the pipes were too short to perturb the head field.

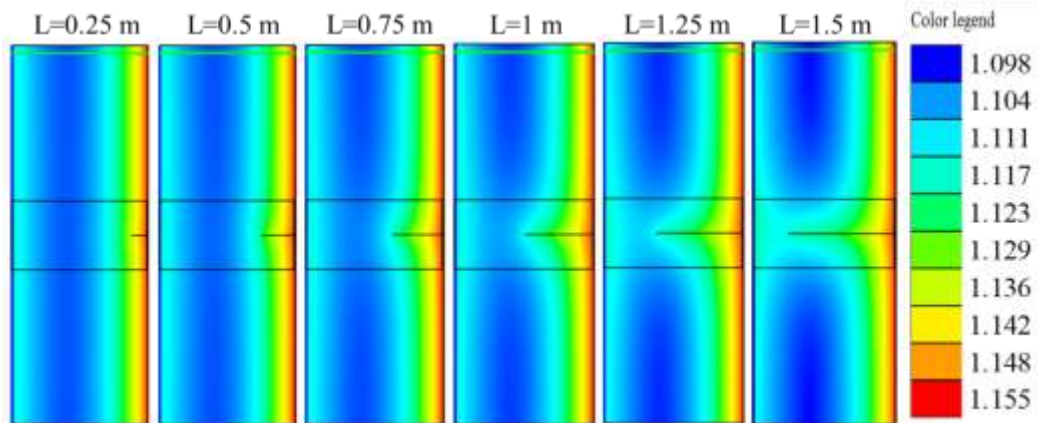


**Figure 2.6: Hydraulic head maps for various pipe lengths at  $t=1$  hr. At low soil pipe lengths (i.e.  $L=0.25$  m) the potentiometric surface is a straight ridge line, and at high soil pipe lengths, there is a significant protrusion of high head.**

Hyporheic volume increased with  $D$  (by 35%) until  $D \sim 1$  cm and then levelled off (Figure 2.5c). This effect was different than for a regular pipe where flow rate increases proportionally to the square of pipe diameter (i.e. cross-sectional area) because the end of the pipe was blocked by soil matrix. The effect of  $D$  was therefore less than other parameters we evaluated. There was almost no effect of  $H$  on hyporheic volume until the soil pipes were above baseflow (i.e., above height=0 in Figure 2.5d), when hyporheic volume decreased by 6% between heights of 0.1 m and 0.3 m. There was a non-linear increase in hyporheic volume with  $\lambda$ , although the effect was small for the parameter range we used in our sensitivity analysis (9.86%, Figure 2.5e). Increasing the connectivity decreased the overall resistance in the pipe, thereby increasing the flow rate (see also discussion section). There was a roughly linear increase with respect to  $\tau$ . This is because there was more exchange length created with the increase in tortuosity (virtually created through the manipulation of the  $\tau_{ip}$  term in equations [2.3] and [2.4]). There was a slight leveling off of the curve, probably due to the fact that tortuosity slows down the flow in the pipe, coupled with the fact that meanders adjacent to each other start to lessen the head gradient of their neighboring meanders as the tortuosity becomes large and meanders come closer to each other. We do not see a non-linear increase as with length because the soil pipes do not protrude further into the bank; thus, there is not much change in the potentiometric surface.

As matrix  $K$  increased, the percent increase in hyporheic volume due to adding a single soil pipe increased overall (Figure 2.7). However, this increase was nonlinear, first increasing from  $\sim 25\%$  at  $K=10^{-7}$  m/s to a local maximum of  $\sim 35\%$  at about  $K \sim 10^{-5}$  m/s, then decreasing to a local minimum of  $\sim 32\%$  at  $K \sim 10^{-4}$  m/s, then finally increasing more dramatically to  $\sim 66\%$  at  $K=10^{-3}$  m/s. There were a few competing phenomena that resulted in this highly nonlinear curve. As  $K$  increased, resistance to water exchange between soil pipe and riparian groundwater decreased, but head gradient driving flow simultaneously decreased (see discussion section for more detail).

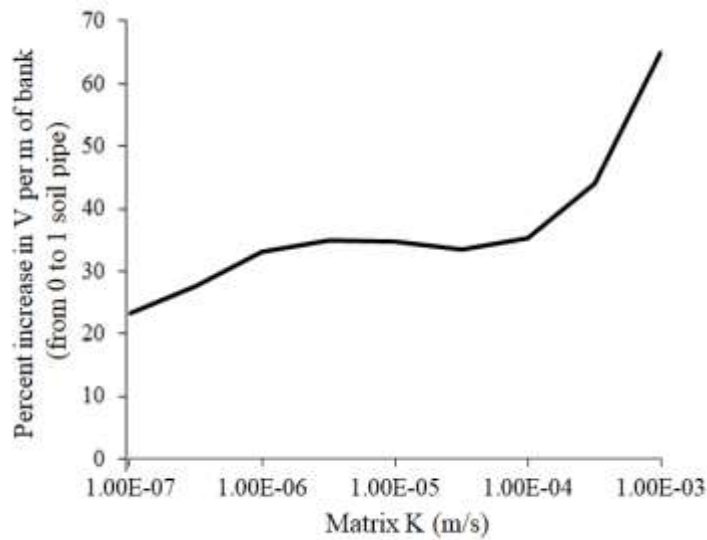


**Figure 2.7: Percent increase in hyporheic volume from adding 1 soil pipe vs. matrix K.** Because the y-axis represents the “value added” from a single soil pipe, the graph decreasing from  $K=10^{-5}$  m/s to  $10^{-4.5}$  m/s, for example, does not mean there is less hyporheic volume but rather that it makes a smaller relative change for  $K=10^{-4.5}$  m/s than for  $K=10^{-5}$  m/s.

## 2.4 Discussion and Further Analysis

### 2.4.1 Soil Pipe Preferential Flow Processes in Streambanks

In the general case of a single streambank soil pipe, high head propagates along the soil pipe and then enters the matrix, driving particles away from the pipe (Figure 2.8) because the soil pipe comes to an end and water is forced into the matrix. This is consistent with Jones (2010), where a storm event caused water to move from soil pipes to the surrounding riparian groundwater. However, once the head in the channel falls, the gradient reverses, and the particles flow back toward the pipe, following the path of least resistance. The latter is consistent with studies where water gravitates towards hillslope soil pipes and deeper zones of high matrix K (Wilson et al. 2017, Wilson et al. 1990, Wilson et al. 2016, Winter 1999).

Fully 40-70% of our observed hyporheic volume flows through a single soil pipe rather than the matrix (Figure B10), consistent with hillslope studies that show soil pipes as the primary conveyance of precipitation to the stream (Mosley 1982, Wilson et al. 2017, Wilson et al. 1990, Wilson et al. 2016). Thus, when present, soil pipes dominated subsurface flow regardless whether from riparian groundwater to the channel or vice-versa. Similarly, Zhou et al. (2014) showed that in heterogeneous river beds, 70% of the total hyporheic exchange occurred across 30% of the channel boundary with the higher K.

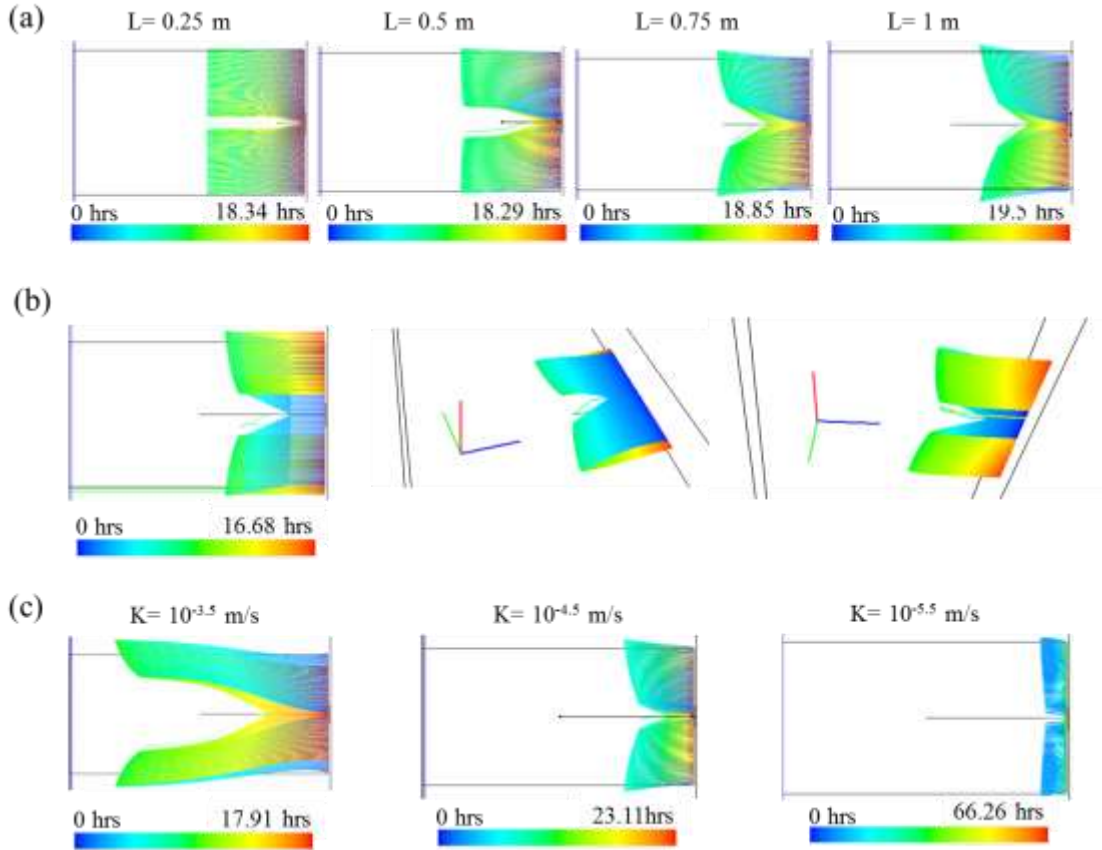


**Figure 2.8:** (a) Plan (2D) view of particle paths with 1 soil pipe of  $L = 0.25, 0.5, 0.75,$  and  $1$  m. (b) Particles paths with 1 soil pipe at  $H=0.3$ ; left is a 2D plan view, middle and right are 3-D views from over and under the model domain, respectively. (c) Plan (2-D) view of particle paths with 1 soil pipe with matrix  $K = 10^{-3.5}, 10^{-4.5},$  and  $10^{-5.5}$  m/s. Stream channel is on right side of all plots, and pathline colors indicate cumulative residence time at that location. Water particles were released 10 minutes into the simulation at the stream channel boundary.

#### 2.4.2 Controls on Soil Pipe Preferential Flow in Streambanks

Our study was able to establish pipe density ( $\rho$ ) and length ( $L$ ) as dominant controls within the parameter ranges we tested. By contrast,  $D$ ,  $H$ , and  $\lambda$  were less important. Here, we examine the process reasons why the relationships in Figures 2.5 and 2.7 have the shapes they do. As pipe length ( $L$ ) increased (Figure 2.5b), all head contours were initially parallel to the channel (Figure 2.6, leftmost), but at greater  $L$  the soil pipe created a high head protrusion into the riparian groundwater (Figure 2.6, right), non-linearly increasing the flux boundary length. Specifically, applying Darcy's Law by taking the line integral of the flow vector field along the length of a head contour (Figure 2.9a) gives

$$Q_{H_2O} = \oint \vec{q} ds = \oint K \vec{\nabla} h ds \quad [2.8]$$

where  $\Gamma$  is the length of the head contour (L). We fit a curve of the form  $y(x) = c_1 + c_2 e^{-c_3 x^2}$  to the particular head contour which intersects the end of the soil pipe away from the channel, where  $x$  is distance from the soil pipe perpendicularly along the channel (L), and  $y$  is the distance of the head contour from the channel margin (L). To obtain  $\Gamma$ , we applied the formula for the length of a curve in the domain of interest  $x = [-0.5 \text{ m}, 0.5 \text{ m}]$ .

$$\Gamma = \int_{-0.5}^{0.5} \sqrt{dy(x)^2 + dx^2} dx \quad [2.9]$$

Evaluating Equation [2.7] along a head contour and assuming constant matrix  $K$ , the non-linear relationship between pipe length and  $\Gamma$  (Figure 2.9b) yields a similarly-shaped non-linear relationship between  $V/V_0$  and  $L$  (Figure 2.5b). At the same time, as the soil pipe and the high head protrusion both lengthened (Figure 2.6), flowpaths were pushed further away from the soil pipe (Figure 2.8a).

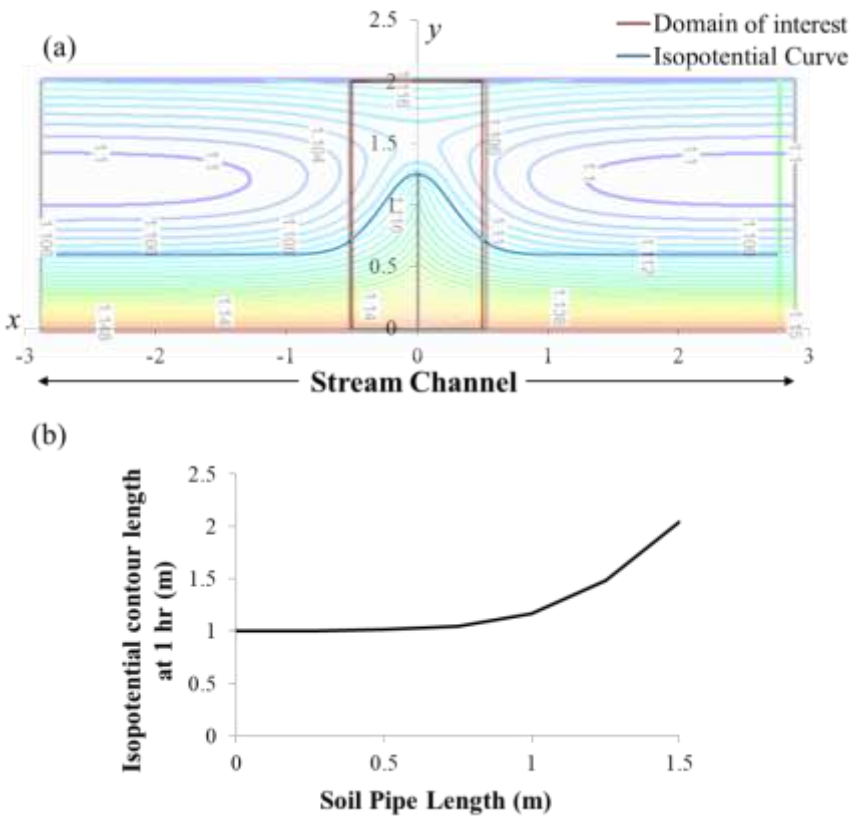


**Figure 2.9:** (a) The high head protrusion created by the insertion of a soil pipe of  $L = 1.25 \text{ m}$ . A curve of the form  $y(x) = c_1 + c_2 e^{-c_3 x^2}$  was fit to the isopotential line which goes through the end of the soil pipe (highlighted in blue). (b) Isopotential contour length ( $\Gamma$ , equation 2.8) vs. soil pipe length (length of blue curve in panel a within the red box).

The nonlinear relationship between hyporheic volume and soil pipe diameter ( $D$ , Figure 2.5c) reflects a shifting balance between flow capacity in the pipe and exchange between pipe

and matrix. The capacity for exchange with the matrix is greater at small pipe diameters, and the capacity for flow within the pipe itself is greater at larger pipe diameters. The reason for this is that matrix flow is governed by head gradient, which does not change with diameter (Figure 2.10). On the other hand, pipe flow capacity per Hagen-Poiseuille or Darcy-Weisbach is partially a function of  $D$ . As  $D$  increases, pipe capacity limitation decreases until  $D = \sim 0.95$  cm, when matrix flow starts to limit. Since this matrix capacity remains relatively the same with diameter, hyporheic volume levels off at higher diameters (Figure 2.5c).

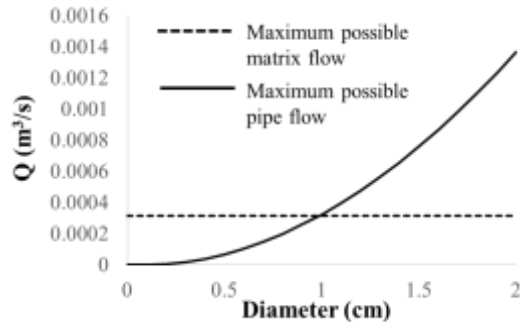


**Figure 2.10. Maximum possible exchange rate between a single pipe ( $L = 1.0$  m) and matrix, and maximum possible pipe flow in a single pipe, vs. pipe diameter at a head gradient of 1 m/m. Compare to Figure 2.5c.**

As height above baseflow ( $H$ ) increased, hyporheic volume decreased (Figure 2.5d) because exchange with the bank increasingly disengaged with the soil pipe. When  $H > 0$ , groundwater flow is initially beneath the soil pipe with particles moving perpendicularly away from the stream channel. Once the soil pipes become filled, the particles are driven away from the soil pipe because the head in the soil pipe is high relative to the surrounding matrix (Figure 2.8b). As channel heads subsequently drop on the falling limb, but are still above the pipe, the particles head straight back to the pipe. Note the maximum residence time in the  $H = +0.3$  m case is 16.68 hr. (Figure 2.8b), whereas the base-case ( $H = -0.5$  m) has a maximum residence time of 19.5 hr. The residence time is shorter for the higher  $H$  because in that case the particles are driven away from the pipes at an angle after the stream rises above the soil pipe and thus do not travel as far from the stream channel, and then the particles travel straight back after the soil pipes are no longer hydraulically active, creating a shorter particle path.

As connectivity ( $\lambda$ ) increased from addition of connector pipes, the number of possible paths the flow could take through the soil pipe network increased exponentially (Figure 2.11). This explains a similarly shaped trend in Figure 2.5e. However, the trend in Figure 2.5e is not as strong as that in Figure 2.11, because the increase in number of possible paths is partially cancelled out by increasing redundancy of those paths. This study only examines connectivity amongst soil pipes that are already connected to the stream bank. We would expect connectivity to play an even bigger role if some of the soil pipes are not connected to the stream bank.

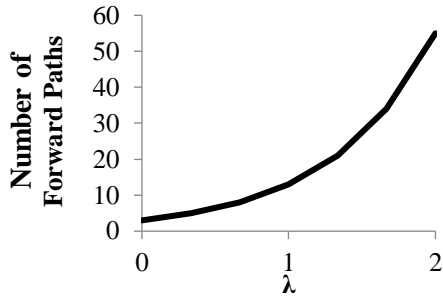


**Figure 2.11: Number of possible flow paths vs.  $\lambda$**

The complex and nonlinear relationship between effect of soil pipe addition and matrix K (Figure 2.7) is likely due to a variety of factors that vary in importance across the range of K values. Overall, an increase with K is intuitive, but specific portions of the curve bear further evaluation. For example, as matrix K increased, the head gradient between channel/soil pipe and riparian groundwater decreased (Figures 2.12a and Figure B11). This likely contributed to the slight decrease in soil pipe's effects on hyporheic volume from  $K=10^{-5}$  m/s to  $K=10^{-4.5}$  m/s (Figure 2.7). Another factor is how long the riparian groundwater spent in losing conditions (Figure 2.12b). At higher matrix K, the head signal propagated fast and the riparian groundwater head remained close to but below the channel stage height for a long time, and at lower K, the riparian groundwater head stayed relatively low, leading to a longer duration that the channel stage height is above the riparian groundwater head. This may also have contributed to the decrease in relative effect of soil pipes from  $K=10^{-5}$  m/s to  $K=10^{-4.5}$  m/s (Figure 2.7). At low K (from  $10^{-7}$  m/s to  $10^{-6.5}$  m/s) and high K (from  $10^{-3.5}$  m/s to  $10^{-3}$  m/s) the proportion of water that flowed through the soil pipes (vs. the matrix) was greater than for intermediate K (Figure 2.12c). Flow through the soil pipes at high matrix K was enhanced because that flow could easily continue on into the matrix given less resistance to flow exiting the soil pipe away from the stream channel. This explains the large effect of adding a soil pipe at high K (i.e.  $10^{-4}$  m/s to  $10^{-3}$  m/s, right side of Figure 2.7), which is mostly added via the soil pipe rather than the matrix (Figure B10).

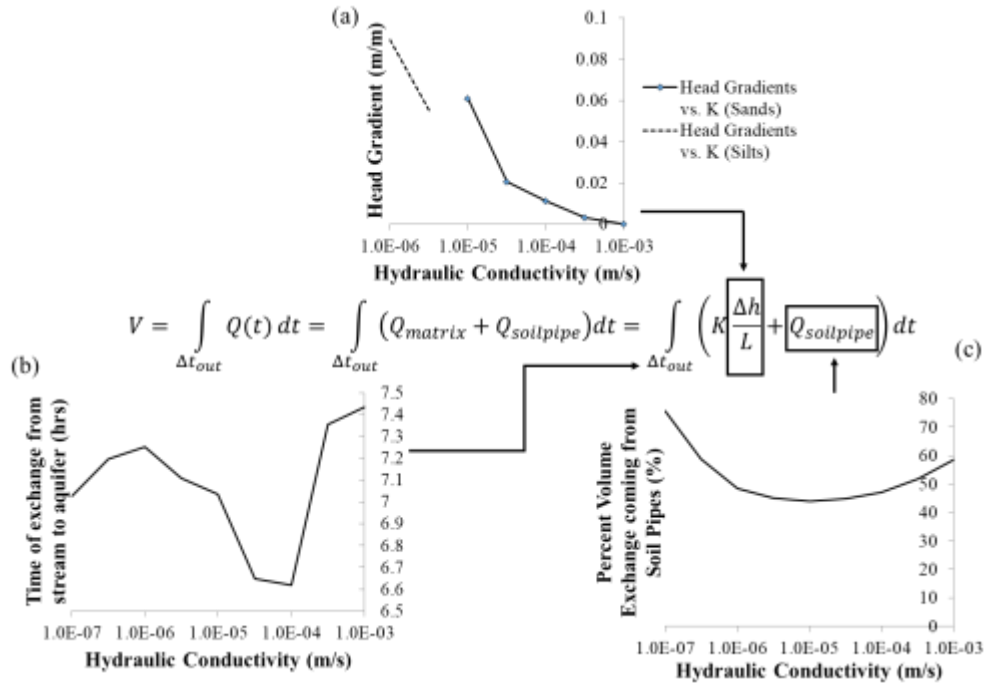


**Figure 2.12: A breakdown of matrix K effects on various controls of hyporheic volume for a single streambank soil pipe ( $L = 1.0$  m,  $D = 2$  cm). (a) The head gradient between the lowest contour line (e.g. 1.14 in Figure B12a and 1.018 in Figure B12b) and the point on the soil pipe closest to the lowest contour line at  $t = 1$  hr. for each K (note there is a discontinuity in head gradient between  $K = 10^{-5}$  m/s and  $K = 10^{-5.5}$  m/s as we have transitioned from sand to silt and the discontinuity in specific yield (Table 2.2) has propagated to head gradient). (b) The duration when water goes from channel to riparian groundwater rather than vice-versa (e.g., the distance between the x-intercepts in Figure 2.4), (c) The percentage of flow that is soil pipe flow (vs. matrix flow). We calculated the percentage by dividing the volume of water which flowed into the riparian groundwater during the simulation via the soil pipe by the entire volume of water exchanged (i.e. the area under the positive part of the curve in Figure 2.4 which included both matrix and pipe flow).**

Particles travel much further in systems of high matrix K (Figure 2.8c), since there is less resistance to flow. In addition to flowing further into the riparian groundwater, the particles also are pushed further away from the soil pipe, as the flow of particles is much more sensitive to changes in the potentiometric surface (Figure 2.8c). Despite the longer flow paths, residence times are still shortest for the highest K. The great distance to which the water particles are driven away from the soil pipe also illustrates how much easier water can flow into the riparian groundwater from the soil pipes at high K, reinforcing what we see in Figure 2.7 and Figure B10 in section B3 of the supporting information— that more water flows through soil pipes at high K and thus adding a soil pipe has a greater impact at high matrix K. In short, high matrix K reduced the resistance that water in the pipe has to exchange with the matrix.

Finally, we note field studies indicate that soil pipes are more abundant in streambanks with low matrix K dominated by silts and clays than they are in high K soils such as coarse sand

and gravel (McEwen and Hester 2019). By itself, this fact would argue that soil pipes will have more effect on overall hyporheic exchange/bank storage at lower matrix K, which calls into question the conventional assumption that hyporheic exchange is always proportional to K with low K streams having very little exchange (Gomez-Velez and Harvey 2014, Hester and Doyle 2008). Nevertheless, this trend may be cancelled out to some extent by the reverse trend in Figure 2.7. The net sum of these effects may play out in complex ways to affect the distribution of hyporheic exchange along stream corridors, a fertile area for future research.

#### *2.4.3 Model Limitations and Future Studies*

There is ample scope to examine the effects of soil pipes on hyporheic volume with more complicated boundary conditions. For example, one might simulate a time-varying hillslope boundary (Schmadel et al. 2016), or incorporate recharge, percolation from the vadose zone, or evapotranspiration. Yet a key barrier to progress is a dearth of field data for validation. Our results matched those from the most relevant field study of which we are aware (Figure 2.2), but more diverse data are needed. There have been attempts to map the spatial layout of soil pipes in many contexts (Allaire et al. 2009, Gormally et al. 2011) and there are many studies on soil pipe effects on flow in hillslope settings (Holden and Burt 2002, Putty and Prasad 2000, Terajima et al. 1996, Wilson et al. 2017, Wilson et al. 1990, Wilson et al. 2016). In riparian zones, there have been some field efforts to characterize the abundance and distribution of soil pipe openings (McEwen and Hester 2019, Menichino et al. 2015), and we are aware of two case field studies on the effects of soil pipes on hyporheic exchange (Menichino and Hester 2015, Menichino et al. 2014). But to our knowledge, no studies have systematically mapped riparian/riverbank soil pipes in multiple streams/rivers and built up a database of statistics around soil pipe geometry that would be needed for more realistic modeling.

We were not able to calculate meaningful residence time distributions because MODPATH does not simulate particle movement in conduits. Yet a sizeable amount of the flow coming from the channel enters the soil pipe (~40-70%, Figure 2.12c). There may also be particles which start out in the pipe and enter the soil matrix further into the riparian groundwater, and vice versa. Future work could modify MODPATH to track particles through conduits. In addition, MT3D-USGS (Bedekar et al. 2016) could be modified to run with the CFP package to extend this work to water quality simulation.

#### *2.4.4 Practical Application*

Hyporheic exchange benefits stream ecology by providing oxygen and other nutrients to organisms burrowed in the hyporheic zone. It also improves water quality by physicochemical processes occurring in the bank where contaminants such as excess nitrate are consumed by microbes in the bank and/or sorbed onto the soil matrix. The simple addition of five short soil pipes ( $L = 1$  m,  $D = 1.5$  cm) increased hyporheic exchange volume 135% for a 10-hour peak flow event, and just one long soil pipe ( $L = 1.5$  m,  $D = 1.5$  cm) increased hyporheic volume 73.4%. In the Chesapeake Bay Region, significantly more restoration credits (Berg et al. 2014) could be given for locations with more or longer pipes, but future studies would need to confirm

the translation of enhanced hyporheic exchange modeled here to enhanced removal of excess nutrients travelling down the channel. Strategies for creating soil pipes (e.g., auguring) could also be explored. Whether naturally or artificially created, pipe morphology and therefore nutrient effects may change over time, which bears further study. Perhaps more importantly, the results of our study show that when monitoring water quality and hydraulic data in the floodplain, one should consider whether or not monitoring wells are near soil pipes, since the hydraulic behavior of the system near soil pipes is fundamentally different from the matrix (Figure 2.8), with possibility for misinterpretation.

## 2.5. Conclusions

Our results suggest that soil pipes have a significant impact on transient hyporheic exchange volume (bank storage) during a high channel flow event as the addition of five soil pipes per m to a system more than doubled (135% increase) hyporheic volume. The soil pipe parameter that had by far the most impact on hyporheic volume was length, as adding just one soil pipe of 1.5 m caused a 73.4% increase in hyporheic volume. This happened because the soil pipe creates a high head protrusion into riparian groundwater, which increases the effective length of the boundary condition exponentially as the length of the soil pipe is increased. In lower K soils, soil pipes have the most profound impact in silty soils ( $K \sim 10^{-5.5}$  m/s), but do not have very much impact for more impermeable soils ( $K \sim 10^{-7}$  m/s). Soil pipes have the most impact in coarse sand and fine gravel ( $K \sim 10^{-3.5}$ - $10^{-3}$  m/s) although they are less likely to form there due to reduced soil cohesion. The effect of soil pipe diameter on hyporheic volume leveled off at  $D \sim 1$  cm as the system switched from pipe flow limited to exchange-flow limited, which stays constant with diameter. The high head propagating along soil pipes drives flow into the riparian groundwater under losing conditions, causing the particles to take a longer tortuous path. The exception is when the soil pipe is positioned significantly above base flow water levels in the channel, where the maximum residence times were actually shorter. This study has gained significant insight about how soil pipe parameters affect the hydraulics of the hyporheic zone during a peak flow event with implications for river management and monitoring.

## Acknowledgements

We thank the National Science Foundation under award #1446481 for support to W. Lotts and E. Hester. The opinions expressed are those of the authors and not necessarily those of the NSF. Data are published in HydroShare at <https://doi.org/10.4211/hs.fbf812c4d72d4a89b941645ffb69df75> .

## References

Allaire, S.E., Roulier, S. and Cessna, A.J. (2009) Quantifying preferential flow in soils: A review of different techniques. *Journal of Hydrology* 378(1-2), 179-204.

- Allen, D.C. and Vaughn, C.C. (2009) Burrowing behavior of freshwater mussels in experimentally manipulated communities. *Journal of the North American Benthological Society* 28(1), 93-100.
- Anderson, M.P., Woessner, W.W. and Hunt, R.J. (2015) *Applied Groundwater Modeling: Simulation of Flow and Advective Transport*. Second Edition. Academic Press: Elsevier Inc.
- Anderson, W.P., Storniolo, R.E. and Rice, J.S. (2011) Bank thermal storage as a sink of temperature surges in urbanized streams. *Journal of Hydrology* 409(1-2), 525-537.
- Aubertin, G.M. (1971) Nature and extent of macropores in forest soils and their influence on subsurface water movement. Res. Pap. NE-192. Upper Darby, PA: U.S. Department of Agriculture, Forest Service, Northeastern Forest Experiment Station. 33 p.
- Bear, J. (1972) *Dynamics of fluids in porous media*, Dover Publications, Inc., New York, NY.
- Beasley, R.S. (1976) Contribution of subsurface flow from the upper slopes of forested watersheds to channel flow. *Soil Science Society of America Journal* 40, 955-957.
- Bedekar, V., Morway, E.D., Langevin, C.D. and Tonkin, M. (2016) MT3D-USGS version 1: A U.S. Geological Survey release of MT3DMS updated with new and expanded transport capabilities for use with MODFLOW. U.S. Geological Survey Techniques and Methods 6-A53, 69p.
- Bell, A.H., Coles, J.F., McMahon, G. and Woodside, M.D. (2012) Urban development results in stressors that degrade stream ecosystems. U.S. Geological Survey.
- Berg, J., Burch, J., Cappuccitti, D., Filoso, S., Fraley-McNeal, L., Goerman, D., Hardman, N., Kaushal, S., Medina, D. and Meyers, M. (2014) Recommendations of the Expert Panel to Define Removal Rates for Individual Stream Restoration Projects. Chesapeake Bay Program.
- Bernatek-Jakiel, A. and Poesen, J. (2018) Subsurface erosion by soil piping: significance and research needs. *Earth-Science Reviews* 185, 1107-1128.
- Bernatek-Jakiel, A., Vannoppen, W. and Poesen, J. (2017) Assessment of grass root effects on soil piping in sandy soils using the pinhole test. *Geomorphology* 295, 563-571.
- Beven, K. and Germann, P. (1982) Macropores and water-flow in soils. *Water Resources Research* 18(5), 1311-1325.
- Beven, K. and Germann, P. (2013) Macropores and water flow in soils revisited. *Water Resources Research* 49(6), 3071-3092.
- Blackwell, P.S. (2000) Management of water repellency in Australia, and risks associated with preferential flow, pesticide concentration and leaching. *Journal of Hydrology* 231, 384-395.
- Briggs, M.A., Hare, D.K., Boutt, D.F., Davenport, G. and Lane, J.W. (2016) Thermal infrared video details multiscale groundwater discharge to surface water through macropores and peat pipes. *Hydrological Processes* 30(14), 2510-2511.
- Brown, T.T. and Brown, S. (2011) *Pocketguide to eastern streams* 1st edition. Stackpole Books, Mechanicsburg Pennsylvania.
- Brunke, M. and Gonser, T. (1997) The ecological significance of exchange processes between rivers and groundwater. *Freshwater Biology* 37(1), 1-33.
- Bryan, R.B. and Jones, J.A.A. (1997) The significance of soil piping processes: inventory and prospect. *Geomorphology* 20(3-4), 209-218.

- Caldwell, R.R. and Eddy-Miller, C.A. (2013) Groundwater and surface-water interaction within the upper Smith River Watershed, Montana 2006-2010. U.S. Geological Survey Scientific Investigations Report 2013-5051, 1-88.
- Cardenas, M.B., Wilson, J.L. and Zlotnik, V.A. (2004) Impact of heterogeneity, bed forms, and stream curvature on subchannel hyporheic exchange. *Water Resources Research* 40(8), W08307.
- Climent, M.J., Herrero-Hernández, E., Sánchez-Martín, M.J., Rodríguez-Cruz, M.S., Pedreros, P. and Urrutia, R. (2019) Residues of pesticides and some metabolites in dissolved and particulate phase in surface stream water of Cachapoal River basin, central Chile. *Environmental Pollution* 251, 90-101.
- Coles, J.F. and Geological Survey (U.S.) (2012) Effects of urban development on stream ecosystems in nine metropolitan study areas across the United States, U.S. Geological Survey, Reston, Va.
- Connolly, N.M., Pearson, R.G., Loong, D., Maughan, M. and Brodie, J. (2015) Water quality variation along streams with similar agricultural development but contrasting riparian vegetation. *Agriculture Ecosystems & Environment* 213, 11-20.
- Crosbie, R.S., Doble, R.C., Turnadge, C. and Taylor, A.R. (2019) Constraining the Magnitude and Uncertainty of Specific Yield for Use in the Water Table Fluctuation Method of Estimating Recharge. *Water Resources Research* 55, 7343-7361.
- Cummins, K.W. and Klug, M.J. (1979) Feeding Ecology of Stream Invertebrates. *Annual Review of Ecology and Systematics* 10, 147-172.
- Darnault, C.J.G., Garnier, P., Kim, Y.J., Oveson, K.L., Steenhuis, T.S., Parlange, J.Y., Jenkins, M., Ghiorse, W.C. and Baveye, P. (2003) Preferential transport of *Cryptosporidium parvum* oocysts in variably saturated subsurface environments. *Water Environment Research* 75(2), 113-120.
- DiStefano, R.J., Magoulick, D.D., Imhoff, E.M. and Larson, E.R. (2009) Imperiled crayfishes use hyporheic zone during seasonal drying of an intermittent stream. *Journal of the North American Benthological Society* 28(1), 142-152.
- Du, X.Z., Shrestha, N.K. and Wang, J.Y. (2019) Assessing climate change impacts on stream temperature in the Athabasca River Basin using SWAT equilibrium temperature model and its potential impacts on stream ecosystem. *Science of the Total Environment* 650, 1872-1881.
- Elder, J.F., Flagg, S.D. and Matraw Jr., H.C. (1988) Hydrology and Ecology of the Apalachicola River, Florida: A Summary of the River Quality Assessment. U.S. Geological Survey Water-Supply Paper 2196-D, D1-D46.
- Fitts, C.R. (2012) *Groundwater Science*, Second Edition. 57.
- Fleckenstein, J.H., Niswonger, R.G. and Fogg, G.E. (2006) River-aquifer interactions, geologic heterogeneity, and low-flow management. *Ground Water* 44(6), 837-852.
- Fox, G.A. and Durnford, D.S. (2003) Unsaturated hyporheic zone flow in stream/aquifer conjunctive systems. *Advances in Water Resources* 26(9), 989-1000.
- Fox, G.A., Heeren, D.M., Miller, R.B., Mittelstet, A.R. and Storm, D.E. (2011) Flow and transport experiments for a streambank seep originating from a preferential flow pathway. *Journal of Hydrology* 403(3-4), 360-366.
- Francis, B.A., Francis, L.K. and Cardenas, M.B. (2010) Water table dynamics and groundwater-surface water interaction during filling and draining of a large fluvial island due to dam-induced river stage fluctuations. *Water Resources Research* 46.

- Freeze, R.A. and Cherry, J.A. (1979) Groundwater, Prentice-Hall, Inc, Englewood Cliffs, NJ.
- Gaiser, R.N. (1952) Root channels and roots in forest soils. *Soil Science Society of America Journal* 16, 62-65.
- Gallegos, J.J., Hu, B.X. and Davis, H. (2013) Simulating flow in karst aquifers at laboratory and sub-regional scales using MODFLOW-CFP. *Hydrogeology Journal* 21(8), 1749-1760.
- Gerecht, K.E., Cardenas, M.B., Guswa, A.J., Sawyer, A.H., Nowinski, J.D. and Swanson, T.E. (2011) Dynamics of hyporheic flow and heat transport across a bed-to-bank continuum in a large regulated river. *Water Resources Research* 47.
- Gomez-Velez, J. and Harvey, J.W. (2014) A hydrogeomorphic river network model predicts where and why hyporheic exchange is important in large basins. *Geophysical Research Letters* 41(18), 6403-6412.
- Gormally, K.H., McIntosh, M.S., Mucciardi, A.N. and McCarty, G.W. (2011) Ground-Penetrating Radar Detection and Three-Dimensional Mapping of Lateral Macropores: II. Riparian Application. *Soil Science Society of America Journal* 75(4), 1236-1243.
- Gu, C.H., Anderson, W. and Maggi, F. (2012) Riparian biogeochemical hot moments induced by stream fluctuations. *Water Resources Research* 48.
- Harbaugh, A.W. (2005) MODFLOW-2005, the U.S. Geological Survey modular ground-water model -- the Ground-Water Flow Process: U.S. Geological Survey Techniques and Methods 6-A16. U.S. Geological Survey, Reston, VA.
- Harvey, J.W. and Wagner, B.J. (2000) Streams and ground waters. Jones, J.B. and Mulholland, P.J. (eds), pp. 3-44, Academic Press, San Diego, CA.
- Hassett, B.A., Sudduth, E.B., Somers, K.A., Urban, D.L., Violin, C.R., Wang, S.Y., Wright, J.P., Cory, R.M. and Bernhardt, E.S. (2018) Pulling apart the urbanization axis: patterns of physiochemical degradation and biological response across stream ecosystems. *Freshwater Science* 37(3), 653-672.
- Hedeff, I.E. and Caldwell, R.R. (2017) Evaluating the impact of irrigation on surface water - groundwater interaction and stream temperature in an agricultural watershed. *Science of the Total Environment* 599-600, 581-596.
- Heeren, D.M., Miller, R.B., Fox, G.A., Storm, D.E., Halihan, T. and Penn, C.J. (2010) Preferential flow effects on subsurface contaminant transport in alluvial floodplains. *Transactions of the ASABE* 53(1), 127-136.
- Hester, E.T. and Doyle, M.W. (2008) In-stream geomorphic structures as drivers of hyporheic exchange. *Water Resources Research* 44(3), W03417.
- Hester, E.T. and Gooseff, M.N. (2010) Moving Beyond the Banks: Hyporheic Restoration Is Fundamental to Restoring Ecological Services and Functions of Streams. *Environmental Science & Technology* 44(5), 1521-1525.
- Hester, E.T., Young, K.I. and Widdowson, M.A. (2014) Controls on mixing-dependent denitrification in hyporheic zones induced by riverbed dunes: A steady state modeling study. *Water Resources Research* 50(11), 9048-9066.
- Hillel, D. (1987) Unstable Flow in Layered Soils - a Review. *Hydrological Processes* 1(2), 143-147.
- Holden, J. and Burt, T.P. (2002) Piping and pipeflow in a deep peat catchment. *Catena* 48(3), 163-199.
- Huet, M. (1959) Profiles and biology of Western European streams as related to fish management. . *Transactions of the American Fisheries Society* 88, 155-163.

- Huggenberger, P., Hoehn, E., Beschta, R. and Woessner, W. (1998) Abiotic aspects of channels and floodplains in riparian ecology. *Freshwater Biology* 40(3), 407-425.
- Jarvis, N., Larsbo, M. and Koestel, J. (2017) Connectivity and percolation of structural pore networks in a cultivated silt loam soil quantified by X-ray tomography. *Geoderma* 287, 71-79.
- Jarvis, N.J. (2007) A review of non-equilibrium water flow and solute transport in soil macropores: principles, controlling factors and consequences for water quality. *European Journal of Soil Science* 58(3), 523-546.
- Jones, C.S., C.W., D., Hruby, C.E., Schilling, K.E. and Wolter, C.F. (2018) Livestock manure driving stream nitrate. *AMBIO- A Journal of the Human Environment*.
- Jones, J.A.A. (1988) Modelling pipeflow contributions to stream runoff. *Hydrological Processes* 2, 1-17.
- Jones, J.A.A. (2010) Soil piping and catchment response. *Hydrological Processes* 24(12), 1548-1566.
- Jones, J.A.A. and Cottrell, C.I. (2007) Long-term changes in stream bank soil pipes and the effects of afforestation. *Journal of Geophysical Research-Earth Surface* 112(F1).
- Jones, J.A.A. and Crane, F.G. (1984) Pipeflow and pipe erosion in the Maesnant experimental catchment. *Geobooks (Catchment Experiments in Fluvial Geomorphology)*, 55-72.
- Jung, M., Burt, T.P. and Bates, P.D. (2004) Toward a conceptual model of floodplain water table response. *Water Resources Research* 40(12).
- Kalbus, E., Schmidt, C., Molson, J.W., Reinstorf, F. and Schirmer, M. (2009) Influence of aquifer and streambed heterogeneity on the distribution of groundwater discharge. *Hydrology and Earth System Sciences* 13(1), 69-77.
- Karay, G. and Hajnal, G. (2015) Modelling of groundwater flow in fractured rocks. 7th Groundwater Symposium of the International Association for Hydro-Environment Engineering and Research (Iahr), 142-149.
- King, G.D., Chapman, J.M., Cooke, S.J. and Suski, C.D. (2016) Stress in the neighborhood: Tissue glucocorticoids relative to stream quality for five species of fish. *Science of the Total Environment* 547, 87-94.
- Kladivko, E.J., Brown, L.C. and Baker, J.L. (2001) Pesticide transport to subsurface tile drains in humid regions of North America. *Critical Reviews in Environmental Science and Technology* 31(1), 1-62.
- Knillmann, S., Orlinskiy, P., Kaske, O., Foit, K. and Liess, M. (2018) Indication of pesticide effects and recolonization in streams. *Science of the Total Environment* 630, 1619-1627.
- Larsbo, M., Koestel, J. and Jarvis, N. (2014) Relations between macropore network characteristics and the degree of preferential solute transport. *Hydrology and Earth System Sciences* 18(12), 5255-5269.
- Laube, G., Schmidt, C. and Fleckenstein, J.H. (2018) The systematic effect of streambed conductivity heterogeneity on hyporheic flux and residence time. *Advances in Water Resources* 122, 60-69.
- Lautz, L. and Seigel, D.I. (2005) Modeling surface and groundwater in the hyporheic zone using MODFLOW and MT3D. *Advances in Water Resources* 29, 1618-1633.
- Lehmann, P., Hinz, C., McGrath, G., Tromp-van Meerveld, H.J. and McDonnell, J.J. (2007) Rainfall threshold for hillslope outflow: an emergent property of flow pathway connectivity. *Hydrology and Earth System Sciences* 11(2), 1047-1063.

- Liao, H.H., Sarver, E. and Krometis, L.A.H. (2018) Interactive effects of water quality, physical habitat, and watershed anthropogenic activities on stream ecosystem health. *Water Research* 130, 69-78.
- Lin, Y.C. and Medina, M.A. (2003) Incorporating transient storage in conjunctive stream-aquifer modeling. *Advances in Water Resources* 26(9), 1001-1019.
- Loheide, S.P. and Lundquist, J.D. (2009) Snowmelt-induced diel fluxes through the hyporheic zone. *Water Resources Research* 45, W07404.
- Lundquist, J.D. and Cayan, D.R. (2002) Seasonal and spatial patterns in diurnal cycles in streamflow in the western United States. *Journal of Hydrometeorology* 3(5), 591-603.
- Luo, L.F., Lin, H. and Li, S.C. (2010) Quantification of 3-D soil macropore networks in different soil types and land uses using computed tomography. *Journal of Hydrology* 393(1-2), 53-64.
- McEwen, A.M. and Hester, E.T. (2019) Abundance, distribution, and geometry of naturally occurring macropores and soil pipes in stream banks. *Freshwater Science*, In review.
- Meghdadi, A. and Javar, N. (2018) Evaluation of nitrate sources and the percent contribution of bacterial denitrification in hyporheic zone using isotope fractionation technique and multi-linear regression analysis. *Journal of Environmental Management* 222, 54-65.
- Menichino, G.T. and Hester, E.T. (2015) The Effect of Macropores on Bi-Directional Hydrologic Exchange between a Stream Channel and Riparian Groundwater. *Journal of Hydrology* 529(3), 830-842.
- Menichino, G.T., Scott, D.T. and Hester, E.T. (2015) Abundance and dimensions of naturally occurring macropores along stream channels and the effects of artificially constructed large macropores on transient storage. *Freshwater Science* 34(1), 125–138.
- Menichino, G.T., Ward, A.S. and Hester, E.T. (2014) Macropores as preferential flow paths in meander bends. *Hydrological Processes* 28(3), 482-495.
- Meyer, J.L. and Edwards, R.T. (1990) Ecosystem Metabolism and Turnover of Organic-Carbon Along a Blackwater River Continuum. *Ecology* 71(2), 668-677.
- Molina-Navarro, E., Andersen, H.E., Nielsen, A., Thodsen, H. and Trolle, D. (2018) Quantifying the combined effects of land use and climate changes on stream flow and nutrient loads: A modelling approach in the Odense Fjord catchment (Denmark). *Science of the Total Environment* 621, 253-264.
- Morales, V.L., Parlange, J.Y. and Steenhuis, T.S. (2010) Are preferential flow paths perpetuated by microbial activity in the soil matrix? A review. *Journal of Hydrology* 393(1-2), 29-36.
- Morris, D.A. and Johnson, A.I. (1967) Summary of hydrologic and physical properties of rock and soil Materials, as analyzed by the hydrologic laboratory of the U.S. Geological Survey 1948-60. Geological Survey Water Supply Paper 1839-D. United States Government Printing Office, Washington.
- Mosley, M.P. (1979) Streamflow generation in a forested watershed, New Zealand. *Water Resources Research* 15, 795-806.
- Mosley, M.P. (1982) Subsurface Flow Velocities through Selected Forest Soils, South Island, New-Zealand. *Journal of Hydrology* 55(1-4), 65-92.
- Newman, A. and Keim, R. (2013) Mesoscale connectivity through a natural levee. *Hydrology and Earth System Sciences* 17, 691-704.
- Nieber, J.L. and Sidle, R.C. (2010) How do disconnected macropores in sloping soils facilitate preferential flow? *Hydrological Processes* 24(12), 1582-1594.

- O'Driscoll, M., Clinton, S., Jefferson, A., Manda, A. and McMillan, S.K. (2010) Urbanization effects on watershed hydrology and in-stream processes in the southern United States. *Water* 2, 605-648.
- Pales, A.R., Li, B.T., Clifford, H.M., Kupis, S., Edayilam, N., Montgomery, D., Liang, W.Z., Dogan, M., Tharayil, N., Martinez, N., Moysey, S., Powell, B. and Darnault, C.J.G. (2018) Preferential flow systems amended with biogeochemical components: imaging of a two-dimensional study. *Hydrology and Earth System Sciences* 22(4), 2487-2509.
- Pescimoro, E., Boano, F., Sawyer, A.H. and Soltanian, M.R. (2019) Modeling Influence of Sediment Heterogeneity on Nutrient Cycling. *Water Resources Research*.
- Pinder, G.F. and Sauer, S.P. (1971) Numerical simulation of flood wave modification due to bank storage effects. *Water Resources Research* 7(1), 63-70.
- Pollock, D.W. (2012) User Guide for MODPATH Version 6 -- A Particle-Tracking Model for MODFLOW. U.S. Geological Survey Survey Techniques and Methods 6-A41, 58 p.
- Pryshlak, T.T., Sawyer, A.H., Stonedahl, S.H. and Soltanian, M.R. (2015) Multiscale hyporheic exchange through strongly heterogeneous sediments. *Water Resources Research* 51(11), 9127-9140.
- Putty, M.R.Y. and Prasad, R. (2000) Runoff processes in headwater catchments - an experimental study in Western Ghats, South India. *Journal of Hydrology* 235(1-2), 63-71.
- Quaglietta, L., Pauperio, J., Martins, F.M.S., Alves, P.C. and Beja, P. (2018) Recent range contractions in the globally threatened Pyrenean desman highlight the importance of stream headwater refugia. *Animal Conservation* 21(6), 515-525.
- Rezanezhad, F., Vogel, H.J. and Roth, K. (2006) Experimental study of fingered flow through initially dry sand. *Hydrology and Earth System Sciences* 3, 2595-2620.
- Richter, D.D. and Mobley, M.L. (2009) Monitoring Earth's Critical Zone. *Science* 326(5956), 1067-1068.
- Rizzi, C., Finizio, A., Maggi, V. and Villa, S. (2019) Spatial-temporal analysis and risk characterisation of pesticides in Alpine glacial streams. *Environmental Pollution* 248, 659-666.
- Saller, S.P., Ronayne, M.J. and Long, A.J. (2013) Comparison of a karst groundwater model with and without discrete conduit flow. *Hydrogeology Journal* 21(7), 1555-1566.
- Sawyer, A.H., Cardenas, M.B., Bomar, A. and Mackey, M. (2009) Impact of dam operations on hyporheic exchange in the riparian zone of a regulated river. *Hydrological Processes* 23(15), 2129-2137.
- Schmadel, N.M., Ward, A.S., Lowry, C.S. and Malzone, J.M. (2016) Hyporheic exchange controlled by dynamic hydrologic boundary conditions. *Geophysical Research Letters* 43(9), 4408-4417.
- Selker, J.S., Steenhuis, T.S. and Parlange, J.Y. (1996) An engineering approach to fingered vadose pollutant transport. *Geoderma* 70(2-4), 197-206.
- Shields, S.J. and Kelly, J.F. (1997) Nest-site selection by belted kingfishers. (*Ceryle alcyon*) in Colorado. *American Midland Naturalist* 137, 401-403.
- Shoemaker, W.B., Kuniandy, E.L., Birk, S., Bauer, S. and Swain, E.D. (2007) Documentation of a Conduit Flow Process (CFP) for MODFLOW-2005. U.S. Geological Survey Techniques and Methods Book 6, Chapter A24, 50p.
- Sidle, R.C., Noguchi, S., Tsuboyama, Y. and Laursen, K. (2001) A conceptual model of preferential flow systems in forested hillslopes: evidence of self-organization. *Hydrological Processes* 15(10), 1675-1692.

- Šimůnek, J., Jarvis, N.J., van Genuchten, M.T. and Gardenas, A. (2003) Review and comparison of models for describing non-equilibrium and preferential flow and transport in the vadose zone. *Journal of Hydrology* 272(1-4), 14-35.
- Smock, L.A., Gladden, J.E., Riekenberg, J.L., Smith, L.C. and Black, C.R. (1992) Lotic Macroinvertebrate Production in 3 Dimensions - Channel Surface, Hyporheic, and Floodplain Environments. *Ecology* 73(3), 876-886.
- Stahl, M.O., Tarek, M.H., Yeo, D.C.J., Badruzzaman, A.B.M. and Harvey, C.F. (2014) Crab burrows as conduits for groundwater-surface water exchange in Bangladesh. *Geophysical Research Letters* 41(23), 8342-8347.
- Stanford, J.A. and Ward, J.V. (1993) AN ECOSYSTEM PERSPECTIVE OF ALLUVIAL RIVERS - CONNECTIVITY AND THE HYPORHEIC CORRIDOR. *Journal of the North American Benthological Society* 12(1), 48-60.
- Stehle, S. and Schulz, R. (2015) Agricultural insecticides threaten surface waters at the global scale. *Proceedings of the National Academy of Sciences of the United States of America* 112(18), 5750-5755.
- Tang, K.H.D. (2019) Climate change in Malaysia: Trends, contributors, impacts, mitigation and adaptations. *Science of the Total Environment* 650, 1858-1871.
- Terajima, T., Sakamoto, T., Nakai, Y. and Kitamura, K. (1996) Pipe flow significance on subsurface flow from the valley head of a small watershed. *J. Jpn. For. Soc.* 78, 20-28.
- Thoms, M.C. (2003) Floodplain-river ecosystems: lateral connections and the implications of human interference. *Geomorphology* 56(3-4), 335-349.
- Triska, F.J., Kennedy, V.C., Avanzino, R.J., Zellweger, G.W. and Bencala, K.E. (1989) Retention and Transport of Nutrients in a 3rd-Order Stream in Northwestern California - Hyporheic Processes. *Ecology* 70(6), 1893-1905.
- Troch, P.A., Carrillo, G.A., Heidbuchel, I., Rajagopal, S., Switanek, M., Volkmann, T.H.M. and Yaeger, M. (2009) Dealing with Landscape Heterogeneity in Watershed Hydrology: A Review of Recent Progress toward New Hydrological Theory. *Geography Compass* 3(1), 375-392.
- Uchida, T., Kosugi, K. and Mizuyama, T. (2001) Effects of pipeflow on hydrological process and its relation to landslide: a review of pipeflow studies in forested headwater catchments. *Hydrological Processes* 15(11), 2151-2174.
- Villholth, K.G., Jarvis, N.J., Jacobsen, O.H. and de Jonge, H. (2000) Field investigations and modeling of particle-facilitated pesticide transport in macroporous soil. *Journal of Environmental Quality* 29(4), 1298-1309.
- Vogel, H.J. and Kretzschmar, A. (1996) Topological characterization of pore space in soil - Sample preparation and digital image-processing. *Geoderma* 73(1-2), 23-38.
- Vorosmarty, C.J., McIntyre, P.B., Gessner, M.O., Dudgeon, D., Prusevich, A., Green, P., Glidden, S., Bunn, S.E., Sullivan, C.A., Liermann, C.R. and Davies, P.M. (2010) Global threats to human water security and river biodiversity. *Nature* 467(7315), 555-561.
- Waite, I.R., National Water-Quality Assessment Program (U.S.) and Geological Survey (U.S.) (2008) Effects of urbanization on stream ecosystems in the Willamette River basin and surrounding area, Oregon and Washington, U.S. Dept. of the Interior, U.S. Geological Survey, Reston, Va.
- White, S.A., Santos, I.R. and Hessey, S. (2018) Nitrate loads in sub-tropical headwater streams driven by intensive horticulture. *Environmental Pollution* 243, 1036-1046.

- Williams, D.D. and Hynes, H.B.N. (1974) Occurrence of benthos deep in substratum of a stream. *Freshwater Biology* 4(3), 233-255.
- Williams, D.D., Williams, N.E. and Hynes, H.B.N. (1974) Observations on the life history and burrow construction of the crayfish *Cambarus fodiens* (Cottle) in a temporary stream in southern Ontario. *Canadian Journal of Zoology* 52, 365-370.
- Wilson, G., Nieber, J.L., Fox, G.A., Dabney, S.M., Ursic, M. and Rigby, J.R. (2017) Hydrologic connectivity and threshold behavior of hillslopes with fragipans and soil pipe networks. *Hydrological Processes* 31(13), 2477-2496.
- Wilson, G.V., Jardine, P.M., Luxmoore, R.J. and Jones, J.R. (1990) HYDROLOGY OF A FORESTED HILLSLOPE DURING STORM EVENTS. *Geoderma* 46(1-3), 119-138.
- Wilson, G.V., Nieber, J.L., Sidle, R.C. and Fox, G.A. (2013) INTERNAL EROSION DURING SOIL PIPEFLOW: STATE OF THE SCIENCE FOR EXPERIMENTAL AND NUMERICAL ANALYSIS. *Transactions of the Asabe* 56(2), 465-478.
- Wilson, G.V., Rigby, J.R., Ursic, M. and Dabney, S.M. (2016) Soil pipe flow tracer experiments: 1. Connectivity and transport characteristics. *Hydrological Processes* 30(8), 1265-1279.
- Winston, R.B. (2014) Modifications made to ModelMuse to add support for the Saturated-Unsaturated Transport model (SUTRA):. U.S. Geological Survey Techniques and Methods book 6, A49, 6 p. .
- Winter, T.C. (1999) Relation of streams, lakes, and wetlands to groundwater flow systems. *Hydrogeology Journal* 7(1), 28-45.
- Winter, T.C., Harvey, J.W., Franke, O.L. and Alley, W.M. (1998) Ground Water and Surface Water, A Single Resource, Circular 1139., U.S. Geological Survey, Denver, CO.
- Wright, D.H., Lomeli, H., Hofmann, P.S. and Nguyen, C. (2011) Burrow occupancy and nesting phenology of bank swallows along the Sacramento River. *California Fish and Game* 97, 138-147.
- Xu, Z., Hu, B.X., Davis, H. and Kish, S. (2015) Numerical study of groundwater flow cycling controlled by seawater/freshwater interaction in a coastal karst aquifer through conduit network using CFPv2. *Journal of Contaminant Hydrology* 182, 131-145.
- Zarnetske, J.P., Haggerty, R., Wondzell, S.M., Bokil, V.A. and Gonzalez-Pinzon, R. (2012) Coupled transport and reaction kinetics control the nitrate source-sink function of hyporheic zones (vol 48, W11508, 2012). *Water Resources Research* 48.
- Zhou, Y., Wilson, G.V., Fox, G.A., Rigby, J.R. and Dabney, S.M. (2016) Soil pipe flow tracer experiments: 2. Application of a streamflow transient storage zone model. *Hydrological Processes* 30(8), 1280-1291.
- Zhou, Y.Q., Ritzi, R.W., Soltanian, M.R. and Dominic, D.F. (2014) The Influence of Streambed Heterogeneity on Hyporheic Flow in Gravelly Rivers. *Groundwater* 52(2), 206-216.

### **CHAPTER 3: Pipe dreams: the effects of stream bank soil pipes on hyporheic denitrification caused by a peak flow event**

Status: published in *Water Resources Research* on March 21, 2022. reprinted here with permission from Wiley ©2022. American Geophysical Union. All Rights Reserved.

Lotts, W. S., & Hester, E. T. (2022). Pipe dreams: The effects of stream bank soil pipes on hyporheic denitrification caused by a peak flow event. *Water Resources Research*, 58, e2021WR030312. <https://doi.org/10.1029/2021WR030312>.

**Authors:** W. Seth Lotts<sup>1</sup>, Erich T. Hester<sup>1</sup>

<sup>1</sup>Department of Civil and Environmental Engineering, Virginia Tech, Blacksburg, Virginia 24061 USA

**Corresponding Author:** Erich T. Hester, [ehester@vt.edu](mailto:ehester@vt.edu)

#### **Key Points:**

- Soil pipe effects on denitrification in riparian groundwater were modeled during hyporheic exchange induced by a peak flow event
- Denitrification was mostly transport limited, with exceptions including coarse soils and soil pipes above initial channel stage
- Adding a single 1.5-meter soil pipe increased riparian denitrification by 76%

#### **Key words:**

- Hyporheic Zone
- Preferential Flow
- Floodplains
- Riparian Zone

#### **Abstract:**

Peak flow events in gaining stream/river channels cause lung model hyporheic exchange with the banks (bank storage), which fosters beneficial reactions as polluted channel water cycles through riparian groundwater. Soil pipes are common along stream/riverbanks, and enhance exchange, yet their effect on reactions such as denitrification is unknown. We used MODFLOW with the Conduit Flow Package to simulate lung model exchange during a peak flow event in a section of streambank/riparian soil with soil pipes, and MT3D-USGS to estimate nitrate transport and denitrification. We varied soil matrix hydraulic conductivity (K) and first-order reaction constant (k), as well as soil pipe density, length, and height above the initial channel water surface elevation (H). The addition of soil pipes enhanced streambank (riparian) denitrification

relative to banks without pipes, for example a 76% increase due to adding a single 1.5-m pipe. Denitrification increased linearly with pipe density but exhibited non-linear trends with other parameters. Sensitivity analysis revealed length and density to be most influential. Soil pipe enhancement of denitrification was governed by hyporheic volume in most cases in our study. Exceptions included 1) coarse soil ( $K=10^{-3}$  m/s) and 2) low  $k$  and  $H>0$ . Scaling our results to the stream corridor scale estimated that five soil pipes per m cumulatively induced 3% nitrate removal along a 1-km reach. Overall, soil pipes enhanced advection of nitrate into the banks, and also increased residence times of that nitrate under certain conditions, which together enhanced denitrification. This enhancement has implications for excess nitrate management in watersheds.

### 3.1 Introduction

Excess nitrogen (N) remains a problem in streams and rivers, lakes, and estuaries (Damashek and Francis, 2018; Dubrovsky et al., 2010; Lunau et al., 2013; Royer et al., 2006; Schindler and Vallentyne, 2008; USEPA, 2016; Vilmin et al., 2018). Nitrate is the most significant component of total nitrogen (N) in areas impacted by humans (Vilmin et al., 2018). Nitrate contributes to eutrophication worldwide (Bergstrom et al., 2018; Dalu et al., 2019; Le Moal et al., 2019; Nguyen et al., 2019; Sinha et al., 2017), and can harm human health (Inoue-Choi et al., 2015; Ward et al., 2018). Thus, it is beneficial to understand natural phenomena that can reduce nitrate in waterways.

The hyporheic zone is the connective tissue between stream/rivers channels and surrounding groundwater, including beneath floodplains and in riparian zones (Brunke and Gonser, 1997; Hester and Gooseff, 2011; Stanford and Ward, 1988; Triska et al., 1993). Many field studies have shown the hyporheic zone to be a hotbed for denitrification (Duff and Triska, 1990; Harvey et al., 2013; Hinshaw et al., 2020; Triska et al., 1993; Vidon et al., 2010; Zarnetske et al., 2015). Modeling studies have investigated denitrification in approximately steady-state (gill-model) hyporheic flow, quantifying the effect of varying biogeochemical parameters (e.g., reaction rates, reactant concentrations), transport parameters (e.g., dispersion coefficient, advective water velocity), hydrologic conditions (e.g., baseflow discharge), hydrogeological parameters (e.g., soil hydraulic conductivity), and geomorphic parameters (e.g., dunes, instream structures; Hester et al., 2018; Marzadri et al., 2011; Zarnetske et al., 2012).

Contrastively, lung model exchange (Gerecht et al., 2011; Sawyer et al., 2009; Schmadel et al., 2016), otherwise known as bank storage (Pinder and Sauer, 1971), refers to dynamic hydraulic gradient reversals driving water into and then out of stream and river banks, and has been shown to increase hyporheic denitrification (Boano et al., 2014; Gu et al., 2012; Rahimi et al., 2015; Triska et al., 1993). Many studies have examined the effects of hydrologic and biogeochemical parameters on hyporheic denitrification caused by stage fluctuations of streams and rivers (Gu et al., 2012; Rahimi et al., 2015; Shuai et al., 2017). Spatial heterogeneity of soil hydraulic conductivity has been shown to be an important control on nitrate removal in steady state upwelling groundwater (Sawyer, 2015) and intertidal mixing zones in coastal aquifers

(Heiss et al., 2020). Yet to our knowledge, the effect of preferential flow through soil pipes on hyporheic denitrification has not been assessed.

Soil pipes are long void spaces in the subsurface formed by burrowing fauna (Allen and Vaughn, 2009; DiStefano et al., 2009; Stahl et al., 2014; Williams et al., 1974; Wright et al., 2011), decayed plant roots (Aubertin, 1971; Beasley, 1976; Mosley, 1982), physicochemical processes such as desiccation and freeze/thaw (Beven and Germann, 1982; 2013), and internal erosion (Wilson et al., 2013). Soil pipes form in the vast majority of USDA soil types (Bernatek-Jakiel and Poesen, 2018), and are common along stream banks (Hester et al., 2020; Jones and Cottrell, 2007; Menichino et al., 2015). Soil pipes exhibit markedly faster flow than surrounding soil matrix which often cannot be accurately simulated using traditional Darcy-Richards equations (Anderson et al., 2009; Beven and Germann, 2013; Jarvis, 2007; Tsuboyama et al., 1994). Soil pipes account for the majority of stormwater interflow, dominating the hydrologic response of the watershed flow network (Bernatek-Jakiel and Poesen, 2018; Jones, 2010; Wilson et al., 1990). Soil pipes enable rapid flow in hillslopes and uplands to receiving waterbodies compared to surrounding soil matrices (Beven and Germann, 2013; Koch et al., 2017; Laine-Kaulio et al., 2014; Wilson et al., 2016).

Soil pipes also enhance hydrologic flow near channels (Menichino et al., 2015; Zhou et al., 2016). For example, thermal imaging from Briggs et al. (2016) show massive unidirectional inflow into a stream from a 2.5 cm diameter soil pipe along the stream bank compared to no visible inflow from the surrounding soil matrix. Menichino et al. (2014) showed that a soil pipe in a meander bend had 29 to 550 times greater hydraulic conductivity and 9% to 21% faster transport velocities than when the soil pipe was partially plugged, but only addressed hydraulics. In another field study, Menichino and Hester (2015) illustrated how floodplain soils with soil pipes are more hydraulically connected to stream stage fluctuations than floodplain soils without soil pipes, but did not quantify how that affects solute transport or reaction. Lotts and Hester (2020) explored the effects of soil pipes on hyporheic hydraulics caused by gradient reversals resulting from peak flow events. However, we are unaware of studies of the effect of soil pipes in stream or riverbanks on solute transport or reactions during lung model exchange.

Here we sought to simulate the effects of soil pipes on denitrification of stream-borne nitrate in adjacent riparian groundwater. Our objectives were to determine 1) how soil pipes in stream/river banks affect denitrification occurring in riparian groundwater due to lung model hyporheic exchange (bank storage) caused by a peak flow event in the channel, 2) how such denitrification is affected by variation of geomorphic, hydraulic, and reactive transport parameters, 3) whether denitrification is primarily transport limited or reaction limited, and 4) and to conduct simple upscaling of these riparian-scale results to estimate order-of-magnitude removal along a 1-km reach of channel. We conducted a sensitivity analysis using a multi-dimensional numerical groundwater flow and transport model, varying soil pipe density, length, spacing, and height above water surface elevation; matrix hydraulic conductivity and porosity; and reactive transport parameters first order reaction rate, concentration in the stream, and longitudinal dispersivity.

## 3.2. Methods

We used MODFLOW and MT3D-USGS to simulate 2-D nitrate transport and denitrification in transient hyporheic exchange flows occurring in a small length of streambank, which we call the “streambank scale.” Then we upscaled the 2-D streambank scale results using a 1-D stream corridor model to provide a rough estimate of the cumulative effect of streambank exchange on downstream nitrate transport in longer channel reaches, which we call the “stream corridor scale.”

### 3.2.1 Streambank Scale Analysis

#### 3.2.1.1 Hydraulics

We used the same hydraulic model as Lotts and Hester (2020), which used MODFLOW (Harbaugh, 2005) to solve the 2-D unconfined, isotropic, saturated groundwater flow (Boussinesq) equation (Equation 3.1) on a rectangular prismatic domain, 5.5 m in the  $x$ -direction (parallel to the stream channel), 2.0 m in the  $y$ -direction (perpendicular to the stream channel), and 2.0 m in the  $z$ -direction corresponding to depth (gray area in Figure 3.1).

$$\frac{\partial}{\partial x} \left( h \frac{\partial h}{\partial x} \right) + \frac{\partial}{\partial y} \left( h \frac{\partial h}{\partial y} \right) + \frac{R}{K} = \frac{S_y}{K} \frac{\partial h}{\partial t} \quad [3.1]$$

$K$  is the matrix hydraulic conductivity ( $LT^{-1}$ ),  $R$  is a volumetric flux per unit volume corresponding to sources and sinks ( $T^{-1}$ ),  $h$  is the hydraulic head (L),  $S_y$  is specific yield (dimensionless), and  $x$ ,  $y$ , and  $z$  are Cartesian spatial coordinates (L), and  $t$  is time (T). Model computational cells were 2.0 cm by 2.0 cm in the  $x$  and  $y$  directions, respectively, with 275 rows and 100 columns; the model had one layer 2.0 m thick with a time-varying water table. The stream channel was represented hydraulically with a temporally-varying specified head boundary condition namely a half sinusoid with an amplitude of 0.5 m and duration of 10 hours (Figure 3.1 and Equation 3.2; Lotts and Hester, 2020).

$$h(t) = 1 + 0.5 \sin \left( \frac{\pi t}{36,000} \right), t \rightarrow [s], h \rightarrow [m] \quad [3.2]$$

The upland boundary condition opposite the stream channel was general head to simulate a far-field condition which produces the same head profile as the winter gaining conditions in Menichino and Hester (2015). We positioned no-flow boundaries in the longitudinal direction far enough away from the soil pipes located in the “Domain of Interest” (Figure 3.1) to remove the boundary effects (Lotts and Hester, 2020).

We chose a saturated groundwater flow model even in this situation where flood waves propagate into the riparian aquifer because saturated models can address our research objectives while being computationally parsimonious. This choice is justified for our study in multiple ways. Most fundamentally, a saturated model reliably establishes trends and relationships between aquifer parameters and system response variables (e.g. denitrification, residence time, hyporheic flux) in scenarios where hyporheic exchange in the banks are induced by a flood wave



overlaps a node in the groundwater domain. The CFP applies Kirchhoff's Law (Equation 3.3) to all the nodes (index  $in$ ) in the pipe domain,

$$\sum_{ip=1}^{np} Q_{ip} - Q_{ex} + Q_s = 0 \quad [3.3]$$

where  $\sum_{ip=1}^{np} Q_{ip}$  is the sum of all flows from pipe segment  $ip$  coming from other nodes,  $np$  is the total segments coming into a node  $in$ ,  $Q_{ex}$  is flow from or to the matrix, and  $Q_s$  is storage. Hagen Poiseuille (Equation 3.4) and the Darcy-Weisbach equations (Equation 3.5) for laminar and turbulent flows, respectively, transform the flows in Kirchhoff's Law to head.

$$Q_{ip} = -\frac{\pi d_{ip}^4 g (h_{in} - h_{neighbor})}{128 \nu \Delta l_{ip} \tau_{ip}} \quad [3.4]$$

$$Q_{ip} = -\sqrt{\frac{|h_{in} - h_{neighbor}| g d_{ip}^5 \pi^2}{2 \Delta l_{ip} \tau_{ip}}} \log \left( \frac{2.51 \nu}{4 \sqrt{\frac{2 |h_{in} - h_{neighbor}| g d_{ip}^3}{\Delta l_{ip} \tau_{ip}}}} + \frac{k_c}{3.71 d_{ip}} \right) \frac{(h_{in} - h_{neighbor})}{|h_{in} - h_{neighbor}|} \quad [3.5]$$

For pipe segment at index  $ip$ ,  $Q_{ip}$  is the flow rate ( $L^3 T^{-1}$ );  $d_{ip}$  is the diameter (L),  $\Delta l_{ip}$  is the length of the pipe segment (L),  $k_c$  is the roughness height (L), and  $\tau_{ip}$  is the tortuosity (dimensionless);  $h_{in}$  is the head (L) at node index  $in$ , and  $h_{neighbor}$  is the head (L) at the node on other end of the pipe segment;  $g$  is the gravitational acceleration ( $L T^{-2}$ ), and  $\nu$  is the viscosity ( $L^2 T^{-1}$ ) of water at 25°C. The corresponding nodes of the pipe and matrix domains are coupled with an exchange term (Equation 3.6),

$$Q_{ex} = \alpha_{i,j} (h_{in} - h_{i,j}) \quad [3.6]$$

where  $Q_{ex}$  are  $\alpha_{i,j}$  are the volumetric flow rate ( $L^3 T^{-1}$ ) and conductance ( $L^2 T^{-1}$ ) between the pipe and soil matrix at MODFLOW cell  $i,j$ , respectively; and  $h_{i,j}$  is the hydraulic head (L) in cell  $i,j$  (Shoemaker et al., 2007). The conductance for the base-case was set to  $6.28 \times 10^{-6} \text{ m}^2/\text{s}$  to match  $K$  of the surrounding soil matrix. We then varied  $\alpha$  with  $K$  in our sensitivity analysis (Sections 3.2.1.3 and 3.3.1). Hydraulic boundary conditions are discussed below in Section 3.2.1.4.

### 3.2.1.2 Nitrate Transport and Reaction

We solved the reactive advective-transport equation for dissolved nitrate in the modeling domain (gray area in Figure 3.1) with MT3D-USGS (Bedekar et al., 2016),

$$\frac{\partial C}{\partial t} = \frac{\partial}{\partial x_i} \left( \mathbf{E}_{ij} \frac{\partial C}{\partial x_j} \right) - \frac{\partial}{\partial x_i} (v_i C) - kC \quad [3.7]$$

where:

$C$  is the concentration of contaminants dissolved in groundwater,  $ML^{-3}$ ;  
 $t$  is time, T;

$x_i$  is the distance along the respective Cartesian coordinate axis, L;  
 $E_{ij}$  is the hydrodynamic dispersion tensor,  $L^2 T^{-1}$ ;  
 $v_j$  is the seepage or linear pore water velocity,  $LT^{-1}$ ;  
 $q_s$  is the volumetric flux of water per unit volume of aquifer representing sources; (positive) and sinks (negative),  $T^{-1}$ ;  
 $C_s$  is the concentration of the sources or sinks,  $ML^{-3}$ ;  
 $\theta$  is the porosity of the porous medium dimensionless;  
 $k$  is a first order rate constant  $T^{-1}$ .

We modeled the chemical reaction with first order kinetics rather than Monod. Since our purpose is to establish how characteristic reaction time scales interrelate with soil pipe effects on transport, first order kinetics are a more parsimonious way to achieve this objective. Monod kinetics necessitates coupling aerobic respiration, nitrification, denitrification, and microbial  $NH_4^+$  uptake (Zarnetske et al., 2012), and specifying values for their many associated parameters, each of which adds uncertainty to the solution. Further, we conducted additional simulations where we used Monod kinetics (and incorporated aerobic respiration) which showed that first order kinetics produce the exact same trends of system response (Figure C2). While first order kinetics if anything overestimates raw denitrification (i.e. at higher nitrate concentrations), it actually underestimates soil pipe impacts on denitrification as soil pipes will actually add more substrate thereby increasing the reaction rates (for further discussion refer to C2.1). Hence, by using first order kinetics we actually provide a conservative estimate of the impact of soil pipes. Several studies reasonably fit first order kinetic models to denitrification field data in the hyporheic zone (Boyer et al., 2006; Gilles et al., 2009; Pittroff et al., 2017; Rahimi et al., 2015; Sheibley et al., 2003; Zarnetske et al., 2015), and other studies have used first order kinetics with literature rate data to establish meaningful relationships between denitrification and various hydrologic parameters (Hester et al., 2018; Hester et al., 2016). Zarnetske et al. (2012) examined the entire Monod kinetics parameter space and determined that reaction rate constants are more influential on denitrification than half-saturation constants or the  $O_2$  inhibition term, and the majority of scenarios within the parameter literature ranges favored denitrification. Furthermore, first order kinetics closely resemble Monod kinetics when nitrate concentrations are below the half-reaction constant of a typical riparian soil ( $\sim 1.64$  mg/L; Hester et al., 2018; Hester et al., 2016; Zarnetske et al., 2012), and our base case is 1.0 mg/L. Thus, first order kinetics are an acceptable and parsimonious way to simulate denitrification in a large subset of hyporheic zones, allowing us to isolate the effects of soil pipes. Because we are only interested in the fate of nitrate entering the hyporheic zone along one meter of bank, the constant concentration boundary on the channel side was set for a smaller sub-domain one meter long in the  $x$ -direction (“Domain of Interest” in Figure 3.1). Contaminant transport in the pipes themselves was not explicitly modeled. Rather, the pipes’ effects were incorporated through the hydraulic model and their influence on the flow field which was then accounted for in the advection portion of the transport model.

### 3.2.1.3 Parameter Selection and Sensitivity Analysis

We conducted a sensitivity analysis of soil pipe, soil matrix, and reactive transport parameters (Table 3.1). We varied each parameter independently while holding other parameters to the base case. Justification for parameter ranges are included in Table 3.1 and Lotts and Hester (2020). Our primary hydraulic response variable was total hyporheic exchange volume due to the 10 hr. storm event,  $V$  ( $L^3$ ; i.e. the amount of water that entered the bank from the channel and then returned to the channel as a result of the peak flow event in the channel), divided by the total hyporheic exchange volume occurring without soil pipes ( $\rho=0$   $m^{-1}$ ),  $V_0$  ( $L^3$ ), i.e. the normalized hyporheic volume  $V/V_0$  ( $L^3L^{-3}$ ; Lotts and Hester 2020). Our primary transport response variable was total mass denitrified  $D$  (M) within the total hyporheic volume, again normalized by total mass denitrified that occurred without soil pipes ( $\rho=0$   $m^{-1}$ )  $D_0$  (M), yielding normalized total mass denitrified,  $D/D_0$  ( $MM^{-1}$ ). For transport and reaction parameters  $K$ ,  $k$ ,  $\alpha_L$ ,  $C_0$ , and  $\theta$ ,  $D_0$  varied with the soil matrix or reactive-transport parameter. In that case, normalized denitrification is denoted as  $D/D_0^*$ .

**Table 3.1. Sensitivity Analysis Parameters**

Parameter varied	Range;	Base	Units	Sources for values
Soil pipe density, $\rho$	0–5; 1	1	soil pipes per m	(Hester et al., 2020; Menichino et al., 2015)
Soil pipe longitudinal (horizontal) spacing in a three-pipe configuration, $\delta$	0.1, 0.18, 0.24, 0.32, 0.39, 0.43, 0.5	0.24	M	(Hester et al., 2020; Menichino et al., 2015)
Soil pipe length, $L$	0–1.5; 0.25	1	M	(Gormally et al., 2011)
Soil matrix hydraulic conductivity, $K$	$10^{-7}$ , $10^{-6.5}$ , ..., $10^{-3}$ †	$10^{-4}$	m/s	$D=2$ cm, $S_y$ varied simultaneously to match material (Lotts and Hester, 2020)
Soil pipe height above or below baseflow water level, $H$	-0.5–+0.3; 0.1	-0.5	m above (+) or below (-) baseflow	(Menichino et al., 2015)
Longitudinal dispersivity, $\alpha_L$	0.005, 0.01, 0.02, 0.04†	0.01	(m)	Fig 1 of Gelhar et al. (1992)
Porosity, $\theta$	0.1-0.4; 0.15	0.25	dimensionless	Table 1 of Gelhar et al. (1992)

Biodegradation first-order rate constant, $k$	0.6, 6, 36	6	$d^{-1}$	(Hester et al., 2016)
Stream water column dissolved $NO_3^-$ concentration, $C_0$ ††	0.5-3;0.5	1	mg/L	(Hester et al., 2016)

† not a uniform interval since the scale spans several orders of magnitude

†† this differs from the initial aquifer concentration (which is 0 mg/L) and the soil pipe boundary concentration which is modeled with a stair step function (Equations 3.8-3.9)

#### 3.2.1.4 Boundary Conditions

For the hydraulic model, the half-sinusoid time-varying specified head boundary on the channel side of the model domain (right hand boundary gray area, Figure 3.1) represented a generic peak flow event from storms or diel fluctuation in human withdrawal from or discharge to the channel, dam releases, or snowmelt (Lotts and Hester, 2020). The amplitude and duration are roughly based on field data in Menichino and Hester (2015). The upland side of the model domain was set as a general head boundary simulating far-field conditions (left hand boundary, Figure 3.1), and all other boundaries were no flow (Lotts and Hester, 2020). The soil pipes implemented via the CFP acted as head-dependent flux boundaries (cylinders in the “Domain of Interest,” Figure 3.1). For  $H > 0$ , the head-dependent flux boundaries only act when the stage height is above the soil pipe elevation. The soil pipes for the base case were already inundated at the beginning of the peak flow event (i.e.  $H = -0.5$  m).

For the transport model, the channel was represented as a specified concentration boundary that was constant with time (base case  $C_0 = 1$  mg/L dissolved nitrate; Hester et al., 2016). Since we only computed denitrification in nitrate coming from one meter of bank, we confined the specified concentration to the “Domain of Interest” (Figure 3.1).

Because we did not explicitly simulate transport in the soil pipes, the pipes were designated in MT3D-USGS as concentration boundary conditions at the location of the pipes, in this case as a time-varying concentration (Equations 3.8a-3.8b). Time-varying was necessary due to the transient nature of the simulations. Early in the simulations, as water flowed from the channel into the banks (rising limb), the soil pipe boundary concentration was set to a constant (Equation 3.8a), because during such conditions the concentration of nitrate in the soil pipe will approximately equal the constant concentration in the channel. Although the pipe would be initially free of nitrate given nitrate-free groundwater flows toward the channel during baseflow, we assumed the entire length of the soil pipe was contaminated from the start of the simulation due to generally low residence times in the soil pipes compared to the matrix. For example, at the base case soil matrix hydraulic conductivity of  $10^{-4}$  m/s, the residence time of flow through the soil pipe was only around 13 min according to linear interpolations from CFP flow rate data. This was the case for all model scenarios in the sensitivity analysis (Table 3.1) except lower  $K$ . At lower values of  $K$ , it was not reasonable to assume advection of dissolved nitrate from the

channel into the soil pipe early in the simulation was approximately instantaneous, and doing so caused more than 1% error in D. Thus, we instituted a “growing” time-varying specified concentration boundary condition, where the region of non-zero nitrate concentration within the pipe grew away from the channel with time (Section C1.1). Finally, we assumed that concentration was uniform along the length of the soil pipe, which assumes minimal denitrification within the pipes themselves, again consistent with comparatively low residence times in the pipes. The initial nitrate concentration in the riparian soil matrix was 0 mg/L, and we also assumed water coming from the upslope did not contain nitrate.

Later in the simulations, after undergoing at least some denitrification in riparian groundwater, the nitrate plume flowed back to and through the pipes as water moved back to the channel (falling limb; e.g., see Animations SI-1-10). During these conditions, MT3D-USGS concentrations at the locations of the soil pipes were set to the average concentration of the nitrate plume upgradient from the pipe (e.g., Equation 3.8b for base case) which was approximated from the average of the maximum concentration and the minimum concentration of all cells contributing flow to the pipe (Equation 3.9). All cells in a given soil pipe were assigned the same time-varying concentrations, which is reasonable because mixing occurs once the water is in the soil pipe. In scenarios with more than one soil pipe, each pipe had a different time-varying boundary concentration history based on the concentration of the plume upgradient from the soil pipe (Equation 3.9).

$$\text{Rising Limb (example: base case)} \quad C_{sp}(t) = 1; \quad 0 < t < 26400 \quad [3.8a]$$

$$\text{Falling Limb (example: base case)} \quad C_{sp}(t) = \begin{cases} 0.7; & 26400 < t < 27600 \\ 0.6; & 27600 < t < 28800 \\ 0.52; & 28800 < t < 30000 \\ 0.47; & 30000 < t < 31200 \\ 0.43; & 31200 < t < 32400 \\ 0.38; & 32400 < t < 33600 \\ 0.29; & 33600 < t < 34800 \\ 0.24; & 34800 < t < 36000 \\ 0.18; & 36000 < t < 43200 \\ 0; & 43200 < t < 86400 \end{cases} \quad [3.8b]$$

$$\text{Avg. up-gradient plume conc. approximation} \quad C_{sp}(t) \approx \frac{C_{max}(t) + C_{min}(t)}{2}; \quad [3.9]$$

where  $C_{sp}(t)$  is the concentration in the soil pipe ( $\text{gm}^{-3}$ ) at time  $t$  (s), and  $C_{max}$  (mg/L) and  $C_{min}$  (mg/L) are the maximum and minimum concentration of the returning up-gradient nitrate plume in the model cells adjacent to and upgradient from the soil pipe. Equation 3.8b was determined by making an initial guess and then manually examining the concentration maps at the beginning of each stress period, identifying the maximum and minimum concentration, and resetting the concentration to equal the average of the two as in Equation 3.9. This procedure converged very quickly, with only a 0.00017% change in D from the first iteration to a subsequent additional iteration in the base case scenario.

### 3.2.1.5 Residence Time Calculation

We used MODPATH7 (Pollock, 2016) to track particles and determine residence times of hyporheic flowpaths within riparian groundwater. For each simulation, we released 12 particles in each cell of the stream channel boundary as well as the soil pipes within the “Domain of Interest” (Figure 3.1). This amounted to 1188 particles for the base case with one soil pipe, with more particles for longer and more soil pipes. We released particles 0.167 hours into the simulation, when the channel first becomes losing to riparian groundwater. We calculated average residence time (RT) of the 1188 particles. In some cases, it was necessary to extend the model domain in the y-direction (Figure 3.1) so that particles did not terminate on the general head boundary (low porosity  $\theta = 0.1$ ,  $K > 10^{-4}$  m/s, and  $L > 1$  m). In such cases, the general head boundary was modified with the new grid to achieve the same steady state head profile in the domain of interest.

### 3.2.2 Stream Corridor Scale Analysis

We extrapolated our MODFLOW/MT3D results to estimate the cumulative effect of soil pipes along one kilometer of stream channel. 1 km is arbitrary but represents a reasonable estimate for the length of mainstem channel in third or higher order watersheds (Hack, 1957). We assumed that there were no other inflows or outflows into the system other than the hyporheic exchange we simulated in MODFLOW. This included no baseflow, which allowed us to isolate the effects of hyporheic exchange and represents an intermediate condition between typically gaining watersheds in humid climates and often losing watersheds in arid climates. These stream corridor level assumptions limit the applicability of the extrapolation to a narrower subset of scenarios than the streambank scale analysis; this more limited scope of scenarios includes storms that occur significantly upstream of the reach, or diel cycles of glacial melt, dam releases (e.g., hydropower peaking), human water withdrawals, or evapotranspiration. As detailed below, we made many simplifications to yield rough, order of magnitude upper and lower bound estimates of percent nitrate removal in channel flow due to lung model hyporheic denitrification. Our goal is to gain a preliminary understanding of how stream and soil pipe parameters interact to affect percent nitrate removal in the stream itself. The use of an idealized scenario facilitates varying the parameters and helps uncloak the relationships between the parameters.

We assumed a rectangular channel cross section with constant width and slope and calculated channel flow rate as a function of stage and time using Manning’s equation:

$$Q(t) = \frac{1}{n} A(t) R_h(t)^{2/3} S_0^{0.5} \quad [3.10]$$

where  $n$  is Manning’s roughness coefficient ( $L^{-1/3}T$ ),  $Q$  is channel flow rate ( $L^3T^{-1}$ ),  $A$  is channel cross sectional area ( $L^2$ ),  $R_h$  is channel hydraulic radius ( $L$ ), and  $S_0$  is channel slope (-). We then

assumed an upstream nitrate source, and calculated the nitrate mass inflow rate at the upstream end of the 1 km reach with respect to time as:

$$\dot{M}(t) = C_0 Q(t) \quad [3.11]$$

where  $\dot{M}(t)$  is mass flow rate of nitrate ( $MT^{-1}$ ), and  $C_0$  is 1 mg/L. The total (cumulative) nitrate mass that enters from the upstream pollutant source during the 10 hr. storm duration  $M$  (M) is found by integrating the mass flow rate with respect to time.

$$M = \int_0^{10 \text{ hrs}} \dot{M}(t) dt \quad [3.12]$$

Because hyporheic exchange simulated by the MODFLOW model would attenuate the hydrograph in the channel over the one kilometer of channel, calculating the actual denitrification for the attenuated hydrograph would require a fully coupled surface water-groundwater flow and transport code, which was beyond the scope of this study. Instead, we estimated an upper and lower bound on denitrification using simplified equations. We estimated the upper bound total mass denitrified (M) by applying total mass denitrified (D) in one meter of the hyporheic zone during the peak flow event from the MODFLOW/MT3D simulations (for  $\rho=0,1$ , and  $5 \text{ m}^{-1}$ , section 3.2.1.3) across the entire 1 km reach as:

$$\text{Total Mass Denitrified} = \int_0^{1,000 \text{ m}} D|_{x=0} dx \quad [3.13]$$

where  $x$  is the downstream spatial coordinate (L),  $D|_{x=0}$  is the total mass denitrified calculated in section 3.2.1.3 per meter of MODFLOW model domain ( $ML^{-1}$ ), e.g., 0.325 g for base case. The D evaluated at  $x=0$  means the D in the first meter of the reach, and should not be confused with the sum of D at  $x=0$ . This value for D in reality applies only to the upstream most 1.0 m of the channel ( $x \in 0.0-1.0 \text{ m}$ ) because further downstream the hydrograph would have been attenuated due to hyporheic exchange with the banks upstream. Thus, applying this upper bound D to the whole channel overestimates denitrification in the 1 km reach. The percentage removal was calculated as:

$$\%D(\text{upperbound}) = 100 \frac{\int_0^{1,000 \text{ m}} D|_{x=0} dx}{M} \quad [3.14]$$

Next, we estimated the lower bound of total mass denitrified by first estimating the hydrograph in the downstream end of the 10 km channel as:

$$Q(t)|_{x=1,000} = Q(t) - \int_0^{1,000 \text{ m}} Q_{hyp}(t) |_{x=0} dx \quad [3.15]$$

Equation 3.15 multiplies the hyporheic flow hydrograph from the MODFLOW model (which applies to the first 1 m segment) by 1,000 m to estimate the total hyporheic exchange along the 1 km reach, and then subtracted that from the stream's flow rate hydrograph  $Q(t)$  from Equation 3.10. This overestimates the hyporheic exchange because in reality there is a progressively attenuated flood wave driving the water into the banks and hence a progressively attenuated hyporheic flow hydrograph. Positive  $Q_{hyp}$  indicates losing conditions where water flows from the stream to the riparian soil. Next, we substituted  $Q(t)|_{x=1,000}$  into Manning's

equation and solved the implicit equation for  $h(t)|_{x=1,000}$  at all time steps using the `fsolve` function in Python 3. Finally, we used  $h(t)|_{x=1,000}$  as the specified head boundary condition in MODFLOW, and then reran MT3D-USGS. This actually overestimates the hydrograph attenuation experienced in the 1 km reach, thus the hyporheic exchange calculated by MODFLOW and the denitrification calculated MT3D for the downstream end of the 1 km reach is underestimated. Denitrification for all other locations along the stream channel between  $x=0$  km and  $x=1$  km was linearly interpolated using

$$\%D(\text{lower bound}) = 100 \frac{\int_0^{1,000 \text{ m}} \left(1 - \frac{x}{1,000}\right) (D_{NO_3}|_{x=0}) + \left(\frac{x}{1,000}\right) (D_{NO_3}|_{x=1,000}) dx}{M} \quad [3.16]$$

We ran the calculations for three channel widths ( $w = 3, 6, \text{ and } 9 \text{ m}$ ) and slopes ( $S_0 = 0.01, 0.001, 0.0001$ ) for three soil pipe densities ( $\rho = 0, 1, \text{ and } 5$ ). Among all scenarios, we kept the initial upstream depth constant, which meant that flow increased as we varied  $w$  and  $S_0$ . This choice was made to maintain consistency with the channel stage hydrograph from Lotts and Hester (2020). We discuss the implications of this choice on our results in Section 3.4.4. Although channel width and slope can be correlated (Garcia, 2008), for completeness we performed simulations across the entire Cartesian cross-product of the three parameter sets, for a total of 27 calculations. We chose the Manning's coefficient to be 0.03 as a reasonable value for natural settings (Mays, 2011). Our approach yields a rough approximation, but is useful to estimate order-of-magnitude effects, and also gives initial insight into the interrelation of  $\rho$ ,  $w$ ,  $S_0$ , and stream denitrification.

### 3.3 Results

#### 3.3.1 Effect of Soil Pipe and Soil Matrix Parameters at Streambank Scale

To better isolate the effect of soil pipes on denitrification, we mainly present denitrification normalized to that which occurs when no soil pipes are present. Total mass denitrified in peak-flow induced lung model hyporheic exchange ( $D$ ) normalized to that for no soil pipes (i.e.  $\rho=0$ ;  $D/D_0$ ) increased with the length ( $L$ ) of a single soil pipe (Figure 3.2a). This increase was nonlinear, increasing more rapidly at greater pipe length to 76% for  $L = 1.5 \text{ m}$ .  $D/D_{\delta=0.24\text{m}}$  exhibited a similar but subtler trend with pipe spacing ( $\delta$ ) for a three-pipe configuration (Figure 3.2b). As  $\delta$  increased from  $\delta = 0.24 \text{ m}$  (base case) to  $0.5 \text{ m}$ ,  $D$  increased 10.6% for  $k = 6 \text{ days}^{-1}$ . Here, we normalized to the base case (i.e.  $D_{\delta=0.24\text{m}}$ ) as opposed to  $D_0$  to magnify the effects of spacing, since  $D \gg D_0$  for all  $\rho = 3$  configurations.  $D/D_0$  stayed relatively constant as the height of a single soil pipe above initial (baseflow) channel water surface elevation ( $H$ ) increased from  $-0.5 \text{ m}$  to  $0 \text{ m}$ , but then decreased for  $H > 0 \text{ m}$  for soils with reaction rate ( $k$ ) =  $6 \text{ days}^{-1}$  (Figure 3.2c). By contrast, for  $k = 0.6 \text{ days}^{-1}$  soil,  $D/D_0$  increased 15% with respect to base case  $H$  for  $0.0 < H \leq 0.1 \text{ m}$ , but then decreased again for  $H > 0.1 \text{ m}$ .  $D/D_0$  increased generally linearly with pipe density ( $\rho$ ), and  $D/D_0$  increased at a noticeably greater rate for low  $k$  ( $k = 0.6 \text{ days}^{-1}$ ) than with the other reaction rates (Figures 3.2d and 3.2e). We include

normalized hyporheic volume,  $V/V_0$ , and normalized residence time,  $R/RT_0$ , in Figure 3.2 to help visualize the connection between  $D/D_0$  and both  $V/V_0$  and  $R/RT_0$ .

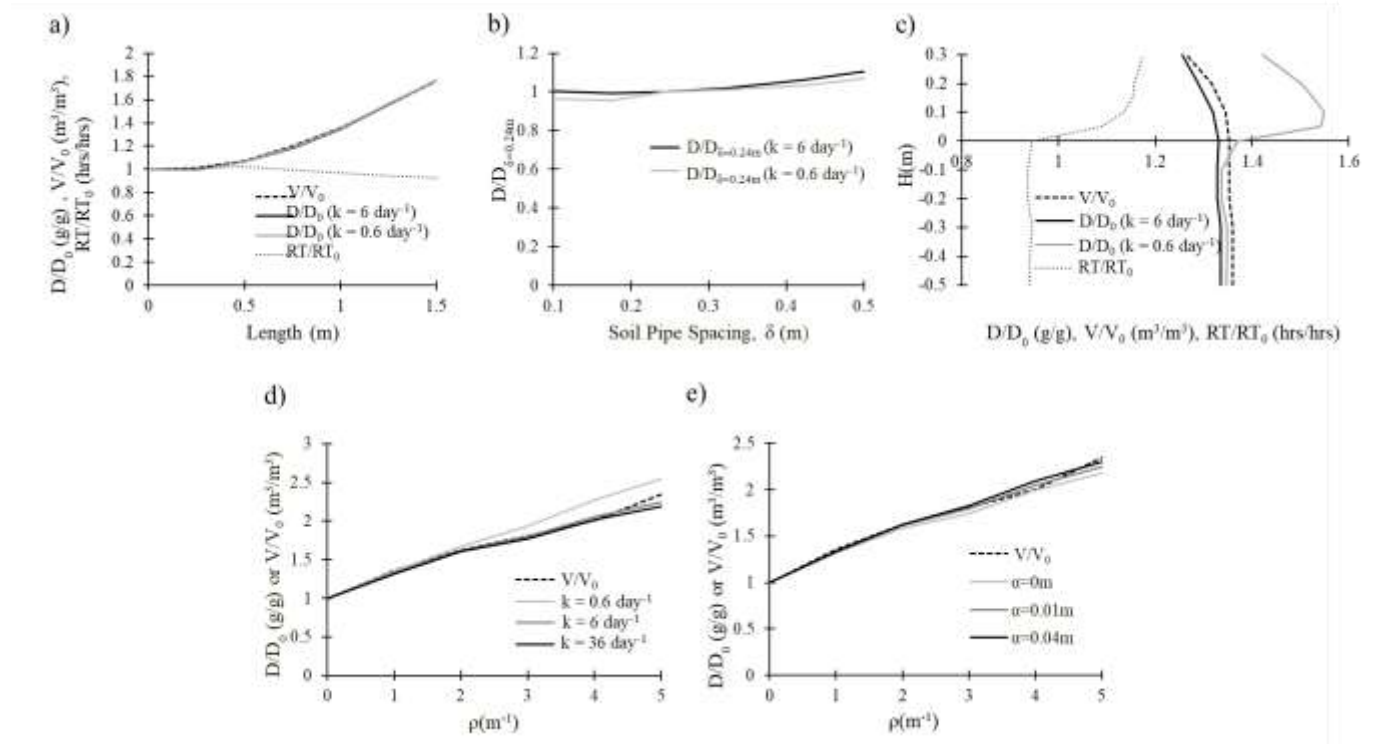


**Figure 3.2. Streambank scale effects of soil pipe parameters. a) Total mass denitrified in peak-flow induced lung model hyporheic exchange ( $D$ ) normalized to case without soil pipes (soil pipe density  $\rho = 0 \text{ m}^{-1}$ ;  $D/D_0$ ) vs. the length ( $L$ ) of a single soil pipe, b)  $D/D_{\delta=0.24m}$  vs. soil pipe spacing ( $\delta$ ) for  $\rho=3 \text{ m}^{-1}$ , c)  $D/D_0$  for a single soil pipe vs. its height above or below starting water surface elevation ( $H$ ; negative is an initially submerged soil pipe), d)  $D/D_0$  vs. soil pipe density ( $\rho$ ) for various reaction constants ( $k$ ), and e)  $D/D_0$  vs.  $\rho$  for various longitudinal dispersivities ( $\alpha_L$ ).  $V/V_0$  and  $RT/RT_0$  are hyporheic volume and residence time normalized to a case without soil pipes ( $\rho=0$ ), respectively. In panel b,  $D$  for the three soil pipe case ( $\rho=3 \text{ m}^{-1}$ ) is normalized by  $D$  for  $\delta =0.24 \text{ m}$ ; this choice best illustrates the effect of  $\delta$  on  $D$ , as the trend is undetectable when dividing by  $D_0$ . In panel c, axes are swapped to enhance physical intuition of stage height.  $k$  is reaction constant.**

As hydraulic conductivity ( $K$ ) increased,  $D/D_0^*$  increased until  $K = 1 \times 10^{-3.5} \text{ m/s}$ , after which it decreased sharply (Figure 3.3a). The \* in  $D_0^*$  denotes that  $D_0^*$  changes with each  $K$ . Similarly,  $D$  increased until  $K = 1 \times 10^{-3.5} \text{ m/s}$ , and then declined (Figure 3.3b). Many  $D/D_0$  trends mimicked those for normalized hyporheic volume ( $V/V_0$ ; Lotts and Hester, 2020), which we discuss in the Discussion section, below. Note that the  $D/D_0^*$  vs.  $K$  curve will drop far more drastically with increasing  $K$  where aerobic respiration is considered since respiration does not have time to finish at higher  $K$  values (section C2.1). This is the only case in our study where

$D/D_0 \ll 1$ . Overall,  $D/D_0$  appeared to vary most with  $L$  and  $\rho$  among the parameters and parameter ranges we evaluated.

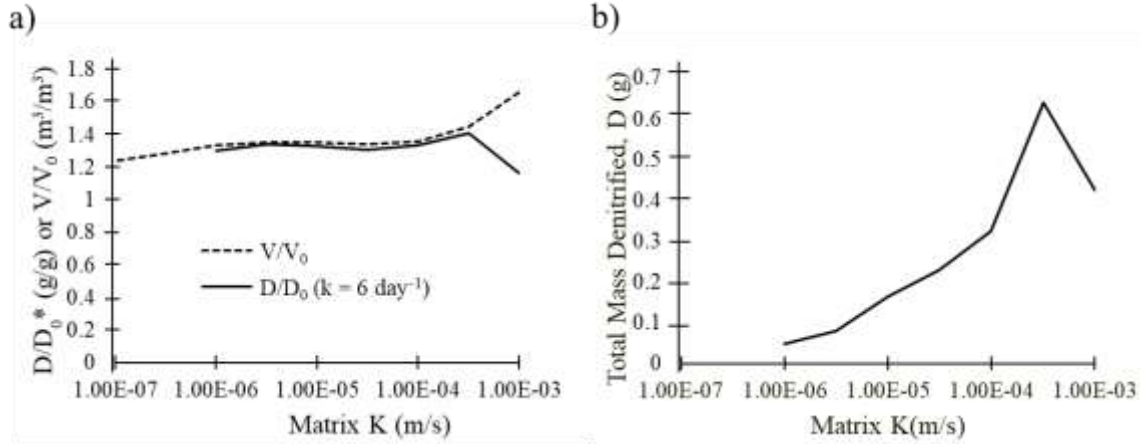


**Figure 3.3. Streambank scale effects of matrix hydraulic conductivity (K). a) Total mass denitrified in peak-flow induced lung model hyporheic exchange (D) normalized to case without soil pipes (soil pipe density  $\rho = 0 \text{ m}^{-1}$ ;  $D/D_0^*$ ) vs. K for adding a single soil pipe, and b) D vs. K. \* signifies that  $D_0$  varies with each value of K, i.e. D was normalized by a different  $D_0$  for each K.  $V/V_0$  is hyporheic volume normalized to that for case without soil pipes ( $\rho=0$ ).**

### 3.3.2 Effect of Transport Parameters at Streambank Scale

Due to our focus on the effects of soil pipes, in evaluating the effect of transport parameters on denitrification, rather than trends of total denitrification (D), we focus again on normalized denitrification  $D/D_0^*$  (note that the \* denotes that we are normalizing by a different  $D_0$  for each value of  $k$ ,  $\alpha_L$ ,  $C_0$ , or  $\theta$ ). However, for completeness, relationships between D and transport parameters are shown in Section C2.2.  $D/D_0^*$  overall was not very sensitive to changes in transport parameters, indicated by mostly horizontal lines (Figure 3.4), meaning that adding soil pipes caused the same relative increase in denitrification as with no soil pipes ( $\rho = 0 \text{ m}^{-1}$ ). This is an important finding that we would like to emphasize, because it means that changes in these transport parameters do not affect the impact of soil pipes on hyporheic transport. The two exceptions were for low  $k$  and low  $\alpha_L$ .  $D/D_0^*$  was elevated for low  $k$ , particularly for high  $\rho$  (Figure 3.4a). This means that the relative increase in denitrification caused by adding soil pipes was highest at low  $k$ , for riparian soil with many soil pipes. The percent decrease in  $D/D_0^*$  from  $k = 0.6 \text{ days}^{-1}$  to  $k = 36 \text{ days}^{-1}$  for  $\rho=1,2,3,4$ , and 5 was 2.5%, 4.1%, 9.2%, 12.6%, and 16.3%, respectively. Similarly,  $D/D_0^*$  increased very slightly with  $\alpha_L$  for  $\rho \geq 3 \text{ m}^{-1}$ , (Figure 3.4b; increasing from  $\alpha_L = 0 \text{ m}$  to  $\alpha_L = 0.04 \text{ m}$  caused a 4.4%, 5.0%, and 5.5% increase in  $D/D_0^*$  for  $\rho=3,4$ , and 5 respectively). These results mean that as the number of soil pipes increased, normalized denitrification became more sensitive to changes in  $k$  or  $\alpha_L$ .

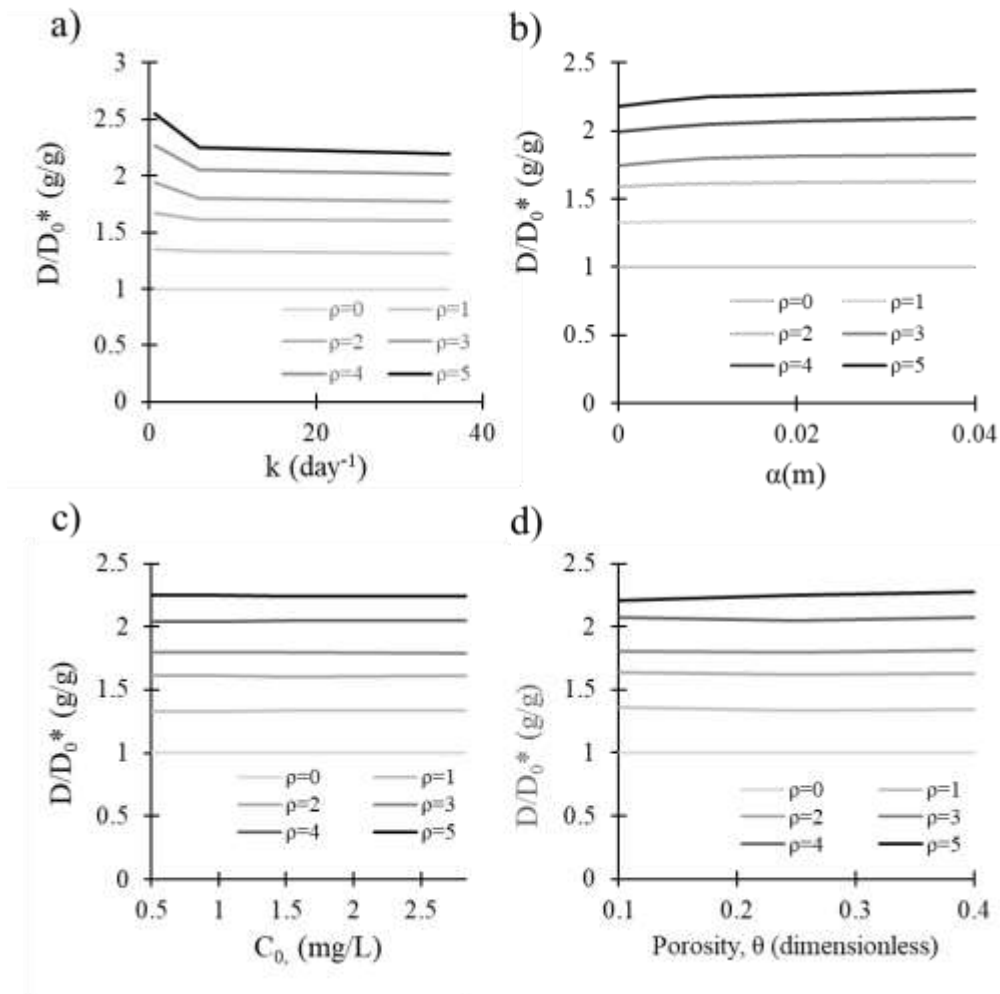


**Figure 3.4. Streambank scale effects of transport parameters. Total mass denitrified in peak-flow induced lung model hyporheic exchange ( $D$ ) normalized to the base case ( $D/D_0^*$ ) versus a) reaction constant ( $k$ ), b) longitudinal dispersivity ( $\alpha_L$ ), c) initial concentration ( $C_0$ ), and d) porosity ( $\theta$ ) for various soil pipes densities ( $\rho$ ). \* signifies that normalization is by a different value of  $D_0$  unique for each value of  $k$ ,  $\alpha_L$ ,  $C_0$ , or  $\theta$ .**

### 3.3.3 Effect of Channel Width and Slope at Stream Corridor Scale

At the stream corridor scale, the sinusoidal pulse entering the upstream end of the simulated channel (Figure 3.1) attenuated in the downstream direction due to the cumulative effect of lung model hyporheic exchange (Figure 3.5). This effect is manifest in slightly lower flow and stage (channel depth) hydrographs at the downstream end of the model domain than at the upstream end, as well a slight decrease in maximum channel flow depth ( $h_{\max}$ ) with distance down the channel. Channel flow rate was overall higher for greater channel widths and channel

slopes because the same stage height hydrograph at  $x=0$  is used. These effects are relatively small compared to uncertainties of other parameters that we have idealized such as  $w$ ,  $S_0$ , and  $K$ , so they likely would not be noticed in practice. Channel flow rate was overall higher for greater  $w$  and  $S_0$  because the same stage height hydrograph at  $x=0$  is used.

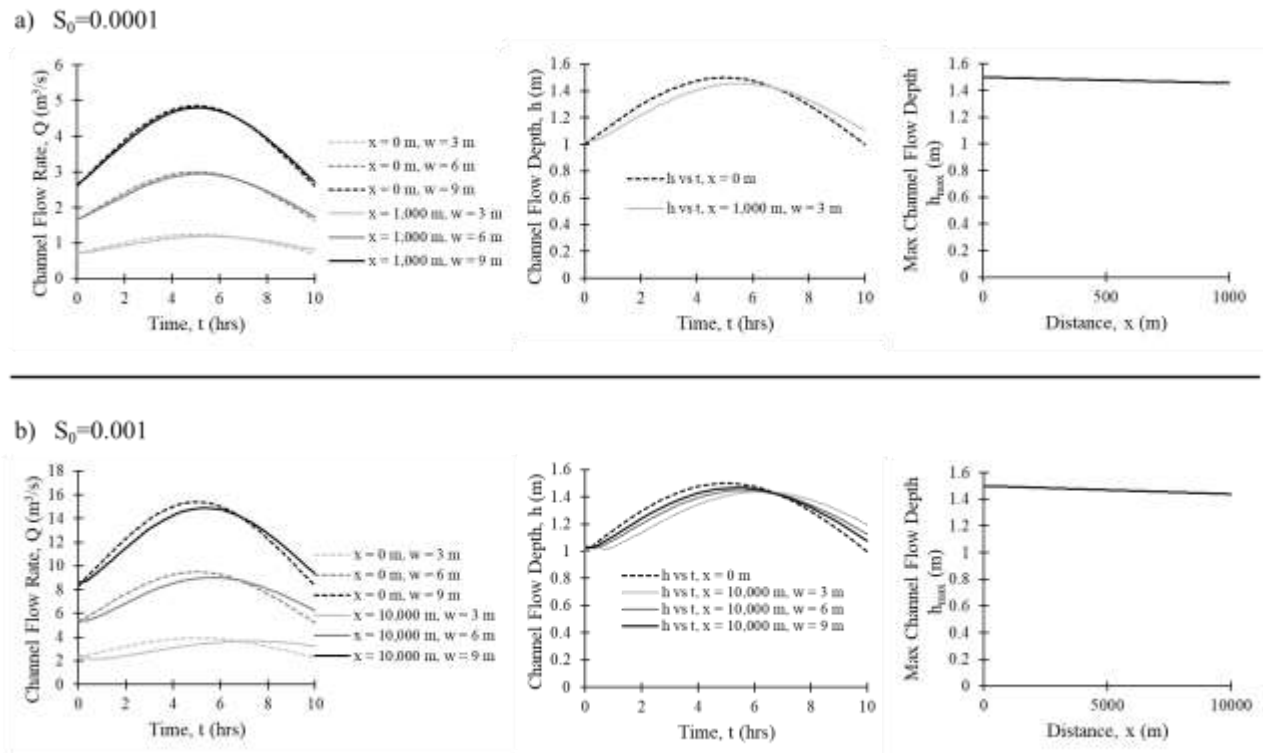


**Figure 3.5. Stream corridor scale hydraulic results. Channel flow rate ( $Q$ ) and channel flow depth ( $h$ ) vs. time for selected channel locations and widths ( $w$ ), and max channel flow depth ( $h_{max}$ ) vs. distance down the channel from upstream end of model domain ( $x$ ), for channel slope of a) 0.0001 and b) 0.001. We only show max channel flow depth vs. longitudinal distance for  $w = 3$  m. There is less attenuation for  $w = 6$  and  $9$  m, and thus the curves are flatter. We only show 1,000 m of channel for  $S_0 = 0.0001$  because the flood wave was mostly attenuated by that distance down the channel. Soil pipe density ( $\rho = 5 \text{ m}^{-1}$ ) for all plots.**

We estimated that for a stream channel 3 m wide ( $w$ ) with bed slope ( $S_0$ ) = 0.0001, that denitrification from bank storage removed approximately 3% of the nitrate flowing into the upstream end of a 1.0-km reach with 5 soil pipes per m of channel ( $\rho = 5.0 \text{ m}^{-1}$ , Figure 3.6) during flood wave propagation down the channel. This is three times greater than that without soil pipes (1% of nitrate removed). As channel length increased, or equivalently as one moves down the channel, nitrate removal increased. On the other hand, as  $w$  increased, nitrate removal decreased because channel flow rate increases with  $w$  and thus a smaller proportion of channel

flow cycled through the hyporheic zone. As  $S_0$  increased, denitrification similarly decreased (Figure 3.6) because channel velocities increased so a lower percentage of channel flow passed through the hyporheic zone. Within our selected parameter range, a 100-fold decrease of  $S_0$  caused a 10-fold increase in nitrate removal, and a 3-fold decrease in  $w$  increased nitrate removal by a factor of 3.85. Under those circumstances,  $w$  was 12.9 times more sensitive than  $S_0$ . Some of these conclusions are specific to our choice of upstream boundary condition, as discussed further in Section 3.4.4.

As  $\rho$  decreased, denitrification decreased because fewer soil pipes led to reduced hyporheic exchange. Finally, as  $K$  decreased, nitrate removal also decreased (Figure B4) due to reduced hyporheic exchange. Nevertheless, denitrification was still noticeable at  $K=10^{-6}$  m/s with narrow streams and flat slopes ( $w=3$  m and  $S_0 = 0.0001$ ) i.e. 0.5% removal after 1 km.

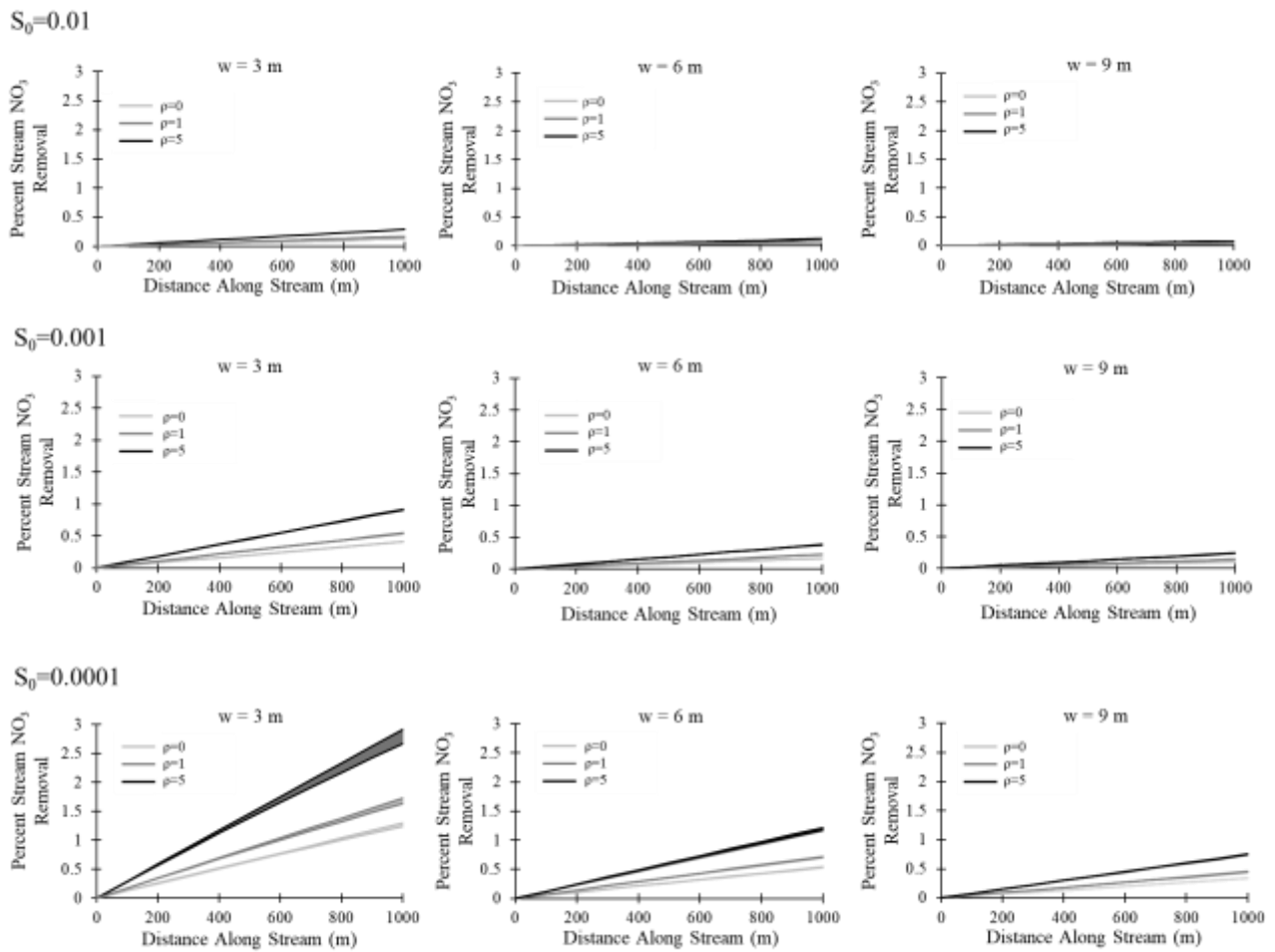


**Figure 3.6. Stream corridor scale transport results. Estimated percent channel influent nitrate load removed by denitrification in bank hyporheic exchange in a 1 km reach for varying  $w$ ,  $\rho$ , and  $S_0$ .  $K = 1 \times 10^{-4}$  m/s for all curves.**

### 3.4. Discussion

#### 3.4.1 *How Soil Pipes Alter Hyporheic Flowpaths and Hence Denitrification*

We observed a series of interesting transport phenomena caused by strong preferential flow induced by soil pipes in the context of dynamic response to hydraulic perturbation in the adjacent channel. Below we discuss specific transport patterns caused by soil pipes that alter nitrate storage, residence times (RTs), and hence reaction within riparian groundwater.

##### 3.4.1.1 *Adjacent Soil Pipes Constrain Lateral Extent of Nitrate Plumes*

The shape of the relationship between normalized denitrification ( $D/D_0$ ) and soil pipe density ( $\rho$ ) was the same as that for hyporheic volume ( $V/V_0$ ) at lower  $\rho$  but dipped below that for  $V/V_0$  at higher  $\rho$  for  $k = 6$  and  $36 \text{ days}^{-1}$  (Figures 3.2d and 3.2e). This divergence occurred because nitrate plumes emanating from the middle soil pipes at higher  $\rho$  were constrained by those from pipes on the ends (Figure 3.7). These middle plumes at higher  $\rho$  were not able to spread out in space due to opposing gradients created by high heads propagating into the bank along the adjacent pipes, leading to narrower plumes and hence less denitrification in the soil matrix. Thus, while total mass denitrified ( $T$ ) increased with additional soil pipes (i.e. with increased  $\rho$ , Figures 3.2d and 3.2e), denitrification per pipe declined. This is similar to the way groundwater contributions to the riparian zone from adjacent valley slopes inhibit flow from the channel and hence decrease hyporheic RTs in Schmadel et al. (2016). Conversely, when  $\rho$  decreased by increasing soil pipe spacing ( $\delta$ ), holding the number of pipes constant, the plumes spread out (Figure 3.7b), leading to higher  $D/D_{\delta=0.24\text{m}}$  (Figure 3.2b).

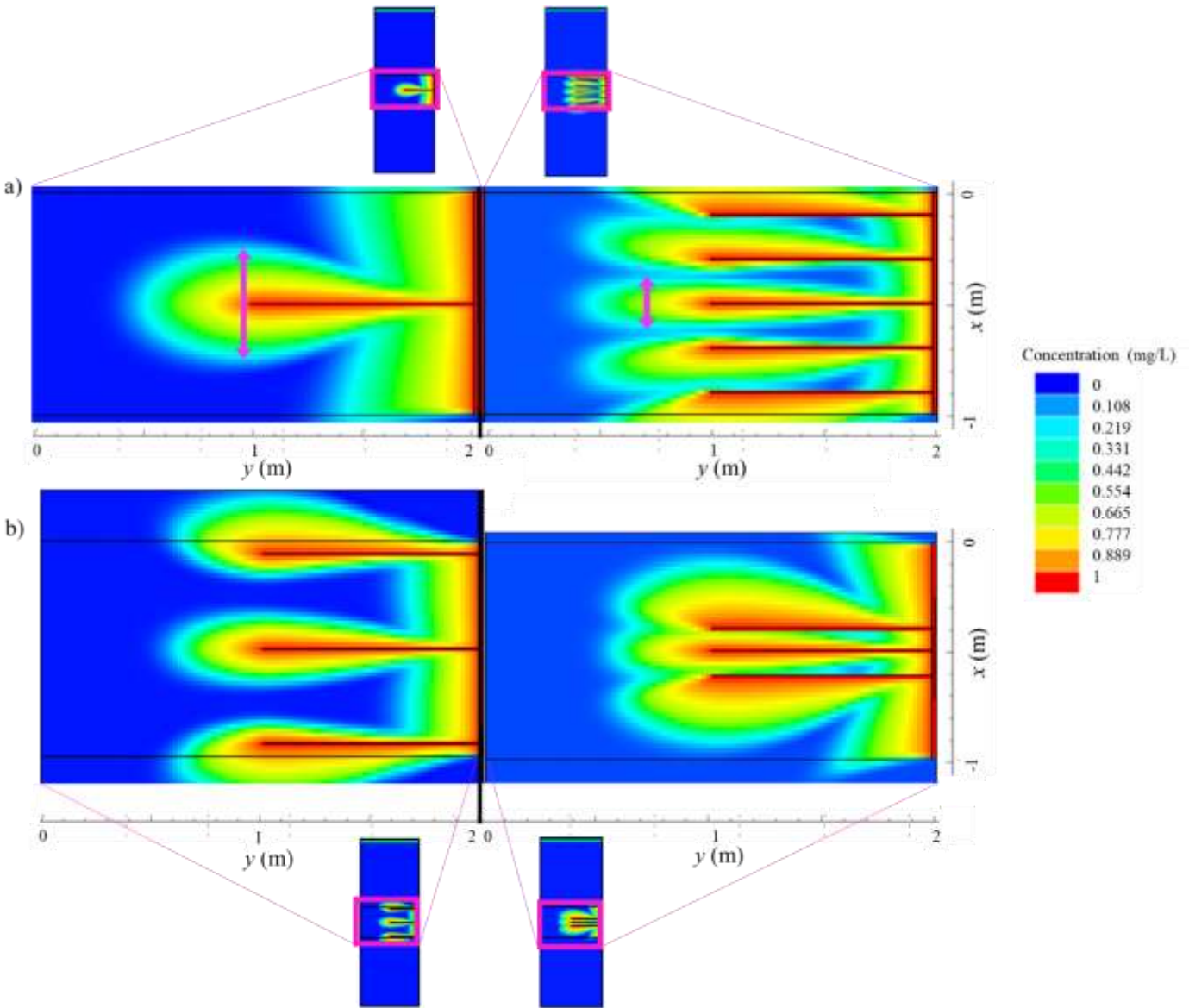


**Figure 3.7. a) Plan view nitrate concentration maps 3.3 hrs. after the start of the peak flow event as soil pipe density ( $\rho$ ) was varied by a) varying number of pipes ( $\rho=1 \text{ m}^{-1}$  at left,  $\rho=5 \text{ m}^{-1}$  at right) and b) varying pipe interspacing ( $\delta = 0.43 \text{ m}$  at left,  $\delta = 0.1 \text{ m}$  at right). In both cases, as  $\rho$  decreased, the plume width of middle plumes increased, leading to increased denitrification per pipe. The concentration maps are cropped from the larger domain to show more detail.**

#### *3.4.1.2 Soil Pipe Groupings Create Transverse Head Gradients that Push Nitrate Back into the Matrix*

The effect of adding soil pipes on normalized denitrification ( $D/D_0$ ) for  $\rho \geq 3 \text{ m}^{-1}$  was noticeably greater for slower-reacting soils ( $k = 0.6 \text{ days}^{-1}$ ) than it was for faster-reacting soils ( $k = 6 \text{ days}^{-1}$  and  $36 \text{ days}^{-1}$ ; Figures 3.2d and 3.4a). This difference arose because head gradients

perpendicular to the soil pipes (Figure 3.8a) drove nitrate from the pipes back into the soil matrix a second time after it had already returned to the pipe (Figure 3.8b). This allowed additional denitrification as nitrate got stored in the matrix between pipes. This effect was less at higher  $k$  because more of the nitrate had already reacted by the time it reached the pipe the first time. Thus, adding additional soil pipes for  $\rho \geq 3 \text{ m}^{-1}$  in fast-reacting soils only enhanced denitrification to the extent that adding pipes increased  $V/V_0$ . The perpendicular head gradients themselves are caused by the grouping or clustering of the soil pipes, where such gradients are strongest at the pipes at the end of the grouping where the potentiometric surface is curving back toward the background condition without pipes on either side (Figure 3.8a and Animations SI 8-10). Thus, we expect that pipes spaced continuously along a stream bank would reduce this effect.

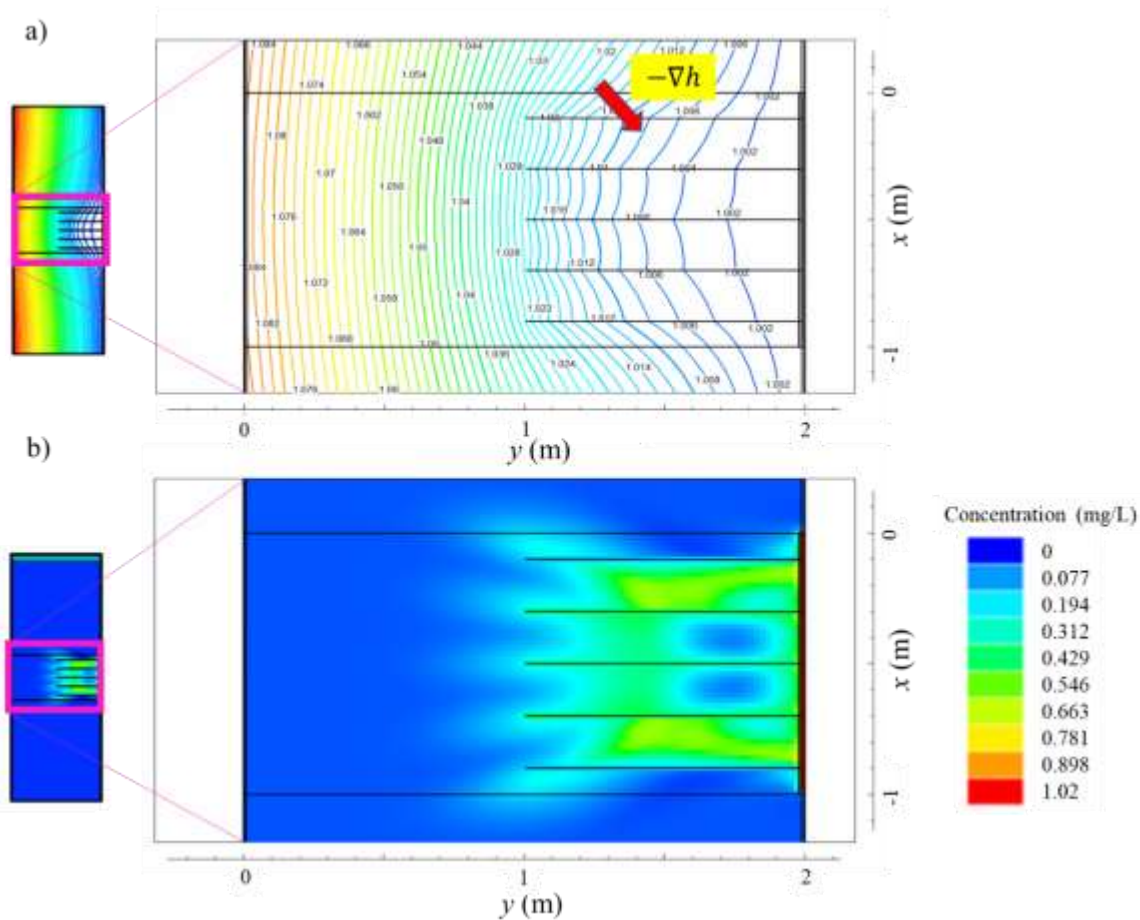


**Figure 3.8. a) Plan view potentiometric contours showing transverse head gradients 18.9 hrs. after the start of the peak flow event. Red contours correspond to higher head, and blue contours correspond to lower head. b) Plan view nitrate concentration map showing nitrate pushed back into the matrix between the pipes. The concentration maps are cropped from the larger domain to show more detail.**

### 3.4.1.3 High Dispersivity Enhances Nitrate Storage on “Potentiometric Shelves”

$D/D_0$  increased with  $\alpha_L$  at high  $\rho$  (Figures 3.2e and 3.4b). High  $\alpha_L$  induced the nitrate plume to spread out more and get trapped on “potentiometric shelves” (Figure 3.9a) beyond the ends of the soil pipes away from the channel as water started to return to the pipes (Figure 3.9b). This led to mildly increased denitrification relative to lower  $\alpha_L$ . This phenomenon is similar to the way the phase lag between an upslope and stream stage boundary condition in Schmadel et al. (2016) causes water parcels to stall in riparian aquifers, thereby extending RT.

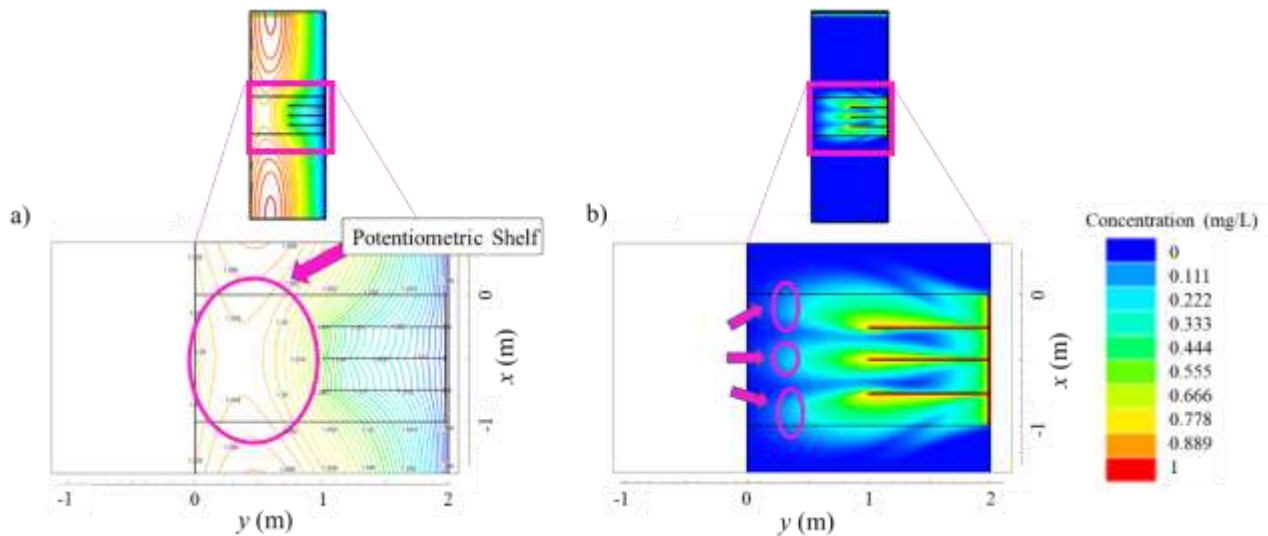


**Figure 3.9. Plan view maps for model runs late in the simulation of a) hydraulic head showing a “potentiometric shelf” 7.33 hours after the start of the peak flow event and b) its effects on nitrate transport for high longitudinal dispersivity ( $\alpha_L=0.02$  m) at 8.66 hours. In panel a) red contours correspond to higher head, and blue contours correspond to lower head. The slightly later time in b) depicts solute that has been stuck on the shelf formed roughly an hour earlier. The concentration maps are cropped from the larger domain to show more detail.**

### 3.4.1.4 Soil Pipes Being Situated Above Baseflow Leads to Stranded Nitrate Plumes

The shape of the relationship between soil pipe height above baseflow channel stage ( $H$ ) and increase in denitrification due to addition of a single ( $\rho=1$  m<sup>-1</sup>) one meter long ( $L=1$  m) soil pipe where  $K=10^{-4}$  m/s (we divide  $D$  computed at each  $H$  by  $D_0$ , hence  $D/D_0$ ) was similar to that for hyporheic volume ( $V/V_0$ ) for the base case reaction rate ( $k = 6$  days<sup>-1</sup>; Figure 3.2c). Yet the  $D/D_0$  and  $V/V_0$  curves diverge for slower-reacting soil ( $k = 0.6$  days<sup>-1</sup>) when the soil pipe is above the baseflow channel stage (i.e.  $H > 0$ ). This divergence for lower  $k$  was caused later in the simulation when dropping water levels in the channel caused water receding toward the channel

in the soil to drop below the pipes and get caught in much slower moving water in the soil matrix rather than continuing to exit via the pipes (Figure 3.10 and Animation SI 11). The effects on  $D/D_0$  of the water table dropping below the soil pipes was significant for the slower-reacting soil but not the base case because the latter situation is not as kinetics limited, and thus the additional RT does not have the same effect on denitrification (see also Section 3.4.2).

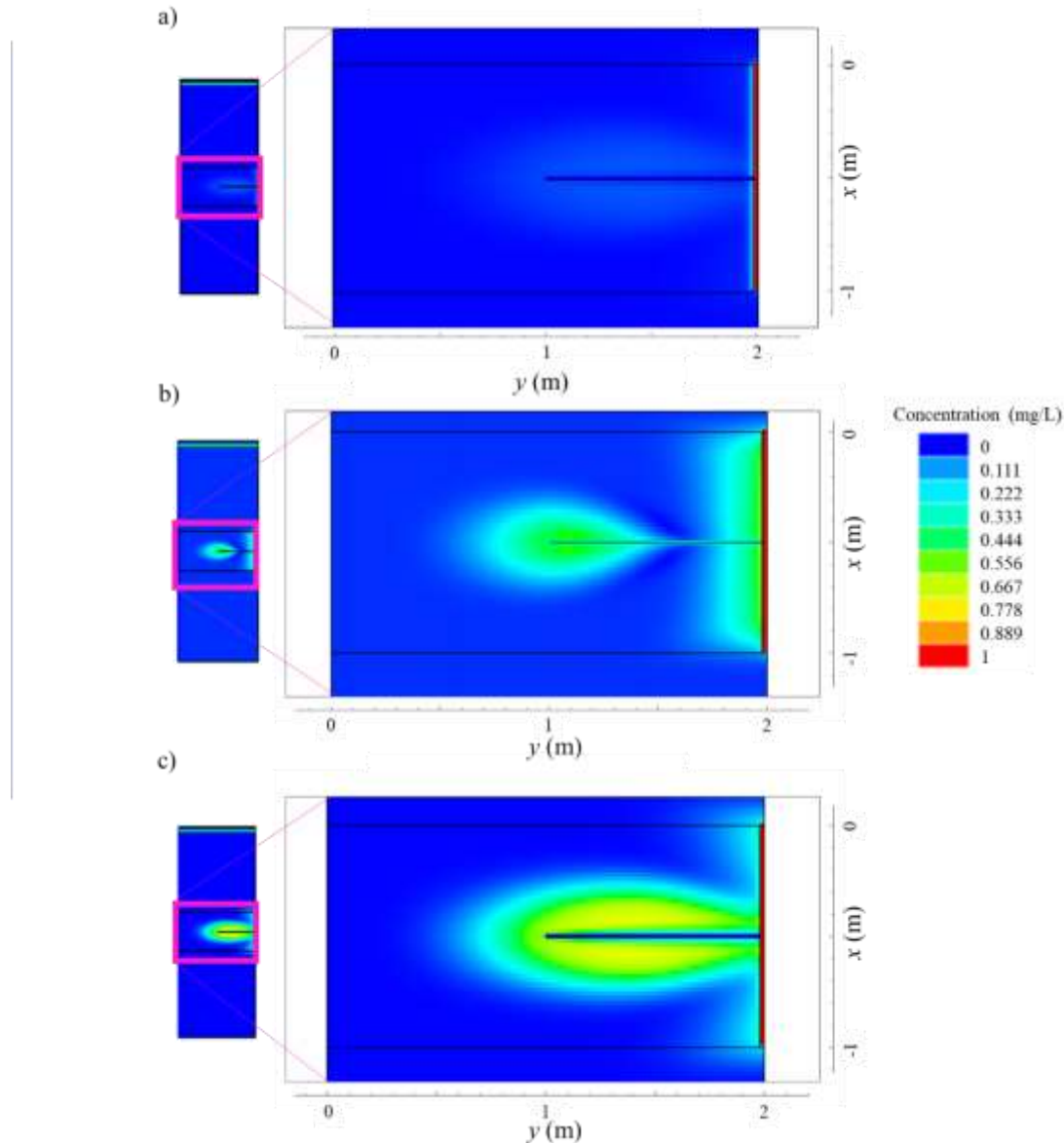


**Figure 3.10. Plan view nitrate concentration maps for 16.7 hrs. after the start of the peak flow event for a) soil pipe height above channel stage ( $H = 0.1$  m for reaction rate ( $k = 6$  days $^{-1}$ ); b) for  $H = -0.5$  for reaction rate ( $k = 0.6$  days $^{-1}$ ); and c) for  $H = 0.1$  m for reaction rate ( $k = 0.6$  days $^{-1}$ ). Note for the slow reacting soils for  $H = -0.5$  m, much of the nitrate has**

left via the pipe, but in the  $H = 0.1$  m case the nitrate plume is trapped in the soil matrix beneath the pipe, most of which will be denitrified. In the  $6 \text{ days}^{-1}$  case the water particles emanating from the soil pipes at the start of the scenario are still in the soil matrix; however, all of the nitrate has biodegraded. Hydraulic conductivity ( $K$ ) =  $10^{-4}$  m/s and  $H=0.1$  m for both panels. The concentration maps are cropped from the larger domain to show more detail.

### 3.4.2 Relative Importance of Transport and Reaction Processes

The presence of soil pipes in a streambank alters the flow patterns of surface water-groundwater exchange, which in turn affects denitrification. From a mechanistic standpoint, the changes induced by pipes shown in Figure 3.2 can be understood by considering how they change the relative balance of transport and reaction processes by evaluating hyporheic residence RT and Damköhler number (Da). The Damköhler number (Da) is the ratio of the reaction rate to the transport rate, and is useful for quantifying the balance of reaction and transport processes, and thus determining reaction ( $Da \ll 1$ ) vs. transport ( $Da \gg 1$ ) limitation (Harvey et al., 2013; Schnoor, 1996; Zarnetske et al., 2012).

$$Da = RT \cdot k_{NO_3} \quad [3.17]$$

Normalized denitrification ( $D/D_0$ ) in a system is a function of Da and the amount of mass that enters the system, with the latter proportional to hyporheic volume. Most  $D/D_0$  curves follow the hyporheic volume  $V/V_0$  curves (Figures 3.2a and 3.3), suggesting that  $D/D_0$  in our parameter space varies predominately as a result of changes in  $V/V_0$  (Lotts and Hester, 2020). In other words,  $D/D_0$  did not vary as a result of changes in RT for most scenarios. For example, where  $Da \gg 1$  (i.e. where  $k \geq 6 \text{ days}^{-1}$  for all scenarios where  $K \leq 10^{-4}$  m/s; Figures 3.2 and 3.3), a change in RT made no difference since all the nitrate is removed for all RTs where  $Da \gg 1$ , i.e. where the system is transport limited. By contrast, a change in RT would have made a difference for scenarios with  $Da \ll 1$ , but such model runs in our study happened to not show significant changes in RT. For example, RT remained invariant as soil pipe length (L) varied (Figure 3.2a,  $k = 0.6 \text{ days}^{-1}$ ) such that associated changes in  $D/D_0$  were a result of changes induced in  $V/V_0$  but not RT. In other words, for most of the scenarios modeled herein, the dimensionless significance index,  $I_s$ , defined by Equation 10 of Gu et al. (2012) would be equal to unity ( $36 \text{ days}^{-1}$  and  $k = 6 \text{ days}^{-1}$ ) or not change with the presence or absence of soil pipes (as is the case with the L sensitivity analysis). Note that these observations are only valid for the ideal denitrification scenario with abundant DOC, no oxygen, and plenty of denitrifying bacteria.

There are two notable exceptions to transport limitation. The first occurs where the  $D/D_0$  vs. H curve for low  $k$  ( $= 0.6 \text{ days}^{-1}$ ) shows a spike for baseflow channel stage ( $H$ )  $> 0$  whereas the other curves decrease for  $H > 0$  (Figure 3.2c). In this situation, RTs are elevated because water returns to the channel via the matrix below the pipes rather than via the pipes themselves (Figure 3.11a). Moreover, the ratio of peak RT to base case RT ( $RT_{\text{peak}}/RT_{\text{base}}$ ) was 1.18, which is similar to the ratio of peak D to base case D ( $D_{\text{peak}}/D_{\text{base}}$ ) of 1.15, and reinforces that the spike in  $D/D_0$  (Figure 3.2c) was due to increased RT, which suggests reaction limitation. We should

expect the ratio for  $RT_{\text{peak}}/RT_{\text{base}}$  to be slightly more than  $D_{\text{peak}}/D_{\text{base}}$  because there is less hyporheic exchange volume with increasing  $H$  for  $H > 0$ .  $Da$  results are consistent with  $Da$  increasing for  $H > 0$  (Figure 3.11c).

The second exception to transport limitation occurs where the  $D/D_0$  vs hydraulic conductivity ( $K$ ) curve for  $K > 10^{-3.5}$  m/s decreases drastically with respect to the  $V/V_0$  curve (Figure 3.3a). This decrease in  $D/D_0$  was due to a simultaneous decrease in total mass denitrified ( $D$ , Figure 3.3b), due in turn to a decrease in  $RT$  (Figure 3.11b). For  $K > 1 \times 10^{-3.5}$  m/s, the system shifts from transport limitation to reaction limitation and nitrate has short enough  $RT$  in the riparian soil such that a good portion of nitrate is not getting removed. This is consistent with  $Da \rightarrow 2$  as  $K \rightarrow 10^{-3}$  m/s (Figure 3.11d). Note that  $Da$  was calculated with particles released immediately only at the instant when the channel switches from gaining to losing, but a more holistic residence time which includes particles released continuously all throughout the rising limb of the peak flow event would yield a  $Da$  of about half as much, so is consistent with the normal transition from transport to reaction limitation at  $Da=1$ . Accounting for aerobic respiration increases the reaction time scale, and so the system becomes transport limited at higher residence times and therefore lower  $K$ .

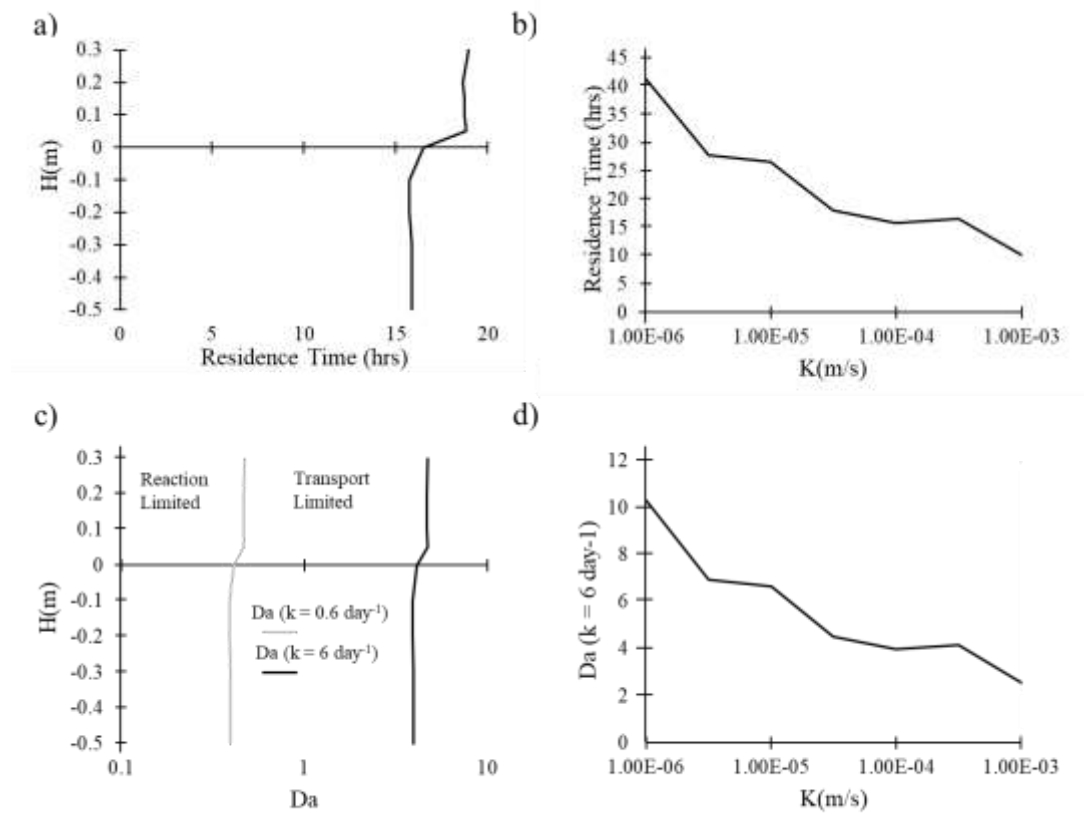


**Figure 3.11. a) Average residence times (RTs) of hyporheic flowpaths versus baseflow channel stage ( $H$ ) for 1188 water particles released at the bank face and soil pipe immediately after the channel switches from gaining to losing ( $t=0.167$  hours). b) Average**

**RT of hyporheic flowpaths vs. matrix hydraulic conductivity (K) for 1188 water particles starting at same time/locations as those in panel a. c) Damköhler number (Da) vs. baseflow channel stage (H) for slow-reacting soils ( $k = 0.6 \text{ days}^{-1}$ ) and fast-reacting soils ( $k = 6 \text{ days}^{-1}$ ). d) Da vs. matrix K for fast-reacting soils ( $k = 6 \text{ days}^{-1}$ ). Panel a) shows that average RT experiences roughly the same relative increase from the base case at  $H > 0$ , as normalized denitrification ( $D/D_0$ ) in Figure 3.2c.**

### *3.4.3 Scientific Impact and Practical Application*

Our results further the understanding of transport and reaction processes governing denitrification in riparian zones, and lay the groundwork for field studies to confirm the theoretical concepts presented here. A recurring theme is that soil pipes create strongly preferential flow which creates strongly heterogeneous nitrate flux patterns into and out of streambanks which result in increased storage and thus denitrification in certain parts of the soil matrix. In other words, soil pipes increase denitrification by simultaneously increasing flux of water and therefore nitrate into riparian groundwater from sources in the channel, and also enhancing storage of that nitrate in riparian groundwater where it then has opportunity to react.

Most scenarios we modeled were transport limited. Thus, parameters that most strongly control hyporheic volume ( $V/V_0$ ) such as matrix K and soil pipe length (L; Lotts and Hester, 2020) will also control denitrification in our scenarios. The variation of soil pipe presence and streambank soil texture along stream networks (Hester et al., 2020) will thus provide a key control on the significance of soil pipes for nitrate transport in watersheds. Key exceptions where reaction limitation occurs include slow-reacting soils ( $k = 0.6 \text{ days}^{-1}$ ), soil pipes above baseflow channel stage ( $H > 0$ ), and mildly coarse soils (matrix  $K > 1 \times 10^{-3.5} \text{ m/s}$ ). An example implication would be in urban areas where baseflow can be artificially increased or decreased (O'Driscoll et al., 2010), soil pipe vertical distribution relative to the baseflow channel stage may affect H and hence hyporheic denitrification.

A clear understanding of preferential flow in streambanks can help properly assign stream restoration credits for enhanced denitrification as pioneered in the Chesapeake Bay watershed (Altland et al., 2020; Berg et al., 2014). Stream credits are currently given for prevented sediment erosion, hyporheic denitrification, floodplain reconnection, and dry channel regenerative stormwater conveyance (Altland et al., 2020; Berg et al., 2014). Future versions of the protocols might more explicitly incorporate lung model exchange with the effects of preferential flow such as that through soil pipes. Further, our stream-corridor-scale order-of-magnitude approximation implies that soil pipes' effects on denitrification is more important for low order streams in the headwaters of a watershed (i.e. low width), in sections of the reaches that are flat (i.e. low  $S_0$ ). Therefore, location of a stream in the overall watershed may have implications in terms of soil pipe's effects on stream credit allocation.

### *3.4.4 Model Limitations and Future Study*

Currently, MT3D-USGS does not work with the CFP to model reactive transport in soil pipes. Thus, in this study, we represented soil pipes in the transport model as a boundary condition. The loss of accuracy with this approach is minimal for  $\rho=1 \text{ m}^{-1}$  because all flows in the soil matrix domain converge on the one pipe, which was most cases in this study. However, for  $\rho>1 \text{ m}^{-1}$ , transverse gradients perpendicular to the pipes pushed nitrate back into the matrix, and thus these scenarios would benefit more from explicit simulation of transport in the soil pipes themselves. Nonetheless, our existing approach still demonstrated the basic effects of such transverse gradients, and estimated the resulting added denitrification within a reasonable error bound (Section C3).

Another limitation is that our study applies only to riparian zones with favorable conditions for denitrification, where anoxic conditions, denitrifiers, and effectively infinite labile organic carbon are present. In reality, this would over-estimate denitrification in cases where aerobic respiration and nitrification occur at the upstream end of hyporheic flowpaths. Future studies could use Monod kinetics to explore the parameter space of controlling factors more broadly, and include other processes such as nitrification where important. Such a sensitivity analysis in conjunction with field surveys could also reveal exactly how prevalent transport-limitation is in nature. Nevertheless, prior studies have shown that conditions favorable for denitrification are widespread in streams (Zarnetske et al., 2012). Furthermore, in this study we are focused on trends in the effects of soil pipes on nitrate consumption rather than absolute values of consumption, and such trends are the same for both first-order and Monod kinetics (Section C.1). Finally, use of full Monod kinetics requires many additional parameters, all of which have associated uncertainty.

We further recognize that while our soil pipe dimensions are drawn from field data (Hester et al., 2020), certain aspects of our model geometry (e.g., straight pipes) is simplified relative to field conditions. Future studies could incorporate more realistic soil pipe alignments as field data become available, and Monte-Carlo simulations of randomly generated layouts could be tested creating a distribution of possible  $D/D_0$ . Nevertheless, our more conceptual conclusions regarding the impact of soil pipes on nitrate transport and storage in riparian groundwater would remain the same. Furthermore, in the cases where antecedent oxygen is significant, unsaturated zone processes need to be included to model oxygen being cycled from the above, which may affect the trends we observed.

Our model simulations represent a range of scenarios where a stage increase occurs in the channel without a similar head increase at the upslope general head boundary (Lotts and Hester, 2020). This is a reasonable approach for situations where 1) precipitation occurs only upstream of the reach (Elder et al., 1988), 2) significant lag time exists between hillslope peak and channel stage fluctuations (Holden and Burt, 2002; Jones, 1988; Jones and Crane, 1984), 3) channel fluctuations occur due to dam release schedules (Francis et al., 2010; Sawyer et al., 2009), 4) channel fluctuations occur due to snowmelt runoff (Loheide and Lundquist, 2009), and 5) channel fluctuations occur due to diel irrigation cycles (Caldwell and Eddy-Miller, 2013; Hedeff and Caldwell, 2017). Nonetheless, future studies could add this upslope forcing. For example, Schmadel et al. (2016) examined such hillslope forcing without soil pipes, and noted that the

maximum stream to aquifer flux occurs at a phase lag of 12 hr. They found that subjecting the riparian aquifer to different phase lags caused hyporheic flow path lengths and RT's to span several orders of magnitude. Hillslope forcing would therefore affect the amount of hyporheic flux (increasing or decreasing depending on phase lag), and path lengths and RT's. Moreover, there are scenarios where the impact of the unsaturated zone is significant to hyporheic flux and residence time such as high amplitude peak flow events (Welch et al., 2015), or lower soil hydraulic conductivity (Doble et al., 2012), and further research could see if the unsaturated zone's impeding of hyporheic flux would impact normalized denitrification in these scenarios.

Moreover, for our stream corridor scale model, when we varied parameters such as stream width ( $w$ ) and slope ( $S_0$ ), we kept the boundary depth at the upstream end of the channel reach constant, such that channel discharge ( $Q$ ) varied with both  $w$  and  $S_0$ . We recognize that this is only one possible way to handle the upstream boundary condition, and another valid approach would be to keep  $Q$  constant, such that upstream boundary depth would change with  $w$  and  $S_0$ . This would change trends with  $w$  and  $S_0$  but not with distance downstream or soil pipe density (Figure 3.6), nor would it change the overall order of magnitude of our range of nitrate removals. We acknowledge that  $S_0$ ,  $w$ , and soil pipe density would not remain uniform throughout the reach, and clustering of soil pipes would occur (Hester et al., 2020; Menichino et al., 2015) creating a similar effect as spacing (Figure 3.3b). Nonetheless, our model gives nascent insight into how these parameters relate to affect denitrification. More generally, this larger scale model provides only a very coarse estimate of denitrification in a narrow range of scenarios such as a dam release along a stream reach whose riparian soils remain fairly homogeneous. Nevertheless, this work provides a preliminary estimate for total stream denitrification, and a starting point for future application of more rigorous upscaling models.

Finally, the theoretical concepts uncovered by this study should be corroborated by field studies before being widely accepted. Nevertheless, this study serves as motivation for future field work and lab studies.

### 3.5 Conclusions

We simulated the effect of stream bank soil pipes on denitrification occurring during “lung model” exchange (bank storage) induced by a peak flow event in the adjacent channel. We found that denitrification increased approximately linearly with pipe density but exhibited non-linear trends with all other parameters. We found that stream bank soil pipes can significantly increase denitrification in stream banks. For example, at our base case first order reaction coefficient ( $k$ ) of  $6 \text{ days}^{-1}$ , addition of a single soil pipe 1.5 m in length led to 76% more nitrate removal, while addition of five pipes 1.0 m in length led to a 225% increase in denitrification. We found that such enhancement was caused by 1) increased flux of dissolved nitrate from the channel into the banks by the soil pipes themselves, but also 2) storage of nitrate within the bank soil matrix due to the interaction of the geometric configuration soil matrix surrounding the pipes and the dynamic head reversals occurring in response to the peak flow event in the adjacent channel.

Among the model scenarios in our sensitivity analysis, denitrification was generally either transport limited as quantified by Damköhler Number ( $Da \gg 1$ ), and/or the sensitivity did not impact residence time (such with  $D/D_0$  at  $k = 0.6 \text{ days}^{-1}$ ). In such cases, total mass denitrified in peak-flow induced lung model hyporheic exchange ( $D$ ) normalized to that for no soil pipes (i.e.  $\rho=0$ ;  $D/D_0$ ) was driven by volume of hyporheic exchange that occurred over the rising and falling limbs of the peak flow event in the neighboring channel (normalized hyporheic volume,  $V/V_0$ ).  $V/V_0$  was in turn controlled by the hydraulic and geomorphic parameters soil matrix hydraulic conductivity ( $K$ ), soil pipe length ( $L$ ), and  $\rho$ . According to our sensitivity analysis,  $D/D_0$  was most sensitive to  $\rho$  and  $L$ . For reactive-transport parameters,  $D/D_0^*$  ( $D/D_0$  normalized by a  $D_0$  that varies with soil matrix or reactive transport parameter) was most sensitive to longitudinal dispersivity ( $\alpha_L$ ) and  $k$  particularly for  $\rho \geq 3 \text{ m}^{-1}$ .

There were two particular situations where  $D/D_0$  was reaction limited ( $Da \ll 1$ ) and governed by RT. The first occurred with low reaction rate constant ( $k = 0.6$ ) and initial water surface elevation below the soil pipes ( $H > 0$ ), where nitrate plumes became stranded in the slow-moving matrix on the falling limb of the hydrograph, when water migrating back to the stream drops below the soil pipes. The second exception to transport limitation occurred when hydraulic conductivity was large ( $K = 10^{-3} \text{ m/s}$ ), leading reduced nitrate removal due to low RTs.

Our stream corridor scale results indicate that channel slope ( $S_0$ ) is important in controlling the cumulative effect of stream bank hyporheic denitrification along longer lengths ( $\geq 1 \text{ km}$ ) of channel. Our simple upscaling showed that hyporheic denitrification can remove about 3% of nitrate over a 1 km reach. Removal increased with decreasing channel slope ( $S_0$ ), increasing channel width ( $w$ ), increasing distance down the channel, and increased soil pipe density. We note that trends with  $S_0$  and  $w$  are due in part to the choice of constant upstream boundary depth among model scenarios. These findings also provide understanding useful to watershed and water quality management engineers and scientists in consideration of adjustments to stream restoration protocols and water quality management practices.

## Acknowledgements

The authors thank the National Science Foundation under award #1446481 for support to W. Lotts and E. Hester. The opinions expressed are those of the authors and not necessarily those of the NSF. The authors also thank the Sussman Foundation and Charles E. Via, Jr. Fellowship for support to W. Lotts. Data are published at Hydroshare: <https://doi.org/10.4211/hs.e8efd71614214497998591661529f69c>.

## References

- Allen, D.C. and Vaughn, C.C. 2009. Burrowing behavior of freshwater mussels in experimentally manipulated communities. *Journal of the North American Benthological Society* 28(1), 93-100.
- Altland, D., Becraft, C., Berg, J., Brown, T., Burch, J., Clearwater, D., Coleman, J., Crawford, S., Barbara, D., Geratz, J., Hanson, J., Hartranft, J., Hottenstain, J., Kaushal, S., Lowe, S.,

- Mayer, P., Noe, G., Oberholzer, W., Parola, A., Scott, D., Stack, W., Sweeney, J. and White, J. 2020. Consensus Recommendation to Improve Protocols 2 and 3 for Defining Stream Restoration Pollutant Removal Credits. Chesapeake Bay Program. .
- Anderson, A.E., Weiler, M., Alila, Y. and Hudson, R.O. 2009. Subsurface flow velocities in a hillslope with lateral preferential flow. *Water Resources Research* 45, 1-15.
- Aubertin, G.M. 1971. Nature and extent of macropores in forest soils and their influence on subsurface water movement. Res. Pap. NE-192. Upper Darby, PA: U.S. Department of Agriculture, Forest Service, Northeastern Forest Experiment Station. 33 p.
- Beasley, R.S. 1976. Contribution of subsurface flow from the upper slopes of forested watersheds to channel flow. *Soil Science Society of America Journal* 40, 955-957.
- Bedekar, V., Morway, E.D., Langevin, C.D. and Tonkin, M. 2016. MT3D-USGS version 1: A U.S. Geological Survey release of MT3DMS updated with new and expanded transport capabilities for use with MODFLOW:. U.S. Geological Survey Techniques and Methods 6-A53, 69p.
- Berg, J., Burch, J., Cappuccitti, D., Filoso, S., Fraley-McNeal, L., Goerman, D., Hardman, N., Kaushal, S., Medina, D. and Meyers, M. 2014. Recommendations of the Expert Panel to Define Removal Rates for Individual Stream Restoration Projects. Chesapeake Bay Program.
- Bergstrom, L., Karlsson, M., Bergstrom, U. and Pihl, L. 2018. Relative impact of fishing and eutrophication on coastal fish assessed by comparing a no-take area with an environmental gradient. *Ambio* 48, 565-579.
- Bernatek-Jakiel, A. and Poesen, J. 2018. Subsurface erosion by soil piping: significance and research needs. *Earth-Science Reviews* 185, 1107-1128.
- Beven, K. and Germann, P. 1982. Macropores and water-flow in soils. *Water Resources Research* 18(5), 1311-1325.
- Beven, K. and Germann, P. 2013. Macropores and water flow in soils revisited. *Water Resources Research* 49(6), 3071-3092.
- Boano, F., Harvey, J.W., Marion, A., Packman, A.I., Revelli, R., Ridolfi, L. and Worman, A. 2014. Hyporheic flow and transport processes: Mechanisms, models, and biogeochemical implications. *Reviews of Geophysics* 52, 603-679.
- Boyer, E.W., Alexander, R.B., Parton, W.J., Li, C., Butterbach-Bahl, K., Donner, S.D., Skaggs, R.W. and Del Gross, S.J. 2006. Modeling denitrification in terrestrial and aquatic ecosystems at regional scales. *Ecological Applications* 16(6), 2123-2142.
- Briggs, M.A., Hare, D.K., Boutt, D.F., Davenport, G. and Lane, J.W. 2016. Thermal infrared video details multiscale groundwater discharge to surface water through macropores and peat pipes. *Hydrological Processes* 30(14), 2510-2511.
- Brunke, M. and Gonser, T. 1997. The ecological significance of exchange processes between rivers and groundwater. *Freshwater Biology* 37(1), 1-33.
- Caldwell, R.R. and Eddy-Miller, C.A. 2013. Groundwater and surface-water interaction within the upper Smith River Watershed, Montana 2006-2010. U.S. Geological Survey Scientific Investigations Report 2013-5051, 1-88.
- Chen, X., Chen, D.Y. and Chen, X.-h. 2006. Simulation of baseflow accounting for the effect of bank storage and its implication in baseflow separation. *Journal of Hydrology* 327, 539-549.
- Chen, X. and Chen, X.H. 2003. Stream water infiltration, bank storage, and storage zone changes due to stream-stage fluctuations. *Journal of Hydrology* 280(1-4), 246-264.

- Dalu, T., Wasserman, R.J., Magoro, M.L., Froneman, W.P. and Weyl, O.L.F. 2019. River nutrient water and sediment measurements inform on nutrient retention, with implications for eutrophication. *Science of the Total Environment* 684, 296-302.
- Damashek, J. and Francis, C.A. 2018. Microbial Nitrogen Cycling in Estuaries: From Genes to Ecosystem Processes. *Estuaries and Coasts* 41, 626-660.
- DiStefano, R.J., Magoulick, D.D., Imhoff, E.M. and Larson, E.R. 2009. Imperiled crayfishes use hyporheic zone during seasonal drying of an intermittent stream. *Journal of the North American Benthological Society* 28(1), 142-152.
- Doble, R.C., Brunner, P., James, M. and Cook, P.G. 2012. An analysis of river bank slope and unsaturated flow effects on bank storage. *Groundwater* 50, 77-86.
- Dubrovsky, N.M., Burow, K.R., Clark, G.M., Gronberg, J., Hamilton, P.A., Hitt, K.J., Mueller, D.K., Munn, M.D., Nolan, B.T. and Puckett, L.J. 2010. The Quality of Our Nation's Water: Nutrients in the Nation's Streams and Groundwater, 1992-2004. USGS Circular 1350. US Department of the Interior, US Geological Survey.
- Duff, J.H. and Triska, F.J. 1990. Denitrification in sediments from the hyporheic zone adjacent to a small forested stream. *Canadian Journal of Fisheries and Aquatic Sciences* 47, 1140-1147.
- Elder, J.F., Flagg, S.D. and Mattraw Jr., H.C. 1988. Hydrology and Ecology of the Apalachicola River, Florida: A Summary of the River Quality Assessment. U.S. Geological Survey Water-Supply Paper 2196-D, D1-D46.
- Fox, G.A. and Durnford, D.S. 2003. Unsaturated hyporheic zone flow in stream/aquifer conjunctive systems. *Advances in Water Resources* 26(9), 989-1000.
- Francis, B.A., Francis, L.K. and Cardenas, M.B. 2010. Water table dynamics and groundwater-surface water interaction during filling and draining of a large fluvial island due to dam-induced river stage fluctuations. *Water Resources Research* 46.
- Garcia, M.H. (2008) Sedimentation Engineering: Processes, Measurements, Modeling, and Practice. ASCE Manual and Reports on Engineering Practice No. 110. Garcia, M.H. (ed), pp. 21-164, American Society of Civil Engineers, Reston, VA.
- Gelhar, L.W., Welty, C. and Rehfeldt, K.R. 1992. A critical-review of data on field-scale dispersion in aquifers. *Water Resources Research* 28(7), 1955-1974.
- Gerecht, K.E., Cardenas, M.B., Guswa, A.J., Sawyer, A.H., Nowinski, J.D. and Swanson, T.E. 2011. Dynamics of hyporheic flow and heat transport across a bed-to-bank continuum in a large regulated river. *Water Resources Research* 47.
- Gilles, P., O'Keefe, T.C., Edwards, R.T. and Naiman, R.J. 2009. Nitrate removal in the hyporheic zone of a salmon river in Alaska. *River Research and Applications* 25, 367-375.
- Gomez-Velez, J., Wilson, J.L., Cardenas, M.B. and Harvey, J.W. 2017. Flow and residence times of dynamic river bank storage and sinuosity-driven hyporheic exchange. *Water Resources Research* 53, 8572-8595.
- Gormally, K.H., McIntosh, M.S., Mucciardi, A.N. and McCarty, G.W. 2011. Ground-Penetrating Radar Detection and Three-Dimensional Mapping of Lateral Macropores: II. Riparian Application. *Soil Science Society of America Journal* 75(4), 1236-1243.
- Gu, C.H., Anderson, W. and Maggi, F. 2012. Riparian biogeochemical hot moments induced by stream fluctuations. *Water Resources Research* 48.
- Hack, J.T. 1957. Studies of longitudinal stream profiles in Virginia and Maryland (294B). U.S. Geological Survey.

- Harbaugh, A.W. 2005. MODFLOW-2005, the U.S. Geological Survey modular ground-water model -- the Ground-Water Flow Process: U.S. Geological Survey Techniques and Methods 6-A16. U.S. Geological Survey, Reston, VA.
- Harvey, J.W., Bohlke, J.K., Voytek, M.A., Scott, D. and Tobias, C.R. 2013. Hyporheic zone denitrification: Controls on effective reaction depth and contribution to whole-stream mass balance. *Water Resources Research* 49(10), 6298-6316.
- Hedeff, I.E. and Caldwell, R.R. 2017. Evaluating the impact of irrigation on surface water - groundwater interaction and stream temperature in an agricultural watershed. *Science of the Total Environment* 599-600, 581-596.
- Heiss, J.W., Michael, H.A. and Koneshloo, M. 2020. Denitrification hotspots in intertidal mixing zones linked to geologic heterogeneity. *Environmental Research Letters* 15, 1-10.
- Hester, E.T., Brooks, K.E. and Scott, D.T. 2018. Comparing reach scale hyporheic exchange and denitrification induced by instream restoration structures and natural streambed morphology. *Ecological Engineering* 115, 105-121.
- Hester, E.T. and Gooseff, M.N. (2011) *Stream Restoration in Dynamic Fluvial Systems: Scientific Approaches, Analyses, and Tools* Simon, A., Bennett, S.J. and Castro, J.M. (eds), American Geophysical Union, Washington, DC.
- Hester, E.T., Hammond, B. and Scott, D. 2016. Effects of inset floodplains hyporheic exchange induced by instream structures on nitrate removal in a headwater stream. *Ecological Engineering* 97, 452-464.
- Hester, E.T., McEwen, A.M., Kim, B. and Rost, E. 2020. Abundance, distribution, and geometry of naturally occurring macropores and soil pipes in stream banks. *Freshwater Science* 39.
- Hinshaw, S.E., Zhang, T., Harrison, J.A. and Dahlgren, R.A. 2020. Excess N<sub>2</sub> and denitrification in hyporheic porewaters and groundwaters of the San Joaquin River, California. *Water Resources Research* 168, 1-11.
- Holden, J. and Burt, T.P. 2002. Piping and pipeflow in a deep peat catchment. *Catena* 48(3), 163-199.
- Inoue-Choi, M., Jones, R.R., Anderson, K.E., Cantor, K.P., James, R.C., Krasner, S., Robien, K., Weyer, P.J. and Ward, M.H. 2015. Nitrate and nitrite ingestion and risk of ovarian cancer among postmenopausal women in Iowa. *International Journal of Cancer* 137, 173-182.
- Jarvis, N.J. 2007. A review of non-equilibrium water flow and solute transport in soil macropores: principles, controlling factors and consequences for water quality. *European Journal of Soil Science* 58(3), 523-546.
- Jones, J.A.A. 1988. Modelling pipeflow contributions to stream runoff. *Hydrological Processes* 2, 1-17.
- Jones, J.A.A. 2010. Soil piping and catchment response. *Hydrological Processes* 24(12), 1548-1566.
- Jones, J.A.A. and Cottrell, C.I. 2007. Long-term changes in stream bank soil pipes and the effects of afforestation. *Journal of Geophysical Research-Earth Surface* 112(F1).
- Jones, J.A.A. and Crane, F.G. 1984. Pipeflow and pipe erosion in the Maesnant experimental catchment. *Geobooks (Catchment Experiments in Fluvial Geomorphology)*, 55-72.
- Koch, J.C., Toohey, R.C. and Reeves, D.M. 2017. Tracer-based evidence of heterogeneity in subsurface flow and storage within a boreal hillslope. *hydrological Processes* 31, 2453-2463.

- Laine-Kaulio, H., Backnäs, S., Karvonen, T., Koivusalo, H. and McDonnell, J.J. 2014. Lateral subsurface stormflow and solute transport in a forester hill slope: a combined measurement and modeling approach. *Water Resources Research* 50, 8159-8178.
- Le Moal, M., Gascuel-Oudou, C., Menesguen, A., Souchon, Y., Etrillard, C., Levain, A., Moatar, F., Pannard, A., Souchu, P., Lefebvre, A. and Pinay, G. 2019. Eutrophication: A new wine in an old bottle? *Science of the Total Environment* 651, 1-11.
- Loheide, S.P. and Lundquist, J.D. 2009. Snowmelt-induced diel fluxes through the hyporheic zone. *Water Resources Research* 45, W07404.
- Lotts, W.S. and Hester, E.T. 2020. Filling the void: the effect of stream bank soil pipes on transient hyporheic exchange during a peak flow event. *Water Resources Research* 56, 1-20.
- Lunau, M., Voss, M., Erickson, M., Dziallas, C., Casciotti, K. and Ducklow, H. 2013. Excess nitrate loads to coastal waters reduces nitrate removal efficiency: mechanism and implications for coastal eutrophication. *Environment Microbiology* 15(5), 1492-1504.
- Marzadri, A., Tonina, D. and Bellin, A. 2011. A semianalytical three-dimensional process-based model for hyporheic nitrogen dynamics in gravel bed rivers. *Water Resources Research* 47.
- Mays, L.W. (2011) *Water resources engineering*, John Wiley & Sons, Inc., Hoboken, NJ.
- Menichino, G.T. and Hester, E.T. 2015. The effect of macropores on bi-directional hydrologic exchange between a stream channel and riparian groundwater. *Journal of Hydrology* 529(3), 830-842.
- Menichino, G.T., Scott, D.T. and Hester, E.T. 2015. Abundance and dimensions of naturally occurring macropores along stream channels and the effects of artificially constructed large macropores on transient storage. *Freshwater Science* 34(1), 125–138.
- Menichino, G.T., Ward, A.S. and Hester, E.T. 2014. Macropores as preferential flow paths in meander bends. *Hydrological Processes* 28 (3), 482-495.
- Mosley, M.P. 1982. Subsurface flow velocities through selected forest soils, South Island, New-Zealand. *Journal of Hydrology* 55(1-4), 65-92.
- Nguyen, T.T.N., Nemery, J., Gratiot, N., Strady, E., Tran, V.Q., Nguyen, A.T., Aime, J. and Payne, A. 2019. Nutrient dynamics and eutrophication assessment in the tropic river system of Saigon - Dongai (southern Vietnam). *Science of the Total Environment* 653, 370-383.
- O'Driscoll, M., Clinton, S., Jefferson, A., Manda, A. and McMillan, S.K. 2010. Urbanization effects on watershed hydrology and in-stream processes in the southern United States. *Water* 2, 605-648.
- Pinder, G.F. and Sauer, S.P. 1971. Numerical simulation of flood wave modification due to bank storage effects. *Water Resources Research* 7(1), 63-70.
- Pittroff, M., Frei, S. and Gilfedder, B.S. 2017. Quantifying nitrate and oxygen reduction rates in the hyporheic zone using Rn-222 to upscale biogeochemical turnover in rivers. *Water Resources Research* 53(1), 563-579.
- Pollock, D.W. 2016. User guide for MODPATH Version 7 -- a particle-tracking model for MODFLOW. U.S. Geological Survey, 35.
- Rahimi, M., Essaid, H.I. and Wilson, J.T. 2015. The role of dynamic surface water-groundwater exchange on streambed denitrification in a first-order, low-relief agricultural watershed. *Water Resources Research* 51(12), 9514-9538.

- Royer, T.V., David, M.B. and Gentry, L.E. 2006. Timing of riverine export of nitrate and phosphorus from agricultural watersheds in Illinois: Implications for reducing nutrient loading to the Mississippi River. *Environmental Science & Technology* 40(13), 4126-4131.
- Sawyer, A.H. 2015. Enhanced removal of groundwater-borne nitrate in heterogeneous aquatic sediments. *Geophysical Research Letters* 42, 403-410.
- Sawyer, A.H., Cardenas, M.B., Bomar, A. and Mackey, M. 2009. Impact of dam operations on hyporheic exchange in the riparian zone of a regulated river. *Hydrological Processes* 23(15), 2129-2137.
- Schindler, D.W. and Vallentyne, J.R. (2008) *The algal bowl: overfertilization of the world's freshwaters and estuaries*, University of Alberta Press.
- Schmadel, N.M., Ward, A.S., Lowry, C.S. and Malzone, J.M. 2016. Hyporheic exchange controlled by dynamic hydrologic boundary conditions. *Geophysical Research Letters* 43(9), 4408-4417.
- Schnoor, J.L. (1996) *Environmental Modeling*, John Wiley & Sons, Inc., New York, NY.
- Sheibley, R.W., Jackman, A.P., Duff, J.H. and Triska, F.J. 2003. Numerical modeling of coupled nitrification-denitrification in sediment perfusion cores from the hyporheic zone of the Shingobee River, MN. *Advances in Water Resources* 26(9), 977-987.
- Shoemaker, W.B., Kuniansky, E.L., Birk, S., Bauer, S. and Swain, E.D. 2007. Documentation of a Conduit Flow Process (CFP) for MODFLOW-2005. U.S. Geological Survey Techniques and Methods Book 6, Chapter A24, 50p.
- Shuai, P., Cardenas, M.B., Knappett, P.S.K., Bennett, P.C. and Neilson, B.T. 2017. Denitrification in the banks of fluctuating rivers: The effects of river stage amplitude, sediment hydraulic conductivity and dispersivity, and ambient groundwater flow. *Water Resources Research* 53(9), 7951-7967.
- Sinha, E., Michalak, A.M. and Balaji, V. 2017. Eutrophication will increase during the 21st century as a result of precipitation changes. *Science* 357(6349), 405-408.
- Stahl, M.O., Tarek, M.H., Yeo, D.C.J., Badruzzaman, A.B.M. and Harvey, C.F. 2014. Crab burrows as conduits for groundwater-surface water exchange in Bangladesh. *Geophysical Research Letters* 41(23), 8342-8347.
- Stanford, J.A. and Ward, J.V. 1988. The Hyporheic Habitat of River Ecosystems. *Nature* 335(6185), 64-66.
- Triska, F.J., Duff, J.H. and Avanzino, R.J. 1993. The role of water exchange between a stream channel and its hyporheic zone in nitrogen cycling at the terrestrial aquatic interface. *Hydrobiologia* 251(1-3), 167-184.
- Tsuboyama, Y., Sidle, R.C., Noguchi, S. and Hosoda, I. 1994. Flow and solute transport through the soil matrix and macropores of a hillslope segment. *Water Resources Research* 30, 879-890.
- USEPA 2016. National Lakes Assessment 2012: A Collaborative Survey of Lakes in the United States. EPA 841-R-16-113. U.S. Environmental Protection Agency, Washington, D.C.
- Vidon, P., Allan, C., Burns, D., Duval, T.P., Gurwick, N., Inamdar, S., Lowrance, R., Okay, J., Scott, D. and Sebestyen, S. 2010. Hot Spots and Hot Moments in Riparian Zones: Potential for Improved Water Quality Management. *J. Am. Water Resour. Assoc.* 46(2), 278-298.

- Vilmin, L., Mogollon, J.M., Beusen, A.H.W. and Bouwman, A.F. 2018. Forms and subannual variability of nitrogen and phosphorus loading to global river networks over the 20th century. *Global and Planetary Change* 163, 67-85.
- Ward, M.H., Jones, R.R., Brender, J.D., de KoK, T., Weyer, P.J., Nolan, B.T., Villanueva, C.M. and van Breda, S. 2018. Drinking Water Nitrate and Human Health: An Updated Review. *International Journal of Environment Research and Public Health* 15(7).
- Welch, C., Harrington, G.A. and Cook, P.G. 2015. Influence of Groundwater Hydraulic Gradient on Bank Storage Metrics. *Groundwater* 53, 782-793.
- Williams, D.D., Williams, N.E. and Hynes, H.B.N. 1974. Observations on the life history and burrow construction of the crayfish *Cambarus fodiens* (Cottle) in a temporary stream in southern Ontario. *Canadian Journal of Zoology* 52, 365-370.
- Wilson, G.V., Jardine, P.M., Luxmoore, R.J. and Jones, J.R. 1990. HYDROLOGY OF A FORESTED HILLSLOPE DURING STORM EVENTS. *Geoderma* 46(1-3), 119-138.
- Wilson, G.V., Nieber, J.L., Sidle, R.C. and Fox, G.A. 2013. Internal erosion during soil pipeflow: state of the science for experimental and numerical analysis. *Transactions of the Asabe* 56(2), 465-478.
- Wilson, G.V., Rigby, J.R., Ursic, M. and Dabney, S.M. 2016. Soil pipe flow tracer experiments: 1. Connectivity and transport characteristics. *Hydrological Processes* 30(8), 1265-1279.
- Wright, D.H., Lomeli, H., Hofmann, P.S. and Nguyen, C. 2011. Burrow occupancy and nesting phenology of bank swallows along the Sacramento River. *California Fish and Game* 97, 138-147.
- Zarnetske, J.P., Haggerty, R. and Wondzell, S.M. 2015. Coupling multiscale observations to evaluate hyporheic nitrate removal at the reach scale. *Freshwater Science* 34(1), 172-186.
- Zarnetske, J.P., Haggerty, R., Wondzell, S.M., Bokil, V.A. and Gonzalez-Pinzon, R. 2012. Coupled transport and reaction kinetics control the nitrate source-sink function of hyporheic zones (vol 48, W11508, 2012). *Water Resources Research* 48.
- Zhou, Y., Wilson, G.V., Fox, G.A., Rigby, J.R. and Dabney, S.M. 2016. Soil pipe flow tracer experiments: 2. Application of a streamflow transient storage zone model. *Hydrological Processes* 30(8), 1280-1291.

## **CHAPTER 4: Take it to the bank: A numerical examination of the effects of soil pipes on bypass of riparian buffer nitrate removal capacity**

Status: Submitted for publication on February 22, 2022; currently in review

**Authors:** W. Seth Lotts<sup>1</sup>, Erich T. Hester<sup>1</sup>

<sup>1</sup>Department of Civil and Environmental Engineering, Virginia Tech, Blacksburg, Virginia 24061 USA

**Corresponding Author:** Erich T. Hester, ehester@vt.edu

### **Key words:**

- Riparian Zone
- Floodplains
- Preferential Flow
- Nutrients

### **Abstract**

Streams are vital landscape ecosystems, and urbanization and modern agriculture have introduced pollutants (including excess nitrate) which threaten these waterways. Riparian zones have been shown to attenuate pollutants, and riparian buffers are commonly implemented to capture these benefits. Nevertheless, preferential flowpaths such as soil pipes have potential to bypass such attenuation. We used a MODFLOW groundwater model with the conduit flow package (CFP), along with the transport code MT3D-USGS, to simulate flow of water and nitrate through riparian groundwater to a gaining stream. We conducted a numerical sensitivity analysis to examine the impact of soil pipe presence and characteristics, as well as soil matrix characteristics, on nitrate transport and uptake by denitrification within the saturated zone. We found that in systems with long soil pipes (2.0 m), low hydraulic conductivity ( $K < 0.0035$ ), low head gradients ( $\nabla h < 10^{-4.75}$  m/s), and high reaction-constant ( $k > 4$  days<sup>-1</sup>), soil pipes increased the transport rate of nitrate across the riparian zone toward the channel by several orders of magnitude. Yet soil pipes simultaneously increased the volumetric flowrate of water across the riparian zone only by up to 3.9 times. This comparatively greater effect on transport occurred because the accelerated advection of nitrate through the soil pipes decreased the residence time available for denitrification. We created a non-dimensional parameter, the riparian bypass potential ( $\psi$ ) that accounts for key governing factors such as volumetric flowrate and Damköhler number. Nitrate bypass starts to increase by orders of magnitude above  $\psi \approx 2.75$ . Our results emphasize the importance of accounting for soil pipes when constructing riparian buffers and predicting their effects on dissolved pollutant transport.

## 4.1. Introduction

Streams and rivers act as a hotbed for biodiversity and nexus for ecological flourishing (Baxter et al., 2005; Colvin et al., 2019; Moore and Palmer, 2005), and play a pivotal role in nitrogen cycling (Peterson et al., 2001). Surface waters account for roughly 70% of drinking water in the United States (Dieter et al., 2018). Therefore, it is important to understand phenomenon which transport pathways to these vital components of our ecosystem.

Urbanization, modern agriculture, and other anthropogenic activities have added increased pollutants including nitrogen. Excess nitrogen (N), and specifically nitrate ( $\text{NO}_3^-$ ) end up in streams due to agriculture and urban development (Royer et al., 2006), and contribute to eutrophication in downstream inland and coastal surface waters around the world (Boesch et al., 2001; Dodds, 2006; Dodds et al., 2009; Kemp et al., 2005; Liu et al., 2015; Sinha et al., 2017; Struijs et al., 2011). Thus, knowledge of the efficacy and limitations of natural denitrification mechanisms in the landscape is paramount.

One of the primary natural filtration and denitrification sites is the riparian zone (Hester and Fox, 2020; Hill, 1996; Hill, 2019). The riparian zone is the strip of land immediately adjacent to the stream banks. It typically includes vegetation, an organic soil layer, unsaturated groundwater (vadose zone), and the saturated groundwater beneath. Riparian buffers are a subset of riparian zones that remove pollutants coming from adjacent human-dominated uplands (Dosskey, 1997). Riparian buffers mitigate bank erosion, enhancing geomorphic stability. They trap sediment-bound contaminants at the surface and attenuate reactive contaminants (e.g., nitrates) in groundwater from anthropogenic sources such as farms, commercial areas, and industrial parks (Fennessy and Cronk, 1997; Mayer and Canfield, 2018; Osborne and Kovacic, 1993; Stutter et al., 2019; Turunen et al., 2019). Unfortunately, various bypass mechanisms offer ways nitrate and other pollutants can circumvent the riparian zone, undermining its filtering capabilities (Inamdar, 2006; O'Donnell and Jones, 2006; Steiness et al., 2021).

One bypass mechanism in riparian groundwater is preferential flow, a phenomenon where a slender portion of soil or sediment exhibits significantly faster flow than the rest of the surrounding area and accounts for a significant portion of the flow in the entire domain (Allaire et al., 2015; Angier and McCarty, 2008; Angier et al., 2001; Angier et al., 2005; Ashby et al., 1998; Bohlke and Denver, 1995; Bohlke et al., 2007; Burt et al., 1999; Devito et al., 2000; Fox et al., 2011; Heeren et al., 2010; Hill et al., 2000; McCarty et al., 2007; O'Driscoll and DeWalle, 2010; Orozco-Lopez et al., 2018; Smethurst et al., 2014; Williams et al., 2014). Soil pipes are a particular type of preferential flow path common along banks of lower order streams (Hester et al., 2020; Menichino et al., 2015). Macropores and soil pipes short circuit hydrologic flow between an agricultural catchment and the stream, allowing pesticides and fertilizers to circumvent or bypass the soil matrix and associated processes (Bernatek-Jakiel et al., 2017). Effluent from soil pipes and macropores can contribute more than half the total nitrate load to channels (Bohlke et al., 2007). While the ability of preferential flow paths to undermine riparian buffer functions has been established, the effects of soil pipe characteristics on riparian nitrate removal have not been systematically quantified.

We seek to quantify the relationships between soil pipe and soil matrix characteristics and riparian bypass of a widespread pollutant, excess nitrate. We used numerical methods to explore the effects of soil pipe length, diameter, density, and the effects of soil matrix hydraulic

conductivity, first-order reaction constant, and hydraulic gradient on nitrate riparian bypass. We also examined the effects of gravel veins for comparison.

## 4.2. Methods

### 4.2.1 Hydraulics; Governing Equations and Boundary Conditions

We modeled riparian groundwater hydraulics adjacent to a gaining stream or river using MODFLOW (Harbaugh, 2005) to solve the 2D transient, unconfined, isotropic, saturated groundwater flow (Boussinesq) equation (Equation 4.1). We ran the model to steady-state on a rectangular prismatic domain, 5.5 m in the  $x$ -direction (parallel to the stream channel), 2.0 m in the  $y$ -direction (perpendicular to the stream channel), and 2.0 m in the  $z$ -direction corresponding to depth (gray area in Figure 4.1).

$$\frac{\partial}{\partial x} \left( h \frac{\partial h}{\partial x} \right) + \frac{\partial}{\partial y} \left( h \frac{\partial h}{\partial y} \right) + \frac{R}{K} = \frac{S_y}{K} \frac{\partial h}{\partial t} \quad [4.1]$$

Cartesian spatial coordinates (L) are denoted by  $x$ ,  $y$ , and  $z$ ;  $h$  is hydraulic head (L),  $R$  is volumetric flux per unit volume of sources and sinks ( $T^{-1}$ ),  $S_y$  is specific yield (dimensionless),  $K$  is the hydraulic conductivity of riparian soil ( $LT^{-1}$ ), and  $t$  is time (T). The model domain is similar to Lotts and Hester (2020) with 275 rows and 100 columns of 2.0 cm by 2.0 cm computational cells in the  $x$  and  $y$  directions, respectively. The model also had one layer 2.0 m thick with a spatially varying water table. The stream channel was represented with a constant head boundary (right-hand of gray area, Figure 4.1) to represent a steady-state channel flow depth of 1 m (stream channel in Figure 4.1), and remained the same throughout all sensitivity analyses. The upslope boundary (left-hand side of gray area in Figure 4.1) was also a constant head boundary, which we set to achieve a desired steady state gaining head gradient toward the channel (Section 4.2.3).

We modeled soil pipe flow in a separate domain using the Conduit Flow Package (CFP)(Shoemaker et al., 2007). The domain consisted of one or more 1D pipe segments within the saturated zone, divided into nodes which correspond in one to one fashion to cells in the soil matrix domain. The CFP applies Kirchhoff's Law (Equation 4.2) to all the nodes,  $in$ , in the pipe domain,

$$\sum_{ip=1}^{np} Q_{ip} - Q_{ex} + Q_s = 0 \quad [4.2]$$

where  $\sum_{ip=1}^{np} Q_{ip}$  is the sum of volumetric flows at node,  $in$ , coming from all pipe segments from neighboring nodes (denoted with index  $ip$ ),  $np$  is the number of pipes coming into a given node,  $Q_{ex}$  is flow from or to the matrix, and  $Q_s$  is storage (only applicable to partially filled pipes). The laminar Hagen Poiseuille equation (Equation 4.3) or the turbulent Darcy-Weisbach equation (Equation 4.4), transform Kirchhoff's Law into a function with respect to head.

$$Q_{ip} = - \frac{\pi d_{ip}^4 g (h_{in} - h_{neighbor})}{128 \nu \Delta l_{ip} \tau_{ip}} \quad [4.3]$$

$$Q_{ip} = -\sqrt{\frac{|h_{in}-h_{neighbor}|gd_{ip}^5\pi^2}{2\Delta l_{ip}\tau_{ip}}} \log\left(\frac{2.51\nu}{4\sqrt{\frac{2|h_{in}-h_{neighbor}|gd_{ip}^3}{\Delta l_{ip}\tau_{ip}}}} + \frac{k_c}{3.71d_{ip}}\right) \frac{(h_{in}-h_{neighbor})}{|h_{in}-h_{neighbor}|} \quad [4.4]$$

The flowrate for the pipe segment at index  $ip$  is given by  $Q_{ip}$  ( $L^3T^{-1}$ ); diameter (L) is expressed as  $d_{ip}$ ; gravitational acceleration ( $LT^{-2}$ ) is denoted as  $g$ ; at node index  $in$ , the head (L) is given by  $h_{in}$ ;  $h_{neighbor}$  is the head (L) at the node on other end of the pipe segment; and  $\nu$  is the viscosity ( $L^2T^{-1}$ ) of water at 25°C; the length of the pipe segment (L), the tortuosity (dimensionless), and the roughness height (L) are all given by  $\Delta l_{ip}$ ,  $\tau_{ip}$ , and  $k_c$ , respectively. The two domains are coupled at each corresponding node with an exchange term (Equation 4.5), and thereby the soil pipes act as a head dependent flux boundary condition to riparian soil matrix domain.

$$Q_{ex} = \alpha_{i,j}(h_{in} - h_{i,j}) \quad [4.5]$$

where  $Q_{ex}$  and  $\alpha_{i,j}$  are the volumetric flowrate ( $L^3T^{-1}$ ) and conductance ( $L^2 T^{-1}$ ) between the soil pipe and riparian soil at MODFLOW, respectively; and  $h_{i,j}$  is the hydraulic head (L) in cell  $i,j$  (Shoemaker et al., 2007). We set  $\alpha$  to  $6.28 \times 10^{-6}$  m<sup>2</sup>/s to match  $K$  of the surrounding soil matrix, and then varied  $\alpha$  with  $K$  in our sensitivity analysis (Sections 4.2.3). We chose to have all soil pipes connect to the stream bank, which we call “bank-facing soil pipes.” This decision reflects their documented commonness along streams (Hester et al., 2020; Menichino et al., 2015), and their heightened potential to affect the stream channel given their direct connection.

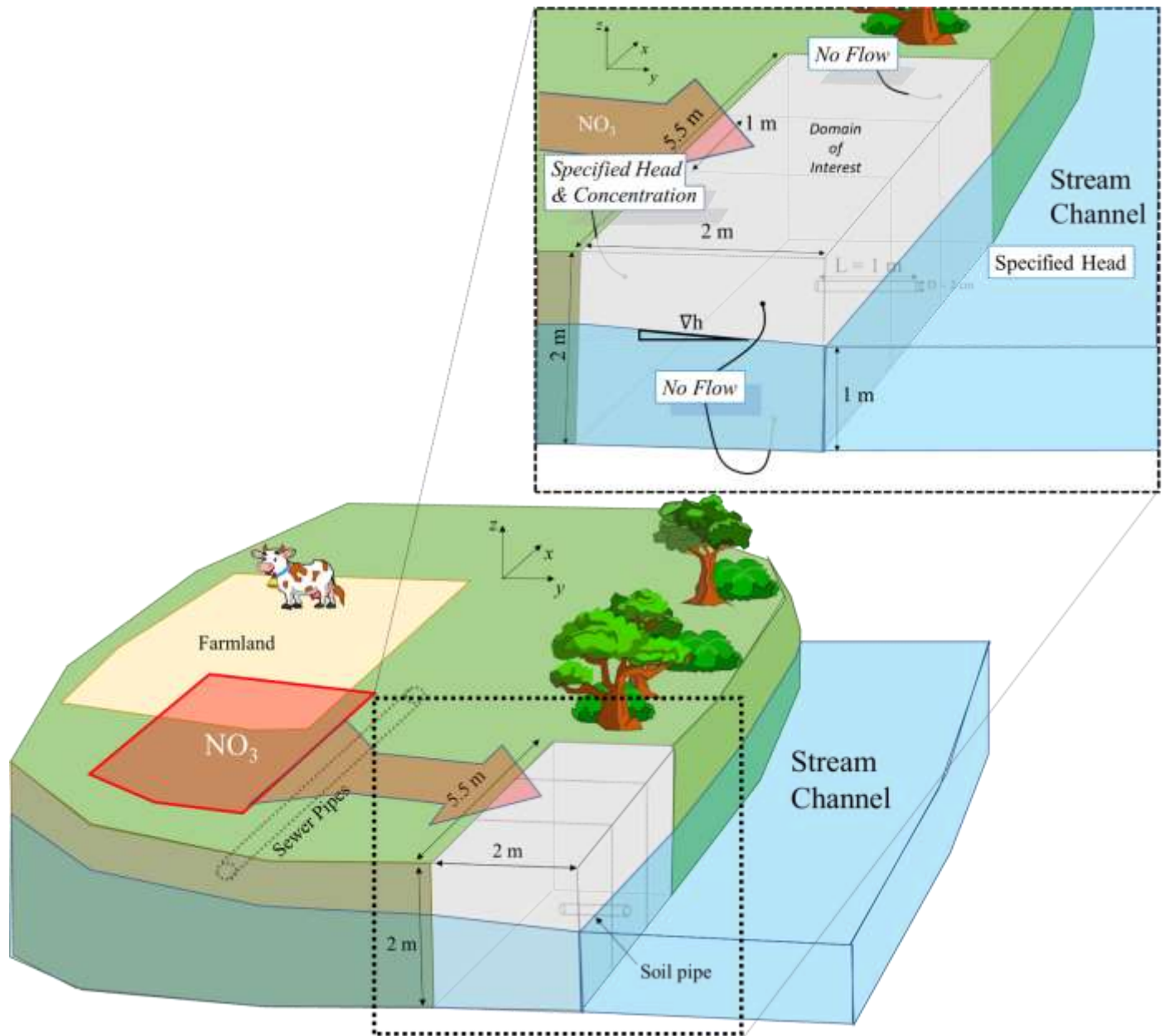


**Figure 4.1 Model schematic.** We modeled the stream and upslope boundary conditions (left and right side of gray model domain) as a steady state specified head which extended the full length of the domain. The upslope was also a specified concentration. All other boundary conditions were no flow boundaries. We recorded mass-flowrate in the 1-meter wide sub-domain called the “domain of interest.” All soil pipes connected to the bank (which we call “bank-facing”).

#### 4.2.2 Nitrate Transport; Governing Equations and Boundary Conditions

We solved the advective-transport equation in saturated groundwater using a first order reaction term in MT3D-USGS (Bedekar et al., 2016) to obtain dissolved nitrate concentration at each node in the modeling domain (gray area in Figure 4.1),

$$\frac{\partial C}{\partial t} = \frac{\partial}{\partial x_i} \left( \mathbf{D}_{ij} \frac{\partial C}{\partial x_j} \right) - \frac{\partial}{\partial x_i} (v_i C) - kC \quad [4.6]$$

where:

- C is the nitrate concentration at a given node  $i, j$ ,  $\text{ML}^{-3}$ ;
- $t$  is time, T;
- $x_i$  is the Cartesian spatial coordinate, L;
- $\mathbf{D}_{ij}$  is the hydrodynamic dispersion tensor,  $\text{L}^2 \text{T}^{-1}$ ;
- $v_j$  is the seepage or linear pore water velocity,  $\text{LT}^{-1}$ ;
- $k$  is a first order reaction rate constant  $\text{T}^{-1}$ .

We are justified in using first order kinetics since we are only interested in the ideal scenario for denitrification, i.e. the subset of riparian soils where redox conditions favor denitrification, where there is effectively infinite labile dissolved carbon, plenty of nitrate, and anoxic conditions. Riparian zones commonly exhibit anoxic conditions (Briggs et al., 2013; Cooper, 1990; Galloway et al., 2004; Hill, 2019; McDowell et al., 1992), and riparian and hyporheic zone soil waters are rich with dissolved organic carbon (Fiebig et al., 1990). First order kinetics in many cases have reliably reproduced nitrate field data in the riparian zone (Boyer et al., 2006; Gilles et al., 2009; Pittroff et al., 2017; Rahimi et al., 2015; Sheibley et al., 2003; Zarnetske et al., 2015). Furthermore, first order kinetics closely resemble Monod kinetics when nitrate concentrations are below the half-reaction constant of a typical riparian soil ( $\sim 1.64$  mg/L; Hester et al., 2018; Hester et al., 2016; Zarnetske et al., 2012), which they are for our study given we set the upslope concentration to 1.0 mg/L. Thus, first order kinetics are a parsimonious way to simulate denitrification and probe our research objectives in a way applicable to a large subset of riparian zones.

We set the upslope boundary (left-hand side of the gray area in Figure 4.1) as specified concentration of 1.0 mg/L, which represented nitrate coming from a source such as farmland or a leaky sewer pipe. While these sources would often be further than two m from the channel, our choice of 2-meter domain reflects current knowledge where very few studies map riparian soil pipes. One of the best extant studies (Gormally et al., 2011) shows many soil pipes approximately perpendicular to the stream roughly 2 or less m in length. Similarly, Menichino et al. (2015) and Hester et al. (2020) show a maximum soil pipe length of 1.2 m. The latter length data were only to the first bend in the soil pipe as measured from the bank face, and thus are underestimates in some cases, but are among the only systematic data available. We discuss the implications of these spatial layout assumptions in Section 4.4.3.

MT3D-USGS cannot directly simulate transport within conduits where flow is simulated by the CFP. Since flow in our simulated riparian soil matrix converged on the soil pipes (except in cases with more than one soil pipe where there were transverse head gradients), we simulated contaminant transport in the soil pipes with a one-way coupled model in Python 3 where we applied mass conservation to each node in the pipe domain (Equation 4.7ab). Since denitrification occurs via the biofilm attached to sediment surfaces, and there is negligible

sediment surface area in the pipes relative to that in the matrix, as a first approximation we assumed no nitrate reaction in the soil pipes.

$$(\dot{M}_{out})_{in} = (\dot{M}_{inflow})_{in} + (\dot{M}_{matrix})_{in} \quad [4.7a]$$

$$(Q_{out}C_{out})_{in} = (Q_{inflow}C_{inflow})_{in} + (Q_{ex}C_{i,j})_{in} \quad [4.7b]$$

where  $(\dot{M}_{out})_{in}$  is the mass flowrate of nitrate flowing out of pipe node, *in*, into the adjacent downslope pipe node ( $MT^{-1}$ ),  $(\dot{M}_{inflow})_{in}$  is the mass flowrate of nitrate into pipe node, *in*, from the adjacent upslope pipe node ( $MT^{-1}$ ), and  $(\dot{M}_{matrix})_{in}$  is the mass flowrate of nitrate flowing into pipe node, *in*, from the riparian soil matrix ( $MT^{-1}$ ).  $Q_{out}$  and  $Q_{inflow}$  are the flow out of and into (respectively) pipe node, *in* ( $L^3T^{-1}$ ), and  $C_{out}$  and  $C_{inflow}$  are the concentrations of nitrate flowing out of and into (from the adjacent upslope pipe node) node *in*, respectively ( $ML^{-3}$ ).  $Q_{ex}$  is the exchange term from eqn 4.5, and  $C_{i,j}$  is the concentration of the corresponding riparian soil matrix node ( $ML^{-3}$ ). Using Python 3, we extracted values from the CFP output files to populate  $Q_{out}$ ,  $Q_{inflow}$ , and  $Q_{ex}$  for all nodes, *in*, in the pipe domain, and concentration values from MT3D-USGS to populate  $C_{i,j}$ .

We calculated the mass balance across the bank face along the “domain of interest” (i.e. total mass flowing into the stream channel) as follows.

$$\dot{M}_{total} = \dot{M}_{pipe} + \dot{M}_{soil} \quad [4.8]$$

where  $\dot{M}_{total}$  is the total nitrate mass flowrate across the bank face ( $MT^{-1}$ ), and  $\dot{M}_{pipe}$  is the nitrate mass flowrate of the soil pipe(s) emptying into the stream channel ( $MT^{-1}$ ) obtained from the  $(\dot{M}_{out})_{in}$  value for the most downslope (rightmost) node in the pipe domain (eqn 4.7). We obtained  $\dot{M}_{soil}$  ( $MT^{-1}$ ) by taking the following line integral across the riparian soil/stream channel boundary,

$$\dot{M}_{soil} = \oint_0^{1m} C(x)h(x)(\vec{q}(x) \cdot \hat{j}) dx \quad [4.9]$$

where we have defined  $x = 0$  m and  $x = 1$  m as the up- and downstream ends of the domain of interest (Figure 4.1) respectively.  $C(x)$  is the concentration along the bank face which varies with  $x$  ( $ML^{-3}$ ),  $h(x)$  is the hydraulic head at the boundary which varies with  $x$  (L),  $\vec{q}(x)$  is the specific discharge at a given point along the bank face ( $LT^{-1}$ ) ( $\vec{q}(x)$  has components in  $x$  and  $y$  direction), and  $\hat{j}$  is the unit vector in the  $y$ -direction (dimensionless).

#### 4.2.3 Parameter Selection and Sensitivity Analysis

We define “riparian bypass” as the ratio of the mass flowrate of nitrate flowing from the domain of interest (Figure 4.1) to the stream channel relative to the equivalent mass flowrate with soil pipes. This shows the extent to which soil pipes intensify mass transport from the upslope pollutant source to the stream. We refer to this ratio as the normalized mass flowrate,  $\dot{M}/\dot{M}_0$  (dimensionless). It is calculated as

$$\dot{M}/\dot{M}_0 = \frac{(\dot{M}_{total})_{\rho \neq 0} m^{-1}}{(\dot{M}_{total})_{\rho = 0} m^{-1}} \quad [4.10]$$

where  $\rho = 0 \text{ m}^{-1}$  is a soil pipe density of zero soil pipes per m, and  $\rho \neq 0$  is a soil pipe per m density other than zero (1, 2, 3, 4, or 5).

We explored how a variety of both soil pipe and soil matrix parameters (Table 4.1) impact  $\dot{M}/\dot{M}_0$ . We examined the effect of three different soil pipe parameters, including soil pipe density (soil pipes per m),  $\rho$  ( $\text{L}^{-1}$ ); soil pipe length,  $L$  (L); and soil pipe diameter,  $D$  (L). We based the range of values of these parameters roughly on those for bank facing soil pipes in Hester et al. (2020) and Menichino et al. (2015). The base case was  $\rho = 1 \text{ m}^{-1}$ , since that value facilitated isolation of the effects of other parameters. We varied  $L$  from 0 m to 2 m based on the bank facing soil pipes mapped with ground penetrating radar (GPR) in Gormally et al. (2011), and we set the base case to the midpoint of that interval (1 m). The diameter range varied from 0 to 5 cm (Hester et al., 2020; Menichino et al., 2015); although there are larger soil pipes, the effects asymptote sharply after  $D = 1$  cm as the system becomes exchanged limited (Section 4.3), and the vast majority of the soil pipes in prior students have diameters below 5 cm (Hester et al., 2020). The base case was set to  $D = 2$  cm.

We examined the effect of three soil matrix parameters: matrix ( $K$ ) ( $\text{L}/\text{T}$ ), nitrate first order reaction/decay rate in the soil matrix ( $k$ ) ( $\text{T}^{-1}$ ), and head gradient perpendicular to the channel and parallel to the soil pipe ( $\nabla h$ ) ( $\text{LL}^{-1}$ ) (Figure 4.1). We varied  $\nabla h$  from 0.0025 to  $\nabla h = 0.025$  which are common in stream and river banks (Lacombe and Rosman, 1997; USGS, 2005) and allows  $\dot{M}/\dot{M}_0$  to span from very small ( $\dot{M}/\dot{M}_0 \approx 1$ ) to large ( $\dot{M}/\dot{M}_0 \approx 3 \times 10^5$ ). We varied matrix  $K$  from  $10^{-5}$  m/s to  $K = 10^{-4}$  m/s, which corresponds to fine sand, silty sand, or silt, which are common in riparian sediments (Anderson et al., 2015; Heath, 1983; Lotts and Hester, 2020), and allows  $\dot{M}/\dot{M}_0$  to span roughly the same range ( $1 - 3 \times 10^5$ ) as the selected  $\nabla h$  interval. Likewise, we varied  $k$  through a subset of the interval examined in Hester et al. (2016) from  $k = 0.6 \text{ days}^{-1}$  to  $k = 6 \text{ days}^{-1}$ , which also spans a similar range of  $\dot{M}/\dot{M}_0$  as with  $\nabla h$  and  $K$ . The base case parameters were  $\nabla h = 0.0025$ ,  $K = 10^{-4}$  m/s,  $k = 0.6 \text{ days}^{-1}$  since they were common in situ (Anderson et al., 2015; Hester et al., 2016; Lacombe and Rosman, 1997; USGS, 2005).

Since the relationships of  $\dot{M}/\dot{M}_0$  versus  $L$  were often strongly exponential (Section 4.3), we chose to conduct sensitivity analyses for each value of  $L$  throughout the entire parameter ranges of the soil matrix and reaction parameters ( $\nabla h$ , matrix  $K$ ,  $k$ ) (Table 4.1). Thus, we explored the controlling parameter space beyond a simple one-at-a-time approach. By contrast, we only conducted  $\dot{M}/\dot{M}_0$  versus  $D$  sensitivity analysis for variation in  $\nabla h$ . Similarly, we only conducted one sensitivity analysis for  $\rho$  for the base case of  $K$ ,  $k$ ,  $\nabla h$ , and  $D$ . We did not perform this at the base case for  $\nabla h = 0.025$ , since we would need two-way coupling (not just a one-way coupling) to model the water and nitrate going back into the matrix due to transverse head gradients. The one-way coupling incorrectly models water driven into the matrix by the transverse head gradient as having no nitrate. For  $\nabla h = 0.025$ , much solute would be ejected back into the matrix and ultimately end up in the stream, and modeling it as without nitrate drastically underestimates  $\dot{M}/\dot{M}_0$ . This assumption does not matter for  $\nabla h = 0.0025$ , since negligible nitrate even makes it to the pipes, and practically none of the nitrate which is ejected back into the matrix makes it to the stream.

**Table 4.1. Sensitivity Analysis Parameters.** We performed  $\dot{M}/\dot{M}_0$  vs.  $L$  sensitivity analyses for each value of  $K$ ,  $k$ , and  $\nabla h$  for a total of 225 simulations. We performed  $\dot{M}/\dot{M}_0$  vs.  $D$  sensitivity analysis for just  $\nabla h$  for a total of 110 simulations. We conducted only one sensitivity for  $\rho$  where the other parameters were set to the base case (except for  $\nabla h$ , a total of 6 simulations). The base case was  $L = 1$  m,  $D = 2$  cm,  $K = 10^{-4}$  m/s,  $k = 0.6$  days $^{-1}$ , and  $\nabla h = 0.025$ . All values that were not varied were set to the base case unless otherwise noted.

Parameter varied	Range; increment	Units	Notes
Soil pipe density, $\rho$	0–5; 1	soil pipes per m	(Lotts and Hester, 2020; Menichino et al., 2015)
Soil pipe length, $L$	0–2.0; 0.25	m	(Gormally et al., 2011)
Soil pipe diameter, $D$	0, 0.25, 0.5, 0.75, 1.0, 1.5, 2.0, 2.5, 3.0, 4.0, 5.0 <sup>†</sup>	cm	(Menichino et al., 2015) (Hester et al., 2020)
Soil matrix hydraulic conductivity, $K$	$10^{-4}$ , $10^{-4.5}$ , $10^{-4.625}$ , $10^{-4.75}$ , $10^{-4.875}$ , $10^{-4.9375}$ , $10^{-5}$ <sup>†</sup>	m/s	$S_y$ varied simultaneously to match soil texture (Anderson et al., 2015; Heath, 1983; Lotts and Hester, 2020)
Soil matrix biodegradation first order, $k$	$k_{\text{react}} = 0.6, 2, 3, 4, 5, 5.5, 5.75, 6$ <sup>†</sup>	d $^{-1}$	(Hester et al., 2016)
Soil matrix head gradient, $\nabla h$	0.0025, 0.00275, 0.003, 0.0035, 0.005, 0.00575, 0.0065, 0.00875, 0.0125, 0.025 <sup>†</sup>	m/m	(Lacombe and Rosman, 1997; USGS, 2005)

<sup>†</sup>Not a uniform interval; more simulations were conducted in intervals where  $\dot{M}/\dot{M}_0$  was more sensitive to changes in parameters.

In addition to soil pipes, preferential flow in alluvium can also occur through areas of higher permeability sediment (Fox et al., 2011; Fuchs et al., 2009). The actual hydraulic conductivity of the sediment in such preferential flowpaths can vary considerably, but for convenience we refer to all such preferential flowpaths as “gravel veins.” While the focus of our study is soil pipes, we conducted a small number of model runs on gravel veins for comparison. In particular, we compared  $\dot{M}/\dot{M}_0$  for a system with a single 1.0 m-long soil pipe to that with a single 1.0 m-long gravel vein.  $\dot{M}/\dot{M}_0$  for gravel veins is mass flow of nitrate in a system with a gravel vein divided by the mass flow of nitrate in a system without a gravel vein. We examined two gravel vein widths (0.16 m and 0.3 m wide). The widths are arbitrary, but make sense within the 1.0 m-wide domain of interest (Figure 4.1) since 0.16 m (8 cells wide) is a very narrow gravel vein, and anything much larger than 0.3 m takes up a sizeable portion of the domain. Since the height of the water table (i.e. model saturated thickness) is 1.0 m at the bank face, the cross-sectional areas of the gravel veins are 0.16 m $^2$  and 0.3 m $^2$ . We varied the hydraulic conductivity in the gravel vein ( $K_{\text{vein}}$ , ms $^{-1}$ ) from  $10^{-3.5}$  m/s to  $10^{-2}$  m/s, ( $K_{\text{vein}} = \{10^{-3.5}, 10^{-3.25}, 10^{-3}, 10^{-2.5}, 10^{-2.25}, \text{ and } 10^{-2} \text{ m/s}\}$ ), commensurate with the  $K$  range found in gravel alluvium alongside streams (Chen, 2004; Cheong et al., 2008; Fox et al., 2011; Miller et al., 2014).

#### 4.2.4 Particle Tracking and Residence Time Calculation

To determine residence times ( $\tau$ , T) of riparian groundwater flowpaths within the matrix, we used the particle tracking package MODPATH7 (Pollock, 2016). For each simulation, we released 8 particles in each cell of the upslope boundary (left-hand side of the gray area) in the domain of interest, and we extended the particle-release past the domain of interest in both directions, so that we calculated residence time for each particle crossing the bank face on the stream channel boundary of the domain of interest (right side of gray area in Figure 4.1). We then calculated the average  $\tau$  across all released particles ( $\tau_{\text{AVG}}$ ). For simplicity, we did not account for residence time in the soil pipes. This approximation is reasonable because the primary removal mechanism is the biofilm attached to the sediment surfaces in the matrix, and the sediment surface area to water volume ratio is much greater in the matrix than the soil pipes. Furthermore, the residence time in the soil pipes are orders of magnitude shorter than the matrix (e.g.  $O(10^3)$  for the base case).

The specific discharge in MODFLOW must be divided by effective porosity to account the fact that water only flows through the sediment void spaces and not through the whole cross-section, (and some of it will adhere to the porous media surface therefore not using the entire void space). Thus, MODPATH calculates the velocity of the particle as follows:  $v = -K\nabla h/\eta_e$ , where  $\eta_e$  is effective porosity. For all particle tracking purposes, we used  $\eta_e$  of 0.25, commensurate with sand, gravel, and silt (Gelhar et al., 1992).

## 4.3. Results

### 4.3.1 Sensitivity Analyses of Soil Pipe and Matrix Physicochemical Parameters

Our results show that soil pipes increased flow towards the streambank by up to 3.9 times within the range of parameter values in our sensitivity analysis (Figure 4.2). The magnitude of that increase varied depending upon the number and dimensions of the soil pipes. For example, as soil pipe length ( $L$ ) increased, the normalized flowrate of water toward the streambank,  $Q/Q_0$ , increased non-linearly up to 3.9 times that without soil pipes (Figure 4.2a). This non-linear behavior is due to a non-linear increase in the length of the isopotentials along which a line-integral of the normal fluxes determines the flux into the pipe (Figure 6 of Lotts and Hester (2020)). By contrast, as soil pipe diameter ( $D$ ) increased,  $Q/Q_0$  quickly increased to  $\sim 1.5$  and then leveled off sharply because the maximum potential pipe flow is greater than the maximum potential exchange rate between the matrix and pipe (i.e. flow in the pipe shifts from pipe-limited to exchange-limited) (Figure 2b and (Lotts and Hester, 2020)).  $Q/Q_0$  increased at a decreasing rate with soil pipe density ( $\rho$ ) since less flow can occur through the middle pipes with each pipe added for  $\rho \geq 3$  (Figure 4.2c). Neither hydraulic head gradient toward the channel ( $\nabla h$ ) nor matrix hydraulic conductivity ( $K$ ) had any effect on  $Q/Q_0$  (Figure 4.2de), since an increase in  $\nabla h$  or  $K$  increased the matrix-to-pipe flow by the same factor they increased flow from the matrix directly to the streambank.

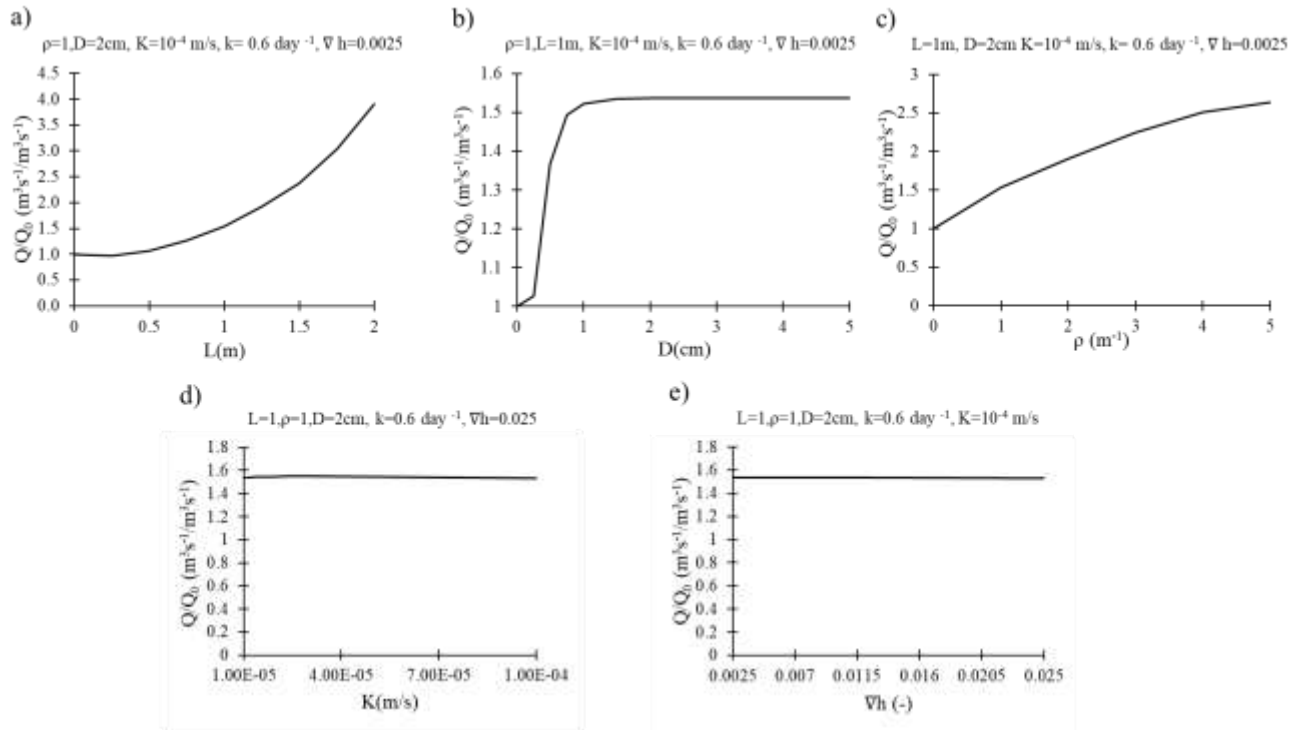


**Figure 4.2.** a) Normalized volumetric-flowrate,  $Q/Q_0$ , (volumetric flowrate of water with soil pipes divided by volumetric flowrate without soil pipes) vs. soil pipe length ( $L$ ), b) soil pipe diameter ( $D$ ), c) soil pipe density ( $\rho$ ), d) matrix hydraulic conductivity ( $K$ ), and e) hydraulic gradient ( $\nabla h$ ). All parameter values are base case conditions (Table 4.1) except for x-axis parameter, and  $\nabla h$  for panels a, b, and c.

Our results show that soil pipes also significantly increased the mass flowrate of nitrate towards the streambank (Figure 4.3). We refer to this increase as “riparian bypass”, which is quantified as the normalized mass flowrate (i.e. mass flowrate of nitrate with soil pipes divided by mass flowrate without soil pipes) ( $\dot{M}/\dot{M}_0$ ). The degree of increase (i.e. magnitude of  $\dot{M}/\dot{M}_0$ ) was highly variable depending on values of controlling parameters, yet the overall magnitude of increase was much greater than the increase in flow, ranging up to hundreds or thousands of times for most parameters. In particular,  $\dot{M}/\dot{M}_0$  grew non-linearly with  $L$  up to  $\sim 300,000x$  (Figures 4.3a).  $\dot{M}/\dot{M}_0$  initially increased rapidly with  $D$  up to  $\sim 350x$  (Figure 4.3b) but then leveled off sharply beyond  $D = 1$  cm because of similar trends in  $Q/Q_0$  (Figure 4.2b). As expected,  $\dot{M}/\dot{M}_0$  spiked as  $k$  increased towards  $6 \text{ days}^{-1}$  (Figure 4.3d).  $\dot{M}/\dot{M}_0$  also spiked sharply where  $\nabla h$  decreased towards  $0.0025$  and as  $K$  decreased towards  $10^{-5} \text{ m/s}$  (Figure 4.3ef). There appeared to be an inflection point near  $k \approx 5 \text{ days}^{-1}$ ,  $K = 1.33 \times 10^{-5} \text{ m/s}$ , and  $\nabla h = 0.005$ , where  $\dot{M}/\dot{M}_0$  started to increase by orders of magnitude with increases in  $k$ , and decreases in  $K$  and  $\nabla h$ .

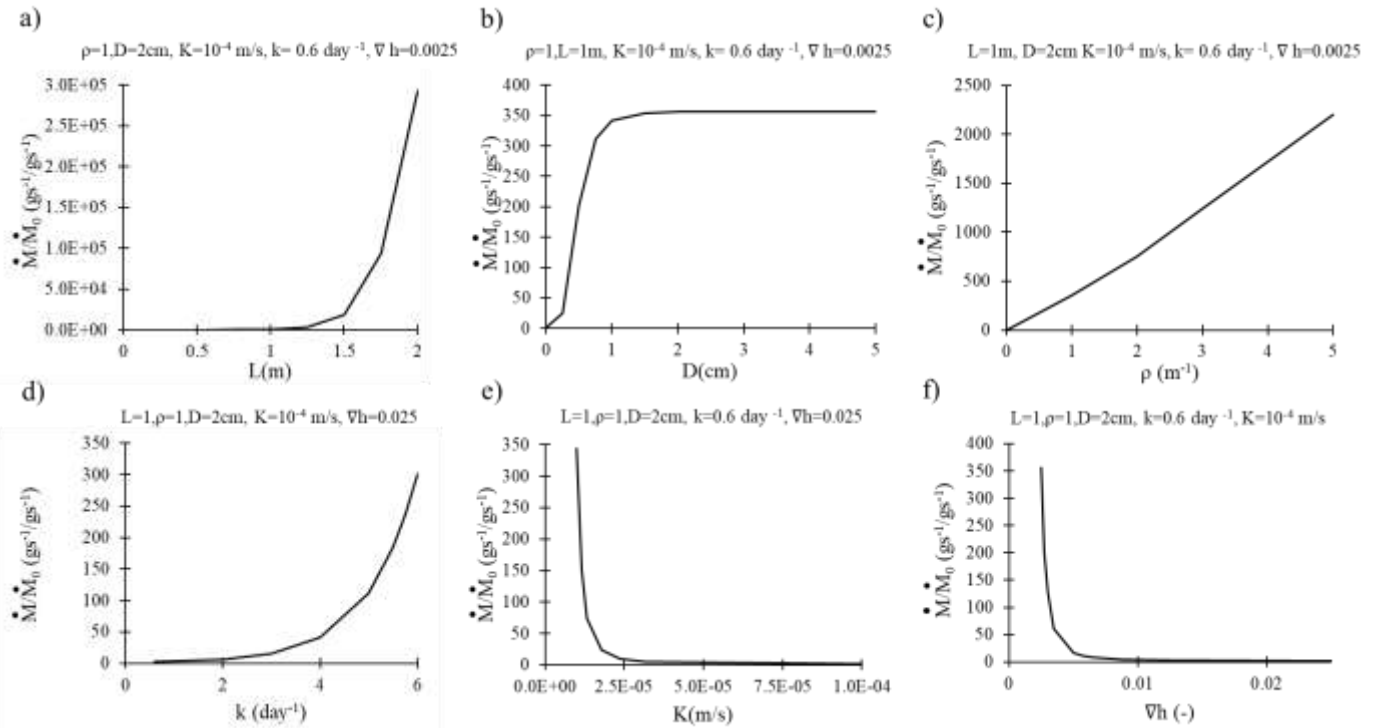


**Figure 4.3.** a) Normalized mass-flowrate ( $\dot{M}/M_0$ , mass flowrate of nitrate with soil pipes divided by mass flowrate without soil pipes) or “riparian bypass” vs. soil pipe length ( $L$ ), b) soil pipe diameter ( $D$ ), c) soil pipe density ( $\rho$ ), d) first order matrix reaction constant ( $k$ ), e) matrix hydraulic conductivity ( $K$ ), and f) hydraulic gradient ( $\nabla h$ ). All parameter values are base case conditions (Table 4.1) except for x-axis parameter, and  $\nabla h$  for panels a, b, and c.

The strong nonlinearity and high values in some parts of Figure 4.3 underscore the profoundness of the impact soil pipes can have in some settings. For this reason, we ran model runs for  $K$ ,  $\nabla h$ , and  $k$  for the full range of  $L$ , and in some cases  $D$  (Figure 4.4). This effect on  $\dot{M}/M_0$  was greatest where there was low  $\nabla h$ , low matrix  $K$ , high  $k$ , and high  $L$ .  $D$  and soil pipe density ( $\rho$ ) had less effect.

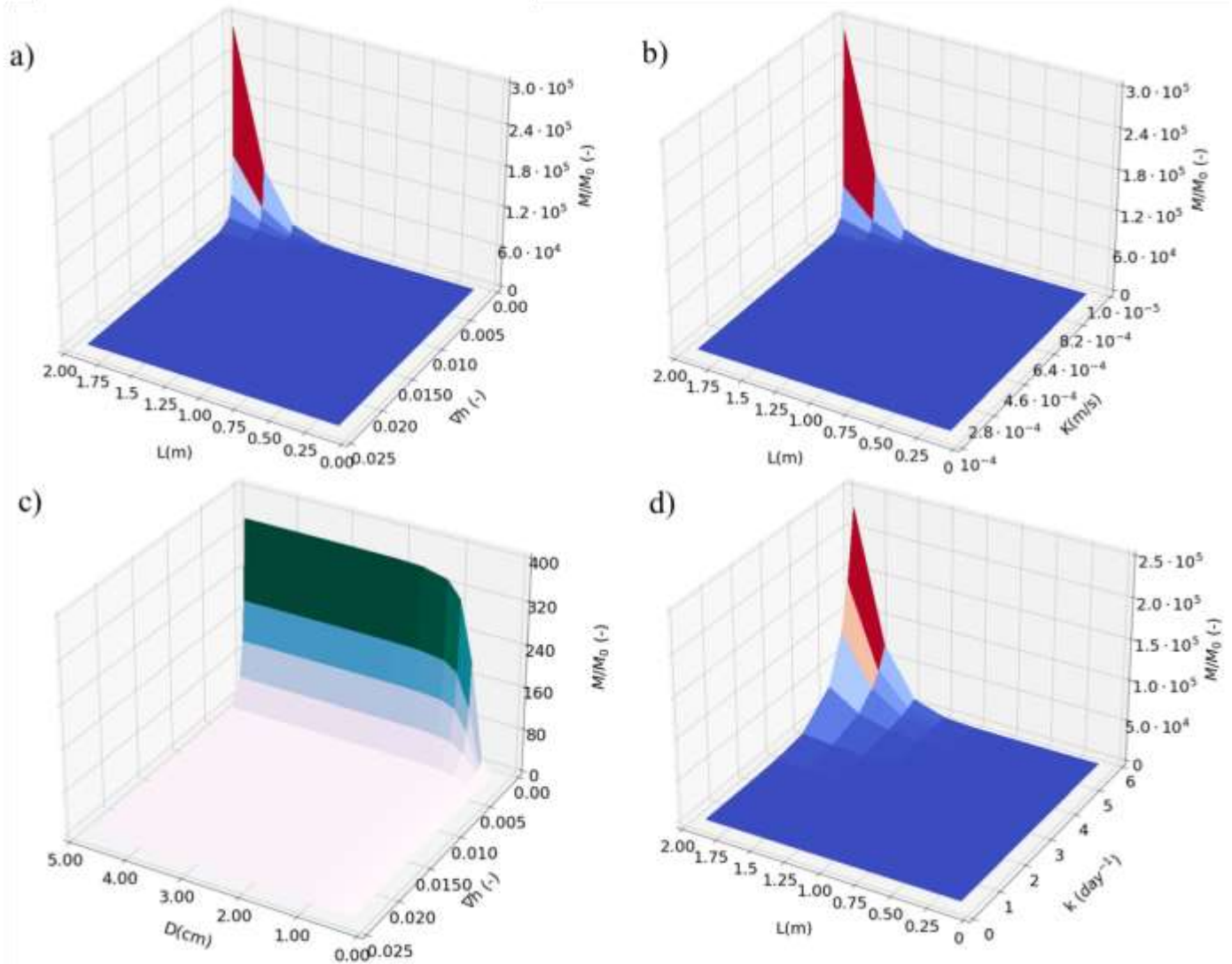


**Figure 4.4.** a) Normalized mass flowrate or “riparian bypass” ( $\dot{M}/\dot{M}_0$ ) vs. hydraulic gradient ( $\nabla h$ ) and soil pipe length ( $L$ ) (soil pipe diameter,  $D = 2$  cm, soil pipe density  $\rho = 1$ , first order matrix reaction constant  $k = 0.6$  days $^{-1}$ , matrix hydraulic conductivity  $K = 10^{-4}$  m/s); b)  $\dot{M}/\dot{M}_0$  vs.  $K$  and  $L$  ( $D = 2$  cm,  $\rho = 1$  m $^{-1}$ ,  $k = 0.6$  days $^{-1}$ ,  $\nabla h = 0.025$ ); c)  $\dot{M}/\dot{M}_0$  vs.  $\nabla h$  and  $D$  ( $L = 1$  m,  $\rho = 1$  m $^{-1}$ ,  $k = 0.6$  days $^{-1}$ ,  $K = 10^{-4}$  m/s); and d)  $\dot{M}/\dot{M}_0$  vs.  $L$  ( $D = 2$  cm,  $\rho = 1$  m $^{-1}$ ,  $\nabla h = 0.025$ ,  $K = 10^{-4}$  m/s).

Another way to highlight the importance of soil pipes and their profound impact on riparian bypass is to quantify non-normalized total mass flowrate ( $\dot{M}$ ) and how the addition of a soil pipe can compensate for lower  $\nabla h$ . For example, a system with a soil pipe where  $L = 1$  m and  $\nabla h = 0.025$  had the same  $\dot{M}$  as a system with  $L = 2$  m roughly three times as small  $\nabla h$  (Figure 4.5). A longer soil pipe was enough to increase  $\dot{M}$  by three times. Furthermore, a riparian zone with no soil pipes has the same  $\dot{M}$  of nitrate as a system with a roughly 32% flatter  $\nabla h$  with a 1 m, 2 cm diameter soil pipe (Figure 4.5).

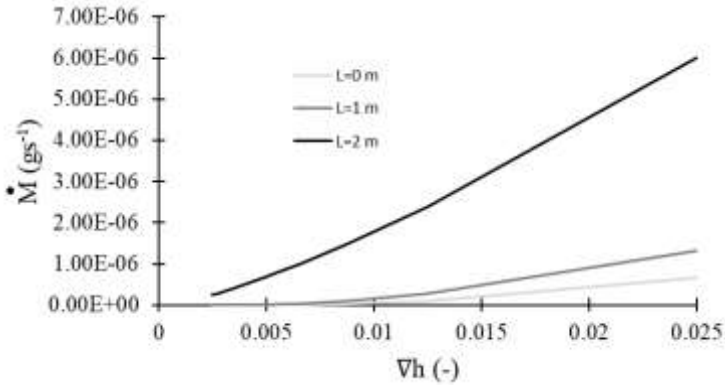


**Figure 4.5. Total mass flowrate  $\text{gs}^{-1}$  ( $\dot{M}$ ) versus hydraulic gradient ( $\nabla h$ ) for a soil pipe of lengths  $L=0$  (no soil pipes),  $L=1$ , and  $L=2$ .**

#### 4.3.2 Comparison with Gravel Veins

The overall magnitude of the effect on flow across the riparian zone of the gravel veins we simulated ( $Q/Q_0$ ) is similar in magnitude to that of the base case soil pipe (Figure 4.6a). This may seem counter-intuitive given that sediment in the gravel vein would obstruct flow relative to a soil pipe. However, the cross-sectional area of the gravel veins ( $0.3 \text{ m}^2$  and  $0.16 \text{ m}^2$ ) even after multiplying by porosity to estimate the effective cross-sectional area of pore space ( $0.075 \text{ m}^2$  and  $0.04 \text{ m}^2$ ) is still much greater than the cross-sectional area of the soil pipes ( $0.00031 \text{ m}^2$  for 2-cm diameter base case). In terms of trends,  $Q/Q_0$  for a system with gravel veins increased with the hydraulic conductivity of the gravel in the vein ( $K_{\text{vein}}$ ), but at a decreasing rate (Figure 4.6a). The rate of increase decreased because the overall  $K$  of a composite layer composed of two  $K$ s (matrix  $K$  and  $K_{\text{vein}}$ ) in series is the harmonic mean both  $K$ s, and there is diminishing return for a single  $K$ 's ability within that harmonic mean to impact the overall matrix  $K$ . In other words, flow into the faster layer is limited by flow out of the slow layer. The flowrate through the gravel vein at high values of  $K_{\text{vein}}$  is therefore exchange-limited as opposed to flow-limited.

In terms of nitrate transport, gravel veins surpass the effect of the base case soil pipe for  $K_{\text{vein}} > 0.0006 \text{ m/s}$  and  $K_{\text{vein}} > 0.0008 \text{ m/s}$  (6 and 8 times greater than the surrounding matrix) at widths  $0.30 \text{ m}$  and  $0.16 \text{ m}$  respectively (Figure 4.6b). At high values of  $K_{\text{vein}}$ , gravel veins of both widths allowed an order of magnitude more nitrate to bypass the riparian zone than the base case soil pipe. Nevertheless, soil pipes are more effective per unit of cross-sectional area, as five soil pipes cause about half of the nitrate bypass as the gravel veins (at highest values of  $K_{\text{vein}}$ ), even though the cross-sectional area of the five soil pipes is orders of magnitude less than that of the gravel veins. Also, doubling the gravel vein width caused much less than a doubling in  $\dot{M}/\dot{M}_0$ . Since the flowrate through the gravel layer is exchange-limited and the length of the gravel layer is greater versus its width, the flux across the boundary of the gravel vein and hence the flowrate within the gravel vein is not enhanced much by an increase in width. In short, increasing the width does not increase relative flux-boundary length into the gravel vein by much.

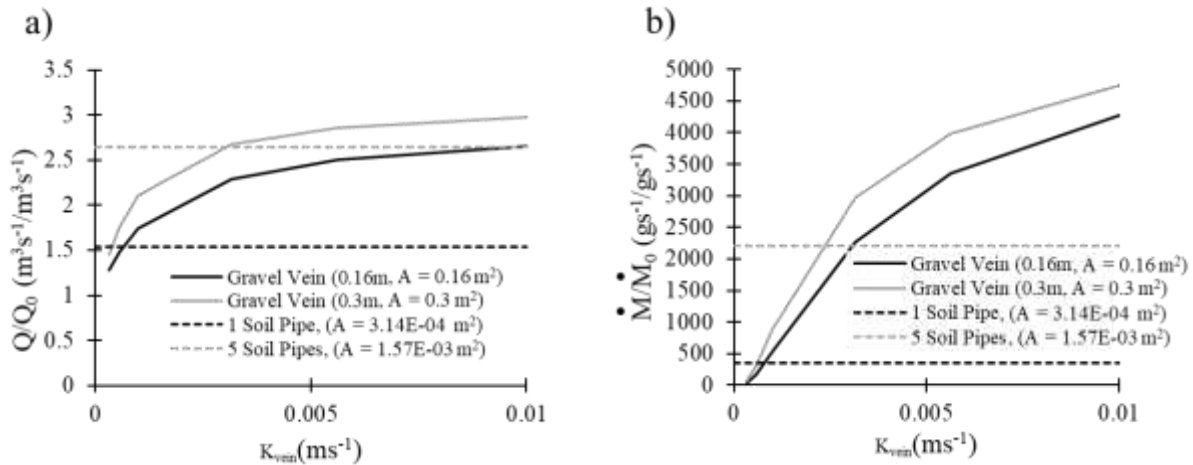


**Figure 4.6. a) Normalized volumetric flowrate,  $Q/Q_0$  (volumetric flowrate of water in a soil pipe or gravel vein system divided by volumetric flowrate of water without soil pipes or gravel veins) vs. gravel vein hydraulic conductivity ( $K_{vein}$ ) for a single 0.16 m or 0.3 m wide gravel vein. b) Normalized mass-flowrate (mass flow of nitrate with soil pipe or gravel vein divided by mass flowrate of nitrate without soil pipes or gravel veins) or “riparian bypass” ( $\dot{M}/\dot{M}_0$ ) vs.  $K_{vein}$  for a single 0.16 m or 0.3 m wide gravel vein. For both panels, the hydraulic conductivity of the matrix ( $K$ ) is kept constant at  $1.0 \times 10^{-4}$  m/s, and  $\nabla h = 0.0025$ . Cross-sectional area of the bank face is given by ( $A$ ). Gravel vein results are compared with those for the base case single soil pipe ( $L = 1$  m,  $D = 2$  cm), and a system with five soil pipes.**

## 4.4 Discussion

### 4.4.1 Significance of Normalized Concentration, Residence Time, Damköhler Number, and Normalized Riparian Flowrate on Riparian Bypass

Soil pipes enhanced the mass flowrate of nitrate ( $\dot{M}$ ) toward the channel by up to several orders of magnitude within the range of parameter values used in our sensitivity analysis (Figure 4.3), yet soil pipes only caused up to a 3.9 times increase in volumetric flowrate of water  $Q$  toward the channel within the same parameter space (Figure 4.2). Thus, the effect of soil pipes on  $Q/Q_0$  only tells part of the story of how pipes impacted nitrate migration through the riparian zone. Nevertheless, the shapes of the relationships between  $Q/Q_0$  and  $\dot{M}/\dot{M}_0$  and  $L$ ,  $D$ , and  $\rho$  were similar (compare Figures 4.2abc to 4.3abc), indicating that normalized volumetric flow is an important control, and is correlated to normalized mass flow.

By contrast, the shapes of the relationships between  $Q/Q_0$  and  $\dot{M}/\dot{M}_0$  and  $K$  and  $\nabla h$  were completely different (compare Figures 4.2de to 4.3ef). The  $Q/Q_0$  curves were flat for these parameters (Figure 4.2de) because as  $K$  and  $\nabla h$  increased, there was a simultaneous increase in volumetric flowrate through both the soil pipes and soil matrix, unlike with  $L$ ,  $D$ , and  $\rho$ , where matrix flow did not increase. Since  $Q/Q_0$  did not change with  $K$  and  $\nabla h$ , the change in  $\dot{M}/\dot{M}_0$  must have been caused by factors other than  $Q/Q_0$  increase. Normalized outlet concentration,  $C/C_0$ , (concentration where the soil pipe flows into the stream channel divided by that at the same location without soil pipes) provides insight into these other factors that contributed to increased

$\dot{M}/\dot{M}_0$  and helps explain the shape of the relationships in Figure 4.3. For example, the relationship between  $\dot{M}/\dot{M}_0$  and  $L$  is more strongly exponential than that for  $Q/Q_0$ , and the strongly exponential relationship between  $C/C_0$  and  $L$  (Figure 4.7a) can explain that difference. In particular, the product of  $Q/Q_0$  (Figure 4.2a) and  $C/C_0$  (Figure 4.7a) is roughly equal to  $\dot{M}/\dot{M}_0$  (Figure 4.3a). Similarly, the shape of the relationships between  $\dot{M}/\dot{M}_0$  and both  $K$  and  $\nabla h$  (Figure 4.3ef) almost exactly mirror those for  $C/C_0$  (Figure 4.7ef). Furthermore, gravel veins exhibited the same relationship between  $\dot{M}/\dot{M}_0$  and the combination of  $Q/Q_0$  and  $C/C_0$  (compare Figures 4.6 and 4.8). Overall then, the combination of the effect soil pipes have on both flows ( $Q/Q_0$ ) and concentrations ( $C/C_0$ ) governs the overall effect on  $\dot{M}/\dot{M}_0$ .

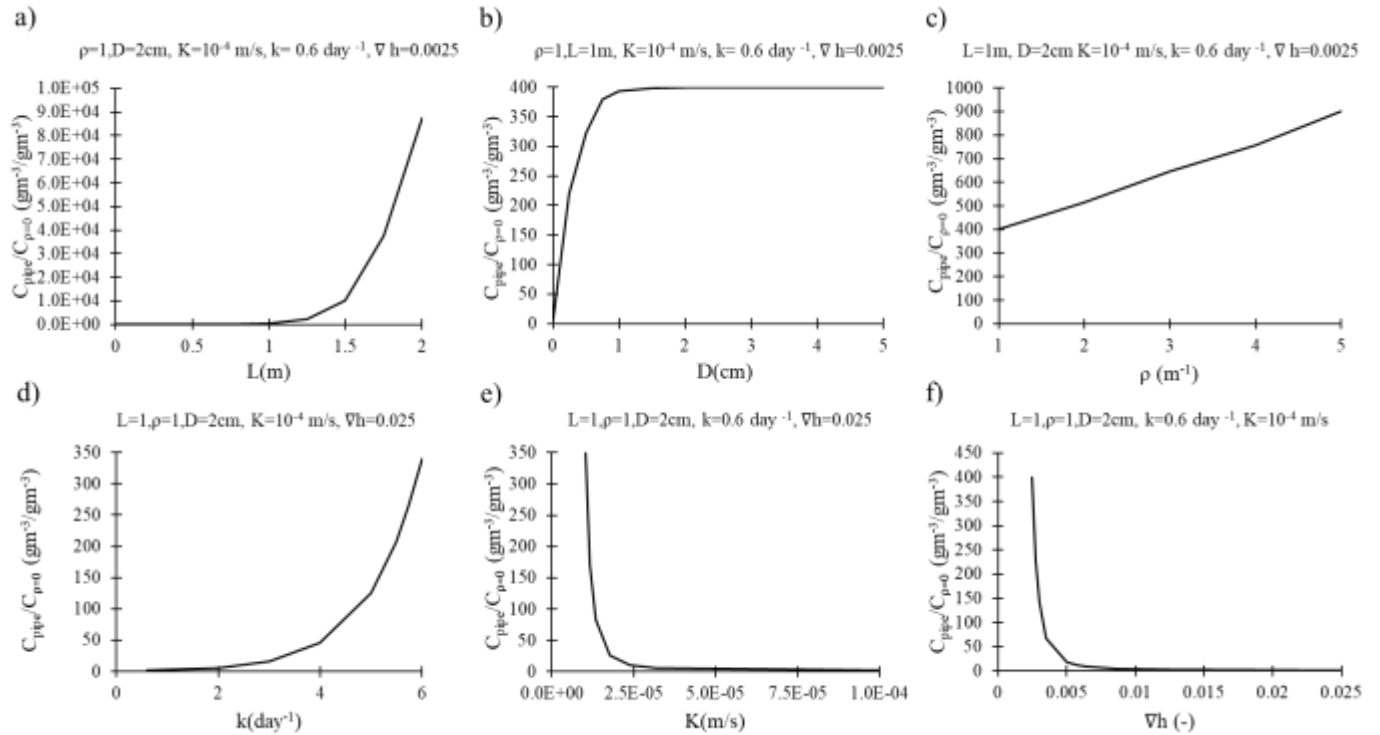


**Figure 4.7.** a) Normalized concentration ( $C/C_0$ , concentration at the outlet of the soil pipe at the channel bank face divided by the concentration at the equivalent location in the soil matrix without soil pipes) vs. soil pipe length ( $L$ ), b) soil pipe diameter ( $D$ ), c) soil pipe density ( $\rho$ ), d) first order matrix reaction constant ( $k$ ), e) matrix hydraulic conductivity ( $K$ ) and f) hydraulic gradient ( $\nabla h$ ). Note:  $C$  in  $\rho > 1$  is the flow-weighted average of the concentration in all the soil pipes. All parameter values are base case conditions (Table 4.1) except for x-axis parameter, and  $\nabla h$  for panels a, b, and c.

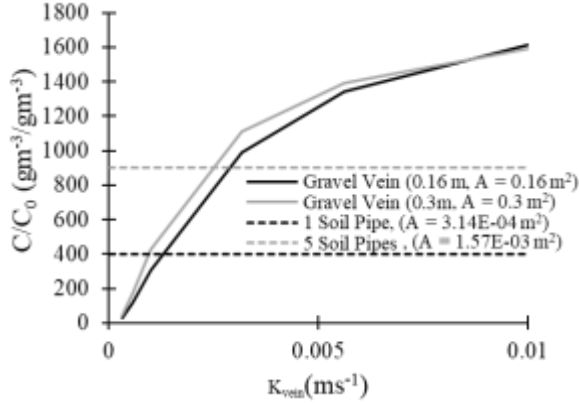


**Figure 4.8. Normalized concentration ( $C/C_0$ , flow-weighted average concentration at the outlet of the soil pipe or outlet of gravel vein versus the concentration in the matrix and bank face without soil pipes). Cross sectional areas ( $A$ ) are denoted on in the legend.**

The reason soil pipes affect  $C/C_0$  so profoundly relates to residence times. Water enters the soil pipe from the upslope and exits the soil pipe into the stream channel after a very short sojourn in the soil pipe relative to that which would occur in the matrix, and thus with significantly less nitrate attenuation than would occur without soil pipes. For example, variation of  $\nabla h$  and  $K$  had almost identical effect on average matrix residence time ( $\tau_{AVG}$ ) (e.g., a tenfold decrease in either causes the same increase in residence time), and consequently had almost identical effect on  $\dot{M}/\dot{M}_0$  (Figure 4.9ab). Thus,  $\dot{M}/\dot{M}_0$  increased non-linearly with  $\nabla h$  and  $K$  (Figure 4.3ef), the same way residence time did (Figure 4.9ab). However,  $\tau_{AVG}$  does not sufficiently explain all the variation throughout the explored parameter space for any given  $L$  value. For example,  $\tau_{AVG}$  was the same for all values of  $k$  (Figure 4.9a), yet  $\dot{M}/\dot{M}_0$  grew non-linearly with increasing  $k$  (Figure 4.3d). Thus, to more comprehensively quantify whether or not bank-facing soil pipes will have an effect on riparian bypass we use the Damköhler number ( $Da$ ), a ratio of characteristic reaction time scale to the characteristic transport time scale.  $Da$  is given by

$$Da = \tau_{AVG} k \quad [4.11]$$

where  $k$  is the first order reaction constant (Harvey et al., 2013). In systems with similar  $Q/Q_0$ , transforming  $K$ ,  $k$ , and  $\nabla h$  into  $Da$  will collapse these curves into one curve (Figure 4.9cd). Also, examining the  $\dot{M}/\dot{M}_0$  vs.  $L$  curves with combinations of  $K$ ,  $k$ , and  $\nabla h$  with roughly the same  $Da$ , show that the curve remains relatively invariant for different systems with the same  $Da$  (Figure 4.10). In other words, a tenfold decrease in  $K$  has the same effect on  $\dot{M}/\dot{M}_0$  as a tenfold decrease in  $\nabla h$  and a tenfold increase in  $k$  (i.e.  $k$  and water particle velocity have opposite effects on characteristic time scale). Thus,  $Da$  is a more efficient, comprehensive way of describing the physical phenomenon which governs  $\dot{M}/\dot{M}_0$  than just focusing on one parameter at a time. Our results show that for systems where  $L=1$  m and  $L = 2$  m, riparian bypass  $\dot{M}/\dot{M}_0$  starts to increase by orders of magnitude (i.e. reaches a threshold) where  $Da > 7$ , and  $Da > 4$ , respectively (Figure 4.9cd). Note, the slight deviation of the  $k$  curve is an artifact of our simplified method for calculating  $\tau_{AVG}$  (we did not do flow weighted residence time).

However, there are more factors that govern riparian bypass, shown by these  $Da$  thresholds varying with  $L$ . A more comprehensive factor accounts for not only the ratio of

characteristic reaction to transport time scales (i.e.  $Da$ ), but also the increase in flowrate from the bank to the stream channel. To account for this additional factor, we introduce the dimensionless riparian bypass potential ( $\psi$ ),

$$\psi = Da^{0.39} \left( \frac{Q}{Q_0} \right)^{0.61} \quad [4.12]$$

$Q/Q_0$  seemed to control the behavior of  $\dot{M}/\dot{M}_0$  more strongly than  $Da$ , indicated by being raised to a higher power. Examining  $\dot{M}/\dot{M}_0$  versus  $\psi$  shows that the data set from the six sensitivity analyses from panel a) and b) of Figure 4.4 collapse into one curve (Figure 4.9e); showing that  $\psi$  accounts for all the factors that govern  $\dot{M}/\dot{M}_0$ . Our riparian bypass metric,  $\dot{M}/\dot{M}_0$ , starts to increase by orders of magnitude at roughly  $\psi > 2.75$ . Though the riparian bypass potential only applies specifically to the six sensitivity analyses in Figure 4.9, it introduces the concept of a non-dimensional parameter which accounts not only for characteristic transport vs. reaction time scale ratios ( $Da$ ), but also soil pipe effects on flowrate and scales both by relative importance with exponents. It provides insight into the relative importance of soil pipe effects on flowrate and  $Da$ , and serves as a foundation upon which future researchers can find a non-dimensional parameter which governs riparian bypass in broader range of scenarios.

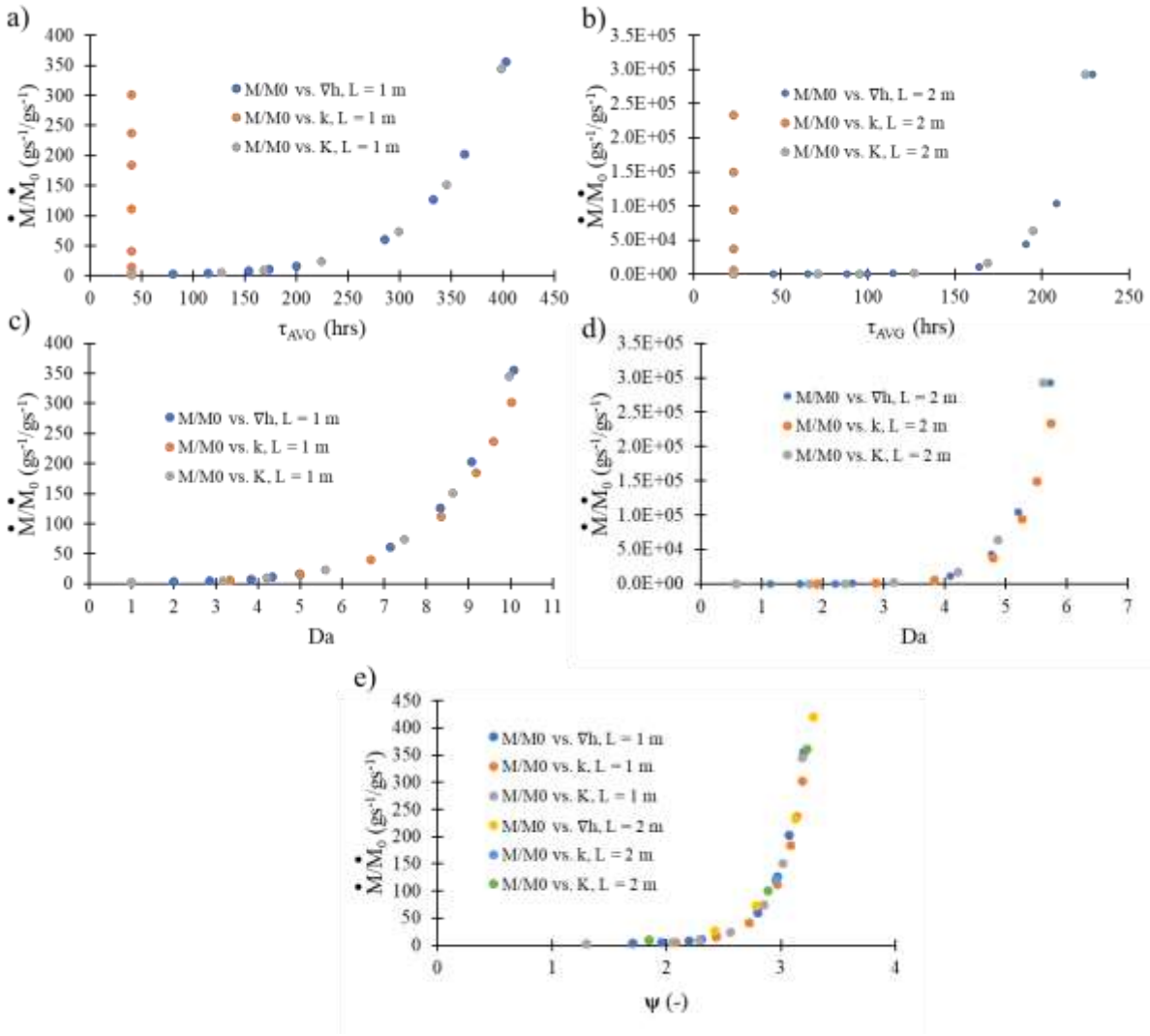


**Figure 4.9.** a) Normalized mass flowrate or “riparian bypass” ( $\dot{M}/\dot{M}_0$ ) vs. average residence time ( $\tau_{AVG}$ ) of water crossing the riparian zone through the soil matrix toward the channel for  $L = 1$  m. The curve was created from the data for three sensitivity curves; ( $\dot{M}/\dot{M}_0$ ) vs.  $\nabla h$  ( $K=10^{-4}$  m/s,  $k = 0.6$  days $^{-1}$ ), ( $\dot{M}/\dot{M}_0$ ) vs.  $K$  ( $\nabla h = 0.025$ ,  $k = 0.6$  days $^{-1}$ ), and ( $\dot{M}/\dot{M}_0$ ) vs.  $k$  ( $\nabla h = 0.025$ ,  $K=10^{-4}$  m/s). b) same as panel a) for  $L = 2$  m. ( $\dot{M}/\dot{M}_0$ ) vs. Damköhler number (Da) for soil pipe length  $L = 1$  m, with the same sensitivity analyses as in panel a). d) same as panel c) for  $L = 2$  m, and the same sensitivity analyses as in panel b). ( $\dot{M}/\dot{M}_0$ ) vs. riparian bypass potential, ( $\psi$ ). This curve was produced with data from six sensitivity analyses from the curves in panel a) and panel b). The various sensitivity analyses were denoted by the colors marked in the legends. Diameter  $D = 2$  cm, and soil pipe density  $\rho = 1$  m $^{-1}$  for all data points.

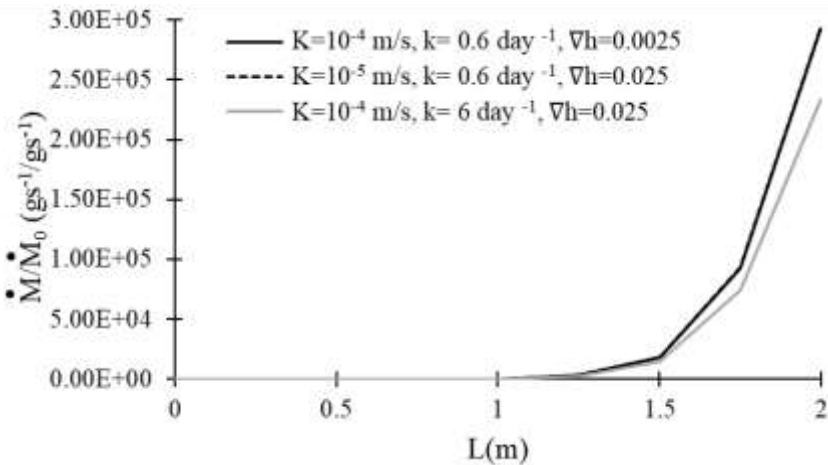


**Figure 4.10. Normalized mass flowrate or “riparian bypass” ( $\dot{M}/\dot{M}_0$ ) vs.  $L$  for three different combinations of hydraulic conductivity ( $K$ ), first order reaction constant ( $k$ ), and hydraulic gradient ( $\nabla h$ ). For any given length, each of three curves has roughly the same Damköhler number ( $Da$ ).**

#### 4.4.2 Scientific Impact and Practical Application

Removal of nitrate by the riparian aquifer is championed as one of the primary pollutant removal mechanisms of the riparian zone (Connolly et al., 2015; Groffman et al., 2002). Our study indicates that soil pipes where present can dominate how much nitrate reaches the stream, particularly for low  $\nabla h$  and matrix  $K$ . Therefore, our results show that soil pipes can undermine the effectiveness of riparian buffers, and thus soil pipes must be accounted for when riparian zones are to be used as a removal mechanism for upslope nitrate. Our study reinforces the recent field study, Steiness et al. (2021), which concluded that bypass flow from various preferential flow mechanisms accounted for a significant portion of the nitrate loads observed in streams. Further, our results also help address the challenge posed in Inamdar (2006), of what level of complexity is justified in modeling groundwater flow in riparian zones. We have shown that even large scale hydrologic models need to include enough complexity to account for small scale features such as soil pipes and other preferential flow mechanisms. By quantifying the magnitude by which soil pipes and gravel veins can induce riparian bypass, we reinforce the findings of Allaire et al. (2015) that riparian buffers would benefit from plant species with fine roots that reduce formation of soil pipes, or filters which require periodic maintenance.

We have also partially addressed another challenge posed by Inamdar (2006) regarding how processes at the riparian scale can be quantified. We crafted a non-dimensional parameter which quantifies the degree to which soil pipes cause riparian bypass. We have shown roughly at what “riparian bypass potential” a riparian buffer begins to experience bypass ( $\psi > 2.75$ ). This is a good starting point for a theoretical framework to describe riparian bypass from a mathematical perspective. Further, our results with gravel veins highlight how important preferential flow paths are in general (not just soil pipes) with respect to riparian bypass.

#### 4.4.3 Model Limitations and Future Study

Riparian buffers are generally wider than 2 m, and nitrate sources in groundwater are often farther than 2m from the channel, thus our upslope boundary condition would ideally be farther than 2 m from the channel. Nevertheless, existing field studies show that the vast majority of bank facing soil pipes are less than 2 m length. Gormally et al. (2011) showed them to be up to ~2 m in length. Menichino et al. (2015) and Hester et al. (2020) show that bank facing soil pipes average length to the first bend was roughly 0.5 m with a maximum of 1.2 m. Length to first bend is likely an underestimate for some soil pipes, and our upland boundary condition represents contaminated water ultimately stemming from the sewer pipes, so our simplification is reasonable.

We also used simplified soil pipe geometries due to the current dearth of information on the spatial layout of riparian soil pipe networks. Gormally et al. (2011) mapped bank facing soil pipes, but we are not aware of other studies that spatially mapped bank facing riparian soil pipes. It seems likely that the further into the streambank we look, the less valid our assumption of a straight perfectly perpendicular and straight soil pipe. Although there were many bank facing soil pipes approximately perpendicular to the channel in Gormally et al. (2011) and in Hester et al. (2020), there were also others with different orientations. Non-bank facing soil pipes could also be examined, and would be expected to have less of impact on flow and nitrate transport than bank facing soil pipes since there is no outlet for the nitrate in the soil pipes other than the flow-restrictive surrounding soil matrix. Thus, more field data on the spatial layout of soil pipe networks are needed, followed by numerical simulations that account for these more realistic and complex networks.

There is also room to explore other hydraulic and hydrological conditions, such as examining the effects of evapotranspiration and recharge, as these may impact the soil pipe's effects on riparian bypass. Furthermore, temporal variations for all boundary conditions could be implemented to replicate diurnal or seasonal variations to examine possible effects on riparian bypass. For example, one could implement sinusoidal temporal boundary conditions like Schmadel et al. (2016) to see if phase lag impacts soil pipes' effects on riparian bypass.

Given these limitations, our modeling offers a rough quantification, as well as a set of foundational principles upon which future studies can build. While the magnitudes of our specific  $\dot{M}/\dot{M}_0$  results should not be interpreted as applicable to all systems, they demonstrate the sheer magnitude of influence of soil pipes on riparian bypass, and the highly non-linear relationships between  $\dot{M}/\dot{M}_0$  and  $K$ ,  $k$ ,  $\nabla h$ , and  $L$ .

## 4.5 Conclusions

We modeled soil pipe impacts to flow and nitrate transport from an upslope pollutant source through a riparian buffer toward a gaining stream using MODFLOW with the CFP package and MT3D-USGS. We found that soil pipes can increase nitrate transport in this setting by several orders of magnitude in certain circumstances (low  $K$ , low  $\nabla h$ , high  $k$ , and high  $L$ ). The most sensitive soil pipe parameter was pipe length. We also found that the amount of riparian bypass is governed by a combination of effects on volumetric flowrate and residence time captured by the non-dimensional parameter we call "riparian bypass potential,"  $\psi$ , which accounts for Damköhler number (the ratio of reaction and transport characteristic timescales) and normalized volumetric flowrate. We have shown that above a riparian bypass potential of

approximately 2.75 ( $\psi > 2.75$ ), an increase in riparian bypass by orders of magnitude results. Our results, combined with the commonness of riparian soil pipes as shown by prior field studies (Menichino et al., 2015), suggest that riparian soil pipes in a riparian buffer context may benefit from mitigation either by plant species with fine roots or filtration systems.

### **Acknowledgements**

We thank the National Science Foundation under award #1446481 for support to W. Lotts and E. Hester. The opinions expressed are those of the authors and not necessarily those of the NSF. We also thank the Sussman Foundation and Charles E. Via, Jr. Fellowship for support to W. Seth Lotts. We would also like to thank Marcus Aguilar for input on riparian nitrate sources and functioning in an urban watershed context. Data will be published in Hydroshare ([www.hydroshare.org](http://www.hydroshare.org)), and a link to the data archive will be included here when the manuscript is accepted for publication.

## References

- Allaire, S.E., Sylvain, C., Lange, S.F., Theriault, G. and Lafrance, P. 2015. Potential Efficiency of Riparian Vegetated Buffer Strips in Intercepting Soluble Compounds in the Presence of Subsurface Preferential Flows. *PLoS One* 10(7).
- Anderson, M.P., Woessner, W.W. and Hunt, R.J. 2015. *Applied Groundwater Modeling: Simulation of Flow and Advective Transport*. Second Edition. Academic Press: Elsevier Inc.
- Angier, J.T. and McCarty, G.W. 2008. Variations in base-flow nitrate flux in a first-order stream and riparian zone. *Journal of the American Water Resources Association* 44(2), 367-380.
- Angier, J.T., McCarty, G.W., Gish, T.J. and Daughtry, C.S.T. 2001. Impact of a first-order riparian zone on nitrogen removal and export from an agricultural ecosystem. *TheScientificWorldJOURNAL* 1(Cited Dec 18, 2001), 642-651.
- Angier, J.T., McCarty, G.W. and Prestegard, K.L. 2005. Hydrology of a first-order riparian zone and stream, mid-Atlantic coastal plain, Maryland. *Journal of Hydrology* 309(1-4), 149-166.
- Ashby, J.A., Bowden, W.B. and Murdoch, P.S. 1998. Controls on denitrification in riparian soils in headwater catchments of a hardwood forest in the Catskill mountains, USA. *Soil Biology & Biochemistry* 30(7), 853-864.
- Baxter, C.V., Fausch, K.D. and Saunders, W.C. 2005. Tangled webs: reciprocal flows of invertebrate prey link streams and riparian zones. *Freshwater Biology* 50, 201-220.
- Bedekar, V., Morway, E.D., Langevin, C.D. and Tonkin, M. 2016. MT3D-USGS version 1: A U.S. Geological Survey release of MT3DMS updated with new and expanded transport capabilities for use with MODFLOW. U.S. Geological Survey Techniques and Methods 6-A53, 69p.
- Bernatek-Jakiel, A., Vannoppen, W. and Poesen, J. 2017. Assessment of grass root effects on soil piping in sandy soils using the pinhole test. *Geomorphology* 295, 563-571.
- Boesch, D.F., Brinsfield, R.B. and Magnien, R.E. 2001. Chesapeake Bay eutrophication: Scientific understanding, ecosystem restoration, and challenges for agriculture. *Journal of Environmental Quality* 30(2), 303-320.
- Bohlke, J.K. and Denver, J.M. 1995. Combined use of groundwater dating, chemical, and isotopic analyses to resolve the history and fate of nitrate contamination in 2 agricultural watersheds, Atlantic coastal-plain, Maryland. *Water Resources Research* 31(9), 2319-2339.
- Bohlke, J.K., O'Connell, M.E. and Prestegard, K.L. 2007. Ground water stratification and delivery of nitrate to an incised stream under varying flow conditions. *Journal of Environmental Quality* 36(3), 664-680.
- Boyer, E.W., Alexander, R.B., Parton, W.J., Li, C., Butterbach-Bahl, K., Donner, S.D., Skaggs, R.W. and Del Gross, S.J. 2006. Modeling denitrification in terrestrial and aquatic ecosystems at regional scales. *Ecological Applications* 16(6), 2123-2142.
- Briggs, M.A., Lutz, L.K., Hare, D.K. and Gonzalez-Pinzon, R. 2013. Relating hyporheic fluxes, residence times, and redox-sensitive biogeochemical processes upstream of beaver dams. *Freshwater Science* 32(2), 622-641.
- Burt, T.P., Matchett, L.S., Goulding, K.W.T., Webster, C.P. and Haycock, N.E. 1999. Denitrification in riparian buffer zones: the role of floodplain hydrology. *Hydrological Processes* 13(10), 1451-1463.

- Chen, X. 2004. Streambed hydraulic conductivity for rivers in south-central nebraska. *J. Am. Water Resour. Assoc.* 40, 561-573.
- Cheong, J.-Y., Hamm, S.-Y., Kim, H.-S., Ko, E.-J., Yang, K. and Lee, J.-H. 2008. Estimating hydraulic conductivity using grain-size analyses, aquifer tests, and numerical modeling in a riverside alluvial system in South Korea. *Hydrogeol. J.* 16, 1129-1143.
- Colvin, A.R.S., Sullivan, S.M.P., Shirey, P.D., Colvin, R.W., Winemiller, K.O., Hughes, R.M., Fausch, K.D., Infanta, D.M., Olden, J.D., Bestgen, K.R., Danehy, R.J. and Eby, L. 2019. Headwater streams and wetlands are critical for sustaining fish, fisheries, and ecosystem services. *American Fisheries Society* 44, 73-91.
- Connolly, N.M., Pearson, R.G., Loong, D., Maughan, M. and Brodie, J. 2015. Water quality variation along streams with similar agricultural development but contrasting riparian vegetation. *Agriculture Ecosystems & Environment* 213, 11-20.
- Cooper, A.B. 1990. Nitrate depletion in the riparian zone and stream channel of a small headwater catchment. *Hydrobiologia* 202, 13-26.
- Devito, K.J., Fitzgerald, D., Hill, A.R. and Aravena, R. 2000. Nitrate dynamics in relation to lithology and hydrologic flow path in a river riparian zone. *Journal of Environmental Quality* 29(4), 1075-1084.
- Dieter, C.A., Maupin, M.A., Caldwell, R.R., Harris, M.A., Ivahnenko, T.I., Lovelace, J.K., Barber, N.L. and Linsey, K.S. 2018. Estimated use of water in the United States in 2015, p. 65 p., Reston, VA.
- Dodds, W.K. 2006. Eutrophication and trophic state in rivers and streams. *Limnology and Oceanography* 51(1), 671-680.
- Dodds, W.K., Bouska, W.W., Eitzmann, J.L., Pilger, T.J., Pitts, K.L., Riley, A.J., Schloesser, J.T. and Thornbrugh, D.J. 2009. Eutrophication of US Freshwaters: Analysis of Potential Economic Damages. *Environmental Science & Technology* 43(1), 12-19.
- Dosskey, M.S., Dick; Isenhardt, Tom 1997. Riparian Buffers for Agriculture Land. *Agroforestry Notes*, USDA Forest Service.
- Fennessy, M.S. and Cronk, J.K. 1997. The effectiveness and restoration potential of riparian ecotones for the management of nonpoint source pollution, particularly nitrate. *Critical Reviews in Environmental Science and Technology* 27(4), 285-317.
- Fiebig, D.M., Lock, M.A. and Neal, C. 1990. Soil water in the riparian zone as a source of carbon for a headwater stream. *Journal of Hydrology* 116, 217-237.
- Fox, G.A., Heeren, D.M., Miller, R.B., Mittelstet, A.R. and Storm, D.E. 2011. Flow and transport experiments for a streambank seep originating from a preferential flow pathway. *Journal of Hydrology* 403(3-4), 360-366.
- Fuchs, J.W., Fox, G.A., Storm, D.E., Penn, C.J. and Brown, G.O. 2009. Subsurface Transport of Phosphorus in Riparian Floodplains: Influence of Preferential Flow Paths. *Journal of Environmental Quality* 38(2), 473-484.
- Galloway, J.N., Dentener, F.J., Capone, D.G., Boyer, E.W., Howarth, R.W., Seitzinger, S.P., Anser, G.P., Michaels, A.F., Porter, J.H., Townsend, A.R. and Vorosmarty, C.J. 2004. Nitrogen cycles: past, present, and future. *Biogeochemistry* 70, 153-226.
- Gelhar, L.W., Welty, C. and Rehfeldt, K.R. 1992. A critical-review of data on field-scale dispersion in aquifers. *Water Resources Research* 28(7), 1955-1974.
- Gilles, P., O'Keefe, T.C., Edwards, R.T. and Naiman, R.J. 2009. Nitrate removal in the hyporheic zone of a salmon river in Alaska. *River Research and Applications* 25, 367-375.

- Gormally, K.H., McIntosh, M.S., Mucciardi, A.N. and McCarty, G.W. 2011. Ground-Penetrating Radar Detection and Three-Dimensional Mapping of Lateral Macropores: II. Riparian Application. *Soil Science Society of America Journal* 75(4), 1236-1243.
- Groffman, P.M., Boulware, N.J., Zipperer, W.C., Pouyat, R.V., Band, L.E. and Colosimo, M.F. 2002. Soil nitrogen cycle processes in urban riparian zones. *Environmental Science & Technology* 36(21), 4547-4552.
- Harbaugh, A.W. 2005. MODFLOW-2005, the U.S. Geological Survey modular ground-water model -- the Ground-Water Flow Process: U.S. Geological Survey Techniques and Methods 6-A16. U.S. Geological Survey, Reston, VA.
- Harvey, J.W., Bohlke, J.K., Voytek, M.A., Scott, D. and Tobias, C.R. 2013. Hyporheic zone denitrification: Controls on effective reaction depth and contribution to whole-stream mass balance. *Water Resources Research* 49(10), 6298-6316.
- Heath, R.C. 1983. Basic ground-water hydrology: U.S. Geological Survey Water-Supply 2220. 86.
- Heeren, D.M., Miller, R.B., Fox, G.A., Storm, D.E., Halihan, T. and Penn, C.J. 2010. Preferential flow effects on subsurface contaminant transport in alluvial floodplains. *Transactions of the ASABE* 53(1), 127-136.
- Hester, E.T., Brooks, K.E. and Scott, D.T. 2018. Comparing reach scale hyporheic exchange and denitrification induced by instream restoration structures and natural streambed morphology. *Ecological Engineering* 115, 105-121.
- Hester, E.T. and Fox, G.A. 2020. Preferential Flow in Riparian Groundwater: Gateways for Watershed Solute Transport and Implications for Water Quality Management. *Water Resources Research* 56(12).
- Hester, E.T., Hammond, B. and Scott, D. 2016. Effects of inset floodplains hyporheic exchange induced by instream structures on nitrate removal in a headwater stream. *Ecological Engineering* 97, 452-464.
- Hester, E.T., McEwen, A.M., Kim, B. and Rost, E. 2020. Abundance, distribution, and geometry of naturally occurring macropores and soil pipes in stream banks. *Freshwater Science* 39.
- Hill, A.R. 1996. Nitrate removal in stream riparian zones. *Journal of Environmental Quality* 25(4), 743-755.
- Hill, A.R. 2019. Groundwater nitrate removal in riparian buffer zones: a review of research progress in the past 20 years. *Biogeochemistry* 143, 347-369.
- Hill, A.R., Devito, K.J., Campagnolo, S. and Sanmugas, K. 2000. Subsurface denitrification in a forest riparian zone: Interactions between hydrology and supplies of nitrate and organic carbon. *Biogeochemistry* 51(2), 193-223.
- Inamdar, S. 2006. Challenges in modeling hydrologic and water quality processes in riparian zones. *Journal American Water Resources Association* 42, 5-14.
- Kemp, W.M., Boynton, W.R., Adolf, J.E., Boesch, D.F., Boicourt, W.C., Brush, G., Cornwell, J.C., Fisher, T.R., Glibert, P.M., Hagy, J.D., Harding, L.W., Houde, E.D., Kimmel, D.G., Miller, W.D., Newell, R.I.E., Roman, M.R., Smith, E.M. and Stevenson, J.C. 2005. Eutrophication of Chesapeake Bay: historical trends and ecological interactions. *Marine Ecology Progress Series* 303, 1-29.
- Lacombe, P.J. and Rosman, R. 1997. Water levels in, extent of freshwater in, and water withdrawal from eight major confined aquifers, New Jersey Coastal Plain, 1993. U.S. Department of the Interior, U.S.G.S. (ed).

- Liu, T.K., Chen, P. and Chen, H.Y. 2015. Comprehensive assessment of coastal eutrophication in Taiwan and its implications for management strategy. *Marine Pollution Bulletin* 97(1-2), 440-450.
- Lotts, W.S. and Hester, E.T. 2020. Filling the void: the effect of stream bank soil pipes on transient hyporheic exchange during a peak flow event. *Water Resources Research* 56, 1-20.
- Mayer, P.M. and Canfield, T. 2018. Effectiveness of riparian buffers for managing nitrogen. National Risk Management Research Laboratory, Groundwater and Ecosystems Restoration Research, United State Environmental Protection Agency. Downloaded November 11, 2018.
- McCarty, G.W., Mookherji, S. and Angier, J.T. 2007. Characterization of denitrification activity in zones of groundwater exfiltration within a riparian wetland ecosystem. *Biology and Fertility of Soils* 43(6), 691-698.
- McDowell, W.H., Bowen, W.B. and Asbury, C.E. 1992. Riparian nitrogen dynamics in two geomorphologically distinct tropical rain forest watershed: subsurface solute pattern. *Biogeochemistry* 18, 53-75.
- Menichino, G.T., Scott, D.T. and Hester, E.T. 2015. Abundance and dimensions of naturally occurring macropores along stream channels and the effects of artificially constructed large macropores on transient storage. *Freshwater Science* 34(1), 125–138.
- Miller, R.B., Heeren, D.M., Fox, G.A., Halihan, T., Storm, D.E. and Mittelstet, A.R. 2014. The hydraulic conductivity structure of gravel-dominated vadose zones within alluvial floodplains. *Journal of Hydrology* 513, 229-240.
- Moore, A.A. and Palmer, M.A. 2005. Invertebrate biodiversity in agricultural and urban headwater streams: Implications for conservation and management. *Ecological Applications* 15(4), 1169-1177.
- O'Donnell, J.A. and Jones, J.B. 2006. Nitrogen retention in the riparian zone of catchments underlain by discontinuous permafrost. *Freshwater Biology* 51, 854-864.
- O'Driscoll, M.A. and DeWalle, D.R. 2010. Seeps Regulate Stream Nitrate Concentration in a Forested Appalachian Catchment. *Journal of Environmental Quality* 39(1), 420-431.
- Orozco-Lopez, E., Munoz-Carpena, R., Gao, B. and Fox, G.A. 2018. Riparian Vadose Zone Preferential Flow: Review of Concepts, Limitations, and Perspectives. *Vadose Zone Journal* 17(1), 20.
- Osborne, L.L. and Kovacic, D.A. 1993. Riparian vegetated buffer strips in water-quality restoration and stream management *Freshwater Biology* 29(2), 243-258.
- Peterson, B.J., Wollheim, W.M., Mulholland, P.J., Webster, J.R., Meyer, J.L., Tank, J.L., Marti, E., Bowden, W.B., Valett, H.M., Hershey, A.E., McDowell, W.H., Dodds, W.K., Hamilton, S.K., Gregory, S. and Morrall, D.D. 2001. Control of nitrogen export from watersheds by headwater streams. *Science* 292(5514), 86-90.
- Pittroff, M., Frei, S. and Gilfedder, B.S. 2017. Quantifying nitrate and oxygen reduction rates in the hyporheic zone using Rn-222 to upscale biogeochemical turnover in rivers. *Water Resources Research* 53(1), 563-579.
- Pollock, D.W. 2016. User guide for MODPATH Version 7 -- a particle-tracking model for MODFLOW. U.S. Geological Survey, 35.
- Rahimi, M., Essaid, H.I. and Wilson, J.T. 2015. The role of dynamic surface water-groundwater exchange on streambed denitrification in a first-order, low-relief agricultural watershed. *Water Resources Research* 51(12), 9514-9538.

- Royer, T.V., David, M.B. and Gentry, L.E. 2006. Timing of riverine export of nitrate and phosphorus from agricultural watersheds in Illinois: Implications for reducing nutrient loading to the Mississippi River. *Environmental Science & Technology* 40(13), 4126-4131.
- Schmadel, N.M., Ward, A.S., Lowry, C.S. and Malzone, J.M. 2016. Hyporheic exchange controlled by dynamic hydrologic boundary conditions. *Geophysical Research Letters* 43(9), 4408-4417.
- Sheibley, R.W., Jackman, A.P., Duff, J.H. and Triska, F.J. 2003. Numerical modeling of coupled nitrification-denitrification in sediment perfusion cores from the hyporheic zone of the Shingobee River, MN. *Advances in Water Resources* 26(9), 977-987.
- Shoemaker, W.B., Kuniandy, E.L., Birk, S., Bauer, S. and Swain, E.D. 2007. Documentation of a Conduit Flow Process (CFP) for MODFLOW-2005. U.S. Geological Survey Techniques and Methods Book 6, Chapter A24, 50p.
- Sinha, E., Michalak, A.M. and Balaji, V. 2017. Eutrophication will increase during the 21st century as a result of precipitation changes. *Science* 357(6349), 405-408.
- Smethurst, P.J., Petrone, K.C., Langergraber, G., Baillie, C.C., Worledge, D. and Nash, D. 2014. Nitrate dynamics in a rural headwater catchment: measurements and modelling. *Hydrological Processes* 28(4), 1820-1834.
- Steiness, M., Jessen, S., van't Veen, S.G.M., Kofod, T., Hojberg, A.L. and Engesgaard, P. 2021. Nitrogen-loads to streams: importance of bypass flow and nitrate removal processes. *Biogeosciences* 126, 1-24.
- Struijs, J., Beusen, A., de Zwart, D. and Huijbregts, M. 2011. Characterization factors for inland water eutrophication at the damage level in life cycle impact assessment. *International Journal of Life Cycle Assessment* 16(1), 59-64.
- Stutter, M., Kronvang, B., Huallachain, D.O. and Rozemeijer, J. 2019. Current Insights into the Effectiveness of Riparian Management, Attainment of Multiple Benefits, and Potential Technical Enhancements. *Journal of Environmental Quality* 48(2), 236-247.
- Turunen, J., Markkula, J., Rajakallio, M. and Aroviita, J. 2019. Riparian forests mitigate harmful ecological effects of agricultural diffuse pollution in medium-sized streams. *Science of the Total Environment* 649, 495-503.
- USGS 2005 Louisiana Ground-Water Map No. 18: Potentiometric Surface, 2003, Jasper Aquifer System in West-Central Louisiana. Brantly, J.A. and Seanor, R.C. (eds).
- Williams, M.R., Buda, A.R., Elliott, H.A., Hamlett, J., Boyer, E.W. and Schmidt, J.P. 2014. Groundwater flow path dynamics and nitrogen transport potential in the riparian zone of an agricultural headwater catchment. *Journal of Hydrology* 511, 870-879.
- Zarnetske, J.P., Haggerty, R. and Wondzell, S.M. 2015. Coupling multiscale observations to evaluate hyporheic nitrate removal at the reach scale. *Freshwater Science* 34(1), 172-186.
- Zarnetske, J.P., Haggerty, R., Wondzell, S.M., Bokil, V.A. and Gonzalez-Pinzon, R. 2012. Coupled transport and reaction kinetics control the nitrate source-sink function of hyporheic zones (vol 48, W11508, 2012). *Water Resources Research* 48.

## CHAPTER 5: “Lost in dune translation: the effects of microbial growth dynamics on hyporheic biogeochemistry underneath moving dunes”

Status: This work is in preparation to be submitted for publication

**Authors:** W. Seth Lotts<sup>1</sup>, Erich T. Hester<sup>1</sup>

<sup>1</sup>Department of Civil and Environmental Engineering, Virginia Tech, Blacksburg, Virginia 24061 USA

Corresponding Author: Erich T. Hester, [ehester@vt.edu](mailto:ehester@vt.edu)

### **Key Points:**

- DOC consumption increases with celerity, increasing from 50-100% with just a 0.25 m/s increase in stream velocity
- Modeling growth/death dynamics is important for accurately modeling subsurface biogeochemistry
- DOC consumption increased celerity’s increasing turnover exchange, and microbial colony areal spatial distribution

### **Key words:**

- Hyporheic Zone
- Moving Dunes
- Surface water/groundwater modeling
- Biogeochemistry

### **ABSTRACT**

Streams and rivers are elegant systems where terrestrial and aquatic processes collide and mesh to form an ecotone critical to our environment. The hyporheic zone is the interface between groundwater and surface water, and offers many benefits to water quality. Dunes are prevalent at the bottom of streams and rivers, and induce a pressure distribution which drives hyporheic exchange with the bed, and are constantly in motion. Yet few numerical studies simulate dune motion, and even fewer examine the impacts of microbial growth/death on the system. In this study, we seek to expand the knowledge of biogeochemical dynamics of the hyporheic zone by conducting a numerical study which examines the combined effects of microbial growth/death dynamics and dune translation. To do this, we coupled together three models: a surface water model (OpenFOAM), a groundwater model (MODFLOW), and a reactive transport model that simulates dissolved oxygen and organic carbon transport and aerobic consumption, aerobic microbial growth/death, and dune translation through a code modification to implement a moving frame of reference. We found that DOC consumption increased with decreasing stream

depth and with increasing dune celerity, increasing from 50-100% with just a 0.25 m/s increase in stream velocity. We revealed that modeling growth/death dynamics is essential for modeling subsurface biogeochemistry, as the no-growth models herein predict half the DOC consumption as growth/death models despite having over six times the biomass. We showed that DOC consumption increases as increased turnover exchange, and its increase of the plume area to allow the microbe colony to grow to a bigger size. These findings not only provide further understanding into the elegant biogeochemical dynamics, they also implicate techniques to increase hyporheic exchange.

## 5.1. Introduction

Streams and rivers provide societal benefits including drinking water, recreation, and aesthetic beauty, as well as habitat and food for other species which drive important ecosystem functions such as pollination, soil aeration, and vector control. In the United States, surface waters – whose ultimate sources are typically streams or rivers – supply approximately 70% of the drinking water (Balvanera et al., 2006; Dieter et al., 2018; Nakano and Murakami, 2001; Ramey and Richardson, 2017; U.S., 1957). Streams and rivers provide a venue for activities such as freshwater fishing, where Americans spent close to \$30 billion in 2016 (U.S. Department of the Interior, 2018). Streams and rivers are integral to many types of ecosystems and play an important role in the Earth's critical zone (Cummins and Klug, 1979; Huet, 1959; Quaglietta et al., 2018; Richter and Mobley, 2009). Stream and river corridors are a hotbed for biodiversity, and a key indicator of environmental health (McClain et al., 2003; Roley et al., 2012; Sterba et al., 1997; Thoms, 2003; Ward et al., 1999). Yet the health of streams and rivers are jeopardized by pollutant sources including metals (Fuller and Harvey, 2000; Neiva et al., 2019), microplastics (Frei et al., 2019; Klein et al., 2015; Yonkos et al., 2014), pharmaceuticals (Peng et al., 2008; Wiegel et al., 2004), pesticides (Climent et al., 2019; Climent et al., 2018; Knillmann et al., 2018; Rizzi et al., 2019), excess nitrogen (Paerl et al., 2016; Royer et al., 2006; Sinha et al., 2017), and excess phosphorus (Carpenter et al., 1998; Royer et al., 2006). Fortunately, there are natural mechanisms which can help remove these pollutants, for example in the hyporheic zone.

The hyporheic zone is the area beneath and adjacent streams and rivers which acts as the interface between surface water (SW) and groundwater (GW) (Bencala, 2000; Lawrence et al., 2013; Triska et al., 1989; White, 1993; Winter et al., 1998). It is an epicenter for biodiversity and biogeochemical reactions and serves as connective tissue between the channel, floodplains and GW (McClain et al., 2003; Stanford and Ward, 1988). The hyporheic zone can filter out contaminants coming from SW via sorption and biodegradation (Brunke and Gonser, 1997; Moser et al., 2003; Winter et al., 1998). Hyporheic exchange, the small-scale bidirectional exchange of SW and GW, also facilitates nutrient and mineral cycling between biota in the channel and banks (Brunke and Gonser, 1997; Hester and Gooseff, 2011; Stanford and Ward, 1993; Triska et al., 1989; Winter et al., 1998). Hyporheic exchange provides oxygen to microbiota, burrowing fauna, and salmon eggs within the sediment. Further, the hyporheic zone

can be a source or sink for heat, thereby helping to regulate stream temperatures (Arrigoni et al., 2008; Burkholder et al., 2008; Hester et al., 2009).

There are multiple physical mechanisms which drive hyporheic exchange. Turbulent momentum from SW propels water into pore spaces in coarse grained river and streambeds (Nagaoka and Ohgaki, 1990). Peak flow events such as dam releases, snowmelt, diurnal fluctuations, or storms cause temporary hydraulic head-gradient reversals which drive SW into the bed and banks (Pinder and Sauer, 1971; Sawyer et al., 2009). Hyporheic exchange is also driven by variation of hydraulic head along the channel at multiple spatial scales (Poole et al., 2008), including bedforms such as dunes and ripples (Elliott and Brooks, 1997b; Janssen et al., 2012; Zheng et al., 2019), instream structures such as logs or rock-dams (Hester and Doyle, 2008), channel sinuosity (Cardenas, 2009), periodic bedrock outcrops (Hiscock and Grischek, 2002), and catchment topography (Toth, 1963). And finally, turnover exchange occurs by the successive trapping and releasing of water by moving bedforms (Elliott and Brooks, 1997b). Exchange induced by bedforms such as dunes and ripples is one of the most widespread and often of greater magnitude than exchange induced by other mechanisms (Gomez-Velez and Harvey, 2014; Gomez-Velez et al., 2015).

Depending on the Froude number of flow in the channel and the magnitude of bed load velocity relative to SW velocity, the bed can form ripples, dunes, a flat bed, or antidunes (Kennedy, 1969). These criteria can also be expressed in terms of median grain size and mean flow velocity (Ashley, 1990). For example, ripples form at smaller grain sizes and lower velocities, while dunes form at larger grain sizes and higher velocities. Dunes form at higher Froude numbers and have minimum lengths which are far greater than the maximum length of ripples (Kennedy, 1969). Water flowing over static dunes or ripples cause pressure variations along the length of the dune, which induce hyporheic flow cells in the subsurface. More specifically, high pressure forms on the middle of the stoss (upstream) side of the dune, creating downwelling of SW into the sediment. That SW then migrates through the sediment and upwells at low pressure zones near the dune cap and on the lee side of the dune.

Hyporheic flow cells and associated biogeochemical activity have been conventionally examined by a large number of modeling and field studies that assume static dunes (Bardini et al., 2012; Cardenas and Wilson, 2007a; b; Elliott and Brooks, 1997a; b; Fox et al., 2014; Hester et al., 2013; 2014; Janssen et al., 2012; Marzadri et al., 2016). In this body of literature, dissolved organic carbon (DOC) and dissolved oxygen (DO) that enter the sediment from SW via hyporheic flow cells beneath static dunes benefit subsurface aerobic microbes (Boulton et al., 1998; Findlay et al., 1993; Stelzer et al., 2014; Stern et al., 2017). Aerobic biofilms in the pore spaces in turn serve as food for crustaceans, segmented worms, flatworms, rotifers, water mites, and juvenile stages of aquatic insects in the subsurface (Boulton et al., 1998). Thus, these processes may be important to the entire riverbed ecosystem. Nevertheless, while the static dune assumption is a useful starting point for developing understanding of hyporheic zone behavior due to its conceptual simplicity and computational parsimony, most dunes in the field are not static and thus ignoring turnover exchange may not always be justified.

Riverbed dunes move by flowing water shearing sediment grains off the stoss side and depositing them on the lee side. There are many models which predict and quantify particle entrainment necessary for bedform movement to occur, but bedform celerity is generally related to the degree that bed shear stress exceeds a critical minimum value (Coleman and Melville, 1994; Papanicolaou et al., 2002; van Rijn, 1984). There are several ways to model dune translation and thus more accurately model dune-induced hyporheic exchange by explicitly incorporating turnover exchange. Very detailed approaches have examined dune motion on a granular level. For example, Charru et al. (2016) modeled individual particle motion with a Lagrangian model, but the scale domain is microscopic. By contrast, Zhao and Fernando (2007) used a two-phase Eulerian approach to solve the momentum equations in both solid and liquid domains at scales approaching the size of a dune, yet computational times exceeded 260 hours per simulation, rendering sensitivity analysis impractical. For these reasons, a “moving frame of reference” (MFOR) approach was developed that models a moving dune as one cohesive body, which is more tractable yet sufficiently accurate for simulating the impact of dune translation on hyporheic biogeochemical dynamics (Ahmerkamp et al., 2015; Kessler et al., 2015; Zheng et al., 2019). MFOR model output from this small number of recent studies showed hyporheic flow cells induced by mobile dunes no longer exhibited the inverted arch shape of static dunes but rather exhibited a flattened shape where SW simply flows in a straight line horizontally from the lee to the stoss side (Zheng et al., 2019).

Another simplistic assumption of conventional numerical studies of hyporheic biogeochemistry is static microbial populations where microbial communities do not grow or die (Bardini et al., 2012; Cardenas and Wilson, 2007a; b; Elliott and Brooks, 1997a; b; Fox et al., 2014; Hester et al., 2013; 2014; Janssen et al., 2012; Marzadri et al., 2016). Prior studies such as Hester et al. (2014) and Zarnetske et al. (2012) assumed constant concentration of microbial biomass in the pore space, and thus did not account for growth and death dynamics of the microbial colonies. Like the assumption of static dunes, static subsurface microbial populations is clearly not realistic in general (Widdowson et al., 1988). Lowell et al. (2009) demonstrated the spatial heterogeneity of microbial communities in the hyporheic zone, and has linked zones of high nitrate ( $\text{NO}_3^-$ ) and DOC consumption to these microbial communities. Recent modeling (Caruso et al., 2017; Chowdhury et al., 2020) and laboratory flume (Cook et al., 2020) studies demonstrated how microbial growth and subsequent death led to bio-clogging and significantly decreased hyporheic exchange. These studies highlighted the importance of accounting for microbial growth dynamics in accurately modeling biogeochemistry in the subsurface. Finally, Monterroso (2021) examined the impact of microbial dynamics on DOC/DO consumption rates under different DOC/DO loads and varying hydraulic conditions such as upwelling rates, and stream/river velocity and depth. Yet to our knowledge, prior studies have not simultaneously examined the coupled effects of dune migration and microbial dynamics.

The primary question motivating this study was what effect does microbial growth play in hyporheic biogeochemistry in river systems with translating dunes where we account for turnover hyporheic exchange? More specifically, our objectives were to examine the effects of varying 1) river water column (SW) velocity and depth and hence dune translation celerity, 2) GW upwelling rates, and 3) river water column (SW) DOC/DO concentrations and hence influx

rates to GW on microbial growth and death, and ultimately DOC/DO consumption rates in in riverbed dune-induced hyporheic zones.

## 2. Methods

We coupled three models: a surface water (SW) model for river water column hydraulics, a groundwater (GW) model for subsurface hydraulics, and a GW reactive transport model which incorporates microbial growth as well as MFOR to simulate dune translation (Figure 5.2). The SW model was OpenFOAM which simulated SW hydrodynamics and generated the pressure distribution over the dunes which we used as the top boundary condition for the GW code hydraulics MODFLOW. The transport code SEAM3D then solved for GW DOC and DO migration and microbial aerobic metabolism, microbial growth/death, and dune translation which required code modifications to implement a MFOR.

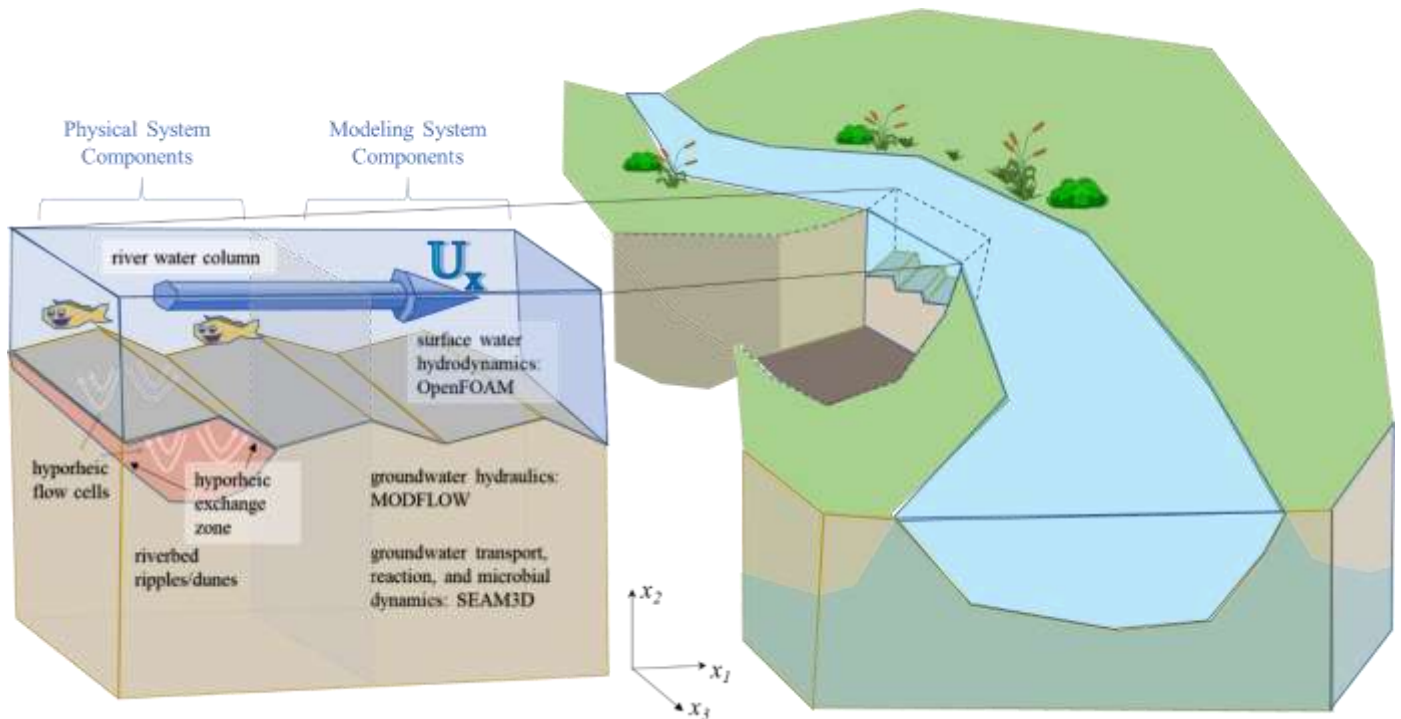


**Figure 5.1. Schematic of modeling approach, including (1) OpenFOAM for SW hydrodynamics, (2) MODFLOW for GW hydraulics, and (3) SEAM3D (modified to incorporate a moving frame of reference) for GW transport and microbial growth and death dynamics.**

### 5.2.1 Surface Water Domain

To model river hydrodynamics along a longitudinal slice of the river water column above three dunes (0.1-m-high, 2-m-long), we solved the 2D incompressible Reynolds Averaged Navier-Stokes (RANS) equations

$$\frac{\partial}{\partial t}(\rho \bar{u}_i) + \frac{\partial}{\partial x_j}(\rho \bar{u}_i \bar{u}_j) = -\frac{\partial \bar{p}}{\partial x_i} + \frac{\partial}{\partial x_j}(\bar{\tau}_{ij} - \rho \overline{u'_i u'_j}), \quad i, j = 1, 2 \quad [5.1]$$

in OpenFOAM on a 300 long x 160 high non-uniform, quadrilateral finite volume grid generated by blockMesh which discretizes a 6-m-long domain at depths (from the free surface to the dune trough) of 0.5, 1.0, and 1.5 m (Weller and Tabor, 1999). In Equation 5.1, the overbar indicates a time-averaged quantity;  $i$  is the free index indicating a 2D vector with components in the first two Cartesian unit basis vector directions (-) (Figure 5.1);  $j$  is the 2D dummy index indicating to sum the terms  $j=1$  and  $j=2$  (-);  $u_i$  is 2D velocity vector in the  $i=1$  or  $i=2$  unit basis vector direction ( $LT^{-1}$ );  $x_i$  is the Cartesian direction based on subscript ( $i=1$  or  $i=2$ ) (L) (see coordinate axis in Figure 5.1);  $t$  is time (T);  $\rho$  is density of water ( $ML^{-3}$ );  $p$  is pressure ( $ML^{-1}T^{-2}$ );  $\rho \overline{u'_i u'_j}$  is the Reynolds stress (effect of time fluctuating eddies on momentum in units of stress,  $ML^{-1}T^{-2}$ ); and  $\bar{\tau}_{ij}$  is the strain tensor ( $ML^{-1}T^{-2}$ ), where

$$\bar{\tau}_{ij} = \mu \left( \frac{\partial \bar{u}_i}{\partial x_j} + \frac{\partial \bar{u}_j}{\partial x_i} \right) \quad [5.2]$$

where  $\mu$  is the dynamic viscosity ( $ML^{-1}T^{-1}$ ). We used the  $k$ - $\omega$  closure scheme to model Reynolds Stress, which implicitly assumes the Boussinesq approximation is valid for the Reynolds Stress tensor,

$$\tau'_{ij} = \rho \overline{u'_i u'_j} = \mu_T \left( \frac{\partial \bar{u}_i}{\partial x_j} + \frac{\partial \bar{u}_j}{\partial x_i} \right) - \frac{2}{3} \rho k \delta_{ij} \quad [5.3]$$

where  $\mu_T$  is the eddy viscosity (a metric measuring the transmissibility of kinetic energy,  $ML^{-1}T^{-1}$ );  $k$  is the turbulent kinetic energy ( $ML^2T^{-2}$ ) given by  $\mu_T = \rho k / \omega$ ; and  $\delta_{ij}$  is the Kronecker delta. Here,  $\omega$  is the specific viscous dissipation rate ( $T^{-1}$ ). The introduction of the Reynolds stress has introduced two unknowns ( $k$  and  $\omega$ ), we calculated them using two new partial differential equations: one for  $k$ , and the other for  $\omega$ . For  $k$ , we have:

$$\rho \frac{\partial k}{\partial t} + \rho \bar{u}_j \frac{\partial k}{\partial x_j} = \bar{\tau}_{ij} \frac{\partial \bar{u}_i}{\partial x_j} - \beta^* \rho k \omega + \frac{\partial}{\partial x_j} \left[ (\mu + \sigma^* \mu_T) \frac{\partial k}{\partial x_j} \right] \quad [5.4]$$

For  $\omega$ , we have:

$$\rho \frac{\partial \omega}{\partial t} + \rho \bar{u}_j \frac{\partial \omega}{\partial x_j} = \alpha \frac{\omega}{k} \bar{\tau}_{ij} \frac{\partial \bar{u}_i}{\partial x_j} - \beta \rho \omega^2 + \frac{\partial}{\partial x_j} \left[ (\mu + \sigma \mu_T) \frac{\partial \omega}{\partial x_j} \right] \quad [5.5]$$

We set the closure coefficients to the defaults in OpenFOAM for high Reynolds numbers and incompressible flows, which are  $\alpha = 0.52$ ,  $\beta = 0.072$ ,  $\beta^* = 0.09$ ,  $\sigma^* = 0.5$ , and  $\sigma = 0.5$  (OpenFOAM, 2021; Wilcox, 1998). We ran the model to steady-state using the boundary conditions and parameters specified in the paragraph below and summarized in Table 5.1 in Section 5.2.5.

For the top boundary condition we specified zero gage pressure consistent with atmospheric pressure ( $L^2T^{-2}$ ) (Figure 5.2) (Elger et al., 2016). We also defined the top longitudinal velocity  $u_x$  such that the average is equal to the target value (Section 5.2.5) for stream velocity (Li et al., 2020). The sides were set as periodic boundary conditions for both pressure and velocity (Li et al., 2020), and the bottom was a wall boundary condition (zero velocity at the wall) (Figure 5.2) (Cardenas and Wilson, 2007a; Li et al., 2020; Zheng et al., 2019). We set the kinematic viscosity as  $\nu = 1 \times 10^{-6} \text{ m}^2\text{s}^{-1}$  (Bayon-Barrachina and Lopez-Jimenez, 2015). We assumed the dunes had a triangular shape (Cardenas and Wilson, 2007a; Elliott and Brooks, 1997b; Hester et al., 2013; 2014).

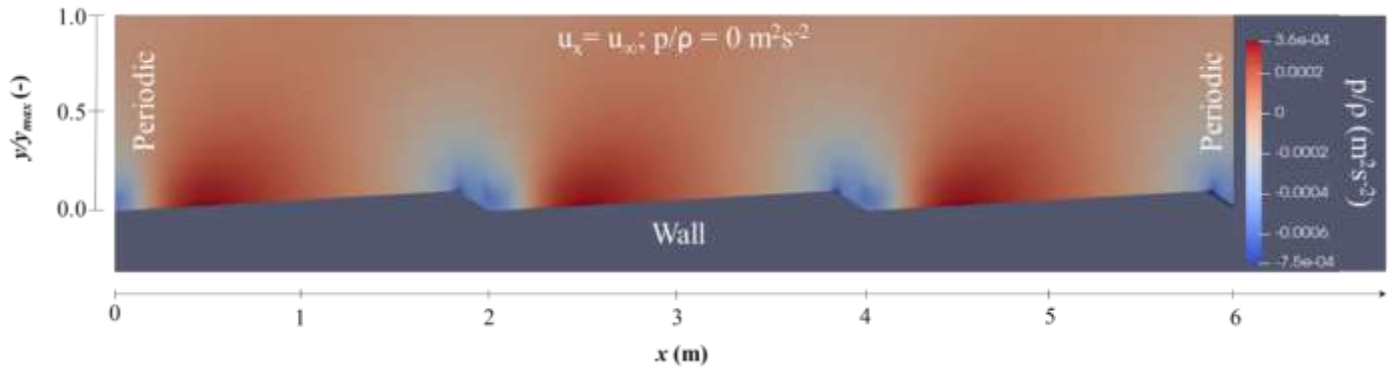


**Figure 5.2: Example OpenFOAM SW pressure solution for channel flow depth = 1.0 m (from dune trough to free surface) and channel slope =  $6.17 \times 10^{-5}$  for base case. The vertical scale is expressed as a normalized length since the depth varied with the sensitivity analysis (i.e.  $y/y_{max} = 1$  corresponds to 0.5 m, 1.0 m, and 1.5 m for the various depths).**

### 5.2.2 Bedload and Celerity

We assumed celerity was related to translation under pure bed load as defined in van Rijn (1984), which related bed-load transport rate to bed shear stress by the following series of equations

$$q_b = 0.053 \left( [(s-1)g]^{0.5} D_{50}^{1.5} \right) \frac{T^{2.1}}{D_*^{0.3}} \quad [5.6]$$

where  $q_b$  is the bedload transport rate ( $L^2T^{-1}$ ),  $s$  is the specific gravity of sediment taken to be 2.65 (-) (United States Interagency Committee on Water Resources Subcommittee on Sedimentation, 1957),  $g$  is the gravitational acceleration constant,  $9.81 \text{ ms}^{-2}$ ,  $D_{50}$  is the median grain size assumed to be  $300 \mu\text{m}$  corresponding to sand-bed rivers in the contiguous United States (Abeshu et al., 2022), where  $D_*$  is the particle parameter (-) given by:

$$D_* = D_{50} \left[ \frac{(s-1)g}{\nu^2} \right]^{1/3} \quad [5.7]$$

and  $T$  (-) is the transport stage parameter, calculated by

$$T = \frac{\tau_* - \tau_{*cr}}{\tau_*} \quad [5.8]$$

where  $\tau_{*cr}$ , ( $\text{ML}^{-1}\text{T}^{-2}$ ) is a critical shear stress parameter given by:

$$\tau_{*cr} = \frac{0.3}{1+1.2D_*} + 0.055(1 - e^{-0.02D_*}) \quad [5.9]$$

$$\tau_* = \sqrt{\tau_b \rho (s - 1) g D_{50}} \quad [5.10]$$

where  $\rho$  is the density of water ( $\text{ML}^{-3}$ ). We exported the bed shear stress from OpenFOAM at each finite volume on the wall boundary, and calculated the bed shear stress as follows:

$$\tau_b = \frac{\sum_{m=1}^N \tau_b^{stoss_m}}{N} \quad [5.11]$$

where  $m$  is an index of stoss-side finite volumes, and  $\tau_b^{stoss_m}$  ( $\text{ML}^{-1}\text{T}^{-2}$ ) is the bed shear stress at index  $m$ , and  $N$  is the number of stoss-side finite volumes. Only the shear stress on the stoss side contributes to the motion of the dunes (Elliott and Brooks, 1997b). Finally, we related bed load transport rate to celerity by the geometry of a triangle,

$$c_b = \frac{2 q_b}{(1-\theta)\Delta} \quad [5.12]$$

where  $c_b$  is bedform celerity ( $\text{LT}^{-1}$ ), and  $\theta$  is porosity (-). In summary, we started with  $D_{50}$ ,  $s$ ,  $g$ ,  $v$ , and the  $\tau_b$  imported from OpenFOAM, and calculated  $\tau_*$ ,  $\tau_{*cr}$ , and  $D_*$ . We then calculated  $T$ , which enabled us to calculate  $q_b$ . Finally, we could use  $q_b$ ,  $\theta$ , and  $\Delta$  to calculate  $c_b$ .

### 5.2.3 Groundwater Hydraulic Equations

We simulated GW hydraulics with and beneath three dunes (0.1-m-high, 2-m-long) by solving the 2D saturated, confined, homogeneous, isotropic GW equations

$$\frac{\partial^2 h}{\partial x^2} + \frac{\partial^2 h}{\partial y^2} + \frac{W}{K} = \frac{S_s}{K} \frac{\partial h}{\partial t} \quad [5.13]$$

in MODFLOW (Harbaugh et al., 2000) using GMS (Aquaveo, 2021), where  $h$  is the hydraulic head (L),  $x$  and  $y$  are Cartesian directions (L) (same as  $x_1$ , and  $x_2$ , in the SW domain);  $W$  is volumetric flux per unit volume of upwelling at the bottom of the domain ( $\text{T}^{-1}$ ),  $K$  is the hydraulic conductivity of subsurface beneath the dunes ( $\text{LT}^{-1}$ ),  $S_s$  is specific storage ( $\text{L}^{-1}$ ), and  $t$  is time (T). The model domain was 6 m long and 0.85 m deep from dune peak to bottom boundary. Using square model cells 1 cm on each side, the finite difference mesh was 600 cells long by 85 cells deep.

The top boundary was constant head, with pressures imported from OpenFOAM and converted from normalized pressure ( $p/\rho$ ,  $\text{m}^2\text{s}^{-2}$ ) to hydraulic head ( $h$ , m) by dividing by  $g$ . The bottom boundary simulated upwelling with a constant flux boundary (Cardenas and Wilson, 2006; 2007b; Hester et al., 2013). The side boundaries were quasi-periodic meaning that while

MODFLOW does not have a periodic boundary condition option, we obtained the effects of periodic boundaries for the middle dune by multiple iterations of substituting the hydraulic heads from the left-most column of the middle dune into the right-most boundary of the model domain in successive model runs (Figure F1). We ran the model to steady-state (Table 5.1). GW hydraulic parameters are given in Section 5.2.5.

#### 5.2.4 Reactive Transport and Microbial Growth/Death Equations

To model the movement and biogeochemical reactions of DOC and DO using GW flow data from MODFLOW, we solved the 2D advection-dispersion-reaction equation in SEAM3D (Widdowson et al., 1997),

$$\frac{\partial(\theta C^k)}{\partial t} = \frac{\partial}{\partial x_i} \left( \theta D_{ij} \frac{\partial C^k}{\partial x_j} \right) - \frac{\partial}{\partial x_i} (\theta v_i C^k) + W C_s^k + \sum R \quad [5.14a]$$

$$v_i = \begin{bmatrix} v_x - c_b \\ v_y \end{bmatrix} \quad [5.14b]$$

where  $C$  is the dissolved concentration ( $\text{ML}^{-3}$ ) of the  $k$ th species, including both substrates and aqueous phase electron acceptors;  $C_s$  is the dissolved concentration of the source term ( $\text{ML}^{-3}$ );  $D_{ij}$  is the hydrodynamic dispersion tensor ( $\text{L}^2\text{T}^{-1}$ );  $W$  is the volumetric fluxes per unit volume of the upwelling coming from deeper GW ( $\text{T}^{-1}$ );  $\sum R$  is the sum of all first-order chemical reaction rates ( $\text{ML}^{-3}\text{T}^{-1}$ );  $v_i$  is the pore-water velocity vector ( $\text{LT}^{-1}$ ), where  $v_x - c_b$  and  $v_y$  are  $x$  and  $y$  velocity components ( $\text{LT}^{-1}$ ) respectively, and  $c_b$  is the celerity calculated in Equation 4.12 ( $\text{LT}^{-1}$ ). Here, it was necessary to modify SEAM3D to implement a MFOR. We accomplished this by modifying the Flow-Model Interface subroutine of the original SEAM3D source code in FORTRAN, where we uniformly subtracted the celerity value from all the  $x$ -components of the porewater velocity. This calculation gave the effect of the domain being in a MFOR where the model domain propagates downstream at the speed of the celerity (Figure F1). SEAM3D uses Monod kinetics to model the movement and reaction of contaminants and accounts for microbial growth dynamics through the following series of equations. The microbial growth rate is given by:

$$\frac{1}{M_\xi} \frac{dM}{dt} = -k_{d\xi} + G_{\xi,ls,le} \quad [5.15]$$

where  $M_\xi$  is the microbial biomass (M) for colony  $\xi$ ,  $k_{d\xi}$  is the effective death rate ( $\text{T}^{-1}$ ), and  $G_{\xi,ls,le}$  is the effective growth rate for substrate  $ls$ , and electron acceptor  $le$  ( $\text{T}^{-1}$ ). The growth rate is proportional to substrate utilization rate, with the constant of proportionality being the yield coefficient (i.e. the amount of addition biomass grown per amount substrate consumed),

$$G_{\xi,ls,le} = \sum_{le} \sum_{ls} Y_{\xi,ls,le} \zeta_{\xi,ls,le} \quad [5.16]$$

where  $Y_{\xi,ls,le}$  is the yield coefficient ( $\text{M}_b\text{M}_{ls}^{-1}$ ), and  $\zeta_{\xi,ls,le}$  is the specific substrate utilization rate ( $\text{M}_{ls}\text{M}_b^{-1}\text{T}^{-1}$ ) growing on microcolony  $\xi$  on substrate  $ls$  and electron acceptor  $le$ . The electron acceptor utilization rate is related to the sum of all the specific substrate utilization rates (for example nitrification and aerobic respiration use ammonium and carbon respectively as substrate but both use oxygen as an electron acceptor) by stoichiometry,

$$\Omega_{\xi} = \sum_{ls} \gamma_{\xi,ls,le} \zeta_{\xi,ls,le} \quad [5.17]$$

where  $\Omega_{\xi}$  is the rate of electron acceptor consumption per unit biomass ( $M_e M_b^{-1}$ ),  $\gamma_{\xi,ls,le}$  is the electron acceptor use coefficient based on stoichiometry ( $M_e M_{ls}^{-1}$ ) which dictates the mass of electron acceptor used per unit mass of substrate  $ls$ .

Many phenomena govern substrate utilization rate: the amount of substrate available, the amount of electron acceptors available, inhibition of the reaction due to the presence of oxygen (if the reaction is denitrification, iron reduction, or other lower Gibbs free energy reactions). Thus, substrate utilization rate is given by:

$$\zeta_{\xi,ls,le} = \zeta_{\xi,ls,le}^{max} \left[ \frac{C_{ls}^k}{K_{\xi,ls,le}^s + C_{ls}^k} \right] \left[ \frac{C_{le}^k}{K_{\xi,ls,le}^e + C_{le}^k} \right] I_{le,li} \quad [5.18]$$

where  $\zeta_{\xi,ls,le}^{max}$  is the maximum specific rate of substrate utilization per unit biomass for microcolony  $\xi$  growing on substrate  $ls$  and electron acceptor  $le$  ( $M_{ls} M_b^{-1} T^{-1}$ );  $C_{ls}^k$  and  $C_{le}^k$  are the concentrations of the substrate ( $M_{ls} L^{-3}$ ) and electron acceptor ( $M_e L^{-3}$ ) respectively;  $K_{\xi,ls,le}^s$  and  $K_{\xi,ls,le}^e$  are half-saturation constants for the substrate ( $M_{ls} L^{-3}$ ) and electron acceptors ( $M_e L^{-3}$ ) respectively.  $I_{le,li}$  is an inhibition term which accounts for the presence of electron acceptors with greater Gibbs free energy,  $li$ , inhibiting the use of electron acceptors that provide the microbial colony with less Gibbs free energy. In our case, we only model aerobic respiration which has the highest Gibbs free energy, and thus  $I_{le,li}$  emerges as unity. The general stoichiometric reaction equation for microbial aerobic respiration (Zarnetske et al., 2012) is:



There are many biogeochemical reactions in the subsurface beyond aerobic respiration, but many important reactions require specific redox conditions such that we chose to simulate aerobic respiration as an important starting point for insight into additional biogeochemical dynamics. Thus, we did not model nutrient dynamics with the implicit assumption that there are enough nutrients in the system to sustain cell growth (i.e. Equation 5.18 does not have a nutrient dynamics term).

We set the top boundary condition to specified concentration, representing SW concentrations of aerobic respiration reactants, in particular base case dissolved organic carbon (DOC) and dissolved oxygen (DO) of 5 mgL<sup>-1</sup>. We set the side boundary conditions to quasi-periodic which represents a fully developed concentration profile given the SW concentrations. In our base case, this means the far-field steady-state concentration profile that results from 0 mg/L of DO and DOC in the aquifer below with a river water column of 5 mg/L (Figure F1). While microbial growth and death are simulated, microbial transport is not, thus there are no microbial boundary conditions. Chemical and microbial parameters are given in Section 5.2.5.

### 5.2.5 Sensitivity Analysis

To examine microbial growth and death and their effects on DO/DOC consumption in a variety of dune migration, hydraulic, and biogeochemical scenarios, we performed sensitivity analyses

(Table 5.1) on the parameters SW water column velocity ( $\text{ms}^{-1}$ ) and depth (m) which control dune celerity, GW upwelling rate ( $\text{m}^3\text{d}^{-1}$ ) which controls hyporheic flow cell formation, and SW DO/DOC concentrations ( $\text{mgL}^{-1}$ ) which control reaction dynamics. We examined the portion of the Cartesian cross-product of the range of SW velocities ( $u_x = 0.25 - 1.00 \text{ m/s}$ ) and depths ( $d = 0.5 - 1.5 \text{ m}$ ) that are physically capable of forming dunes (Table 5.2). We chose typical in situ dune lengths (Bradley and Venditti, 2019; Cisneros et al., 2020), and to maximize flow separation, we chose dunes with the upper end of the lee angle observed in situ in Cisneros et al. (2020) and Bradley and Venditti (2019), and varied the depth in accordance with the range of  $\Delta/d$  ratios, observed in those studies. We then chose the SW velocity range to be reasonably paired with depth range (a range of  $0.25 - 1.0 \text{ m/s}$  is reasonably commensurate for depths of  $0.5 \text{ m}$  or  $1.5 \text{ m}$ ). These SW depths and velocities are consistent with streams of Strahler order 2 to 5 (a height,  $\Delta$ , of  $0.1 \text{ m}$ , a dune length,  $L$ , of  $2 \text{ m}$ , and a lee angle of  $30^\circ$ ) (Bradley and Venditti, 2019; Cisneros et al., 2020; Ward et al., 2016). We chose the same GW upwelling range as Monterroso (2021), whose lower-bound flowrate ( $W = 0.00088 \text{ md}^{-1}$ ) in the static dune scenario led to flow cell which extended to the bottom of the domain, and whose upper-bound flowrate ( $W = 0.3 \text{ md}^{-1}$ ) almost eliminated the flow cell. Our in-stream DO/DOC values are consistent with ranges observed and/or used in other studies (Bardini et al., 2012; Dubrovsky et al., 2010; Hester et al., 2014). Outputs included observed DO/DOC consumption rates ( $\text{gd}^{-1}$ ), growth and death dynamics and spatial distribution of the aerobe colony ( $\text{gm}^{-3}$ ).

**Table 5.1. Summary of sensitivity analyses and parameter selection**

Sensitivity Analysis				
Parameter varied	Range; increment	Base Case	Units	Sources for values used
water column (SW) velocity, $u_x$	0.25-1;0.25	1	ms <sup>-1</sup>	(Bradley and Venditti, 2019; Cisneros et al., 2020)
water column (SW) depth, $d$	0.5-1.5;0.5	1	m	(Bradley and Venditti, 2019; Cisneros et al., 2020)
dune celerity, $c_b$	7.81, 17.02, 28.24, 34.25, 68.67	34.25	md <sup>-1</sup>	Calculated from (van Rijn, 1984)
water column (SW) DOC concentration	5,10	5	mgL <sup>-1</sup>	(Bardini et al., 2012)
water column (SW) DO concentration	5,10	5	mgL <sup>-1</sup>	(Bardini et al., 2012)
GW upwelling rate, $W$	0.00088, 0.0088, 0.03	8.80x10 <sup>-3</sup>	m <sup>3</sup> d <sup>-1</sup>	(Monterroso, 2021)
Constant Parameters				
Parameter	Value	-	Units	Sources for values used
closure coefficients, $\alpha, \beta, \beta^*, \sigma, \sigma^*$	0.52 ,0.072 ,0.09, 0.5, 0.5	-	-	(OpenFOAM, 2021; Wilcox, 1998)
water kinematic viscosity, $\nu$	1.00E-06	-	m <sup>2</sup> s <sup>-1</sup>	(Bayon-Barrachina and Lopez-Jimenez, 2015)
atmospheric boundary pressure, $p/p$	0	-	m <sup>2</sup> s <sup>-2</sup>	(Elger et al., 2016)
dune height, $\Delta$	0.1	-	m	(Bradley and Venditti, 2019; Cisneros et al., 2020)
dune length, $L$	2	-	m	(Bradley and Venditti, 2019; Cisneros et al., 2020)
dune lee angle	30	-	°	(Bradley and Venditti, 2019; Cisneros et al., 2020)
gravitational constant, $g$	9.81	-	ms <sup>-2</sup>	
sediment median grain size, $D_{50}$	300	-	µm	(Abeshu et al., 2022)
$\rho$	998	-	kgm <sup>-3</sup>	(Elger et al., 2016)
sediment hydraulic conductivity, $K$	100	-	md <sup>-1</sup>	(Hester et al., 2013)
sediment porosity, $\theta$	0.3	-	-	(Gelhar et al., 1992)
sediment specific storage, $S_s$	0	-	m <sup>-1</sup>	Steady state
GW longitudinal dispersivity, $\lambda_L$	0.01	-	m	(Hester et al., 2013; Werth et al., 2006)
GW transverse dispersivity, $\lambda_T$	0.001	-	m	(Hester et al., 2013; Werth et al., 2006)
GW DOC concentration	0	-	mgL <sup>-1</sup>	(Chapelle et al., 2012; Hester et al., 2014)
GW DO concentration	0	-	mgL <sup>-1</sup>	(Chapelle et al., 2012; Hester et al., 2014)
minimum substrate concentration, $C_{ls,min}^k$	0.001	-	mgL <sup>-1</sup>	(Kovarova et al., 1996; Monterroso, 2021)
max specific rate of substrate utilization, $\zeta_{\xi,ls,le}^{max}$	23.64	-	gg <sup>-1</sup> d <sup>-1</sup>	Average of (Hester et al., 2014) and (Kindred and Celia, 1989)
electron acceptor use coefficient, $\gamma_{\xi,ls,le}$	1.07	-	gg <sup>-1</sup>	(Hester et al., 2014; Zarnetske et al., 2012)
substrate effective half saturation constant, $K_{\xi,ls,le}^s$	8.68	-	mgL <sup>-1</sup>	(Hester et al., 2014; Zarnetske et al., 2012)
electron acceptor half saturation constant, $K_{\xi,ls,le}^e$	5.28	-	mgL <sup>-1</sup>	(Hester et al., 2014; Zarnetske et al., 2012)
yield coefficient, $Y_{\xi,ls,le}$	0.25	-	g/g	(Kindred and Celia, 1989)

**Table 5.2. Summary of velocity and depth sensitivity analysis. Celerity was calculated by equation 5.12, Fr calculated by the equation  $Fr = u_x / \sqrt{gd}$ , slope was calculated by  $S_0 = \tau_b / \rho g d$ , and shear stress was imported from OpenFOAM. Bold and italicized cells are those velocities and depths which will produce dunes. Velocities < 0.5 m/s would form ripples or not form bedforms at all.**

$u_x$	$d$	$\tau_b$ (N/m <sup>2</sup> )	$S_0$	$Fr$	State	celerity (m/s)	celerity (m/d)	Bedform Type
0.5	0.5	0.37	0.00	0.23	Subcritical	1.60E-05	1.39	ripples
0.5	1	0.29	0.00	0.16	Subcritical	4.53E-06	0.39	ripples
0.5	1.5	0.27	0.00	0.13	Subcritical	2.71E-06	0.23	ripples
<b>0.75</b>	<b>0.5</b>	<b>0.79</b>	<b>0.00</b>	<b>0.34</b>	<b>Subcritical</b>	<b>1.97E-04</b>	<b>17.02</b>	<b>dunes</b>
<b>0.75</b>	<b>1</b>	<b>0.60</b>	<b>0.00</b>	<b>0.24</b>	<b>Subcritical</b>	<b>9.04E-05</b>	<b>7.81</b>	<b>dunes</b>
0.75	1.5	0.57	0.00	0.20	Subcritical	7.51E-05	6.49	ripples
<b>1</b>	<b>0.5</b>	<b>1.36</b>	<b>0.00</b>	<b>0.45</b>	<b>Subcritical</b>	<b>7.95E-04</b>	<b>68.67</b>	<b>dunes</b>
<b>1</b>	<b>1</b>	<b>1.03</b>	<b>0.00</b>	<b>0.32</b>	<b>Subcritical</b>	<b>3.96E-04</b>	<b>34.25</b>	<b>dunes</b>
<b>1</b>	<b>1.5</b>	<b>0.95</b>	<b>0.00</b>	<b>0.26</b>	<b>Subcritical</b>	<b>3.27E-04</b>	<b>28.24</b>	<b>dunes</b>

## 5.2.6 Benchmarking

### 5.2.6.1 Approach

To benchmark our OpenFOAM SW model, we compared our results to those from the recirculating flume experiments of Janssen et al. (2012). We used Janssen's input values, including  $\nu = 1.1 \times 10^{-6} \text{ m}^2\text{s}^{-1}$ , water depth,  $d = 0.10 \text{ m}$ , water velocity,  $u_x = 12 \text{ cm s}^{-1}$ , and dune geometry ( $L = 20 \text{ cm}$ , with a 15 cm trough to crest length, and a  $\Delta = 2\text{cm}$ ). We compared our calculated dune-surface pressure distribution to data from the pressure ports in the sixth ripple of the experimental set up in Janssen et al. (2012). Ripples are shaped identically to dunes, only smaller. Just as in the experiment, we set the pressure at the lee side of the preceding dune as zero.

There are no experimental data to benchmark our GW hydraulics and reactive transport models, so we compared our results to the numerical study by Zheng et al. (2019). We matched the ripple geometry ( $L = 15.7 \text{ cm}$ , with a 12.9 cm trough to crest length, and a  $\Delta = 1.6 \text{ cm}$ ). We also applied periodic boundary conditions and matched Zheng et al. (2019)'s velocity  $u_x = 9 \text{ cm s}^{-1}$  as well as their stream depth of 10 cm We calculated the pressure distribution and imported it into MODFLOW. Zheng et al. (2019) listed a permeability value of  $\kappa = 6.53 \times 10^{-11} \text{ m}^2$ , which we converted to hydraulic conductivity using

$$K = \frac{\kappa g}{\nu} \quad [5.20]$$

where  $\kappa$  is permeability ( $\text{L}^2$ ). Zheng et al. (2019) used values of  $\nu = 1.0035 \times 10^{-6} \text{ m}^2\text{s}^{-1}$  and  $g = 9.81 \text{ ms}^{-2}$ , which yields  $K = 55.15 \text{ md}^{-1}$ . We used their porosity value,  $\theta = 0.37$ . Zheng et al. (2019) has a periodic boundary condition which we mimicked with our multiple dune domain.

Additionally, Zheng et al. (2019) implemented cross-flow from the left side of the GW domain to the right, which was superposed onto their periodic boundary condition. We implemented the same pressure gradient between the left and right boundary. We only modeled transport and reaction of DOC, consistent with the scope of our study. The SW concentrations of DOC and DO were 150 mg/L and 10 mg/L, respectively, which represent a polluted or eutrophic stream. The dispersivities were  $\lambda_L = 3\text{cm}$ , and  $\lambda_T = 0.3\text{cm}$ . The substrate utilization rate was given by  $\zeta_{\xi,ls,le}^{max} = 0.432\text{ d}^{-1}$ .

### 5.2.6.2 Benchmarking Results

Our SW model benchmarked well qualitatively to Janssen et al. (2012). Our pressure distribution was similarly flat along the lee side, and rose roughly to the same amplitude at the peak (Figure 5.3a). The positive pressure spike on the stoss side in our results is slightly steeper on rising side, and then drops to a minimum at the peak of the dune, both consistent with the experimental data. While the amplitudes are not a perfect match and there is a slight phase shift, this does satisfy our purpose of producing a reasonable pressure distribution.

Our GW hydraulics and transport model also produced a satisfactory qualitative match to Zheng et al. (2019). The plume in our static scenario results takes on roughly the same shape as in Zheng et al. (2019), being slightly skewed to the right in both cases (Figure 5.3b). The plumes in the mobile scenario are also roughly the same shape, having the divided plume, with a substantial bud now emanating from the leeside of the dune. Our plume does bubble down a little more than Zheng's, whose was solved with different discretization techniques and solvers in both domains, and both programs have slight differences in terms of coloration depicting the contour maps and legends. Despite these differences, the concentration maps are very similar, lending confidence to our model solution.

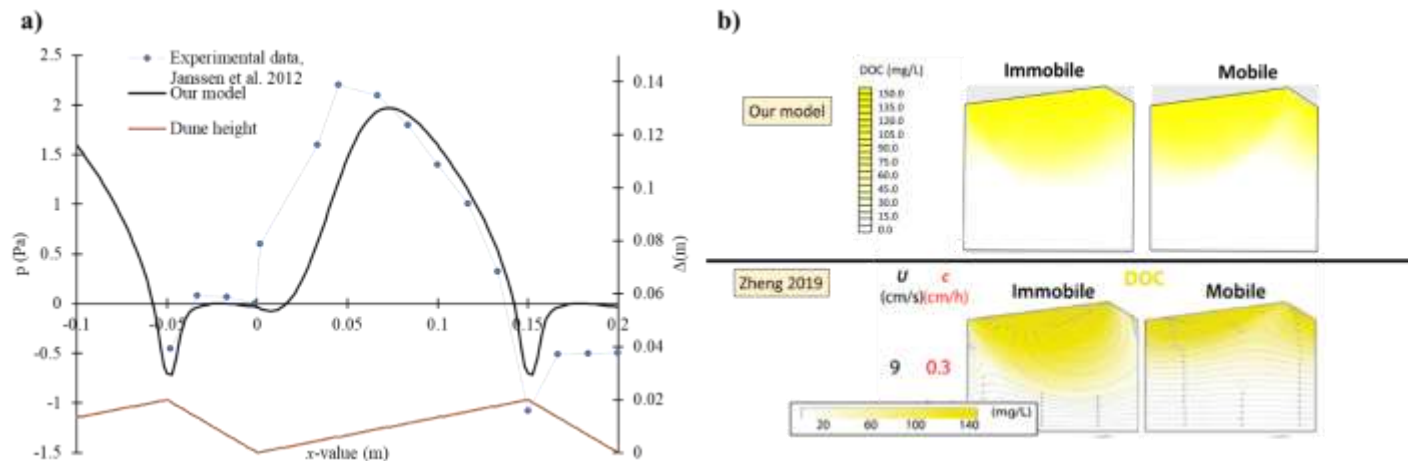


**Figure 5.3. Benchmarking results: a) our surface model results compared with experimental data from Janssen et al. (2012); b) our groundwater reactive transport results compared with Zheng et al. (2019).**

### 3. Results

#### 5.3.1 Surface Water Results

Our OpenFOAM results for pressure distribution across the dune surface follow the same trend as observed in the literature (Ahmerkamp et al., 2015; Janssen et al., 2012; Zheng et al., 2019) with high pressure near the middle of the dune, and low pressure on the extremes (Figures 5.3a, 5.4a). Peak pressures on the dune surface were directly proportional to channel flow velocity,  $u_x$ , (Figure 5.4a) as form drag increased. Conversely, there was an inverse relation between channel flow depth,  $d$ , and the amplitude of the peak pressures (Figure 5.4a – second item on each legend entry) because lower  $d$ 's occur due to steeper bed slopes,  $S_0$ . The shallower of two streams of equal  $u_x$ 's but disparate  $d$ 's has a greater  $S_0$  per equation  $S_0 = \tau_b / \rho g d$ , and the bed roughness has exerted more shear force to hold the shallow stream at the same  $u_x$ 's. As a result of the increased shear force, there is a higher  $c_b$ . Thus, there is a similar inverse relation with  $S_0$ ,  $\tau_b$ , and  $c_b$  versus  $d$  (Figure 5.4bcd). Additionally, comparing the gap between different  $u_x$  curves shows a roughly linear trend with  $S_0$  and  $\tau_b$  versus  $u_x$  (as the gaps between the curves are roughly equal), but a non-linear trend with  $c_b$  versus  $u_x$  (as the gap between the top and middle curve eclipses the gap between middle and bottom curve) (Figure 5.4bcd).

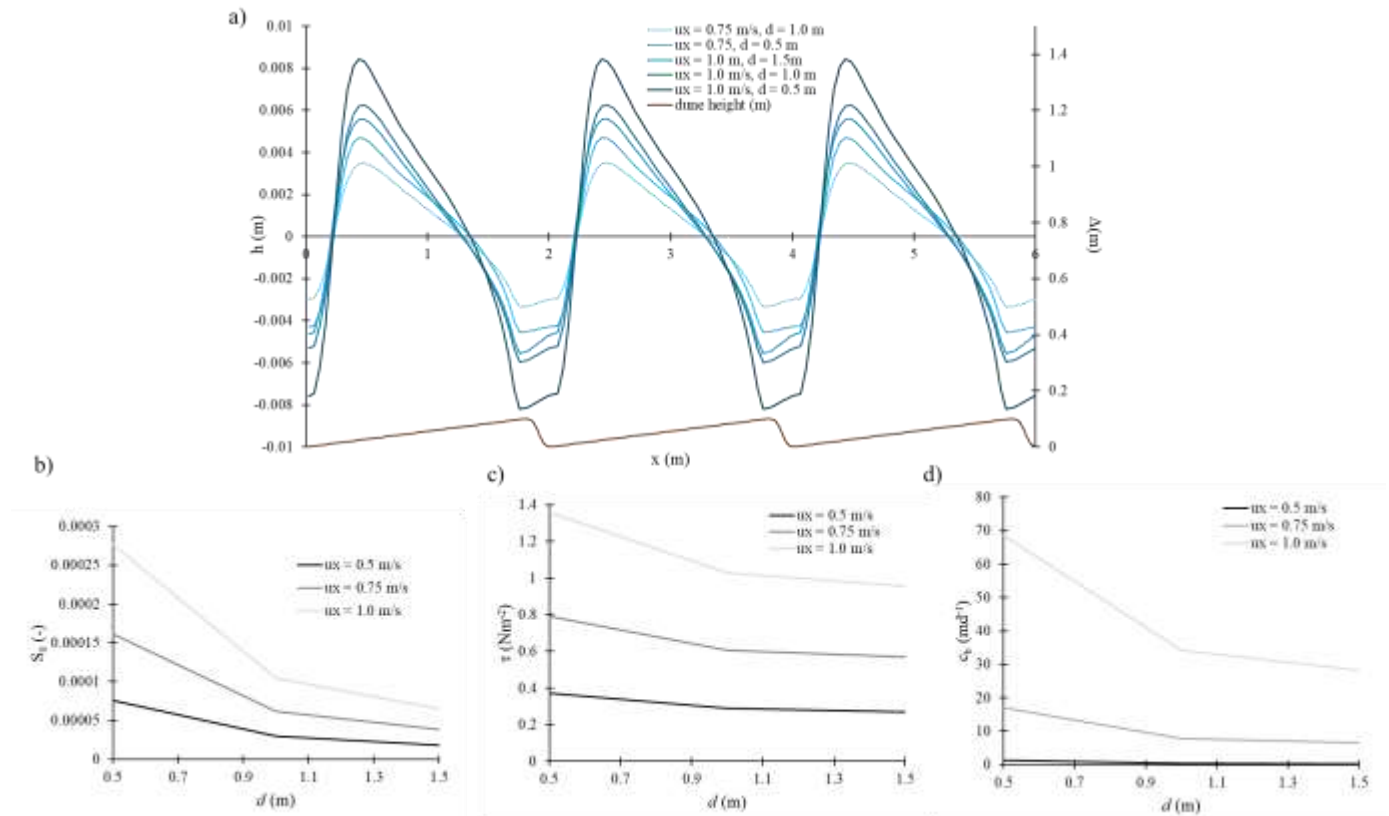


**Figure 5.4. a) Pressure head distribution,  $h$ , at various stream velocities and depths, and dune height,  $\Delta$  (right hand vertical axis) vs. longitudinal distance along dune surface,  $x$ . b) Channel bed slope  $S_0$  vs. channel flow depth above dune trough,  $d$ , at different average channel flow velocities,  $u_x$ . c) Bed shear stress,  $\tau_b$ , versus  $d$  at different  $u_x$ . d) Bedform celerity,  $c_b$  vs.  $d$  at different  $u_x$ .  $c_b$  calculated by equation 5.12,  $Fr$  calculated by  $Fr = u_x/\sqrt{gd}$ ,  $S_0$  calculated by  $S_0 = \tau_b/\rho gd$ , and  $\tau_b$  was imported from OpenFOAM.**

### 5.3.2 Groundwater Results

#### 5.3.2.1 Effect of Channel Velocity and Depth

Our results clearly demonstrate that as dune translation rate ( $c_b$ ) increases, moving dunes create transport conditions that are much different than those of static dunes. The simulated DOC plumes (Figure 5.5) can be used as a surrogate for the hyporheic flow cells that created them. We see that at low  $c_b$ , the portion of the DOC plume created by hyporheic exchange induced by hydrodynamic form drag over the dune (i.e. the only DOC plume in a static dune) was still present as an inverted arch at the bottom of the stoss (left) side of the dune, though not as prominently as in a fully static dune (Monterroso, 2021) (Figure 5.5). As  $c_b$  increased, the hydrodynamic plume decreased, while the portion of the DOC plume created by turnover hyporheic exchange (successive trapping and releasing of water as sediment moves) increased. The latter manifested as a DOC streak emanating from the lee (right) side of the dune, consistent with Zheng et al. (2019). Based on visual comparison, the areal extent of the DOC plume seems lowest at  $c_b = 17.02$  m/d, where the hydrodynamic plume associated with a stationary dune had greatly diminished, but the turnover plume had not yet significantly developed. The turnover plume grew wider and thicker with increasing  $c_b$ , commensurate with Zheng et al. (2019). However, the fully horizontal redox seal of Zheng et al. (2019) did not develop, which we discuss further in Section 5.4.3.

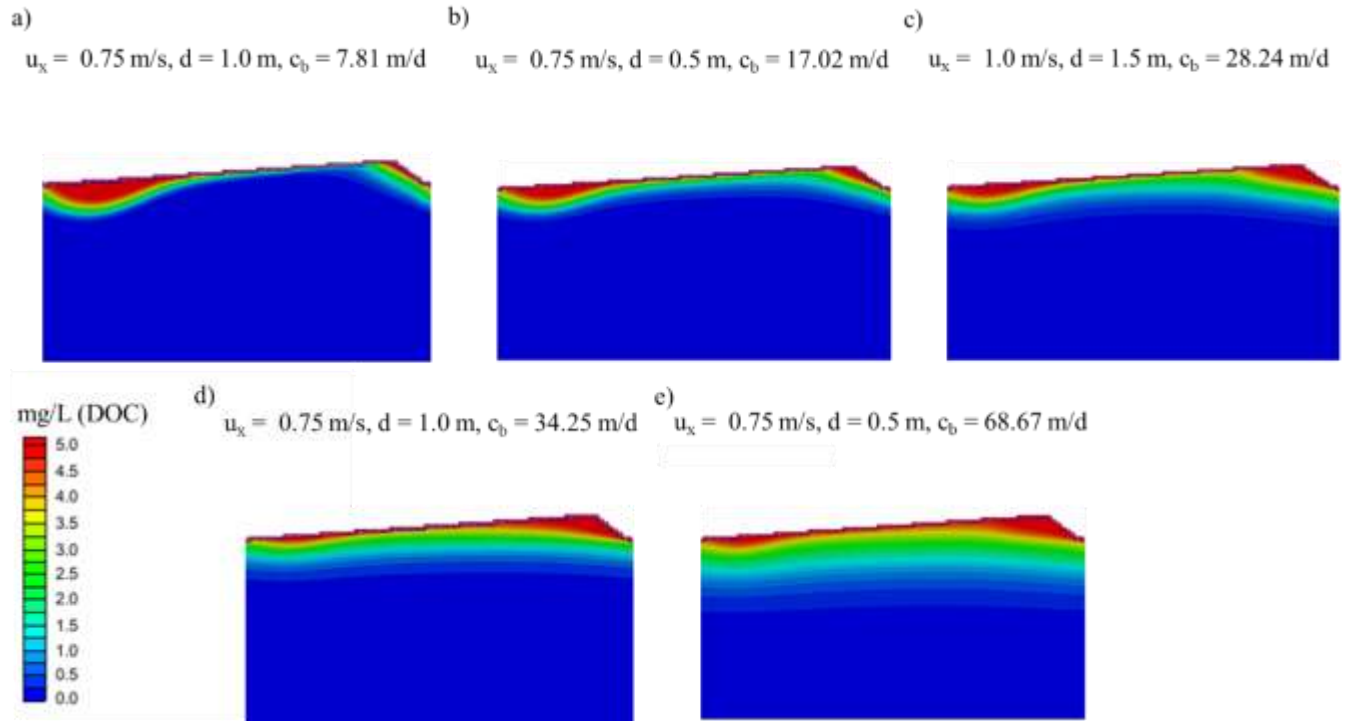


**Figure 5.5. Dissolved organic carbon (DOC) concentration maps at steady state (Figure 5.4) produced with the growth/death model for various velocity and depth combinations. We have ordered the plots based on celerity ( $c_b$ ) starting with the lowest value at the top left and progressing to bottom right. The biomass reached approximately steady state at  $t = 10$  days for  $c_b = 7.81, 17.02,$  and  $28.24$  m/d,  $t = 15$  days for  $c_b = 34.25$  m/d, and  $t = 20$  days for  $c_b = 68.67$  m/d (Figure F4). Note the DO concentration maps are not shown, but are essentially identical to the DOC concentration maps (Figure F2).**

For each channel flow velocity ( $u_x$ ) and depth ( $d$ ) scenario, we compared DOC consumption rates for model scenarios that simulated growth/death processes with those that did not (Figure 5.6a). Despite having almost an order of magnitude less biomass than the no-growth scenario, the growth scenario consumption rate was roughly double the no growth scenario in each case. This is because the biomass was allowed to grow into a denser population around the location of DOC plumes as well as die out in other areas when modeling growth and death dynamics, which did not occur in scenarios where growth and death dynamics were not modeled. In other words, the disparity is largely because in the no-growth scenarios, unrealistically, there are microbes deep in the subsurface far outside the DOC plumes. Thus, this disparity is somewhat a function of how large the domain is. This is commensurate with results in Figure 4 of Monterroso (2021) for static dunes. This shows that neglecting growth and death dynamics could significantly misrepresent biomass distribution and therefore the consumption rate. Note that if we had run scenarios where the biomass in the growth and no-growth scenarios were equivalent (i.e. same total biomass in the model domain)(these model runs are ongoing and will be added later), biomass values would have been even less, so the consumption would be even less, and the disparity would have been bigger. Moreover, viewing the consumption rate through the metric of removal per day per unit biomass (Figure 5.6b) further highlights the disparity

between modeling growth scenarios versus no growth scenarios. There is approximately an order of magnitude less removal per gram biomass in the no growth modeling approach versus the growth and death modeling approach. Note that the DO consumption rates have been relegated to the supporting information (Figure F3) as they are almost identical to the DOC consumption, and therefore do not shed any additional light on the processes.

There was also an overall positive trend of DOC consumption versus  $c_b$  (Figure 5.6). However, values of  $c_b$  in Figure 5.6 are a function of  $d$  and  $u_x$ , which might also affect the pressure head ( $h$ ) distribution which might also in turn affect the consumption rates. Nonetheless, investigating steady state consumption rate versus  $c_b$  (not varied independently but linked to physical scenarios) shows that there is generally a positive relationship between  $c_b$  and consumption rate. There is a slight dip in DOC consumption at a  $c_b$  of 17.02 m/d before it starts its general increase, probably due to the fact that there is less areal extent of the plume (Figure 5.6ab). This will be discussed more in Section 5.4.1. Figure 5.6 also demonstrates the profundity of  $c_b$ 's impact on DOC consumption rate; a stream with  $u_x = 1.0$  m/s, and  $d = 0.5$  m has roughly twice the consumption rate as with  $u_x = 0.75$  m/s, and  $d = 1.0$  m. Thus, a slightly faster, moderately shallower stream will produce significantly higher consumption rates than its slightly slower, moderately deeper counterpart.

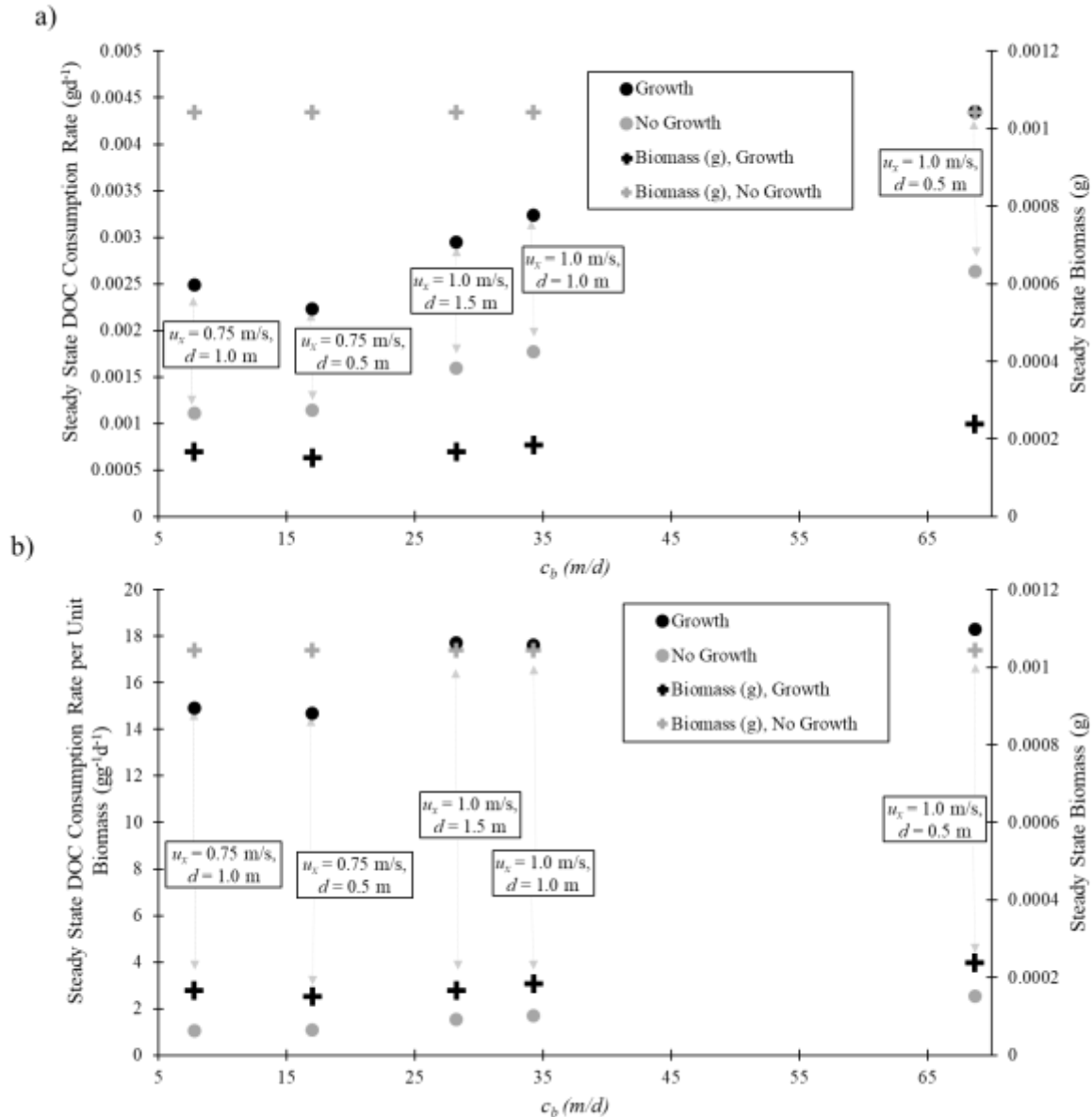


**Figure 5.6. a) Steady state DOC consumption rate and biomass in model domain vs. dune celerity,  $c_b$  (m/d) comparing model scenarios which simulated microbial growth and death with those that did not, for each average stream velocity ( $u_x$ ) and depth ( $d$ , surface to trough) combination. b) Same as in a) but DOC consumption normalized per gram biomass. The biomass reached approximately steady state at  $t = 10$  days for  $c_b$  7.81, 17.02, and 28.24 m/d;  $t = 15$  days for 34.25 m/d; and  $t = 20$  days for 68.67 m/d, (Figure F4).**

In Figure 5.7 we replotted the growth/death results from Figure 5.6 against  $u_x$  and  $d$ . There is a positive correlation between consumption rate and  $u_x$  at all the investigated  $d$ 's because of greater influx of reactants DO and DOC due to greater  $c_b$ . The correlation is more profound at lower  $d$ 's, as the consumption rate at  $u_x = 1.0$  m/s more than doubles that of  $u_x = 0.75$ , when  $d$  is held constant at 0.5 m. When  $u_x$  is fixed at 1.0 m/s, there is clearly an inverse

relationship between  $d$  and  $u_x$ . This is probably due to the fact that lower  $d$  leads to higher  $c_b$ . This is most likely due to higher turnover hyporheic exchange. When  $u_x = 0.75$  m, there is not the same negative correlation. This is probably a special case, most likely due to the areal extent of the plume, as it seems lowest at  $c_b = 17$  m/d, where  $c_b$  has mostly wiped out the hydrodynamic plume, but the turnover exchange coming from the lee side is not high enough yet to compensate for the loss in areal extent of the plume.

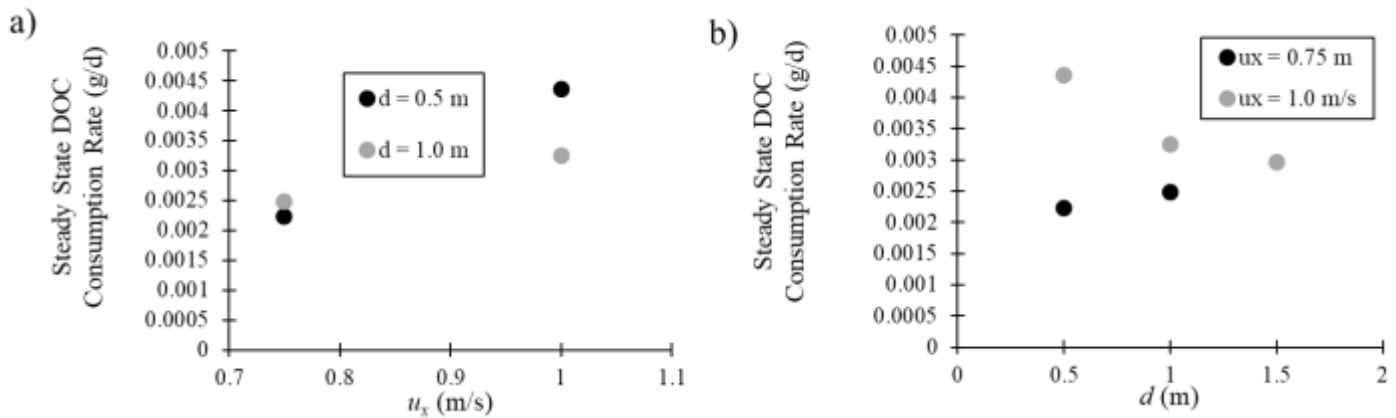


**Figure 5.7. Comparison of predicted steady state ( $t = 10$  days,  $u_x = 0.75$  m/s for both  $d$ 's;  $t = 15$  days for  $u_x = 1.0$  m/s,  $d = 1.0$  m;  $t = 20$  days,  $u_x = 1.0$  m/s,  $d = 1.0$  m; Figure F4) DOC consumption rates between  $u_x$  and  $d$  at dune trough ( $d$ ); a) DOC consumption rates versus  $u_x$  at different  $d$ . Note we did not include  $u_x = 1.0$  m/s,  $d = 1.5$  m, since only one system with a  $d = 1.5$  m, and purpose of the data points in this panel is to visualize DOC consumption with respect to  $u_x$  at fixed  $d$ . b) DOC consumption rates vs.  $d$ . at different  $u_x$ . All data points were produced with the growth/death model.**

### 5.3.2.2 Effects of Channel DOC/DO Concentration and Groundwater Upwelling Rate

When the instream DOC concentration doubled (i.e. increased from 5 mg/L to 10 mg/L), the consumption rates of both DO and DOC more than doubled (Figure 5.8ab). The biomass concentration also more than doubled simultaneously (Figure 5.8c). Biomass concentration did not realize the same growth when we raised the DO concentration from 5 mg/L to 10 mg/L, but kept DOC concentration at 5 mg/L (Figure 5.8c). However, the 10 mg/L DO concentration did exhibit slightly higher DOC consumption rate versus the base case (5 mg/L DOC; 5 mg/L DO). In this scenario, the microbes were not at all inhibited by the lack of DO, therefore the second bracketed term in Equation 5.18 emerges as unity. These trends are congruent with those observed in Figure 10 in Monterroso (2021) for the static case, revealing DOC to be a primary control on the flourishing of microbe colonies.

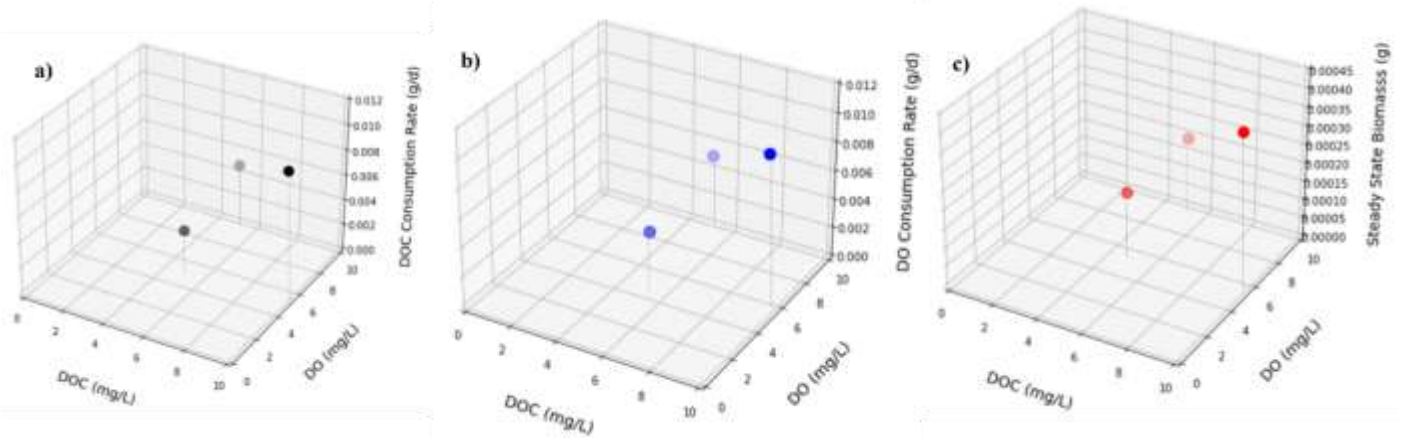


**Figure 5.8.** Comparison of the steady state ( $t = 15$  hrs. for 5 mg/L DOC, 5 mg/L DO;  $t=20$  hrs. for the others) consumption rate of DOC/DO, as well as total steady state biomass (g) under each combination of DOC/DO in-stream concentration; base case 5 mg/L of DOC and 5 mg/L of DO, 10 mg/L of DOC and 5 mg/L of DO, and 5 mg/L of DOC and 10 mg/L of DO we show results for each of these for a) DOC consumption rate, b) DO consumption rate, and c) biomass;  $u_x = 1.0$  m/s,  $d = 1.0$  m, and  $c_b = 34.25$  m/d for all scenarios. Note that the data points which coincide with the vertical axis/DOC axis plane appear shaded.

We found a negative relation between DOC/DO consumption and groundwater upwelling rate,  $W$ , at the bottom model boundary (Figure 5.9). Higher  $W$ 's led to smaller hyporheic flow cells and thus smaller DO/DOC plumes, and therefore less consumption which we discuss further in Section 5.4.1. Increasing the upwelling rate from the lowest up-welling rate of  $0.00088$   $\text{m}^3/\text{d}$  to  $0.0088$   $\text{m}^3/\text{d}$  cuts consumption rates almost in half, and further increasing the upwelling rate from  $0.0088$   $\text{m}^3/\text{d}$  to the highest up-welling rate  $0.03$   $\text{m}^3/\text{d}$  also cuts the consumption rates almost in half again.

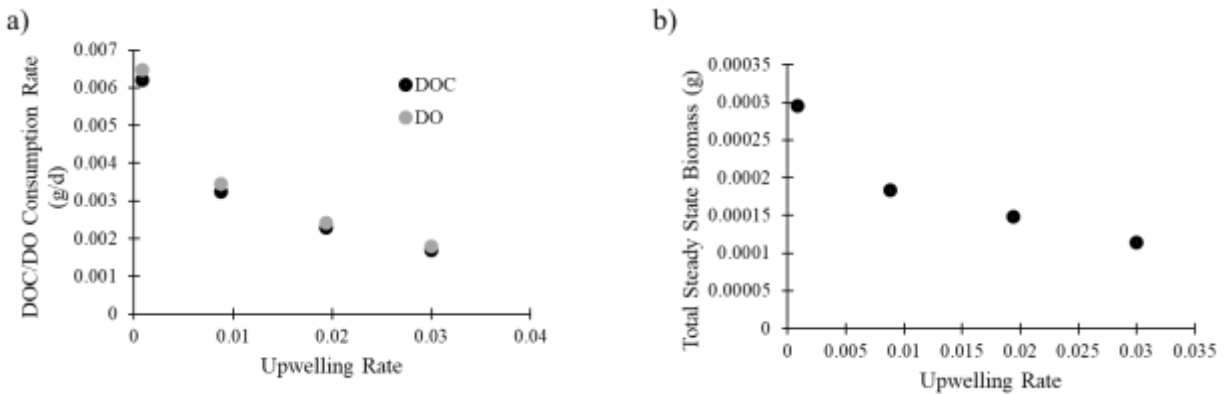


**Figure 5.9.** a) Steady state ( $t=15$  hrs. for  $0.008$   $\text{m}^3/\text{d}$ ,  $t = 10$  hrs. for  $0.03$   $\text{m}^3/\text{d}$ ) DOC/DO consumption rate versus groundwater upwelling rate at model bottom boundary, where we examined the  $W = 0.008$   $\text{m}^3/\text{d}$  (base case) and the  $W = 0.03$   $\text{m}^3/\text{d}$  scenario. Total steady state biomass (g) vs.  $W$ ;  $u_x = 1.0$  m/s,  $d = 1.0$  m, and  $c_b = 34.25$  m/d for all scenarios. (More data points to follow).

## 5.4 Discussion

### 5.4.1 Effects of Increasing Celerity on Biomass and DOC Dynamics

The aerobic biomass spatial distributions (Figure 5.10) mirrored the DOC concentration plumes (Figure 5.5), showing that the aerobes go “where the food is.” The areal extent of these biomass distributions then increased with  $c_b$  (Figures 5.10 and 5.11a). The biomass concentration then directly affects the consumption rate (Equation 5.18). This is reflected in Figure 5.11a mirroring Figure 5.6a, suggesting that consumption rate is related to total biomass. The more biomass, the more the colony as a whole can consume DOC.

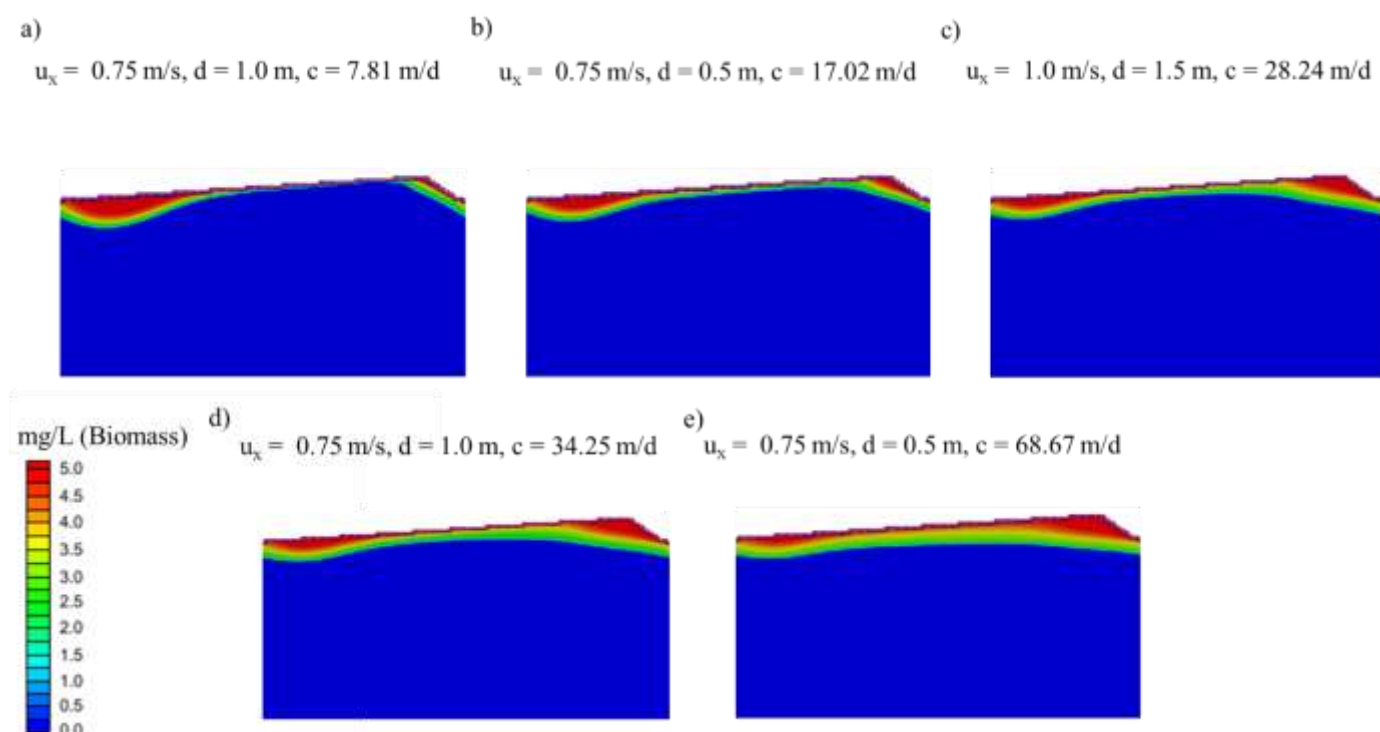


**Figure 5.10. Biomass concentration maps (mg/L) for various velocity and depth combinations, where we have ranked ordered the plots based on celerity starting with the lower value at the top left and progressing from left to right, top to bottom. The biomass reached approximately steady state at  $t = 10$  days for  $c_b = 7.81$ ,  $17.02$ , and  $28.24$  m/d,  $t = 15$  days for  $c_b = 34.25$  m/d, and  $t = 20$  days for  $c_b = 68.67$  m/d (Figure F4).**

Scenarios with higher  $c_b$  values fed more DOC substrate into the system (Figure 5.11b), which sustained larger colonies both in terms of biomass (Figure 5.11a) and area (Figure 5.11c). Also, the dip in Figure 5.6a with respect to the consumption versus  $c_b$  curve at  $c_b = 17.02$  m/d corresponded to a dip in biomass and DOC plume area Figure 5.11ac at  $17.02$  m/d. Further, comparing the growth and no-growth models shows that the dip in DOC consumption only occurs in the growth model (Figure 5.6a) since the biomass migrates and coalesces in the DOC plume. As a consequence of the link between biomass and DOC plume area, the decrease in areal

extent in DOC makes more of an impact in the growth model curve (Figure 5.6a) since it affects both substrate concentration and biomass concentration.

Moreover, the consumption versus celerity curve (Figure 5.6a) does not mimic the behavior of the DOC influx curve (Figure 5.11b), suggesting that DOC consumption is not a direct linear function of DOC influx. Rather, DOC influx most likely affects the rate of consumption indirectly by allowing more DOC to reach the stoss side, thus causing the concentrations to be higher (Figure 15d). Examining equation 15.8 shows that increasing substrate concentration increases the rate of consumption. The DOC curve rises up higher in the  $c_b = 68.67$  m/d case versus the 7.81 m/d than both the biomass and areal distribution (comparing 5.6a with 5.11ac). This is because the DOC consumption increases with celerity not only because there is a bigger microbial colony, but also because the microbial colony is consuming at a higher rate due to higher concentration, especially near the stoss-side of the dune. Note that for all these scenarios, residence time is most likely not a factor that controls consumption. For example, with  $c_b = 68.67$  m/d, we would expect it to halve the residence time as with  $c_b = 34.25$  m/d. If the system were at all affected residence time, it would counteract some of the increased turnover and reduce the aerobic spatial distribution area. However, we do not observe any evidence of the negative effect that increasing  $c_b$  would have on residence time and subsequently DOC consumption rate.

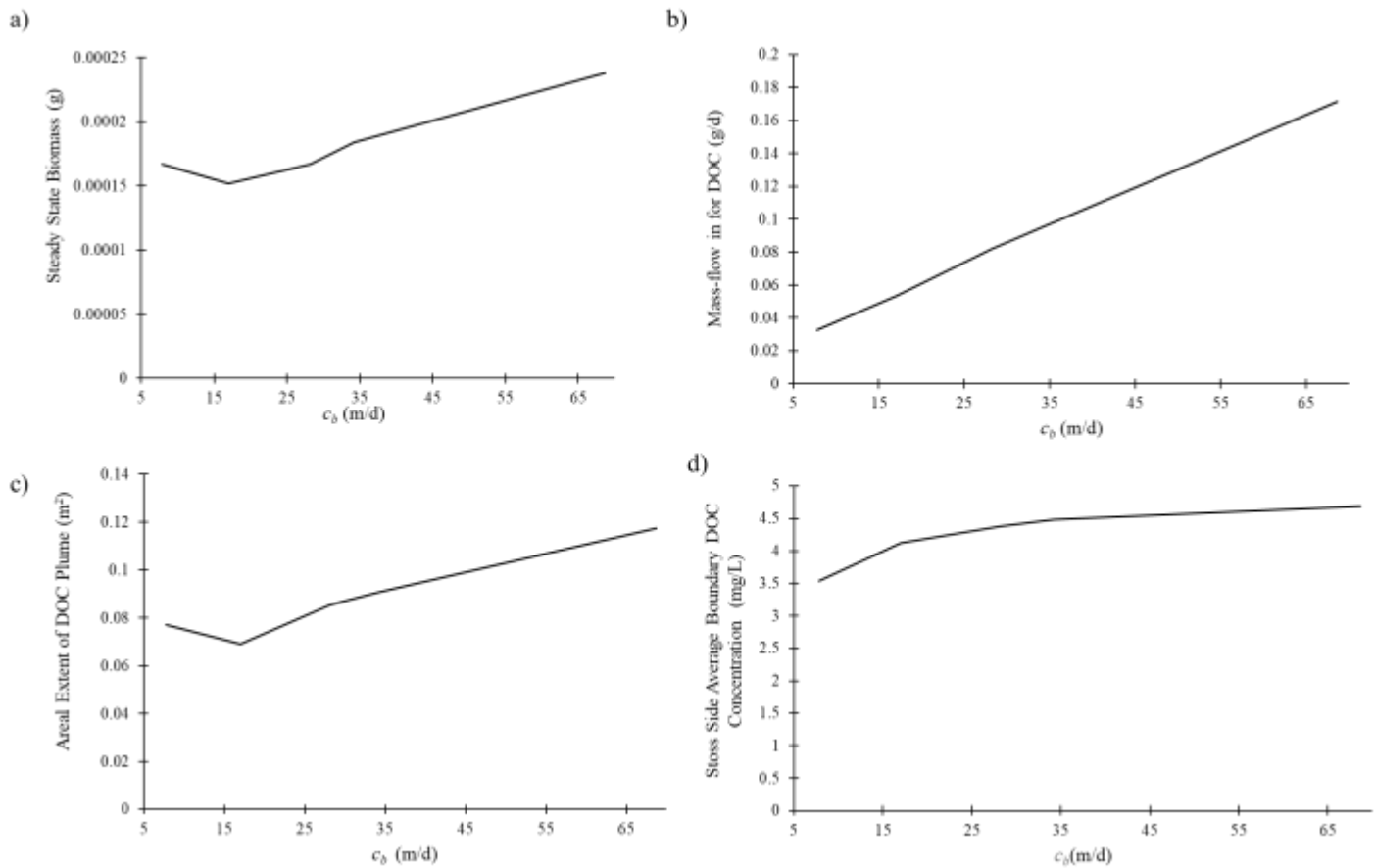


**Figure 5.11. a) Steady state biomass (g) vs.  $c_b$  (m/d). The  $c_b$  values represented here are 7.81, 17.02, 28.24, 34.25, and 68.67 m/d. b) Steady state DOC influx into the system from the surface water (top) boundary. c) Areal extent of DOC plume vs. celerity. d) The average DOC concentration immediately inside the stoss side (the cells immediately below the boundary cells). This was determined by counting the number of cells where  $C_{\text{DOC}} > 3.5$  mg/L and multiplying by the cell area. The biomass reached approximately steady state at  $t = 10$  days for  $c_b = 7.81, 17.02,$  and  $28.24$  m/d,  $t = 15$  days for  $c_b = 34.25$  m/d, and  $t = 20$  days for  $c_b = 68.67$  m/d (Figure F4).**

We recognize that direct comparisons of our results for moving dunes to those for static dunes would be useful to estimate the error incurred by assuming static dunes when conducting numerical simulations. However, such a direct comparison is physically ambiguous because static dunes do not occur in real rivers, and hence we cannot conduct static dune simulations with surface flow depths or channel slopes that are consistent with the moving dune scenarios. For these reasons we do present a static dune comparison, but we have included it in Appendix F. The latter examines the theoretical scenario where the pressure distribution remains constant while we explore the full interval of  $c_b$  values from 0 to 68.67 m/d. But we emphasize that  $c_b \sim 7.81$  m/d is necessary to impel dune formation while anything less would lead to ripples or no bedforms at all.

#### 5.4.2 Relative Importance of Celerity Versus Pore Water Velocity

The non-dimensional ratio of dune celerity ( $c_b$ ) to porewater velocity ( $u_r$ ) can be used to characterize the relative importance of turnover exchange and hydrodynamic exchange. It is calculated as:

$$u_r = \frac{c_b}{u_p} \quad [5.21]$$

where  $u_p$  is characteristic porewater velocity (Ahmerkamp et al., 2015). Characteristic porewater velocity is then given by the following interpretation of Darcy's Law (Ahmerkamp et al., 2015)

$$u_p = 2 \frac{K \Delta h_{max}}{\theta L} \quad [5.22]$$

where we have replaced permeability and viscosity in Ahmerkamp et al. (2015) with hydraulic conductivity,  $K$ .  $\Delta h_{max}$  (m) is the maximum head difference along the dune given by twice the amplitude of the head distributions in Figure 5.4a,  $L$  (m) is dune length and  $\theta$  (-) is the sediment porosity. Examining this ratio for all our  $u_x$  and  $d$  combinations shows that for each scenario, even for the lowest celerity ( $c_b = 7.81$  m/d,  $u_x = 0.75$  m/s;  $d = 1.0$  m), the system was dominated by  $c_b$  as the lowest value of  $u_r$  is  $\sim 3$  (Figure 5.12). There are also some cases where the increase in  $c_b$  was accompanied by an even bigger increase in  $u_p$  (from  $c_b = 17.02$  m/d,  $u_x = 0.75$  m/s,  $d = 0.5$  m, to  $c_b = 28.24$  m/d,  $u_x = 1.0$  m/s,  $d = 1.5$  m), indicating that there are multiple phenomena at work. Thus, since Figure 5.12 represents the lowest  $c_b$  at which dunes form, this means that the system is always dominated by  $c_b$ . Note that we did not go down to zero  $c_b$  because that would be an unphysical scenario. As  $c_b$  decreased much below 7.81 m/d, the system will then

form ripples; and any lower, it will not form bedforms at all. Thus, only quiescent streams would have zero  $c_b$ , but there would also be no dunes, nor would there be form drag if there was somehow a dune. Nevertheless, we note that most prior studies of reactions in dune-induced hyporheic zones assumed static dunes (Bardini et al., 2012; Cardenas and Wilson, 2007a; b; Elliott and Brooks, 1997b; Hester et al., 2013; 2014; Marzadri et al., 2016), which by definition would have  $u_r = 0$ .

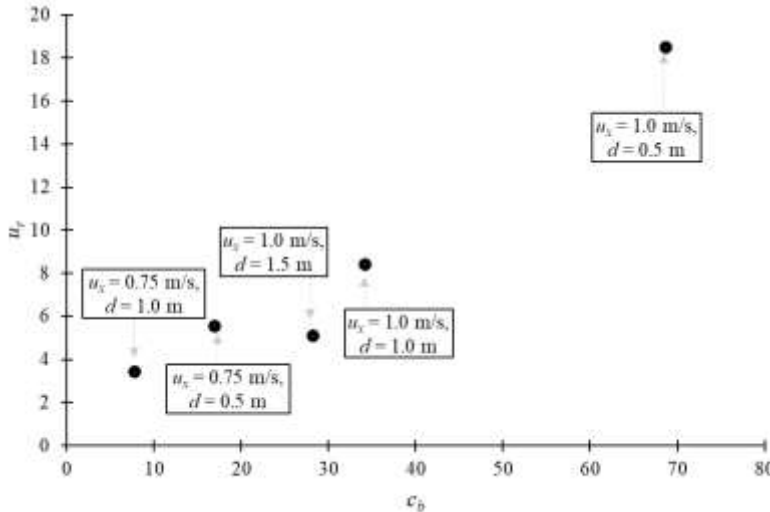


**Figure 5.12. Porewater/celerity ratio,  $u_r$ , versus celerity for each combination of average channel flow velocity,  $u_x$ , and channel flow depth over the dune trough,  $d$ .**

### 5.4.3 Scientific Contribution and Practical Application

While our results are consistent with much existing work on the effects of dune translation on subsurface biogeochemistry (Ahmerkamp et al., 2015; Kessler et al., 2015; Zheng et al., 2019), we did not observe as pronounced a redox seal as Zheng et al. (2019). The latter difference can be explained by examining the differences in conceptual models between the studies. First, our channel flow velocities are almost an order of magnitude more than theirs. It takes much higher flow velocity to achieve the same celerity for a dune versus a ripple. Consequently, a higher amplitude pressure distribution develops, and influences the flow paths by increasing the relative importance of hydrodynamic hyporheic exchange. Secondly, Zheng et al. (2019) did not model upwelling. Upwelling also makes a slightly positive contribution to the y-component of porewater velocity causing flow paths to bend slightly upward in the middle of the dune as water exits the stoss side, and so we would not expect a straight redox seal given that we model upwelling. Finally, Zheng et al. (2019) used longitudinal dispersivity of 3 cm, which was particularly high especially given the fact that their domain is about an order of magnitude smaller than ours. This might blend out or obscure some of the curvature of the DOC plume.

Our results also emphasize the need to incorporate microbial growth/death dynamics to accurately model hyporheic biogeochemistry. As shown in Figure 5.6, even with the total

biomass in the system significantly lower in the growth and death model, the growth and death model predicted roughly double the DOC/DO consumption rate. To model the system accurately while neglecting growth and death, the modeler would somehow have to know the final steady state biomass distribution. Modelers could use data from field studies (Lowell et al., 2009) to assume a microbial concentration of the microbe colony. However, the microbial population density/rate kinetics that are observed at a particular field site at a particular time of year are unlikely to directly apply to a given proposed model scenario since spatial layout of microbial communities in the hyporheic zone is highly heterogeneous and would vary with field conditions such as temperature, soil texture and organic content, reactant concentrations, and hydraulic boundary conditions. Thus, the modeler should use a rate linked to the boundary conditions of the scenario being studied – which can be obtained best by modeling microbial growth and death. Nevertheless, implementing the growth and death model introduces new variables, each of which have uncertainty (such as yield coefficient). So, instead of the assumed microbe colony concentration influencing the model as with a no-growth model, the yield coefficient could influence a growth/death model in the same way, since it drives the rate at which the colony grows.

We have also shown that DOC consumption increases with dune celerity. This is due to the combined effect of increasing the areal extent of the DOC plume, and also increasing the turnover rate thereby increasing DOC flow into the system. We have also shown that DOC consumption is related spatial area the microbes can flourish in, as well as the density to which they can grow to. This has a few implications in terms of practical applications in the area of pollutant attenuation. While we have simulated DOC/DO consumption in this study, future research could include pollutant removal such as denitrification of excess nitrate. In terms of practical application, it may be possible to capitalize on the increased turnover and therefore pollutant consumption by implementing a series of instream structures (such as rock dams) with bed material conducive to dune-formation (i.e. medium to coarse sand). Not only will this potentially increase nitrate removal (and that of other pollutants) due to more turnover, it will also cause more hyporheic exchange (and therefore nitrate removal) by increasing hydrostatic pressure head at the bottom of the upstream side of the rock dam (Hester and Doyle, 2008). Velocities could be manipulated by the instream structures, by manipulating parameters such as the width of the gap in the center of a rock dam. Velocities must be increased only slightly to minimize downstream scouring and erosion. Our results showed that only a modest increase in stream velocity from 0.75 m/s to 1.0 m/s increased the DOC consumption rate by roughly double, and so even slight increases in velocities below scouring and erosion thresholds may still enhance reactions such as nitrate biodegradation significantly. Since there is a negative relationship between upwelling and DOC consumption rates, the rock dams should not be placed where upwelling is prevalent such as where is forced up to the surface by large scale bedrock outcrops (Hiscock and Grischek, 2002). Although even with slight velocities, it is likely that scouring and erosion will occur over time, and the rock dam may require periodic maintenance.

#### *5.4.4 Limitations and Future Study*

Although our study provides valuable insight into the combined effects of dune translation and microbial growth, we acknowledge certain limitations which provide opportunities for future research. First, we did not account for bio-clogging (Caruso et al., 2017; Chowdhury et al., 2020; Cook et al., 2020), which has the potential to significantly affect turnover rate. Nevertheless, our study offers useful insights and understanding about how the system behaves under the combined effects of microbial growth and death, and dune translation.

Secondly, we have not addressed the impact of climate change and seasonal variation. Future studies could be designed to incorporate the effects of both of these phenomena. Climate change may lead to higher flashy peak flowrates in storm events (Apsite et al., 2011), higher temperatures (Du et al., 2019), and high in-stream pollutant rates (Molina-Navarro et al., 2018), which can be incorporated into the OpenFOAM via high velocities and SEAM3D boundary conditions via high pollutant concentration, respectively. Furthermore, SEAM3D could be modified by adding the heat transport equation to model heat flux and the Arrhenius equation to account for temperature changes of climate change on temperature-dependent reaction parameters.

Another limitation is that we only explored a small part of the parameter space in terms of dune geometry (only one case of one type of dune), and a narrow range of upwelling and DOC/DO instream concentrations. We have not explored the case where DOC or DO are limiting, as neither are ever close to being totally consumed in any of the cases studied herein. Nonetheless, our work gives insight into the impacts of these parameters, and lays the foundation for future research. Future studies could also include a more rigorous probe of the porewater space to celerity ratio,  $u_r$  conducting many permutations of hydraulic conductivity (K) values (we used only one K value throughout) and celerity values and to see if there is any universal trend or governing principle that emerges. Further studies could also examine the transient effects of temporally varying surface water boundary conditions. Finally, we have only examined DOC consumption, and although it provides further understanding of the physical system, we have not looked at nitrate removal. Excess nitrate is a pollutant that could be removed using the principles discussed herein. Further studies could investigate nitrate dynamics subjected to the same conditions.

## 5.5 Conclusions

In this study, we numerically simulated the impact of riverbed dune translation and microbial growth/death dynamics on hyporheic aerobic respiration. We coupled three models together: an OpenFOAM surface water model, a MODFLOW groundwater model, and a SEAM3D reactive transport model which incorporates microbial growth/death dynamics that we modified to account for dune migration using a moving frame of reference. We examined the range of channel flow velocity and depth combinations often found in-situ for our selected dune size, as well as impacts of up-welling and change in DO/DOC loading. For the velocity/depth sensitivity analysis, we compared growth models with no-growth models.

We have made several useful insights with this study. First, we have shown that it is important to use a model which accounts for growth/death dynamics, if subsurface biogeochemistry is to be modeled accurately. In our case, neglecting microbial growth/death led to roughly a 50% under-estimation of that predicted by microbial growth/death. We have also shown through calculating a non-dimensional ratio of dune celerity to porewater velocity that turnover exchange always dominated hydrodynamic exchange caused by form drag over the dunes (3 times more important at the lowest  $c_b = 7.81$  m/d). Thus, systems with moving dunes behaved much differently than those with static dunes, as the plumes associated with form drag were extirpated by turnover exchange emanating from the lee side. This highlights the inaccuracies of the conventional approach to modeling hyporheic reactions in riverbed dunes that assumes static dunes. We have also revealed that DOC and DO consumption increase with increased celerity due in part to increased flowrate of DOC and DO into the system, but also due to DOC plume area. Accordingly, there is a local minimum of DOC consumption at a celerity of 17.02 m/s, commensurate with  $u_x = 0.75$  m/s, and  $d = 0.5$ m. Further, we found doubling the DOC consumption rate more than doubles both the steady state DOC and DO consumption rates. We also found that DOC consumption is significantly reduced as upwelling increased.

These results bear implications for enhancing mechanisms of natural pollutant attenuation in streams and rivers. In particular, as a consequence of the positive relationship between celerity and DOC consumption rate, a modest increase in velocity leads to roughly 50-100% increase in DOC consumption (Figure 5.7). This principle could potentially be harnessed through the use of instream structures such as partial rock dams. This study pioneers into the unknown realm of where there is dune translation, with microbial colonies operating under microbial growth/death principles, and we provide good initial insight into the behavior of this system where the biogeochemistry is being lost in dune translation.

## Acknowledgements

We thank the Department of Energy for support to W. Lotts and E. Hester. We would also like to thank Eduardo Mendez for his assistance with FORTRAN. Data will be published in Hydroshare ([www.hydroshare.org](http://www.hydroshare.org)), and a link to the data archive will be included here if the manuscript is accepted for publication.

## References

- Abeshu, G.W., Li, H.-Y., Zhu, Z., Tan, Z. and Leung, L.R. 2022. Median bed-material sediment particle size across rivers in the contiguous US. *Earth Systems Science Data* 14(2), 929-942.
- Ahmerkamp, S., Winter, C., Janssen, F., Kuypers, M. and Holtappels, M. 2015. The impact of bedform migration on benthic oxygen fluxes. *Journal of Geophysical Research-Biogeosciences*, published online.
- Apsite, E., Bakute, A., Elferts, D., Kurpniece, L. and Pallo, I. 2011. Climate change impacts on river runoff in Latvia. *Climate Research* 48, 57-71.
- Aquaveo, L. 2021 Groundwater Modeling System, Aquaveo, LLC, 3210 N. Canyon Road, Suite 300, Provo, Utah 84604, United States, <http://www.aquaveo.com>.

- Arrigoni, A.S., Poole, G.C., Mertes, L.A.K., O'Daniel, S.J., Woessner, W.W. and Thomas, S.A. 2008. Buffered, lagged, or cooled? Disentangling hyporheic influences on temperature cycles in stream channels. *Water Resources Research* 44, W09418.
- Ashley, G.M. 1990. Classification of large-scale subaqueous bedforms: A new look at an old problem-SEPM bedforms and bedding structures. *Journal of Sedimentary Research* 60(1), 160-172.
- Balvanera, P., Pfisterer, A.B., Buchmann, N., Jing-Shen, H., Nakashizuka, T., Raffaelli, D. and Schmid, B. 2006. Quantifying the evidence for biodiversity effects on ecosystem functioning and services. *Ecology Letters* 9, 1146-1156.
- Bardini, L., Boano, F., Cardenas, M.B., Revelli, R. and Ridolfi, L. 2012. Nutrient cycling in bedform induced hyporheic zones. *Geochimica Et Cosmochimica Acta* 84, 47-61.
- Bayon-Barrachina, A. and Lopez-Jimenez, P.A. 2015. Numerical analysis of hydraulic jumps using OpenFOAM. *Journal of Hydroinformatics* 17(4), 662-678.
- Bencala, K.E. 2000. Hyporheic zone hydrological processes. *Hydrological Processes* 14(15), 2797-2798.
- Boulton, A.J., Findlay, S., Marmonier, P., Stanley, E.H. and Valett, H.M. 1998. The functional significance of the hyporheic zone in streams and rivers. *Annual Review of Ecology and Systematics* 29, 59-81.
- Bradley, R.W. and Venditti, J.G. 2019. Transport scaling of dune dimensions in shallow flows. *JGR Earth Surface* 124, 526-347.
- Brunke, M. and Gonser, T. 1997. The ecological significance of exchange processes between rivers and groundwater. *Freshwater Biology* 37(1), 1-33.
- Burkholder, B.K., Grant, G.E., Haggerty, R., Khangaonkar, T. and Wampler, P.J. 2008. Influence of hyporheic flow and geomorphology on temperature of a large, gravel-bed river, Clackamas River, Oregon, USA. *Hydrological Processes* 22(7), 941-953.
- Cardenas, M.B. 2009. A model for lateral hyporheic flow based on valley slope and channel sinuosity. *Water Resources Research* 45, W01501.
- Cardenas, M.B. and Wilson, J.L. 2006. The influence of ambient groundwater discharge on exchange zones induced by current-bedform interactions. *Journal of Hydrology* 331(1-2), 103-109.
- Cardenas, M.B. and Wilson, J.L. 2007a. Dunes, turbulent eddies, and interfacial exchange with permeable sediments. *Water Resources Research* 43(8), W08412.
- Cardenas, M.B. and Wilson, J.L. 2007b. Hydrodynamics of coupled flow above and below a sediment-water interface with triangular bedforms. *Advances in Water Resources* 30(3), 301-313.
- Carpenter, S.R., Caraco, N.F., Correll, D.L., Howarth, R.W., Sharpley, A.N. and Smith, V.H. 1998. Nonpoint pollution of surface waters with phosphorus and nitrogen. *Ecological Applications* 8(3), 559-568.
- Caruso, A., Boano, F., Ridolfi, L., Chopp, D.L. and Packman, A. 2017. Biofilm-induced bioclogging produces sharp interfaces in hyporheic flow, redox conditions, and microbial community structure. *Geophysical Research Letters* 44, 4917-4925.
- Chapelle, F.H., Bradley, P.M., McMahon, P.B., Kaiser, K. and Benner, R. 2012. Dissolved Oxygen as an indicator of bioavailable dissolved organic carbon in groundwater. *Ground Water* 50(2), 230-241.
- Charru, F., Bouteloup, J., Bonometti, T. and Lacaze, L. 2016. Sediment transport and bedforms: a numerical study of two-phase viscous shear flow. *Meccanica* 51, 3055-3065.

- Chowdhury, R.S., Zarnetske, J., Phanikumar, M.S., Briggs, M.A., Day-Lewis, F. and Singha, K. 2020. Formation criteria for hyporheic anoxic microzones: assessing interactions of hydraulics, nutrients, and biofilms. *Water Resources Research* 56, 1-15.
- Cisneros, J., Best, J., van Dijk, T., Paes de Almeida, R., Amsler, M., Boldt, J., Freitan, B., Galeazzi, C., Huizinga, R., Ianniruberto, M., Ma, H., Nittrouer, J.A., Oberg, K., Orfeo, O., Parsons, D., Szupiany, R., Wang, P. and Zhang, Y. 2020. Dunes in the world's big rivers are characterized by low-angle lee-side sloped and a complex shape. *Nature Geoscience* 13, 156-162.
- Climent, M.J., Herrero-Hernández, E., Sánchez-Martín, M.J., Rodríguez-Cruz, M.S., Pedreros, P. and Urrutia, R. 2019. Residues of pesticides and some metabolites in dissolved and particulate phase in surface stream water of Cachapoal River basin, central Chile. *Environmental Pollution* 251, 90-101.
- Climent, M.J., Sanchez-Martin, M.J., Rodriguez-Cruz, M.S., Pedreros, P., Urrutia, R. and Herrero-Hernandez, E. 2018. Determination of Pesticides in River Surface Waters of Central Chile Using Spe-Gc-Ms Multi-Residue Method. *Journal of the Chilean Chemical Society* 63(2), 4023-4031.
- Coleman, S.E. and Melville, B.W. 1994. BED-FORM DEVELOPMENT. *Journal of Hydraulic Engineering-Asce* 120(5), 544-560.
- Cook, S., Price, O., King, A., Finnegan, C., van Egmond, R., Schafer, H., Pearson, J.M., Abolfathi, S. and Bending, G.D. 2020. Bedform characteristics and biofilm community development interact to modify hyporheic exchange. *Science of the Total Environment* 749, 1-12.
- Cummins, K.W. and Klug, M.J. 1979. Feeding Ecology of Stream Invertebrates. *Annual Review of Ecology and Systematics* 10, 147-172.
- Dieter, C.A., Maupin, M.A., Caldwell, R.R., Harris, M.A., Ivahnenko, T.I., Lovelace, J.K., Barber, N.L. and Linsey, K.S. 2018. Estimated use of water in the United States in 2015, p. 65 p., Reston, VA.
- Du, X.Z., Shrestha, N.K. and Wang, J.Y. 2019. Assessing climate change impacts on stream temperature in the Athabasca River Basin using SWAT equilibrium temperature model and its potential impacts on stream ecosystem. *Science of the Total Environment* 650, 1872-1881.
- Dubrovsky, N.M., Burow, K.R., Clark, G.M., Gronberg, J., Hamilton, P.A., Hitt, K.J., Mueller, D.K., Munn, M.D., Nolan, B.T. and Puckett, L.J. 2010. The Quality of Our Nation's Water: Nutrients in the Nation's Streams and Groundwater, 1992-2004. USGS Circular 1350. US Department of the Interior, US Geological Survey.
- Elger, D.F., Lebert, B.A., Crowe, C.T. and Roberson, J.A. (2016) *Engineering Fluid Mechanics* (11th Edition), John Wiley & Sons, Inc., Hoboken, NJ 07030.
- Elliott, A.H. and Brooks, N.H. 1997a. Transfer of nonsorbing solutes to a streambed with bed forms: Laboratory experiments. *Water Resources Research* 33(1), 137-151.
- Elliott, A.H. and Brooks, N.H. 1997b. Transfer of nonsorbing solutes to a streambed with bed forms: Theory. *Water Resources Research* 33(1), 123-136.
- Findlay, S., Strayer, D., Goumbala, C. and Gould, K. 1993. METABOLISM OF STREAMWATER DISSOLVED ORGANIC-CARBON IN THE SHALLOW HYPORHEIC ZONE. *Limnology and Oceanography* 38(7), 1493-1499.

- Fox, A., Boano, F. and Arnon, S. 2014. Impact of losing and gaining streamflow conditions on hyporheic exchange fluxes induced by dune-shaped bed forms. *Water Resources Research* 50(3), 1895-1907.
- Frei, S., Piehl, S., Gilfedder, B.S., Loder, M.G.J., Krutzke, J., Wilhelm, L. and Laforsch, C. 2019. Occurrence of microplastics in the hyporheic zone of rivers. *Scientific Reports* 9, 1-10.
- Fuller, C.C. and Harvey, J.W. 2000. Reactive uptake of trace metals in the hyporheic zone of a mining-contaminated stream, Pinal Creek, Arizona. *Environmental Science & Technology* 34(7), 1150-1155.
- Gelhar, L.W., Welty, C. and Rehfeldt, K.R. 1992. A critical-review of data on field-scale dispersion in aquifers. *Water Resources Research* 28(7), 1955-1974.
- Gomez-Velez, J. and Harvey, J.W. 2014. A hydrogeomorphic river network model predicts where and why hyporheic exchange is important in large basins. *Geophysical Research Letters* 41(18), 6403-6412.
- Gomez-Velez, J.D., Harvey, J., Cardenas, M.B. and Kiel, B. 2015. Denitrification in the Mississippi River network controlled by flow through river bedforms. *Nature Geoscience* 8(12), 941-U975.
- Harbaugh, A.W., Banta, E.R., Hill, M.C. and McDonald, M.G. 2000. MODFLOW-2000, the U.S. Geological Survey modular ground-water model -- User guide to modularization concepts and the Ground-Water Flow Process.
- Hester, E.T. and Doyle, M.W. 2008. In-stream geomorphic structures as drivers of hyporheic exchange. *Water Resources Research* 44(3), W03417.
- Hester, E.T., Doyle, M.W. and Poole, G.C. 2009. The influence of in-stream structures on summer water temperatures via induced hyporheic exchange. *Limnology and Oceanography* 54(1), 355-367.
- Hester, E.T. and Gooseff, M.N. (2011) *Stream Restoration in Dynamic Fluvial Systems: Scientific Approaches, Analyses, and Tools* Simon, A., Bennett, S.J. and Castro, J.M. (eds), American Geophysical Union, Washington, DC.
- Hester, E.T., Young, K.I. and Widdowson, M.A. 2013. Mixing of surface and groundwater induced by riverbed dunes: implications for hyporheic zone definitions and pollutant reactions. *Water Resources Research* 49, 5221-5237.
- Hester, E.T., Young, K.I. and Widdowson, M.A. 2014. Controls on mixing-dependent denitrification in hyporheic zones induced by riverbed dunes: A steady state modeling study. *Water Resources Research* 50(11), 9048-9066.
- Hiscock, K.M. and Grischek, T. 2002. Attenuation of groundwater pollution by bank filtration. *Journal of Hydrology* 266(3-4), 139-144.
- Huet, M. 1959. Profiles and biology of Western European streams as related to fish management. *Transactions of the American Fisheries Society* 88, 155-163.
- Janssen, F., Cardenas, M.B., Sawyer, A.H., Dammrich, T., Krietsch, J. and de Beer, D. 2012. A comparative experimental and multiphysics computational fluid dynamics study of coupled surface-subsurface flow in bed forms. *Water Resources Research* 48, 1-16.
- Kennedy, J.F. 1969. The formation of sediment ripples, dunes, and antidunes. *Annual Review of Fluid Mechanics* 1, 147-168.
- Kessler, A.J., Cardenas, M.B. and Cook, P.L.M. 2015. The negligible effect of bed form migration on denitrification in hyporheic zones of permeable sediments. *Journal of Geophysical Research-Biogeosciences* 120(3), 538-548.

- Kindred, S.J. and Celia, M.A. 1989. Contaminant transport and biodegradation: 2. Conceptual model and test simulations. *Water Resources Research* 25(6), 1149-1159.
- Klein, S., Worch, E. and Knepper, T.P. 2015. Occurrence and Spatial Distribution of Microplastics in River Shore Sediments of the Rhine-Main Area in Germany. *Environmental Science & Technology* 49, 6070-6076.
- Knillmann, S., Orlinskiy, P., Kaske, O., Foit, K. and Liess, M. 2018. Indication of pesticide effects and recolonization in streams. *Science of the Total Environment* 630, 1619-1627.
- Kovarova, K., Zehnder, A.J.B. and Egli, T. 1996. Temperature-Dependent Growth Kinetics of *Escherichia coli* ML 30 in Glucose-Limited Continuous Culture. *Journal of Bacteriology* 178(15), 4530-4539.
- Lawrence, J.E., Skold, M.E., Hussain, F.A., Silverman, D.R., Resh, V.H., Sedlak, D.L., Luthy, R.G. and McCray, J.E. 2013. Hyporheic Zone in Urban Streams: A Review and Opportunities for Enhancing Water Quality and Improving Aquatic Habitat by Active Management. *Environmental Engineering Science* 30(8), 480-501.
- Li, B., Xiaofeng, L., Kaufman, M.H., Turetaia, A., Chen, X. and Cardenas, M.B. 2020. Flexible and Modular Simultaneous Modeling of Flow and Reactive Transport in Rivers and Hyporheic Zones. *Water Resources Research* 56, 1-11.
- Lowell, J.L., Gordon, N., Engstrom, D., Stanford, J.A., Holben, W.E. and Gannon, J.E. 2009. Habitat Heterogeneity and Associated Microbial Community Structure in a Small-Scale Floodplain Hyporheic Flow Path. *Microbial Ecology* 58(3), 611-620.
- Marzadri, A., Tonina, D., Bellin, A. and Valli, A. 2016. Mixing interfaces, fluxes, residence times and redox conditions of the hyporheic zones induced by dune-like bedforms and ambient groundwater flow. *Advances in Water Resources* 88, 139-151.
- McClain, M.E., Boyer, E.W., Dent, C.L., Gergel, S.E., Grimm, N.B., Groffman, P.M., Hart, S.C., Harvey, J.W., Johnston, C.A., Mayorga, E., McDowell, W.H. and Pinay, G. 2003. Biogeochemical hot spots and hot moments at the interface of terrestrial and aquatic ecosystems. *Ecosystems* 6(4), 301-312.
- Molina-Navarro, E., Andersen, H.E., Nielsen, A., Thodsen, H. and Trolle, D. 2018. Quantifying the combined effects of land use and climate changes on stream flow and nutrient loads: A modelling approach in the Odense Fjord catchment (Denmark). *Science of the Total Environment* 621, 253-264.
- Monterroso, H. (2021) Sensitivity Analysis in Growth and Death Dynamics for Hyporheic Zone Aerobic Bacteria in Non-Mobile Dunes, Virginia Polytechnic Institute and State University, Blacksburg, Virginia.
- Moser, D.P., Fredrickson, J.K., Geist, D.R., Arntzen, E.V., Peacock, A.D., Li, S.M.W., Spadoni, T. and McKinley, J.P. 2003. Biogeochemical processes and microbial characteristics across groundwater-surface water boundaries of the Hanford Reach of the Columbia River. *Environmental Science & Technology* 37(22), 5127-5134.
- Nagaoka, H. and Ohgaki, S. 1990. Mass-transfer mechanism in a porous riverbed. *Water Research* 24(4), 417-425.
- Nakano, S. and Murakami, M. 2001. Reciprocal subsidies: dynamic interdependence between terrestrial and aquatic food webs. *PNAS* 98(1), 166-170.
- Neiva, A.M.R., Carvalho, P.C.S., Antunes, I.M.H.R., Albuquerque, A.C.S., Cunha, P.P. and Henriques, S.B.A. 2019. Assessment of metal and metalloid contamination in the waters and stream sediments around the abandoned uranium mine area from Mortorios, central Portugal. *Journal of Geochemical Exploration* 202, 35-48.

- OpenFOAM 2021 OpemFOAM: API Guide v2112, [https://www.openfoam.com/documentation/guides/latest/api/classFoam\\_1\\_1RASModels\\_1\\_1kOmega.html](https://www.openfoam.com/documentation/guides/latest/api/classFoam_1_1RASModels_1_1kOmega.html), accessed on 24 March 2022.
- Paerl, H.W., Gardner, W.S., Havens, K.E., Joyner, A.R., McCarthy, M.J., Newell, S.E., Qin, B. and Scott, J.T. 2016. Mitigating cyanobacterial harmful algal blooms in aquatic ecosystems impacted by climate change and anthropogenic nutrients. *Harmful Algae* 54, 213-222.
- Papanicolaou, A.N., Diplas, P., Evaggelopoulos, N. and Fotopoulos, S. 2002. Stochastic incipient motion criterion for spheres under various bed packing conditions *Journal of Hydraulic Engineering* 128(4), 369-380.
- Peng, X.Z., Yu, Y.J., Tang, C.M., Tan, J.H., Huang, Q.X. and Wang, Z.D. 2008. Occurrence of steroid estrogens, endocrine-disrupting phenols, and acid pharmaceutical residues in urban riverine water of the Pearl River Delta, South China. *Science of the Total Environment* 397(1-3), 158-166.
- Pinder, G.F. and Sauer, S.P. 1971. Numerical simulation of flood wave modification due to bank storage effects. *Water Resources Research* 7(1), 63-70.
- Poole, G.C., O'Daniel, S.J., Jones, K.L., Woessner, W.W., Bernhardt, E.S., Helton, A.M., Stanford, J.A., Boer, B.R. and Beechie, T.J. 2008. Hydrologic spiralling: The role of multiple interactive flow paths in stream ecosystems. *River Research and Applications* 24(7), 1018-1031.
- Quaglietta, L., Pauperio, J., Martins, F.M.S., Alves, P.C. and Beja, P. 2018. Recent range contractions in the globally threatened Pyrenean desman highlight the importance of stream headwater refugia. *Animal Conservation* 21(6), 515-525.
- Ramey, T.L. and Richardson, J.S. 2017. Terrestrial invertebrates in the riparian zone: mechanisms underlying their unique diversity. *Bioscience* 67(9), 808-819.
- Richter, D.D. and Mobley, M.L. 2009. Monitoring Earth's Critical Zone. *Science* 326(5956), 1067-1068.
- Rizzi, C., Finizio, A., Maggi, V. and Villa, S. 2019. Spatial-temporal analysis and risk characterisation of pesticides in Alpine glacial streams. *Environmental Pollution* 248, 659-666.
- Roley, S.S., Tank, J.L., Stephen, M.L., Johnson, L.T., Beaulieu, J.J. and Witter, J.D. 2012. Floodplain restoration enhances denitrification and reach-scale nitrogen removal in an agricultural stream. *Ecological Applications* 22(1), 281-297.
- Royer, T.V., David, M.B. and Gentry, L.E. 2006. Timing of riverine export of nitrate and phosphorus from agricultural watersheds in Illinois: Implications for reducing nutrient loading to the Mississippi River. *Environmental Science & Technology* 40(13), 4126-4131.
- Sawyer, A.H., Cardenas, M.B., Bomar, A. and Mackey, M. 2009. Impact of dam operations on hyporheic exchange in the riparian zone of a regulated river. *Hydrological Processes* 23(15), 2129-2137.
- Sinha, E., Michalak, A.M. and Balaji, V. 2017. Eutrophication will increase during the 21st century as a result of precipitation changes. *Science* 357(6349), 405-408.
- Stanford, J.A. and Ward, J.V. 1988. The Hyporheic Habitat of River Ecosystems. *Nature* 335(6185), 64-66.

- Stanford, J.A. and Ward, J.V. 1993. AN ECOSYSTEM PERSPECTIVE OF ALLUVIAL RIVERS - CONNECTIVITY AND THE HYPORHEIC CORRIDOR. *Journal of the North American Benthological Society* 12(1), 48-60.
- Stelzer, R.S., Scott, J.T., Bartsch, L.A. and Parr, T.B. 2014. Particulate organic matter quality influences nitrate retention and denitrification in stream sediments: evidence from a carbon burial experiment. *Biogeochemistry* 119(1-3), 387-402.
- Sterba, O., Mekotova, J., Krskova, M., Samsonova, P. and Harper, D. 1997. Floodplain forests and river restoration. *Global Ecology and Biogeography Letters* 6(3-4), 331-337.
- Stern, N., Ginder-Vogel, M., Stegen, J.C., Arntzen, E., Kennedy, D.W., Larget, B.R. and Roden, E.E. 2017. Colonization Habitat Controls Biomass, Composition, and Metabolic Activity of Attached Microbial Communities in the Columbia River Hyporheic Corridor. *Applied and Environmental Microbiology* 83(16).
- Thoms, M.C. 2003. Floodplain-river ecosystems: lateral connections and the implications of human interference. *Geomorphology* 56(3-4), 335-349.
- Toth, J. 1963. A theoretical analysis of groundwater flow in small drainage basins. *Journal of Geophysical Research* 68(16), 4795-4812.
- Triska, F.J., Kennedy, V.C., Avanzino, R.J., Zellweger, G.W. and Bencala, K.E. 1989. Retention and Transport of Nutrients in a 3rd-Order Stream in Northwestern California - Hyporheic Processes. *Ecology* 70(6), 1893-1905.
- U.S. 1957 Measurement and Analysis of Sediment Loads in Streams: Report No. 12, Some Fundamentals of Particle Size Analysis, Interagency Committee on Water Resources Subcommittee on Sedimentation, St. Anthony Falls Hydraulic Laboratory, Minneapolis, MN.
- U.S. Department of the Interior, U.S.F.a.W.S., U.S. Department of Commerce, U.S. Census Bureau 2018 2016 National Survey of Fishing, Hunting, and Wildlife-Associated Recreation.
- van Rijn, L.C. 1984. Sediment transport, part I: bed load transport. *Journal of Hydraulic Engineering* 110(10), 1431-1456.
- Ward, A.D., Trimble, S.W., Burckhard, S.R. and Lyon, J.G. (2016) *Environmental hydrology: 3rd edition*, CRC Press, Taylor & Francis Group, 6000 Brokem Sound Parkway, NW, Suite 300.
- Ward, J.V., Tockner, K. and Schiemer, F. 1999. Biodiversity of floodplain river ecosystems: Ecotones and connectivity. *Regulated Rivers-Research & Management* 15(1-3), 125-139.
- Weller, H.G. and Tabor, G. 1999. A tensorial approach to computational continuum mechanics using object-oriented techniques. *Computers in Physics* 12(6), 620.
- Werth, C.J., Cirpka, O.A. and Grathwohl, P. 2006. Enhanced mixing and reaction through flow focusing in heterogeneous porous media. *Water Resources Research* 42(12), W12414.
- White, D.S. 1993. Perspectives on defining and delineating hyporheic zones. *Journal of the North American Benthological Society* 12(1), 61-69.
- Widdowson, M.A., Molz, F.J. and Benefield, L.D. 1988. A numerical transport model for oxygen-based and nitrate-based respiration linked to substrate and nutrient availability in porous-media *Water Resources Research* 24(9), 1553-1565.
- Widdowson, M.A., Waddill, D.W. and Ruiz, C.E. 1997 SEAM3D: A numerical model for three-dimensional solute transport and sequential electron acceptor-based bioremediation in groundwater. Findikakis, A.N. and Stauffer, F. (eds), pp. 83-88, San Francisco, Ca.

- Wiegel, S., Aulinger, A., Brockmeyer, R., Harms, H., Löffler, J., Reincke, H., Schmidt, R., Stachel, B., von Tumpling, W. and Wanke, A. 2004. Pharmaceuticals in the river Elbe and its tributaries. *Chemosphere* 57(2), 107-126.
- Wilcox, D.C. (1998) Turbulence modeling for CFD, DCW Industries, La Canada, California.
- Winter, T.C., Harvey, J.W., Franke, O.L. and Alley, W.M. 1998 Ground Water and Surface Water, A Single Resource, Circular 1139. , U.S. Geological Survey, Denver, CO.
- Yonkos, L.T., Friedel, E.A., Perez-Reyes, A.C., Ghosal, S. and Arthur, C.D. 2014. Microplastics in Four Estuarine Rivers in the Chesapeake Bay, U.S.A. *Environmental Science & Technology* 48, 14195-14202.
- Zarnetske, J.P., Haggerty, R., Wondzell, S.M., Bokil, V.A. and Gonzalez-Pinzon, R. 2012. Coupled transport and reaction kinetics control the nitrate source-sink function of hyporheic zones (vol 48, W11508, 2012). *Water Resources Research* 48.
- Zhao, Z. and Fernando, H.J.S. 2007. Numerical simulation of scour around pipelines using an Euler-Euler coupled two-phase model. *Environmental Fluid Mechanics* 7, 121-142.
- Zheng, L., Cardenas, M.B., Wang, L. and Mohrig, D. 2019. Ripple effects: bed form morphodynamics cascading into hyporheic zone biogeochemistry. *Water Resources Research* 55, 7320-7342.

## CHAPTER 6: Conclusion

### *6.1 Summary of Research Work*

Streams and rivers are the lifeblood of our ecosystem, providing drinking water, serving as a biodiversity epicenter, and providing food sources for pollinators, aerators, and disease vector regulators. They represent delicate physical systems, with many interrelated physical phenomena merging and intermingling into a complex web of ecological and biogeochemical processes. Here, we sought to disentangle some of that web by further understanding the physics and biogeochemistry of streams and rivers, how they interact with the surrounding groundwater, and how the dynamics of those interactions benefit general ecological flourishing. Specifically, we examined how two types of geomorphic structures (soil pipes and dunes) affect stream and river physics and chemistry, and we subsequently explored ways this knowledge can help inform natural attenuation of existing stream/river pollution and reduce pollutant loading. We have focused on excess nitrate as a pollutant, which remains a problem (USGS 2022), yet can be removed through biogeochemical reactions in the subsurface. In Chapters 2 and 3, we have explored the efficacy of soil pipes as a way to increase bidirectional surface/groundwater (SW/GW) exchange (hyporheic exchange), thereby enhancing nitrate removal. Further, in Chapter 4, we have quantified the potential effect of soil pipes on pollutant bypass of riparian filtration mechanisms, highlighting the need to implement appropriate mitigating measures. Additionally, in Chapter 5, we have probed the effect of microbial growth/death and sediment transport on the efficacy of dune bedforms to enhance hyporheic exchange and pollutant biodegradation. In each of Chapters 2-5 we have revealed novel theoretical concepts as well as uncovered practical application insights. The research herein contributes to the body of knowledge required to understand, preserve, and restore stream and river functions and health.

In Chapter 2, we used MODFLOW with the Conduit Flow Package (CFP) to quantify soil pipe impacts on transient hyporheic hydraulics in river banks due to peak-flow events. We performed a sensitivity analysis of normalized hyporheic volume (i.e. divided by hyporheic volume in the absence of soil pipes) to soil pipe density, length, diameter, connectivity, tortuosity, and height above baseflow water surface elevation, as well as soil matrix hydraulic conductivity (K). We found that adding five soil pipes per meter to a stream bank increased hyporheic volume by 234% relative to that without soil pipes. We also identified that soil pipe length was the most important controlling parameter. Adding just one 1.5-m-long soil pipe caused a 73.4% increase in hyporheic volume. These magnitudes of increase in hyporheic volume reinforced the findings of some previous works; such as Menichino et al. (2014) who showed that an unblocked soil pipe had 9% to 21% faster velocities and 29 to 550 times greater K than a partially blocked soil pipe in a meander bend; and Briggs et al. (2016) who shared infrared video of significant flow emanating from a soil pipe in the bank versus none from the surrounding matrix. In terms of fascinating physical phenomena, we discovered that the increase in hyporheic volume induced by the presence of soil pipes increased non-linearly with soil pipe length. Furthermore, our study unmasked a new concept of matrix-pipe exchange limitation versus pipe flow limitation. More specifically, the effect of increasing soil pipe diameter on hyporheic volume leveled off sharply at ~1 cm, as flow limitation switched from pipe flow to

pipe-matrix exchange. In other words, flow gets “held up” in the soil matrix and cannot exit the soil matrix fast enough to maximize the amount of flow the pipe can accommodate. All of these findings have implications in terms of stream credits and mitigation techniques that we discuss in Section 6.2

In Chapter 3, we expanded on our hydraulics study in Chapter 2, and examined soil pipe effects on denitrification during transient peak-flow events. Again, we used MODFLOW and the CFP for the hydraulics and added MT3D-USGS to model nitrate transport and biodegradation. We performed a sensitivity analysis where we examined several geomorphic parameters (soil pipe length, height above baseflow water surface elevation, spacing, density, and soil matrix K), and also reactive transport parameters (first order reaction rate constant, dispersivity, initial concentration, and porosity) and their effects on soil pipe impact on denitrification. We also performed a rough upscaling where we examined the effects of stream channel slope and width, as well as soil pipe density on percentage nitrate removal during migration down 1 km of the channel itself. We reinforced the concepts from Chapter 2 of non-linear increase in both hyporheic volume and denitrification from the addition of soil pipes when plotted versus length, and similar to hydraulics the most influential parameters were pipe length and density. Adding a single 1.5-m-long soil pipe caused a 76% increase in hyporheic denitrification – an almost identical increase as for hyporheic volume. Moreover, we showed through our rough upscaling analysis that five soil pipes per m cumulatively induced up to 3% nitrate removal along a 1-km reach. More generally, we showed that percentage nitrate removal increased with decreasing channel slope, increasing channel width, increasing distance down the channel, and increased soil pipe density.

In terms of factors that govern removal, we showed that soil pipe enhancement of denitrification was governed by hyporheic volume as opposed to residence time in most cases in our study. Exceptions included coarse soil ( $K=10^{-3}$  m/s) and low reaction rate constant with soil pipes above the baseflow water surface elevation. We unveiled several interesting physical phenomena such as when soil pipes that are located above the baseflow water surface elevation get temporarily inundated during a peak flow event, a nitrate plume becomes stranded in the riparian soil matrix as the water recedes below the soil pipes. We also discovered potentiometric shelves, which are flat areas of the potentiometric surface in which nitrate becomes temporarily stranded. This stranding is similar to the way Schmadel et al. (2016) showed water parcels become stranded in riparian aquifers due to similar effects of the potentiometric surface as a result of the phase lag between a sinusoidal upslope and stream stage boundary condition. Furthermore, we showed that when pipes were clustered, that transverse head gradients develop at the ends of the cluster and push the nitrate back into the riparian soil pipe and cause more removal. We also showed that soil pipes constrain the lateral extent of nitrate plumes of its adjacent neighbors. These findings help gain insight into understanding the physicochemical mechanisms occurring in bank hyporheic exchange in the presence of soil pipes, and have implications for excess nitrate management in watersheds.

In Chapter 4, we looked at the reverse scenario where we quantified soil pipe enhancement of water and nitrate movement through riparian zone groundwater from uplands

toward the channel, thereby bypassing riparian buffer nitrate removal mechanisms. As with Chapter 3, we used MODFLOW and the CFP for the groundwater hydraulics and MT3D-USGS to model nitrate transport and biodegradation. We modeled transport in the soil pipes with the conservation of mass equation in Python. We conducted a numerical sensitivity analysis to examine the impact of soil pipe characteristics (density per meter, length, diameter), as well as soil matrix characteristics ( $K$ , hydraulic head gradient) on the quantity of nitrate that reached the channel. We found that in systems with long soil pipes (2.0 m), low hydraulic conductivity ( $K < 10^{-4.75}$  m/s), low head gradients ( $\nabla h < 0.0035$ ), and high reaction-constant ( $k > 4 \text{ day}^{-1}$ ), soil pipes increased nitrate flow rate to the channel by sometimes over five orders of magnitude. This finding reinforced the conclusions of studies such as Allaire et al. (2015) which showcased soil pipe potential to act as a bypass mechanism for nitrate to circumvent riparian buffers, as well as the recent field study of Steiness et al. (2021) which linked nitrate loads observed in streams to nitrate bypass of riparian zones. It is interesting to note that the same soil pipe parameters which benefit hyporheic exchange and hyporheic denitrification as discussed in Chapters 2 and 3 (e.g., increasing soil pipe length) also exacerbate riparian bypass in Chapter 4. A more general point is that soil pipes enhance water quality in some cases and worsen it in others. Nevertheless, soil pipes affected riparian bypass by orders of magnitude in systems with low  $K$ , whereas the addition of one soil pipe made about the same increase in hyporheic denitrification throughout the parameter space.

Methodologically, our results helped determine what level of complexity is required to model riparian groundwater accurately, a challenge posed by Inamdar (2006). We have shown that large scale hydrologic models must include enough complexity to capture the effects of small scale features such as soil pipes and other preferential flow mechanisms such as gravel veins. We also created a non-dimensional parameter, the riparian bypass potential ( $\psi$ ) that accounts for key governing factors such as volumetric flowrate and Damköhler number. For example, we determined that nitrate bypass started to increase by orders of magnitude above  $\psi \approx 2.75$ . This parameter helped gain insight into which systems will experience the worst nitrate bypass as a result of soil pipes. In creating this parameter, we have also partially addressed the challenge of how processes at the riparian scale can be quantified, again posed by Inamdar (2006), and our results offer a good foundation upon which to build a theoretical framework to describe riparian bypass from a mathematical perspective. Our results underscore the critical need to account for and mitigate the bypass effects of soil pipes when constructing riparian buffers, which we discuss in more depth in Section 6.2.

Finally, in Chapter 5, we delved into the physics and biogeochemistry of surface water-groundwater interactions through and around moving riverbed dunes to further understand the physical system and garner insight on the efficacy of dune bedforms as pollutant removal mechanisms. In Chapter 5, we used OpenFOAM to model the surface water hydraulics, MODFLOW to model the groundwater hydraulics, and SEAM3D to model the biogeochemistry, which included microbial growth and death dynamics. We modified SEAM3D to implement a moving frame of reference so that we could investigate the combined impact of dune translation and microbial growth and death dynamics on subsurface biogeochemistry, the first time anyone has merged the two in one study. We found that moving dunes wipe out the hyporheic flow cell

associated with a static dune, i.e. the inverted arch flow paths along which surface water flows through the dune due to hydrodynamically-induced pressure distributions along the dune surface (Elliott and Brooks 1997b, a, Cardenas and Wilson 2007b, a, Bardini et al. 2012, Janssen et al. 2012, Hester et al. 2013, Fox et al. 2014, Hester et al. 2014, Marzadri et al. 2016). We also found that accounting for microbial growth and death shows that denitrification is actually higher than predicted by the conventional no-growth/no-death model approach because the microbe population is able to grow to more dense concentrations. We also showed that dunes with higher celerity (i.e. higher dune translation speed associated with river flow conditions of lower depths and higher velocity) grew larger microbial colonies, and removed more carbon than their slower counterparts due to higher turnover hyporheic exchange. Turnover exchange occurs where water is exchanged between the water column and groundwater by the successive trapping and release of interstitial water as sediment moves along the bed, in this case through the stoss and lee sides of dunes as they move downstream (Elliott and Brooks 1997a). Thus, although dunes do lead to significant biodegradation as attested to in prior literature, it is less via the static inverted-arches of the static dune hyporheic flow cells than originally thought, with substantial (and often dominating) contributions from turnover exchange.

## *6.2 Engineering Significance and Implication*

The knowledge developed by this dissertation research could be applied in a number of different ways. For example, the existence of soil pipes could be accounted for in nutrient management strategies incorporating riparian buffers and stream-restoration credits. For example, a layer of deeply and finely rooted plants immediately downslope of pollutant sources (between sources and the receiving channel) could be applied to prevent the formation of soil pipes and the associated bypass by nitrate of riparian buffer function. And then substantially downstream of pollutant sources, soil pipes could be installed in the stream banks to supplement naturally existing soil pipes and enhance hyporheic removal of nitrate migrating down the channel. Finally, partial rock dams with a gap in the middle might be utilized to manipulate water velocities by adjusting the width of the gap (Figure 6.1) to enhance biodegradation due to turnover exchange (Elliott and Brooks 1997b) across dunes in sections with beds of medium to coarse sand. We explain each of these ideas in more detail in the paragraphs below.

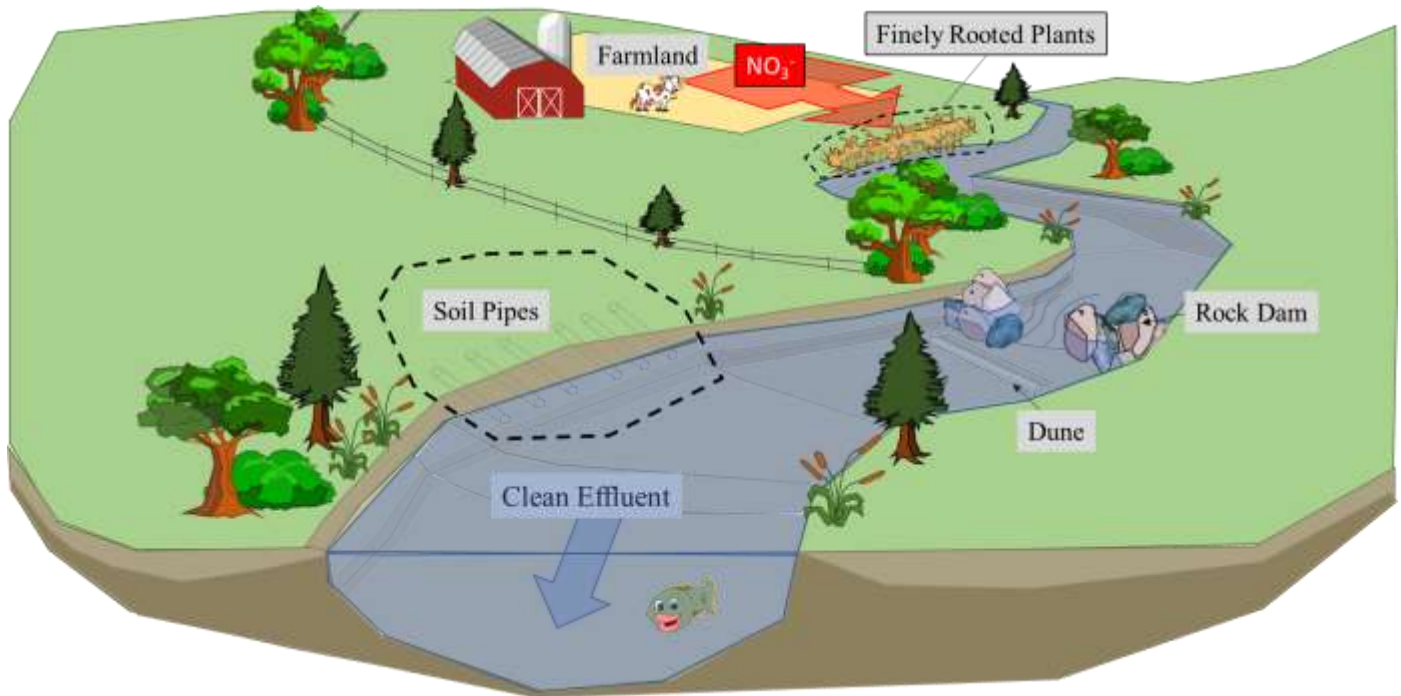


**Figure 6.1. Schematic summary of applications of research insights from Chapters 2 through 5. Directly downslope from a pollutant source such as a farm, planting grasses or shrubs with deep, fine roots along the stream banks can prevent bypass of the riparian nitrate removal mechanisms due to preferential flow from soil pipes. Further downstream far enough away to avoid runoff from the source, soil pipes can be manually installed to enhance hyporheic nitrate removal.**

Preferential flow paths such as soil pipes should be accounted for by stream-restoration nutrient mitigation credit systems such as those developed for the Chesapeake Bay watershed (Berg et al. 2014, Altland et al. 2020). The current Chesapeake Bay stream-restoration credit system gives credit for prevented sediment erosion, hyporheic denitrification, floodplain reconnection, and dry channel regenerative stormwater conveyance (Berg et al. 2014, Altland et al. 2020). Chapters 2 and 3 of this dissertation have shown that soil pipes clearly enhance both hyporheic volume and hyporheic denitrification for reaches downstream of pollutant sources. We propose that further versions of the Chesapeake Bay guidance expand the hyporheic denitrification protocol to account for the enhancing effects of soil pipes. Stream credits could be given to those whose pollutant source has significant number of naturally occurring soil pipes downstream, or manmade soil pipes (e.g., created by auguring) might also be constructed to gain stream credits and supplement naturally occurring soil pipes. More credit should specifically be given to longer soil pipes, soil pipes slightly above the baseflow water surface area, and densely arrayed soil pipes. Further, based on our stream-corridor-scale approximation in Chapter 3, soil pipe effects on denitrification are more important for low order headwater (i.e. low width) and flat (i.e. low slope) channel reaches. Therefore, stream credit allocations should be greater for reaches with narrower channel widths and flatter longitudinal slopes. Moreover, location relative to nitrate sources are critical, as Chapter 4 has shown that soil pipes immediately downslope

from pollutant sources could have the reverse effect and exacerbate nitrate pollution. Thus, negative stream credits should be assigned to sections of reaches with soil pipes immediately downslope from pollutant sources – particularly in sections of reach with long soil pipes. On the other hand, stream credits could be given where a layer of finely rooted plants are installed to mitigate the bypassing effects of soil pipes. In sections of stream where there are soil pipes and excess nitrate both laterally to the channel in the upland area and also coming down the channel from upstream, a layer of finely rooted plants could be installed upslope of the soil pipes, and credit can be given for both soil pipes and buffer enhancement layer of fine roots.

We acknowledge that manually installing soil pipes would be a novel practice, embarking into the unknown. A downside of their installation is their unknown durability, and frequent maintenance may be required. Further, the impact of soil pipes on bank stability is largely unknown, and drilling too many soil pipes might lead to significant erosion or bank collapse. Removal of nitrate by the riparian aquifer is extolled as a highly effective removal mechanism for nitrate (Groffman et al. 2002, Connolly et al. 2015), but Chapter 4 demonstrated that soil pipes can dominate nitrate transport to the channel, particularly for low groundwater head gradients toward the channel and matrix K. Thus, soil pipes can undermine the effectiveness of riparian buffers, and their effects must be mitigated when implementing riparian buffers as a removal mechanism for upslope nitrate. Allaire et al. (2015) suggested that riparian buffers would benefit from plant species with deep and fine roots (such as prairie grass) that reduce formation of soil pipes, or filters which require periodic maintenance. Currently, there is no requirement for stormwater best management practices (BMPs) in Virginia to contain a strip of finely rooted plants (VDOT 2021). We clarify that replacing trees and shrubs with exclusively grass is not recommended. Doing so would lower the vegetation uptake discussed in Hill (2019). Further, tall trees offer shade which creates cooler water temperatures, and provides habitats for fauna. Trees also have a higher Manning's coefficient (Mays, 2011), and therefore dampen flood waves more leading to less sediment and turbidity in the channel, and less erosion on the banks. Thus, maximizing riparian buffer function is complex and site specific. Future versions of stormwater management manuals and regulations could be changed to require a two-meter strip of finely rooted plants to include in riparian buffers to mitigate against soil pipes and preferential flow (Figure 6.1).

The benefits of riparian soil pipes on nitrate removal from water flowing down stream and river channels that we quantified in Chapter 3 of this dissertation are also sensitive to the frequency and magnitude of storm events that create flow pulses in the channel. Thus, any factors that affect the storm hydrology of a stream or river may affect the effectiveness of soil pipes in performing these functions. For example, both urbanization itself and stormwater BMPs that are installed in response to urbanization affect the flashiness of watershed runoff, with potential implications of soil-pipe enhancing hyporheic nitrate removal. Climate change may similarly affect hydrologic magnitude and frequency, with related implications.

Finally, in Chapter 5 we found that increased bedform (dune) celerity led to more turnover hyporheic exchange in riverbeds and thus increased biodegradation within dune-induced hyporheic zones. To harness this principle, in reaches with bed material conducive to

dune-formation (i.e. medium to coarse sand), a series of partial rock dams could be implemented (Figure 6.1). Not only will this increase hyporheic exchange due to the increased depth and therefore hydrostatic pressure head at the bottom of the upstream side of the rock dam (Hester and Doyle 2008), but the flow through the center of the rock dam (Figure 6.1) will increase channel velocities downstream, causing more turnover exchange due to the resulting higher dune celerities. Velocities must be increased only slightly to minimize scouring and erosion downstream of the rock dam. Our results showed that only a modest increase in stream velocity from 0.75 m/s to 1.0 m/s increased the biodegradation rate by roughly double, and so even slight increases in velocities below scouring and erosion thresholds may still enhance biodegradation significantly. Since there is a negative relationship between upwelling and biodegradation rates, the rock dams should not be placed where upwelling is prevalent such as where bedrock outcrops force water back up into the stream (Hiscock and Grischek 2002). Furthermore, turnover exchange could act as a silver lining for issues such as climate change or urbanization. The elevated peak flows of both (if they are only slightly elevated) would increase turnover and therefore biodegradation, which would offer a minor benefit to slightly temper the increased erosion, turbidity, and maximum daily load of pollutants associated with more flashy storm events. Although having a myriad of negative consequences, the warmer water temperatures as a result of climate change would also enhance biodegradation rates, which would further solidify dune turnover as a silver lining.

### *6.3 Future Work*

The research presented in this dissertation paves the way for multiple future numerical and field/laboratory studies. For example, in the transient peakflow event scenarios of Chapters 2 and 3, we did not include an upslope hydrologic forcing representing a pulse of local runoff. Often times, there are pulses of groundwater which come from the hillslopes, which could be added in future numerical studies. Schmadel et al. (2016) examined such hillslope forcing without soil pipes, and noted that the maximum stream to aquifer water flux occurs at a phase lag of 12 h. They found that subjecting the riparian aquifer to different phase lags caused hyporheic flow path lengths and residence times (RTs) to span several orders of magnitude. We expect that soil pipes would affect such hydrologic flow paths and RTs between the two hydraulic boundary conditions (hillslope and channel), and it would be interesting to evaluate the impact of hillslope forcing on the amount of hyporheic flux (increasing or decreasing depending on phase lag), and path lengths and RTs in the presence of soil pipes. Groundwater dynamics in scenarios such as high amplitude peak flow events (Welch et al. 2015), or lower soil hydraulic conductivity (Doble et al. 2012) are affected greatly by the vadose zone, and further research could assess if the impeding effect of the vadose zone on hyporheic flux would impact the hyporheic volume and denitrification in these scenarios.

Furthermore, in Chapter 3 we simplified simulation of denitrification by using first order kinetics. Thus, we did not assess the effects of using more accurate but more complex Monod kinetics, nor include aerobic respiration or nitrification. Like Zarnetske et al. (2012) did for homogeneous riparian aquifers, a thorough probe of the entire parameter space of all Monod kinetic parameters (half-saturated constants, consumption rate constants, etc.) would determine

more precisely under what conditions it is and is not necessary to simulate nitrification and aerobic respiration in settings with soil pipes. Such an exercise would also determine precisely what subset of the Monod parameter space the conclusions presented here are valid.

Considering a wider range of chapters, there is room to explore other hydraulic and hydrological conditions in Chapters 2-4, such as the effects of evapotranspiration and recharge, as these may impact soil pipe effects on hyporheic exchange and/or riparian bypass. Future work could account for both seasonal variations and climate change. Seasonal temperatures would affect the microbial activity which could be accounted for in the governing equations by adding the heat transport equation and the Arrhenius equation to the transport code to model heat flux and its resulting effects on temperature dependent reaction parameters. Seasonal variations and climate change would also affect the stage hydrographs and so the boundary conditions must reflect which season or climate prediction model was used.

In addition to future numerical work, our study has set the conditions for many opportunities for future field work. For example, in Chapters 2-4, the layout of the soil pipes was geometrically very simple, and thus not necessarily fully representative of naturally forming soil pipes. While our work provided an important starting point for conceptually understanding the physical system, soil pipe layout is quite complex in actuality (Gormally et al. 2011, Guo et al. 2014). However, there is a dearth of information on spatial layout from the field, particularly with regards to riparian soils. There are many studies which have mapped macropores (smaller vertically oriented void spaces often in agricultural settings) and soil pipes in agricultural soils (Amin et al. 1998, Koestel and Larsbo 2014, Larsbo et al. 2014, Snehota et al. 2015, Xu et al. 2016, Jarvis et al. 2017, Yu and Lu 2019). There are also several studies which map the layout of soil pipes in hillslopes (Guo et al. 2014, Wilson et al. 2016, Zhou et al. 2016, Bernatek-Jakiel and Kondracka 2019). However, with the exception of a few studies such as Gormally et al. (2011), no one has mapped soil pipes in riparian soils. Understanding soil pipe spatial layout is important to accurate incorporation in mathematical models, and more importantly proper accounting when devising protective measures such as stormwater best management practices (BMPs). The latter include, for example, vegetative strips designed to reduce peak flows and filter out pollutants. Allaire et al. (2009) surveys many different field methods to map preferential flow paths, including tracers, skeletalization, simple excavation, smoke injection, and non-intrusive methods (ground penetrating radar (GPR), x-rays, magnetic resonance imaging (MRI), electrical resistivity tomography (ERT)). Thus, there are many different field studies that could characterize the layouts.

In addition to soil pipe geometry, almost all the work contained herein would benefit from laboratory or field corroboration. For example, it would be beneficial to determine whether or not lurking variables and complicated in-situ factors such as extensive spatial/temporal heterogeneity confound some of the theoretical principles from previous chapters. Example principles include non-linear increase in hyporheic volume and denitrification with respect to soil pipe length; increased residence time with soil pipes just above baseflow water surface elevation due to water becoming stranded as the water level drops below the soil pipes; increased biodegradation for dunes with higher celerity due to increased turnover exchange. All of these

theoretical principles remain to be confirmed by experimental data. The range of future study opportunities discussed in this chapter (be they numerical, laboratory, or field), will work together alongside the results contained herein to piece together the beautiful mosaic of knowledge of preserving and restoring stream and river health.

## References

- Allaire, S. E., S. Roulier, and A. J. Cessna. 2009. Quantifying preferential flow in soils: A review of different techniques. *Journal of Hydrology* **378**:179-204.
- Allaire, S. E., C. Sylvain, S. F. Lange, G. Theriault, and P. Lafrance. 2015. Potential Efficiency of Riparian Vegetated Buffer Strips in Intercepting Soluble Compounds in the Presence of Subsurface Preferential Flows. *Plos One* **10**.
- Altland, D., C. Becraft, J. Berg, T. Brown, J. Burch, D. Clearwater, J. Coleman, S. Crawford, D. Barbara, J. Geratz, J. Hanson, J. Hartranft, J. Hottenstain, S. Kaushal, S. Lowe, P. Mayer, G. Noe, W. Oberholzer, A. Parola, D. Scott, W. Stack, J. Sweeney, and J. White. 2020. Consensus Recommendation to Improve Protocols 2 and 3 for Defining Stream Restoration Pollutant Removal Credits. Chesapeake Bay Program. .
- Amin, M. H. G., L. D. Hall, R. J. Chorley, and K. S. Richard. 1998. Infiltration into soils, with reference to its visualization and measurement by magnetic resonance imaging (MRI). *Progress in Physical Geography* **22**:135-165.
- Bardini, L., F. Boano, M. B. Cardenas, R. Revelli, and L. Ridolfi. 2012. Nutrient cycling in bedform induced hyporheic zones. *Geochimica Et Cosmochimica Acta* **84**:47-61.
- Berg, J., J. Burch, D. Cappuccitti, S. Filoso, L. Fraley-McNeal, D. Goerman, N. Hardman, S. Kaushal, D. Medina, and M. Meyers. 2014. Recommendations of the Expert Panel to Define Removal Rates for Individual Stream Restoration Projects. Chesapeake Bay Program.
- Bernatek-Jakiel, A., and M. Kondracka. 2019. Detection of Soil Pipes Using Ground Penetrating Radar. *Remote Sensing* **11**:1-17.
- Briggs, M. A., D. K. Hare, D. F. Boutt, G. Davenport, and J. W. Lane. 2016. Thermal infrared video details multiscale groundwater discharge to surface water through macropores and peat pipes. *Hydrological Processes* **30**:2510-2511.
- Cardenas, M. B., and J. L. Wilson. 2007a. Dunes, turbulent eddies, and interfacial exchange with permeable sediments. *Water Resources Research* **43**:W08412.
- Cardenas, M. B., and J. L. Wilson. 2007b. Hydrodynamics of coupled flow above and below a sediment-water interface with triangular bedforms. *Advances in Water Resources* **30**:301-313.
- Connolly, N. M., R. G. Pearson, D. Loong, M. Maughan, and J. Brodie. 2015. Water quality variation along streams with similar agricultural development but contrasting riparian vegetation. *Agriculture Ecosystems & Environment* **213**:11-20.
- Doble, R. C., P. Brunner, M. James, and P. G. Cook. 2012. An analysis of river bank slope and unsaturated flow effects on bank storage. *Groundwater* **50**:77-86.
- Elliott, A. H., and N. H. Brooks. 1997a. Transfer of nonsorbing solutes to a streambed with bed forms: Laboratory experiments. *Water Resources Research* **33**:137-151.
- Elliott, A. H., and N. H. Brooks. 1997b. Transfer of nonsorbing solutes to a streambed with bed forms: Theory. *Water Resources Research* **33**:123-136.

- Fox, A., F. Boano, and S. Arnon. 2014. Impact of losing and gaining streamflow conditions on hyporheic exchange fluxes induced by dune-shaped bed forms. *Water Resources Research* **50**:1895-1907.
- Gormally, K. H., M. S. McIntosh, A. N. Mucciardi, and G. W. McCarty. 2011. Ground-Penetrating Radar Detection and Three-Dimensional Mapping of Lateral Macropores: II. Riparian Application. *Soil Science Society of America Journal* **75**:1236-1243.
- Groffman, P. M., N. J. Boulware, W. C. Zipperer, R. V. Pouyat, L. E. Band, and M. F. Colosimo. 2002. Soil nitrogen cycle processes in urban riparian zones. *Environmental Science & Technology* **36**:4547-4552.
- Guo, L., J. Chen, and H. Lin. 2014. Subsurface lateral preferential flow network revealed by time-lapse ground-penetrating radar in a hillslope. *Water Resources Research* **50**:9127-9147.
- Hester, E. T., and M. W. Doyle. 2008. In-stream geomorphic structures as drivers of hyporheic exchange. *Water Resources Research* **44**:W03417.
- Hester, E. T., K. I. Young, and M. A. Widdowson. 2013. Mixing of surface and groundwater induced by riverbed dunes: implications for hyporheic zone definitions and pollutant reactions. *Water Resources Research* **49**:5221-5237.
- Hester, E. T., K. I. Young, and M. A. Widdowson. 2014. Controls on mixing-dependent denitrification in hyporheic zones induced by riverbed dunes: A steady state modeling study. *Water Resources Research* **50**:9048-9066.
- Hill, A.R. (2019) Groundwater nitrate removal in riparian buffer zones: a review of research progress in the past 20 years. *Biogeochemistry* **143**, 347-369.
- Hiscock, K. M., and T. Grischek. 2002. Attenuation of groundwater pollution by bank filtration. *Journal of Hydrology* **266**:139-144.
- Inamdar, S. 2006. Challenges in modeling hydrologic and water quality processes in riparian zones. *Journal American Water Resources Association* **42**:5-14.
- Janssen, F., M. B. Cardenas, A. H. Sawyer, T. Dammrich, J. Krietsch, and D. de Beer. 2012. A comparative experimental and multiphysics computational fluid dynamics study of coupled surface-subsurface flow in bed forms. *Water Resources Research* **48**:1-16.
- Jarvis, N., M. Larsbo, and J. Koestel. 2017. Connectivity and percolation of structural pore networks in a cultivated silt loam soil quantified by X-ray tomography. *Geoderma* **287**:71-79.
- Koestel, J., and M. Larsbo. 2014. Imaging and quantification of preferential solute transport in soil macropores. *Water Resources Research* **50**:4357-4378.
- Larsbo, M., J. Koestel, and N. Jarvis. 2014. Relations between macropore network characteristics and the degree of preferential solute transport. *Hydrology and Earth System Sciences* **18**:5255-5269.
- Mays, L.W. (2011) *Water resources engineering*, John Wiley & Sons, Inc., Hoboken, NJ.
- Marzadri, A., D. Tonina, A. Bellin, and A. Valli. 2016. Mixing interfaces, fluxes, residence times and redox conditions of the hyporheic zones induced by dune-like bedforms and ambient groundwater flow. *Advances in Water Resources* **88**:139-151.
- Menichino, G. T., A. S. Ward, and E. T. Hester. 2014. Macropores as preferential flow paths in meander bends. *Hydrological Processes* **28**:482-495.
- Schmadel, N. M., A. S. Ward, C. S. Lowry, and J. M. Malzone. 2016. Hyporheic exchange controlled by dynamic hydrologic boundary conditions. *Geophysical Research Letters* **43**:4408-4417.

- Snehota, M., V. Jelinkova, J. Sacha, M. Frycova, M. Cislerova, P. Vontobel, and J. Hovind. 2015. Experimental investigation of preferential flow in a near-saturated intact soil sample. *Physics Procedia* **69**:496-502.
- Steiness, M., S. Jessen, S. G. M. van't Veen, T. Kofod, A. L. Hojberg, and P. Engesgaard. 2021. Nitrogen-loads to streams: importance of bypass flow and nitrate removal processes. *Biogeosciences* **126**:1-24.
- USGS. 2022. WaterQualityWatch -- Continuous Real-Time Water Quality of Surface Water in the United States, Real-Time Nitrate, in mg/L as N. <https://waterwatch.usgs.gov/wqwatch/?pcode=00630>, accessed on 12 April 2022.
- VDOT. 2021. Drainage Manual. *in* L. a. D. Division, editor. Virginia Department of Transportation, <http://www.virginiadot.org/business/locdes/hydra-drainage-manual.asp>.
- Welch, C., G. A. Harrington, and P. G. Cook. 2015. Influence of Groundwater Hydraulic Gradient on Bank Storage Metrics. *Groundwater* **53**:782-793.
- Wilson, G. V., J. R. Rigby, M. Ursic, and S. M. Dabney. 2016. Soil pipe flow tracer experiments: 1. Connectivity and transport characteristics. *Hydrological Processes* **30**:1265-1279.
- Xu, Z.-h., L.-x. Li, and M.-c. Ma. 2016. The Application of Research Methods in Soil Macropores in Vadose Zone of Well Vegetated Slope. *Applied Mechanics and Materials* **851**:655-659.
- Yu, X., and S. Lu. 2019. Reconfiguration of macropore networks in a silty loam soil following biochar addition identified by X-ray microtomography and network analyses. *European Journal of Soil Science* **70**:591-603.
- Zarnetske, J. P., R. Haggerty, S. M. Wondzell, V. A. Bokil, and R. Gonzalez-Pinzon. 2012. Coupled transport and reaction kinetics control the nitrate source-sink function of hyporheic zones (vol 48, W11508, 2012). *Water Resources Research* **48**.
- Zhou, Y., G. V. Wilson, G. A. Fox, J. R. Rigby, and S. M. Dabney. 2016. Soil pipe flow tracer experiments: 2. Application of a streamflow transient storage zone model. *Hydrological Processes* **30**:1280-1291.

## Appendix A: Soil Pipe GPR Experiments

We started to develop GPR methodology using equipment owned by Dr. Steven Holbrook in Geosciences in order to map soil pipes as discussed in Chapter 6. We conducted two experiments; one on Strouble's creek on June 21, 2019, and another on July 26, 2019 at Slate Branch creek to locate handmade soil pipes with a simple 1Ghz (highest frequency) GPR pass both with very little success. A summary of the method is presented in Figure A1. Results from Line's 1, 2 and 3 are presented in Figure A2.

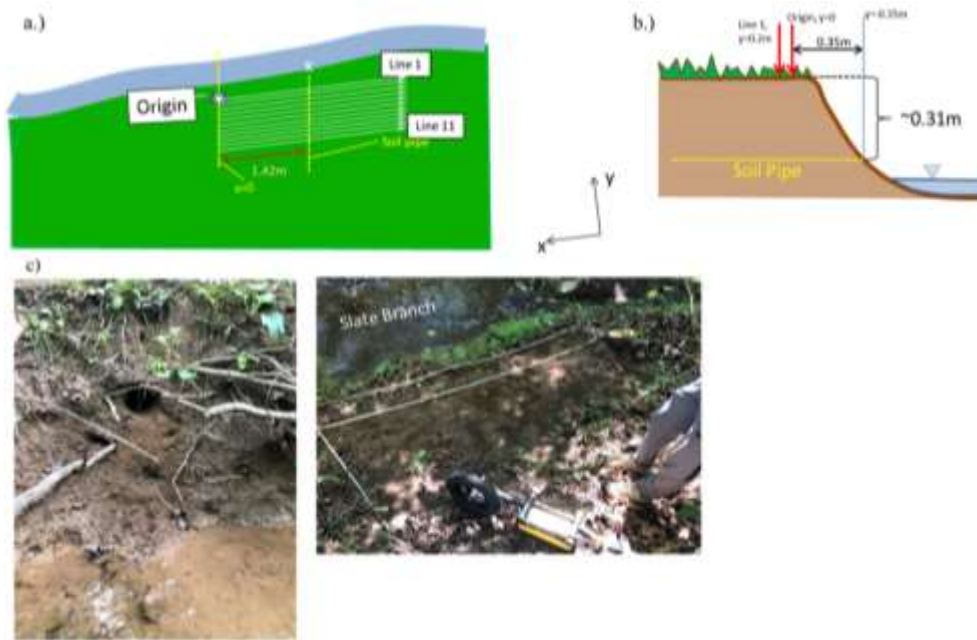


**Figure A1. a) Schematic (plan view) from Slate Branch GPR Site; line 1 is at  $y=20\text{cm}$ ; the soil pipe entrance is at  $(x=1.\text{m}, y=-0.35\text{m})$ ; the soil pipe is  $\sim 5\text{cm}$  (4.8 cm outside diameter PVC pipe); there is 5 cm spacing between lines; the soil pipe is roughly perpendicular to passes; the soil was organic, and silty; 0.005 meter step size; velocity estimation 0.08m/ns. b) Side view schematic (Stream going into the page). c) Pictures from the site.**

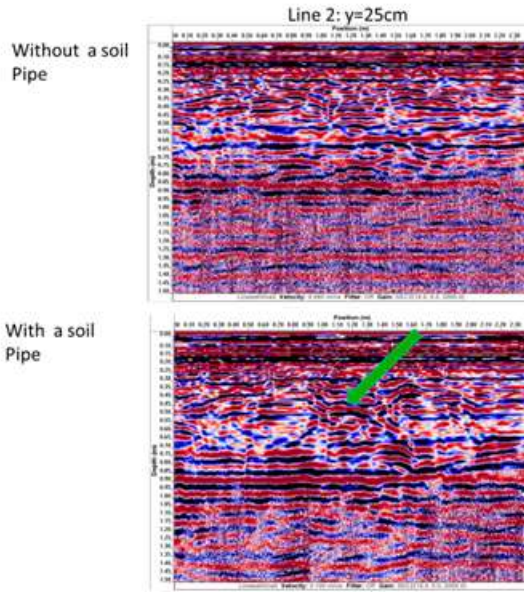


**Figure A2: Radargrams (raw data – not post processes) for line 2. The green arrow marks what we think is the hyperbola associated with the anomaly.**

The hyperbola created by the soil pipe which we thought would be very conspicuous in the radargram, was barely detectable due to massive amount of background noise (Figure A2). Therefore, it is a stretch to think that we can map a soil pipe network we know nothing about simply by examining raw data. It is necessary to employ an extensive post processing procedure to maximize the chance of detecting the anomalies in the radargram. The basic GPR post processing (detrending, dewow, gain, filters, background subtraction) and migration outlined above can help declutter the radargrams and accentuate anomalies (Guo et al. 2014). The image subtraction that is in Guo et al. (2014) would further help accentuate anomalies, because there should be a difference in the wet and dry radargrams of the same transect precisely where the water fills the soil pipes.

### References

Guo, L., Chen, J. and Lin, H. (2014) Subsurface lateral preferential flow network revealed by time-lapse ground-penetrating radar in a hillslope. *Water Resources Research* 50(12), 9127-9147.

**APPENDIX B: Supporting information for CHAPTER 2: Filling the Void: the Effect of Riverbank Soil Pipes on Transient Hyporheic Exchange During a Peak Flow Event.**



*Water Resources Research*

Supporting Information for

**Filling the Void: the Effect of Riverbank Soil Pipes on Transient Hyporheic Exchange During a Peak Flow Event.**

W. Seth Lotts<sup>1</sup>, Erich T. Hester<sup>1</sup>

<sup>1</sup>Department of Civil and Environmental Engineering, Virginia Tech, Blacksburg, Virginia  
24061 USA

**Contents of this file**

B1 Discussion of Numerical Methods

B2 Amplitude and Peak

B3 Comparison of Pipe and Matrix Flow

B4 Head Contour Map at Different Hydraulic Conductivities

Figures B1-B11

**B1: A Discussion of the Numerical Methods and Limitations**

*B1.1 Why the Numerical Method Struggled with Soil Pipe Diameters of 0.5 – 1 cm*

There are three potential ways that a finite difference model could experience the numerical issues we did in the 0.5-1.0 cm pipe diameter range. The scheme could be (1) inconsistent or (2) unstable, or the iterative method used to solve the algebraic system of equations could diverge. The first two pertain to the numerical solution converging to the exact solution of a PDE; therefore, what is meant by convergence in failure type #1 and #2 is that numerical solution converges to the exact solution of a PDE as the grid becomes small. In terms of #3, it is necessary to solve an algebraic system of equation at each time step in MODFLOW, and non-convergence means that the iterative method used to solve those equations diverges. Here we discuss each failure type in turn, and how it pertains to our model. We show that the

numerical issues observed in a narrow range of abscissa values in Figure 2.5c are of type #3, below.

**Failure Type 1: Consistency.** A scheme could hypothetically be inconsistent, i.e. the truncation error (the error associated with using difference approximations as opposed to smooth derivatives) could fail to go to zero as the grid size approaches zero. MODFLOW uses a 2<sup>nd</sup> order central difference scheme for the spatial derivatives and a backwards difference for the time steps (Harbaugh 2005).

For the spatial derivatives, the consistency of the scheme can be proved analytically shown through manipulation of Taylor Series (Pletcher et al. 2013, Sauer 2012). As the mesh approaches zero, so will the truncation error. To address concerns about whether or not we have a fine enough grid so that the truncation is sufficiently small, it is instrumental to compare the solution at two different grid sizes. Below, we look at the  $V/V_0$  vs. diameter curves made with a 2 cm vs. 4 cm grid. The solutions are so close that it appears to be just one curve, indicating that the solution has not gotten much better from 4 cm to 2 cm, which means it is not necessary to refine the grid even further.

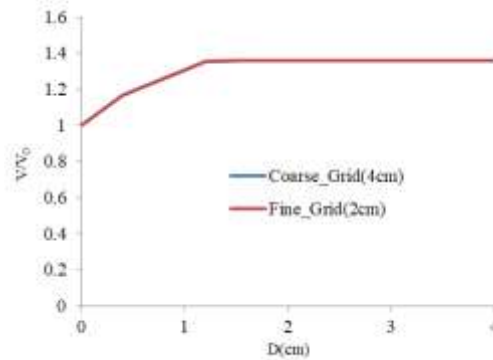


**Figure B1.  $V/V_0$  vs. soil pipe length at 2 cm and 4 cm grid resolutions. The curves are essentially the same demonstrating that not much improvement would be made by additional grid refinement.**

For the temporal derivatives, a rule of thumb established by Wang and Anderson (1982) and (Marsily 1986) for minimum initial time step for a given stress period is

$$\Delta t_i = \frac{S_y \text{Min}(\Delta x, \Delta y)}{4Kb} = \frac{0.32 \cdot 0.02}{4 \cdot 10^{-3} \cdot 1} = 1.6$$

Here we have substituted the parameters out of all our simulations which give the smallest time step. As long as the initial stress period time step we use is shorter than 1.6 seconds than we satisfy the rule of thumb. Our study uses an initial time step of 1 second.

Reilly and Harbaugh (2004) and Prickett and Lonquist (1971) have shown that as long as there are at least six time steps per stress period, the solution will match the analytic solution (the Theis solution) very well. Our study has at least 23 time steps in all stress periods which safely meets the time step multiplier requirement.

Typically, schemes do not fail due to consistency. Such schemes would result in a leading error term of  $O\left(\frac{\Delta t}{\Delta x}\right)$  upon being derived by Taylor Series Expansion. Such a scheme is the DuFort-Frankel scheme (DuFort and Frankel 1953).

Based on these analyses, we have confidence that MODFLOW's scheme is consistent, and that we have chosen a small enough time step, time step multiplier, and mesh size so that truncation error is not a concern.

**Failure Type 2: Stability.** The time integration scheme could hypothetically be unstable. This means that machine errors due to limited precision of computer storage grow over time. MODFLOW 2005 uses a backwards time differencing approach, which is well known to be unconditionally stable (Boyce and DiPrima 2012, Harbaugh 2005, McDonald and Harbaugh 1984, 1988, Pletcher et al. 2013, Sauer 2012), and thus stability is not a concern here. What this means in conjunction with Failure Type #1 is that as long as we can solve the system of equations resulting from the discretization technique, the resulting solution can be trusted to be accurate to the PDE. This is called Lax's equivalence theorem which states that a consistent finite-difference approximation to a well-posed time-dependent linear partial differential equation is convergent to the exact solution if, and only if, the scheme is stable (Pletcher et al. 2013). Thus, knowing that the scheme is consistent and stable, it necessarily converges to the exact solution of the PDE as the truncation error becomes small.

**Failure Type 3: Solver Failure.** The solver could fail to solve the algebraic system that results from applying the discretization method. Discretizing the groundwater flow PDE on an  $N \times M$  grid, results in an algebraic system  $[A]\mathbf{x} = \mathbf{b}$ , which is solved at each time step.  $[A]$  is a  $(N \cdot M) \times (N \cdot M)$  pentadiagonal (for our case of two spatial variables) matrix which is positive definite;  $\mathbf{x}$  is an  $N \cdot M$  long vector of heads at all the nodes; and  $\mathbf{b}$  is the right hand side vector which accounts for terms associated with head-dependent boundaries (i.e. from the general head or soil pipes) and storage terms. The only solver that the CFP package is coded to work with is the preconditioned conjugate gradient (PCG) solver. If we wanted to use another solver we would have to modify the source code. The PCG solver employs an algorithm which numerically finds the minimum of a quadratic hyper-surface:

$$f(\mathbf{x}) = \frac{1}{2} \mathbf{x}^T [A] \mathbf{x} - \mathbf{b}^T \mathbf{x} + c$$

Finding the minimum of such a surface is the same thing mathematically as solving the system  $[A]\mathbf{x} = \mathbf{b}$ . While the positive definiteness of  $[A]$  guarantees a solution to this

minimization problem, the right hand side vector  $\mathbf{b}$  shifts the hyper-surface and makes it hard for the PCG algorithm to find the minimum under certain conditions. For example, if some of the values in  $\mathbf{b}$  were to spike, that would significantly shift the surface  $f(\mathbf{x})$ , which would subsequently affect the convergence of the PCG.

One of the components of this right hand side vector in our case is the matrix-conduit exchange term which involves the heads in the soil pipes computed by solving equations [2.3] or [2.4] by the Newton Raphson Method. The Newton Raphson method procedure in one dimension is executed by picking an initial guess  $x_0$ , finding the derivative at that initial guess, and solving for the tangent line's root (Sauer 2012), as illustrated graphically in Figure B2 below.

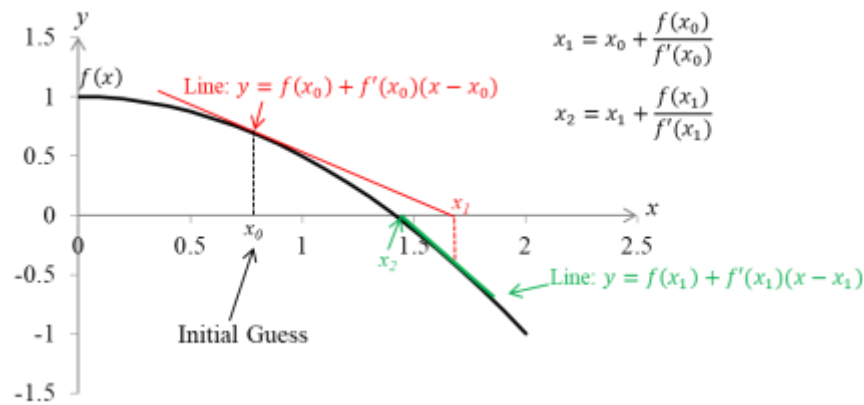


**Figure B2. Graphical depiction of the Newton-Raphson method in 1D.**

To illustrate the short comings of the Newton Raphson Method, consider the function  $f(x) = \left(1 - \frac{3}{4x}\right)^{1/3}$  (Sauer 2012), shown in Figure B3. For many of the initial guesses, due to the chaotic nature of the curve, the solver will have a difficult time converging. For example, if one guesses 0.5 (relatively close to the actual root  $x = 0.75$ ), the method will calculate the estimated root to be at about  $x \approx 1$ . Due to the nature of the derivative (very flat and positive, the next tangent line's root will overshoot  $x = 0.75$  dramatically and occur at a large negative number for  $x$ , and from there the solver will diverge to  $x \rightarrow -\infty$ .

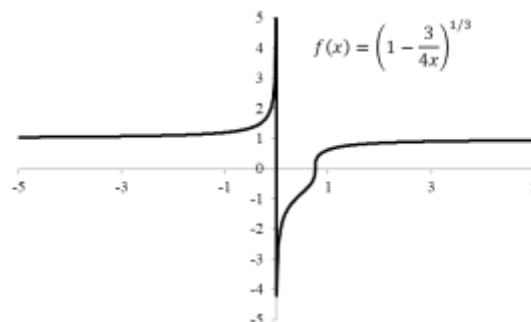


**Figure B3. Graphical illustration of a 1D function which is poorly behaved for the Newton Raphson method, adapted from Sauer (2012).**

Similarly, consider the function  $f(x) = 4x^4 - 6x^2 - \frac{11}{4}$  (Sauer 2012), shown in Figure B4. In this case, depending on the initial guess, the Newton Raphson method may end up oscillating back and forth between  $x_0$  and  $x_1$  forever and never converge.

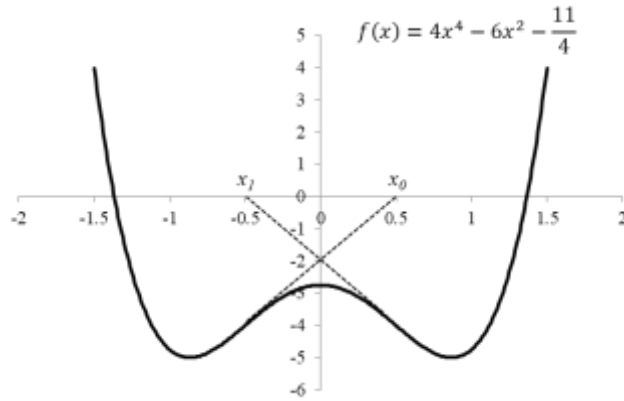


**Figure B4. Graphical Illustration of a 1D function that results in an oscillatory failure of the Newton-Raphson method, adapted from Sauer (2012).**

Therefore, the Newton Raphson method may diverge to infinity, oscillate forever, or fail if a zero derivative is encountered. The same is true for multi-dimensional problems as well. In our case, convergence depends highly on the initial guess for the head vector, and the nature of the functional surface. If the functional surface is chaotic, the solver will have difficulty. The pipe flow equations are very complicated, and thus it is not surprising that there is a range of diameters where the solver has trouble converging. In our case, that range of diameters is from 0.5 – 1.0 cm. This gap is indicated with a dotted line in Figure 2,5c. For an example case of  $D=0.85$  cm, the Newton Raphson method fails for the pipes, which eventually causes the failure of the PCG method for the matrix as well. The model monitor shows that there are three time steps where the Newton Raphson method fails (i.e. “no convergence in the conduit step”), generating giant flow budget errors (Figures B5 and B6).

The Q vs. t solution shows the drastic effect the numerical/mathematical divergence in the pipe domain (Figure B5) has on the entire solution (Figure B6). A system of equations must be solved for both the matrix domain (the preconditioned conjugate gradient method) and the pipe domain (the Newton Raphson method) at each time step. The spikes correspond to time steps where the Newton Raphson method fails to converge. It is evident that failed convergence causes the solution deviate quite a bit from the solution at neighboring time steps.

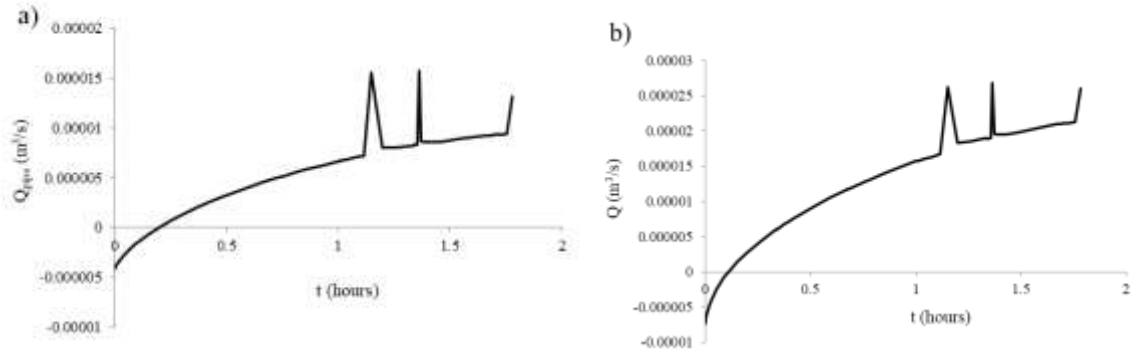


**Figure B5. Q vs. t for (a) pipe flow at D=0.85 cm, and (b) the whole model domain. The three failed Newton-Raphson attempts are evident, and one can see that the error starts in the pipe and propagates to the matrix.**

Plots of the exchange term versus time at one of the nodes of the soil pipes (node #41 approximately 0.2m into the aquifer from the stream) show anomalies/spikes are created in the right hand side vector at these time steps.

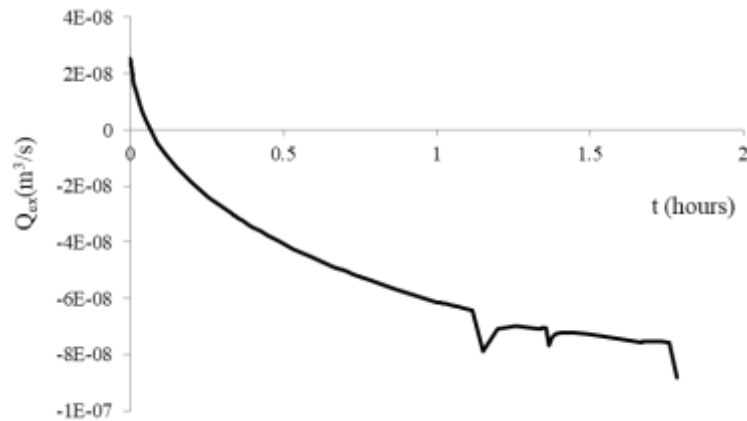


**Figure B6. Exchange terms vs. time. The three instances of Newton Raphson failure manifest in three spikes exchange terms vs. time graph. Input of such spikes into the overall model causes the conjugate gradient method to fail.**

The anomalies shift the surface of  $f(\mathbf{x}) = \frac{1}{2} \mathbf{x}^T [\mathbf{A}] \mathbf{x} - \mathbf{b}^T \mathbf{x} + \mathbf{c}$  to where the conjugate gradient cannot find a minimum in a reasonable amount of iteration steps, and hence the solution fails to converge. We postulate that the Newton Raphson method is having difficulty at the intermediate diameter soil pipes because the Reynolds number is the highest at these diameters. At low diameters, less flow is able to occur in the pipe resulting in viscous forces far outweighing the inertial forces. The slower velocities, and smaller diameter result in a low Reynolds numbers, which mathematically translated to a better behaved pipe flow function. At higher diameters, the flow is *exchange limited*, and so an increase in diameter does not result in more flow and more inertial forces as would be expected in a pipe flow limited scenario.

Consequently, the flow in the pipe slows down significantly with incremental increase in diameter as the pipe cross-sectional area increases proportional to the square of the diameter. Thus, at higher diameters the flow also has a lower Reynolds number, and hence is more stable resulting in a better-behaved pipe flow function. It is at the intermediate diameters (0.5 – 1 cm) where the Reynolds number is at its highest. Regardless, the solver converges for all values presented in the study, and even though the solver does not converge at other diameters, that does not indicate that the solution is invalid for other diameter values where the solver *does* converge. Consider the following two quadratics:

$$2.5x^2 + 10.01x + 10 \text{ vs. } 2.5x^2 + 9.99x + 10$$

The middle term only changed by 0.2%, yet the left hand quadratic has real roots ( $x = -2.30355$ ;  $x = -1.73645$ ), and the right hand quadratic does not have real roots. The fact that quadratic #2 has no real-roots and is just a 0.2% change in one of the parameters away from the quadratic #1 does not invalidate quadratic #1's real roots. Similarly, just because the solver has trouble converging for diameters between 0.5 and 1 cm does not make the remaining solutions invalid. The solver did converge for diameters outside that interval, with flow budget errors less than 1%, and because we have a stable and consistent scheme, the solver renders reliable solutions to the PDE. Thus, among our results, convergence issues were limited to a minority of the abscissa range of one figure panel (Figure 2,5c), and even there we can still ascertain the overall trend in the plot.

### *B1.2 Why Did We Change the Diameter if it Converged for the Length and Soil-pipe Density Study?*

From previous work, we know that the slightest perturbation in a system where the soil matrix has extreme values of hydraulic conductivity (i.e.  $K=10^{-3}$  m/s or  $K=10^{-8}$  m/s) will cause non-convergence of the PCG solver (the only solver package the CFP is coded to work with). Further, in studying the parameter height above base flow, the soil pipes must undergo wetting and drying at positive values of that parameter, which significantly increases the complexity Hagen-Poiseuille or Darcy-Weisbach formula, which increases the chance that the solver will not converge. To give a better chance of completing the entire sensitivity analysis for each parameter without failing to converge for some of the values of matrix K, height above base flow, and connectivity, we decided to change the diameter from 1.5 cm to 2 cm because the solver converges in significantly less iterations for 2 cm than 1.5 cm (compare Figures B7 and B8), and thus is further from the range diameters that gives the solver difficulty.

For 1.5 cm it takes 15 Minutes, 33.216 Seconds

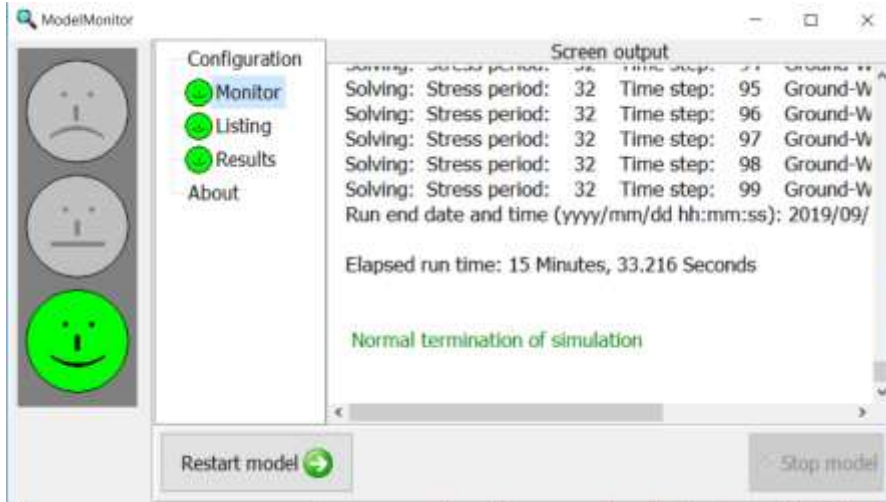


**Figure B7. Simulation information output for D=1.5cm.**

For 2.0 cm it takes 11 minutes, 20.445 seconds.

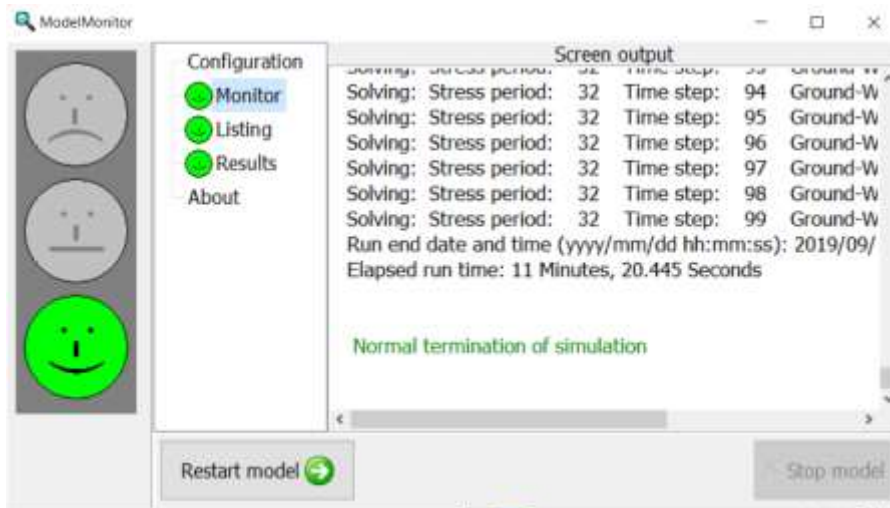


**Figure B8. Simulation information output for D=2.0 cm.**

This is more than a 25% decrease in computation time when going from D=1.5 cm to D=2.0 cm which means the conjugate gradient is finding the minimum of  $f(\mathbf{x}) = \frac{1}{2} \mathbf{x}^T [\mathbf{A}] \mathbf{x} - \mathbf{b}^T \mathbf{x} + \mathbf{c}$  much more quickly at the higher diameter. In other words, the surface for D=2.0 cm is more-well behaved.

## B2: Amplitude and Peak

We varied amplitude and peak as shown in figure B1 to see if the system would behave differently under different boundary conditions. There was little variation in the normalized hyporheic flow volume  $V/V_0$  vs. length (L) curve for each permutation.

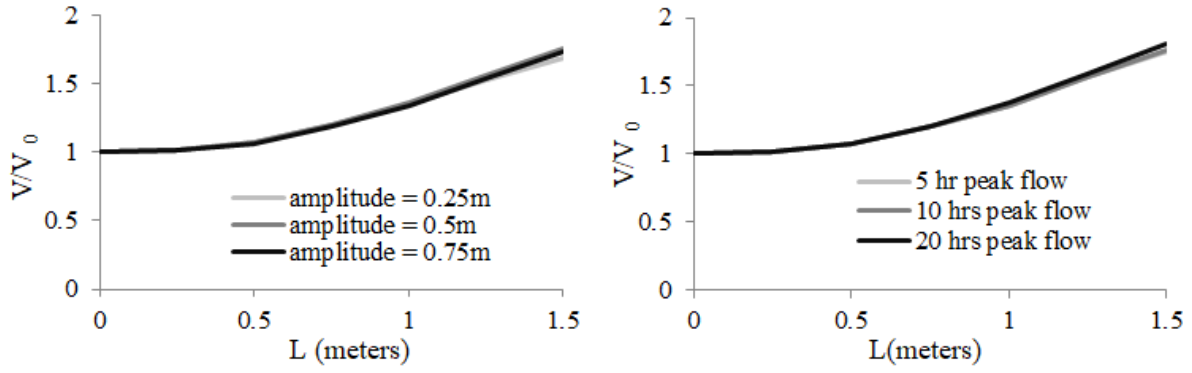
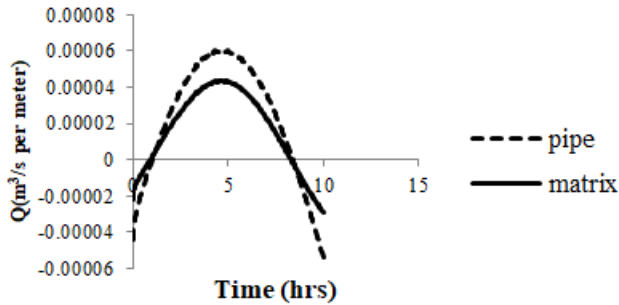


Figure B9:  $V/V_0$  vs.  $L$  for various hydrograph durations and amplitudes.

### B3: Comparison of Pipe Flow vs. Matrix Flow



### B4: Head Contour Maps at different Ks

Figure B10:  $Q$  vs.  $t$  in pipe and matrix at  $K=10^{-3}$  m/s.  $Q_{\text{matrix}}$  is the flow rate across the channel/riparian groundwater interface that occurs in the soil matrix over the domain of interest.  $Q_{\text{pipe}}$  is the flow rate in the soil pipe.

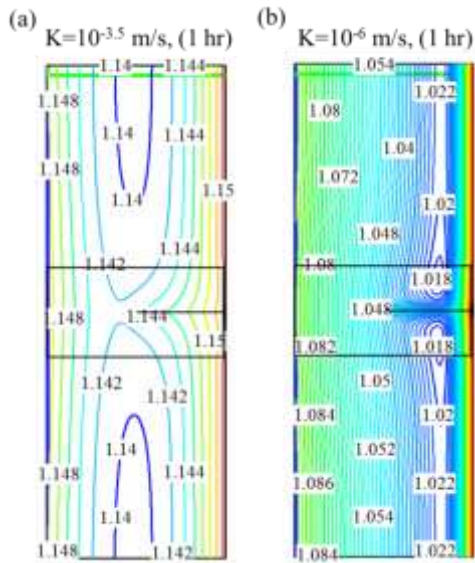


Figure B11: Head gradient comparison between matrix  $K=10^{-3.5}$  m/s and  $K=10^{-6}$  m/s for a single soil pipe ( $L = 1.0$  m,  $D = 2$  cm) at  $t=1$  hr. The contour interval is 0.02 m for both panels. The gradient is much steeper in the soil with lower matrix  $K$ .

### References

Boyce, W.E. and DiPrima, R.C. (2012) Numerical Methods. Elementary Differential Equations and Boundary Value Problems 10th Edition, p. 486.

DuFort, E.C. and Frankel, S.P. (1953) Stability conditions in the numerical treatment of parabolic differential equations. Mathematical Tables and Other Aids to Computation 7, 135-152.

Harbaugh, A.W. (2005) MODFLOW-2005, the U.S. Geological Survey modular ground-water model -- the Ground-Water Flow Process: U.S. Geological Survey Techniques and Methods 6-A16. U.S. Geological Survey, Reston, VA.

Marsily, G.d. (1986) Quantitative Hydrogeology. Academic Press, 440 p.

McDonald, M.G. and Harbaugh, A.W. (1984) A modular three-dimensional finite-difference ground-water flow model. U.S. Geological Survey Open-File Report 83-875, 528p.

McDonald, M.G. and Harbaugh, A.W. (1988) A modular three-dimensional finite-difference ground-water flow model. U.S. Geological Survey Techniques of Water Resources Investigations, 586p.

Pletcher, R.H., Tannehill, J.C. and Anderson, D.A. (2013) Application of Numerical Methods to Selected Model Equations. Computational Fluid Mechanics and Heat Transfer (Third Edition), 114.

Prickett, T.A. and Lonquist, C.G. (1971) Selected Digital Computer Techniques for Groundwater Resource Evaluation. Illinois Water Survey Bulletin 55, 1-62.

Reilly, T.E. and Harbaugh, A.W. (2004) Guidelines for Evaluation Ground-Water Flow Models. U.S. Geological Survey Scientific Investigation Report 2004-5038, 1-30.

Sauer, T. (2012) Numerical Analysis (2nd Edition), p. 382.

Wang, H.F. and Anderson, M.P. (1982) Introduction to Groundwater Modeling: Finite Difference and Finite Element Methods. Academic Press, 237 p.

## APPENDIX C: Supporting Information for CHAPTER 3, Pipe dreams: the effects of stream bank soil pipes on hyporheic denitrification caused by a peak flow event

**Authors:** W. Seth Lotts<sup>1</sup>, Erich T. Hester<sup>1</sup>

<sup>1</sup>Department of Civil and Environmental Engineering, Virginia Tech, Blacksburg, Virginia 24061 USA

### *C1 Supplemental Methods*

#### *C1.1 Growing Boundary Condition*

In low K soils (i.e.  $K \leq 10^{-4.5}$  m/s), it was necessary to institute a “growing” boundary condition that approximated contaminant migration from the channel into the pipes. Because velocities changed with both time and distance along the soil pipe, this needed to be done numerically. The distance that the nitrate front has advanced in the pipe is given by the recursive relation:

$$\hat{y}(t_i) = \hat{y}(t_{i-1}) + v_{\hat{y}}(\hat{y}|_{t=t_{i-1}}, t_{i-1})\Delta t_{i-1}, \text{ for } i = 0, 1, \dots, m \quad [C1]$$

where m is the number of stress periods it takes for the nitrate front to reach the end of the pipe;  $v_{\hat{y}}$  is the velocity in the  $\hat{y}$ -direction (positive is away from the channel);  $\hat{y}$  is distance the nitrate front has traveled in the pipe ( $\hat{y} = 0$  occurs at stream channel, and relates to the global Cartesian coordinate  $\hat{y} = 2 - y$ ) (Figure C1). We divided the boundary condition up into four sections (5 nodes), and the velocity versus time data were extracted from the Conduit Flow Package output files for  $\hat{y}_j$  for all j (Figure C1). In Equations C1 and C2, i indices correspond to stress period number, and the j indices correspond to the section immediate adjacent to the front and furthest from the stream (j=0 corresponds to the stream, and j=4 corresponds to the end of the pipe). The velocity at points in between the known velocities at the j nodes were determined by linear interpretation in Equation C2:

$$v_{\hat{y}}|_{t=t_{i-1}} \approx r v_{\hat{y}_{j-1}} + (1 - r) v_{\hat{y}_j}; \quad r = \frac{\hat{y}_j - \hat{y}}{\hat{y}_j - \hat{y}_{j-1}} \text{ for } j = 0, 1, 2, 3, 4 \quad [C2]$$

Once the front moved past a given value  $\hat{y}_j$ , the segment on the channel side of  $\hat{y}_j$  was set to change from  $C_{sp} = 0$  mg/L to  $C_{sp} = 1$  mg/L at that time (see Animations SI 12-15). Equations C1 and C2 were solved using Microsoft Excel, and the results were then implemented as a time-varying specified concentration boundary condition in MT3D-USGS (see main article).

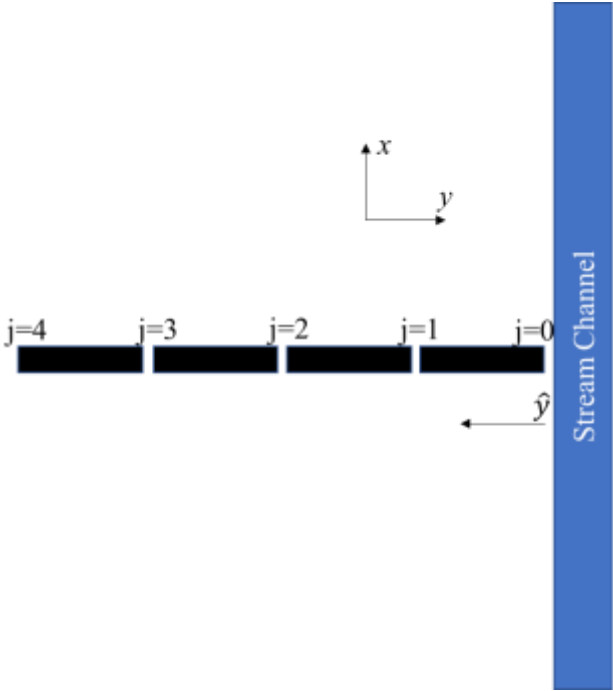


**Figure C1: Schematic of the “growing” time-varying specified concentration boundary condition for MT3D-USGS for  $K \leq 10^{-4.5}$  m/s. Each boundary condition section (i.e. portion of soil pipe between consecutively numbered nodes,  $j$ ) changes from 0 to 1 mg/L during a stress period if the front has migrated farther than that segment away from the stream channel (calculated by equation 3.10) by the time the stress period starts (e.g. the animations for lower  $K$  values in the supporting information, Animations SI 12-15).**

### *C1.2 Effect of Use of First Order Kinetics and Neglecting Aerobic Respiration*

Here, we address key simplifications in the main study related to our approach to modeling denitrification, namely 1) our use of first order kinetics rather than Monod kinetics, and 2) not explicitly modeling aerobic respiration. In particular, we re-ran some of the sensitivity analysis model runs in MT3D-USGS using Monod kinetics for both aerobic respiration and denitrification to demonstrate that first order kinetics produce the same trends. Below, we outline the governing equations, Monod parameters used, and stream concentrations and antecedent riparian aquifer concentrations used.

The rates of aerobic respiration and denitrification are given by equations from Bedekar et al. (2016):

$$R_{O_2}^* = -V_{O_2} Y_{AR} DOC \left( \frac{O_2}{K_{O_2} + O_2} \right) \quad [C3a]$$

$$R_{NO_3}^* = -V_{NO_3} Y_{DN} I \cdot DOC \left( \frac{NO_3}{K_{NO_3} + NO_3} \right) \quad [C3b]$$

with  $I$  given by

$$I = \frac{K_I}{K_I + O_2} \quad [C3c]$$

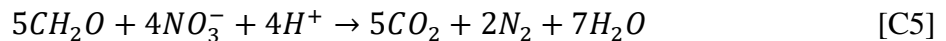
where  $V_{O_2}$  and  $V_{NO_3}$  are the aerobic respiration and denitrification rate respectively, ( $T^{-1}$ ),  $O_2$ , DOC, and  $NO_3$  are the concentrations of dissolved oxygen, dissolved organic carbon, and nitrate respectively ( $ML^{-3}$ ),  $K_{O_2}$ , and  $K_{NO_3}$  are the half-saturation constant for  $O_2$ , and  $NO_3$  respectively ( $ML^{-3}$ ),  $Y_{AR}$  and  $Y_{DN}$  is the yield coefficient for the destruction of DOC, and  $I$  is a non-competitive inhibition factor for  $O_2$ , and  $K_I$  is the inhibition constant for oxygen ( $ML^{-3}$ ). MT3D-USGS does not account for nitrification. We did not include nitrification because it is the more insignificant of the two oxic reactions (Zarnetske et al., 2012). Also, there are conditions where nitrification is minimal, including where there are natural inhibitors produced by various plant and tree roots (Castaldi et al., 2009; Laffite et al., 2020; Subbarao et al., 2012; Tesfamariam et al., 2014), or where heterotrophs outcompete nitrifying bacteria for oxygen (Schramm et al., 1996; Storey et al., 2004).

For ambient groundwater, we assumed anoxic conditions (i.e. 0 mg/L  $O_2$ ) and DOC concentration equal to 9.2 mg/L (both initial conditions within the model domain and for the general head boundary condition), common for riparian zones (Fiebig et al., 1990). We assumed that the stream had a DOC concentration of 24 mg/L, a lower bound for polluted streams (Mineau et al., 2016). We assumed the stream had a DO of 10 mg/L (USGS, 2021). We conducted sensitivity model runs varying soil pipe length ( $L$ ), height above or below WSEL ( $H$ ), and hydraulic conductivity ( $K$ ). The latter two parameters are the only two where the residence time varies significantly with the parameter, thus these parameters are of most concern when accounting for aerobic respiration. We ran two scenarios. The first used values from the experimental reach of Drift Creek (Zarnetske et al., 2012) where  $K_{O_2} = 5.28$  mg/L,  $K_{NO_3} = 1.64$  mg/L,  $K = 0.24$  mg/L,  $V_{O_2} = 5.74 \times 10^{-4} s^{-1}$  and  $V_{NO_3} = 1.11 \times 10^{-3} s^{-1}$ . The second scenario used values (Zarnetske et al., 2012) that would make the process the slowest and hence were more likely to affect denitrification trends, i.e.  $K_{O_2} = 5.80$  mg/L,  $K_{NO_3} = 3.10$  mg/L,  $K = 0.2$  mg/L,  $V_{O_2} = 2.78 \times 10^{-5} s^{-1}$  and  $V_{NO_3} = 7.22 \times 10^{-5} s^{-1}$ . The yield coefficients we calculated from stoichiometry from the following equations:

Aerobic respiration,



Denitrification,



where  $Y_{AR} = 1.07$  mg/L and  $Y_{DN} = 1.65$  mg/L.

The results from the above approach are presented in Section C2.1, below.

## C2 Supplemental Results

### C2.1 Effect of Use of First Order Kinetics and Neglecting Aerobic Respiration

The basic trends in all of the cases produced by Monod kinetics including aerobic respiration were the same as with denitrification only simulated using first order kinetics (Figure C2). The  $D/D_0$  versus  $L$  curves are identically shaped for both methods with a slightly higher percentage increase by adding soil pipes predicted by Monod kinetics. For a fast reacting system which used the Drift Creek stream parameters of Zarnetske et al. (2012), the  $D/D_0$  versus  $H$  followed the same trend as the fast reacting first order models where  $D/D_0$  is strictly a function of hyporheic volume (Figure C2a). For a slower reacting system which used the slowest possible parameter combinations in Zarnetske et al. (2012), the  $D/D_0$  versus  $H$  followed the same trend as the slow reacting first order models where there is a bulge in  $D/D_0$  at  $H > 0$  due to increased residence times caused by nitrate being stranded (Figure C2b). Further, there is also a decrease in  $D/D_0$  at even higher  $H$  (i.e.  $H \approx 0.15\text{m} - 0.3\text{m}$ ) due to less water being advected into the riparian soil just as with the  $D/D_0$  vs.  $H$  curves produced with first order kinetics (Figure C2b). With  $K$  there is a decrease in  $D/D_0$ , but more drastic since the residence time is so short for large  $K$  that aerobic respiration is not finished when the water particles return to the stream or soil pipe (Figure C2c). Other than sharper declines with  $K$ , the only deviation from first order kinetics was that percentage increase in denitrification due to soil pipes is higher with Monod kinetics since more substrate flowed into a system when  $\rho=1$ . This increased the rate of reaction for denitrification and respiration which also causes the oxygen to be depleted faster. So, with first order kinetics, we have actually underestimated normalized denitrification and thereby have provided a conservative estimate of the impact of soil pipes.

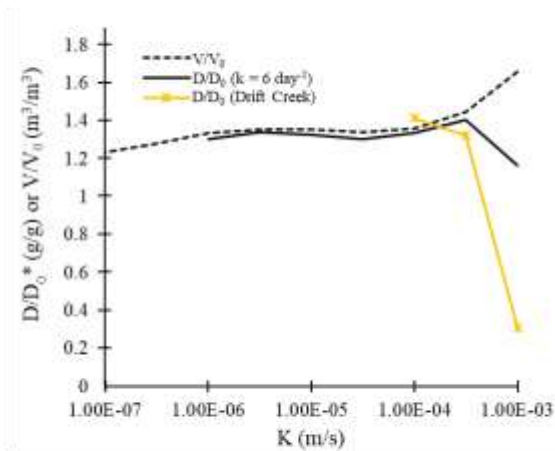
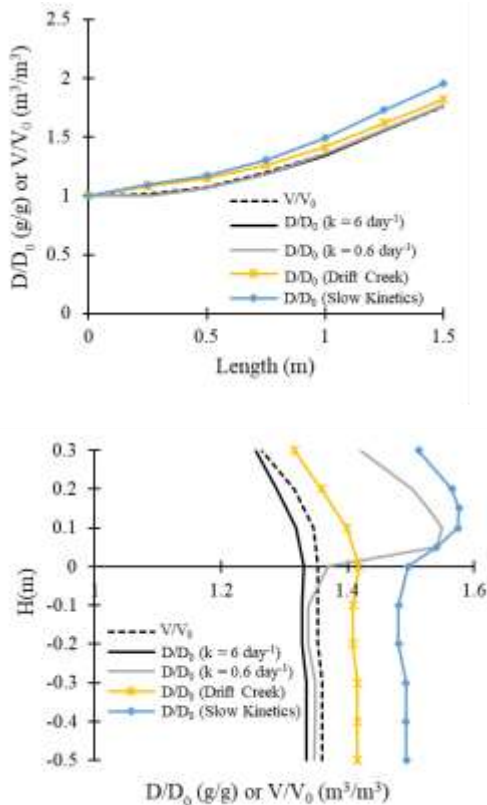


**Figure C2. Streambank scale effects of soil pipe parameters, comparing first-order denitrification with Monod aerobic respiration and denitrification. a) Total mass denitrified in peak-flow induced lung model hyporheic exchange (D) normalized to case without soil pipes (soil pipe density  $\rho = 0 \text{ m}^{-1}$ )(D/D<sub>0</sub>) vs. the length (L) of a single soil pipe b) D/D<sub>0</sub> for a single soil pipe vs. its height above or below starting water surface elevation (H) (negative is an initially submerged soil pipe), and c) D/D<sub>0</sub>\* vs. K. D<sub>0</sub> changes for each scenario in D/D<sub>0</sub>\*. In each panel, the V/V<sub>0</sub>, D/D<sub>0</sub> (k = 0.6 days<sup>-1</sup>), and D/D<sub>0</sub> (k = 6 days<sup>-1</sup>) curves (i.e. the gray and black lines) are unchanged from Figure 3.2 (L and H) and Figure 3.3 (K) from the main manuscript.**

### C2.2 Denitrification vs. Reactive Transport Parameters

Total mass denitrified (D) is most sensitive to changes in k with steep increases at the lower end of the k range but leveled off as reaction rate increases and the reaction became more transport limited (Figure C3a). D slightly increased roughly linearly with increasing  $\alpha_L$  (Figure C3b), and increased linearly with C<sub>0</sub> when first order kinetics are assumed (Figure C3c). Although very subtly, D is slightly elevated at both high and low  $\theta$  (Figure C3d).

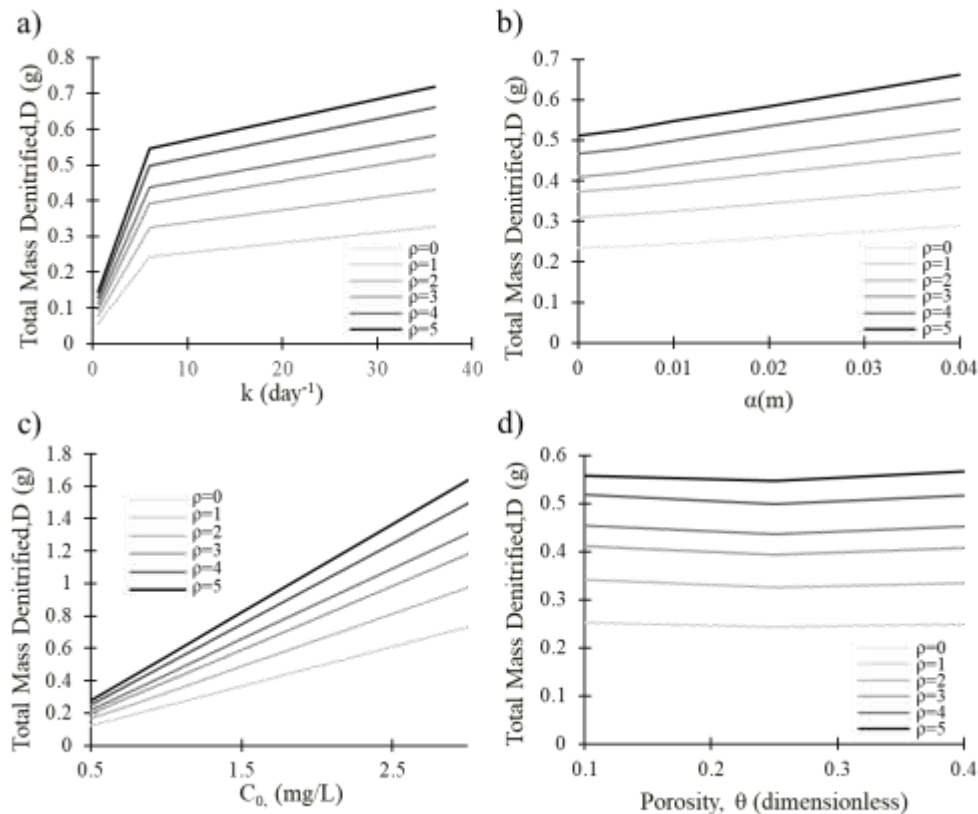


**Figure C3. Total mass denitrified (D) versus a) reaction constant k, b) longitudinal dispersivity,  $\alpha_L$ , c) initial concentration C<sub>0</sub>, d) porosity,  $\theta$  for various  $\rho$ .**

C2.3 Whole Stream Removal for  $K = 1 \times 10^{-6}$  m/s,  $\rho=5$ .

$S_0=0.0001$ ,  $K = 1 \times 10^{-6}$  m/s

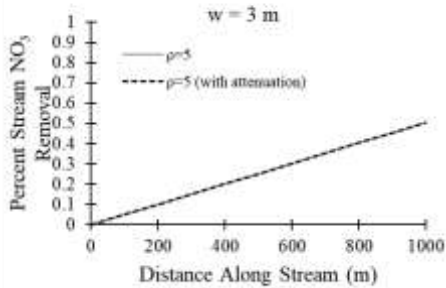


**Figure C4. Denitrification versus distance along stream for  $K = 10^{-6}$  m/s, (reaction constant  $k = 6 \text{ days}^{-1}$ ) at stream width of 3 m, and slope of 0.0001.**

C3 Error of the Stair-Step Boundary Condition

Although it is impossible to precisely quantify the difference between our approach and a more rigorous reactive advective-transport framework applied to the soil pipe domain, it is less than ~4%, the difference between two theoretical extremes: a constant function (one that maintains a constant concentration of 1 mg/L) and a Heaviside function (one that is 1 mg/L from  $t=0$ -10 hours, and then turns to 0 when  $t > 10$  hours) (Table C1). Further, it is probably not greater than the maximum difference between the stairstep boundary condition and a Heaviside function, ~1%, since the stairstep boundary condition is more aligned conceptually to rigorous treatment of soil pipe domain than it is a Heaviside function (immediate vanishing of all nitrate at 10 hours).

**Table C1**

	Percent Difference between Constant and Heaviside function	Percent Difference between Constant and Stair-step function	Percent Difference between Heaviside and Stair-step function
$\rho=0$	N/A	N/A	0
$\rho=1$	0.217	0.194	0.0232
$\rho=2$	0.514	0.500	0.0141
$\rho=3$	2.511	2.443	0.070

$\rho=4$	4.0186	3.796	0.232
$\rho=5$	Not done for Constant	Not done for Constant	0.998

#### C4 Animation Notes

- (1) Animations 1-5 are for  $\rho = 1, 2, 3, 4,$  and  $5 \text{ m}^{-1}$ , respectively, and base case parameters for all other soil pipe, soil matrix, and transport parameter. Animations 6-10 are for  $\rho = 1, 2, 3, 4,$  and  $5,$  and  $k = 0.6 \text{ days}^{-1}$ , respectively, and base case for all other parameters (Table 2.1).
- (2) Animation 11 is for  $H = 0.3 \text{ m}$ , and  $k = 0.6 \text{ days}^{-1}$ , and base case for all other parameters (Table 2.1).
- (3) Animations 12-15 are for  $K = 1 \times 10^{-4.5}, 1 \times 10^{-5}, 1 \times 10^{-5.5},$  and  $1 \times 10^{-6} \text{ m}^{-1}$ , respectively (i.e. the simulations which required a growing boundary condition). All other parameters were base case (Table 2.1).
- (4) The unit for the color legend for the base case scenario is mg/L.
- (5) Each scenario was run until the plume exited into the stream or decomposed all the way; the stream boundary condition shuts off at 24 hours so as not to introduce additional solute into the system via dispersion.
- (6) Nitrate lingered between the soil pipes on animations 8-10 ( $\rho = 3, 4,$  and  $5 \text{ m}^{-1}$  for  $k = 0.6 \text{ days}^{-1}$ , respectively) due to transverse head gradients pushing solute back into the matrix from the soil pipe during the falling limb of the peak flow event. We did not observe this with animations 3-5 ( $\rho = 3, 4,$  and  $5 \text{ m}^{-1}$  for  $k = 6 \text{ days}^{-1}$ , respectively) since it is a faster reacting soil and much of the plume is consumed via biodegradation before it returns to the soil pipe. Consequently, much less is ejected back into the matrix in between the soil pipes.
- (7) Negative concentrations are nonphysical numerical overshoots commonly occurring at sharp gradients (like Gibbs' phenomenon for Fourier Series), and are common for higher order methods. To fit data points that are approximately vertical with respect to each other (ergo the sharp concentration gradient), a higher order polynomial will dip down below the low point and rise up over the point but still fit the data well. The overall solutions though have very little mass balance error. More information about negative concentrations can be found in Bedekar et al. (2016).

#### References

- Bedekar, V., Morway, E.D., Langevin, C.D. and Tonkin, M. 2016. MT3D-USGS version 1: A U.S. Geological Survey release of MT3DMS updated with new and expanded transport capabilities for use with MODFLOW. U.S. Geological Survey Techniques and Methods 6-A53, 69p.
- Castaldi, S., Carfora, A., Fiorentino, A., Natale, A., Messere, A., Miglietta, F. and Cotrufo, M.F. 2009. Inhibition of net nitrification activity in a Mediterranean woodland: possible role of chemicals produced by *Arbutus unedo*. Plant Soil 315, 273-283.

- Fiebig, D.M., Lock, M.A. and Neal, C. 1990. Soil water in the riparian zone as a source of carbon for a headwater stream. *Journal of Hydrology* 116, 217-237.
- Laffite, A., Florio, A., Andrianarisoa, K.S., des Chatelliers, C.C., Schloter-Hai, B., Ndaw, S.M., Periot, C., Schloter, M., Zeller, B., Poly, F. and Le Roux, X. 2020. Biological inhibition of soil nitrification by forest tree species affects *Nitrobacter* populations. *Environmental Microbiology* 22(3), 1141-1153.
- Mineau, M.M., Wollheim, W., Buffam, I., Findlay, S., Hall, R.O., Hotchkiss, E.R., Koenig, L.E., McDowell, W.H. and Parr, T.B. 2016. Dissolved organic carbon uptake in streams: a review and assessment of reach-scale measurements. *Biogeosciences* 121, 2019-2029.
- Schramm, A., Larsen, L.H., Revsbech, N.P., Ramsing, N.B., Amann, R. and Schleifer, K. 1996. Structure and function of a nitrifying biofilm as determined by in situ hybridization and the use of microelectrodes. *Applied and Environmental Microbiology* 62(12), 4641-4647.
- Storey, R.G., Williams, D.D. and Fulthorpe, R.R. 2004. Nitrogen processing in the hyporheic zone of a pastoral stream. *Biogeochemistry* 69, 285-313.
- Subbarao, G.V., Sahrawat, K.L., Nakagawa, H., Ishikawa, T., Kishii, M., Rao, I.M., Hash, C.T., George, T.S., Rao, P.S., Nardi, P., Bonnett, D., Berry, W., Suenega, K. and Lata, J.C. 2012. Chapter six - biological nitrification inhibition - a novel strategy to regulate nitrification in agricultural systems. *Advances in Agronomy* 114, 249-302.
- Tesfamariam, T., Yoshinaga, H., Deshpande, S.P., Rao, P.S., Sahrawat, K.L., Ando, Y., Nakahara, K., Hash, C.T. and Subbaro, G.V. 2014. Biological nitrification inhibition in sorghum: the role of sorgleone. *Plant Soil* 379, 325-335.
- USGS 2021 USGS Surface-Water Daily Statistics for the Nation, USGS 14163900 McKenzie River Near Walterville, OR, USGS.
- Zarnetske, J.P., Haggerty, R., Wondzell, S.M., Bokil, V.A. and Gonzalez-Pinzon, R. 2012. Coupled transport and reaction kinetics control the nitrate source-sink function of hyporheic zones (vol 48, W11508, 2012). *Water Resources Research* 48.

## APPENDIX D: Python code for residence time calculation, implicit solving of Manning's equation in CHAPTER 3

Residence Time Calculator:

```
In [1]: import pandas as pd
import numpy as np
csv_data = pd.read_csv('ResTime_MatrixK_30_3hours.csv')
#ds = pd.read_csv('data.csv', sep=',', header=0)
t = csv_data["t"]
ys = csv_data["y"]
x = csv_data["x"]

y = np.zeros(len(ys))

for i in range(0, len(t)-1):
    if t[i]==0:
        ys[i-1] = "0"
for i in range(0, len(y)-1):
    y[i] = np.float(ys[i])

C:\ProgramData\Anaconda3\lib\site-packages\ipykernel_launcher.py:14: SettingWithCopyWarning:
A value is trying to be set on a copy of a slice from a DataFrame

See the caveats in the documentation: http://pandas.pydata.org/pandas-docs/stable/indexing.html#indexing-view-versus-copy
```

```
In [2]: numpart = 1188
res = np.zeros(numpart)
k=0
for i in range(2, len(t)-1):
    if y[i] >= 2.74 and y[i] <= 2.76 and x[i] >=1 and t[i] > 5000:
        if y[i-1] < 2.74 or y[i-1] > 2.76:
            res[k] = t[i]
        if t[i]==0 and t[i-1]!=0:
            if res[k]==0:
                res[k]=t[i-2]
            k=k+1
res[numpart-1]=t[len(t)-1]
```

```
In [3]: print(res)
[22500. 22500. 22500. ... 27600. 27600. 27600.]
```

```
In [4]: resavg = np.mean(res)
```

```
In [5]: resavg
```

```
Out[5]: 26833.501683501683
```

```

In [6]: resmax = np.max(res)
if resmax == np.max(t):
    print("look into running the flow model longer")
else:
    print("good to go!")

count = 0
for i in range(0, len(res)-1):
    if res[i] < 3000:
        print(i)
        print('blah')
        count = count + 1
    elif res[i] == np.max(t):
        print(i)
        count = count + 1

print("count =", count)

j=0
resnew = np.zeros(len(res)-count-1)
for i in range(0, len(res)-1):
    if res[i] < 3000:
        h=0
    elif res[i] == np.max(t):
        h=0
    else:
        resnew[j] = res[i]
        j=j+1

resavgnew = np.mean(resnew)
print("the new average minus stuck particles", resavgnew)

look into running the flow model longer

```

```

look into running the flow model longer
576
577
578
579
580
581
582
583
584
585
586
587
count = 12
the new average minus stuck particles 26743.31914893617

```

## Implicit Solving of the Manning Equation :

```

In [13]: %pylab inline
%config InlineBackend.figure_format='retina' # hig-res plots for a Retina display
from scipy.optimize import fsolve, newton

# Manning for a trapezoidal or rectangular channel
def manning(y, Q, b, S, n, Co, R):
    A = (b+n*y)*y
    R = A/(b+2*y*(1+n**2)**(1/2))
    return Q-(Co/n)*A*R**(2/3)*S**(1/2)

Populating the interactive namespace from numpy and matplotlib

```

```
In [53]: # channel properties -----
Q= (2.388576847,
2.292377948,
2.358613764,
2.456207289,
2.568066613,
2.689121357,
2.812357483,
2.938649967,
3.056792967,
3.171527217,
3.279564482,
3.376608925,
3.463575312,
3.538603972,
3.600072483,
3.64704041,
3.681872483,
3.698603972,
3.791575312,
3.688908925,
3.661664482,
3.620127217,
3.564792967,
3.496849967,
3.416357483,
3.326121357,
3.226066613,
3.110207289,
3.004613764,
2.885377948,
5.733805387)
```

```
N = len(Q)
b = 3      # channel width (m) w
m = 0      # side slope
So = 0.001 # initial channel slope So
n = 0.03   # manning n value
```

```
In [30]: len(Q)
```

```
Out[30]: 31
```

```
In [54]: # initial conditions
```

```
Co = 1
y = zeros(N)

for i in range(0,N):
    yo = fsolve(manning,i, args=(Q[i], b, So, n, Co, n))[0]
    y[i] = yo

print('normal depth [manning]', around(y, decimals=3))
```

```
normal depth [manning] [1.044 1.014 1.034 1.065 1.1   1.137 1.175 1.212 1.248 1.283 1.315 1.343
1.369 1.391 1.409 1.423 1.432 1.437 1.438 1.435 1.427 1.415 1.398 1.379
1.355 1.328 1.299 1.267 1.233 1.197 2.007]
```

## APPENDIX E: Python code for residence time calculation, and conservation of mass in the soil pipe for CHAPTER 4

Residence Time Calculator:

```
In [1]: import pandas as pd
import numpy as np
csv_data = pd.read_csv('ResTime.csv')
nds = pd.read_csv('data.csv', sep=',', header=0)
t = csv_data["t"]
ys = csv_data["y"]
x = csv_data["x"]

y = np.zeros(len(ys))

for i in range(0, len(t)-1):
    if t[i]==0:
        ys[i-1] = "0"
for i in range(0, len(y)-1):
    y[i] = np.float(ys[i])

numpart = 400
res = np.zeros(numpart)
k=0
for i in range(2, len(t)-1):
    if y[i] >= 2.74 and y[i] <= 2.76 and x[i] >=1 and t[i] > 7500:
        if y[i-1] < 2.74 or y[i-1] > 2.76:
            res[k] = t[i]
        if t[i]==0 and t[i-1]!=0:
            if res[k]==0:
                res[k]=t[i-2]
            k+=1
res[numpart-1]=t[len(t)-1]

resavg = np.mean(res)
```

resavg

C:\ProgramData\Anaconda3\lib\site-packages\ipykernel\_launcher.py:14: SettingWithCopyWarning:  
A value is trying to be set on a copy of a slice from a DataFrame

See the caveats in the documentation: <http://pandas.pydata.org/pandas-docs/stable/indexing.html#indexing-view-versus-copy>

Out[1]: 456670.0

Conservation of Mass Calculator:

```
In [1]: import pandas as pd
import numpy as np

#extract flows from node1, first node in pipe1
read_file = pd.read_csv('NODE0001.OUT')
read_file.to_csv('NODE0001.csv', index=None)
csvdata1 = pd.read_csv('NODE0001.csv')
Qarr1 = csvdata1.to_numpy()
blah = Qarr1[[53]][0][0]
smeh = str.split(blah)
Qmatrix1 = float(smeH[3])
Qout1 = -float(smeH[4])

#test
print(Qmatrix1)
print(Qout1)

#Apply Boundary Condition to top pipe
csv_dataC = pd.read_csv('Conc.csv')
#here we extract the concentrations from the csv file
CmatrixPipe1 = csv_dataC["Conc1"]
#we predesignate an array for Cin and Cout for both pipes
Cinpipe1 = np.zeros(len(CmatrixPipe1))
Coutpipe1 = np.zeros(len(CmatrixPipe1))
#we deal with the node on the end since it is different
Coutpipe1[0] = Qout1*CmatrixPipe1[0]
Cinpipe1[1] = Coutpipe1[0]
```

```

#we now solve for the concentration in pipe1
for i in range(2,49):
    #we extract the flow rates for the respective node
    if((i% 2) and (i% 9)):
        f = "NODE000" +str(i)+".OUT"
        f2 = "NODE000" +str(i)+".CSV"
    else:
        f = "NODE00" +str(i)+".OUT"
        f2 = "NODE00" +str(i)+".CSV"

    read_file = pd.read_csv(f)
    read_file.to_csv (f2, index=None)
    csvdata = pd.read_csv(f2)
    Qarr = csvdata.to_numpy()
    blah = Qarr[[53]][0][0]
    smeh = str.split(blah)
    Qmatrix = float(sme[3])
    Qin = float(sme[4])
    Qout = -float(sme[5])
    Coutpipe1[i-1] = (Cinpipe1[i-1]*Qin+CmatrixPipe1[i-1]*Qmatrix)/Qout
    Cinpipe1[i] = Coutpipe1[i-1]

#record massflow for pipe1
MassFlowP1 = Qout*Coutpipe1[47]

1.83869e-08
1.83866e-08

```

In [2]: print(MassFlowP1)

6.42101002506507e-08

In [2]: Coutpipe1[47]

Out[2]: 0.09056316668850564

In [ ]:

**APPENDIX F: Supporting Information for CHAPTER 5: “Lost in dune translation: the effects of microbial growth dynamics on hyporheic biogeochemistry underneath moving dunes”**

*F1 Quasi-periodic Boundary Condition*

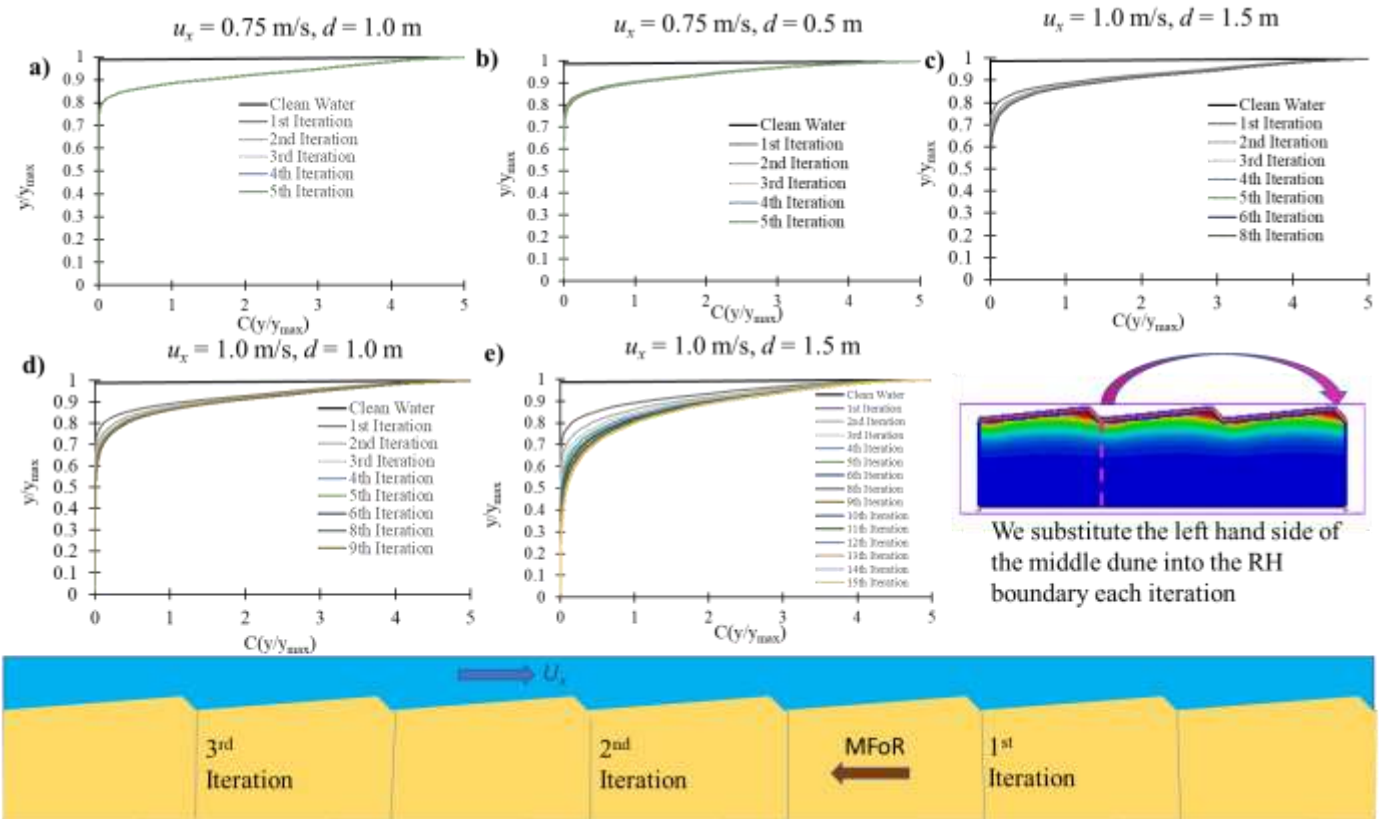
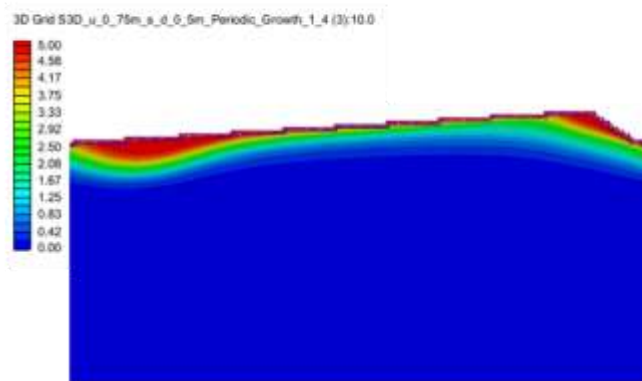


**Figure F1. Quasi-periodic boundary condition. a) thru e) The normalized depth,  $y/y_{max}$  vs. DOC concentration (denoted C) profiles for the left hand boundary of the middle dune, at each surface water velocity ( $u_x$ ) and depth (d) combination.**

*F2 Results for Dissolved Oxygen*

DOC and DO plumes were almost identical. This makes sense because the reactants in Equation 5.19 have a 1:1 stoichiometric ratio, and very similar molar masses ( $\approx 30$ g/mol for  $CH_2O$  and  $\approx 32$ g/mol for  $O_2$ ).

a)  $u_x = 0.75 \text{ m/s}$ ,  $d = 0.5 \text{ m}$ ,  $c_b = 17.02 \text{ m/d}$   
**Growth, DOC**



b)  $u_x = 0.75 \text{ m/s}$ ,  $d = 0.5 \text{ m}$ ,  $c_b = 17.02 \text{ m/d}$   
**Growth, DO**

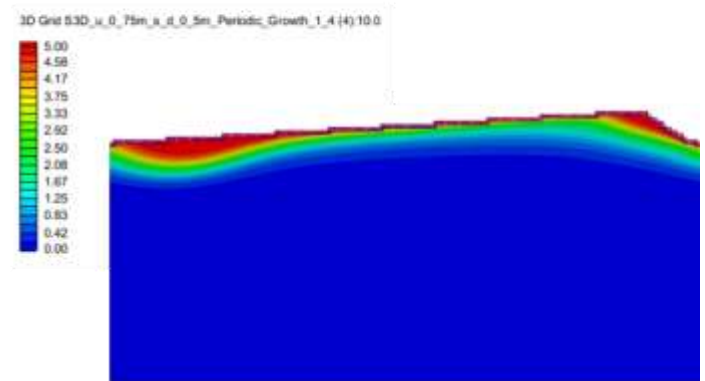


**Figure F2.** This is the concentration map for a) DOC, and b) DO. This is a sample comparison to show that the two color maps are almost identical, so there is no utility in displaying the same results for DO. The (3) in parentheses in the very long color legend label stands for “species 3” for DOC (there are two “tracers” by default), and the (4) stands for “species 4” for DO;  $u_x$  is average stream velocity (m/s),  $d$  is stream depth from dune trough to free surface (m), and  $c_b$  is celerity (m/d).

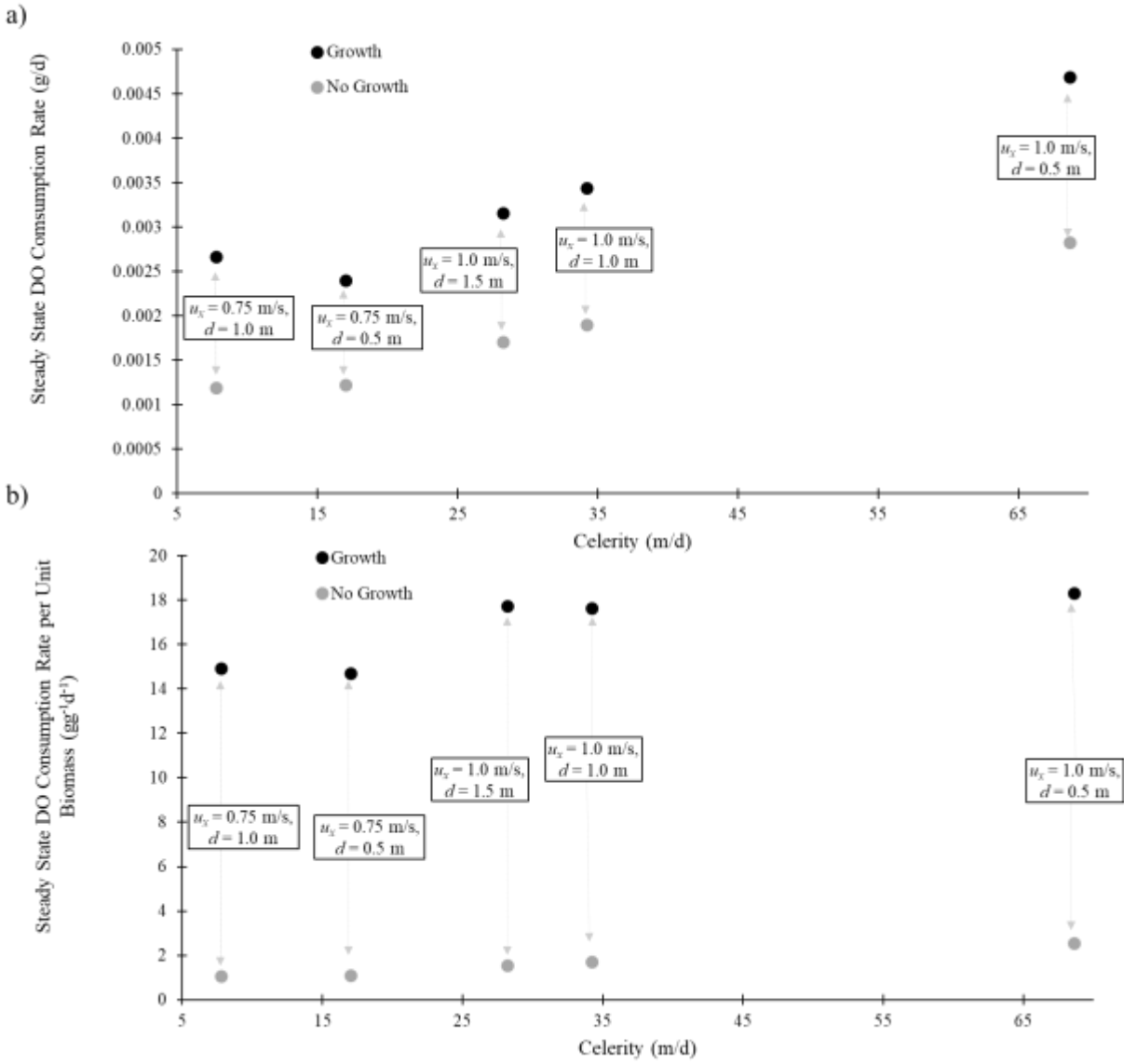
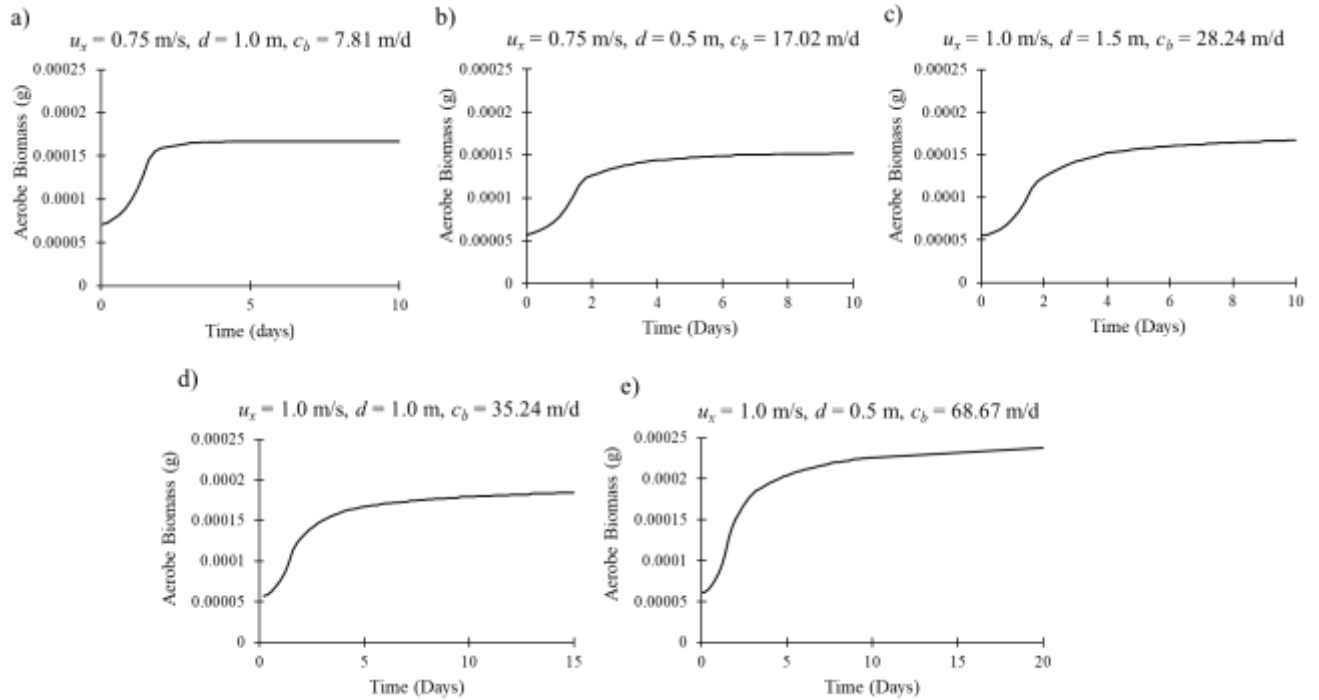


Figure F3. Same as Figure 5.6, except for DO. The graphs are indistinguishable.

F3 Temporal Biomass Curves.



**Figure F4. Biomass versus time curves for each combination of  $u_x$  (m/s) and  $d$  (m).**

#### *F4 Varying Dune Celerity Apart from Stream Hydrodynamics*

In order to compare our moving-dune results with the much more commonly simulated static case (Bardini et al., 2012; Cardenas and Wilson, 2007a; b; Elliott and Brooks, 1997b; Hester et al., 2013; 2014; Marzadri et al., 2016), we held the pressure distribution constant at the mildest pressure distribution we explored in our study produced by the most quiescent stream hydrodynamic conditions ( $u_x = 0.75$  m/s,  $d = 1.0$  m/s,  $c_b = 7.81$  m/d, i.e. the closest to a “zero” celerity case that we explored). We then cycled through all of the  $c_b$  values in the study (7.81, 17.02, 28.24, 34.25, 68.67 m/d) plus three additional  $c_b$  values lower than 7.81 m/d (0, 1, 2 m/d). We explored only changes in  $c_b$  even though changes in  $c_b$  would normally be caused by changes in stream hydrodynamic conditions, which would also cause changes in the pressure distribution. Further, at stream hydrodynamic conditions which would lead to  $c_b = 0, 1,$  and  $2$  m/d for our dune geometry, there would not actually be dunes, but ripples or no bedforms instead.

Our results indicate that as  $c_b$  increased from 0 to 68.67 m/d, the classical hydrodynamically-induced DOC plume associated with the static dune case shrinks back toward the stoss side of the dune (Figure F5), and gets replaced with a turnover-induced streak of DOC emanating from the lee side which gets wider and more highly concentrated with increasing  $c_b$ . The DOC consumption rate predicted by the static scenarios is profoundly higher than the results from the moving-frame of reference model, hinting that that earlier studies significantly over-estimated the impact of dune hyporheic exchange (Figure F6). As with the scenarios studied in the main manuscript, DOC consumption followed almost the exact same shape as steady state biomass curve (Figure F6). Furthermore, by visual inspection the area of the DOC plume in the

static and near static cases (Figure F6abc) are far greater than for  $c_b \geq 7.81$  m/d, which reinforces that DOC consumption is a function of DOC plume area.

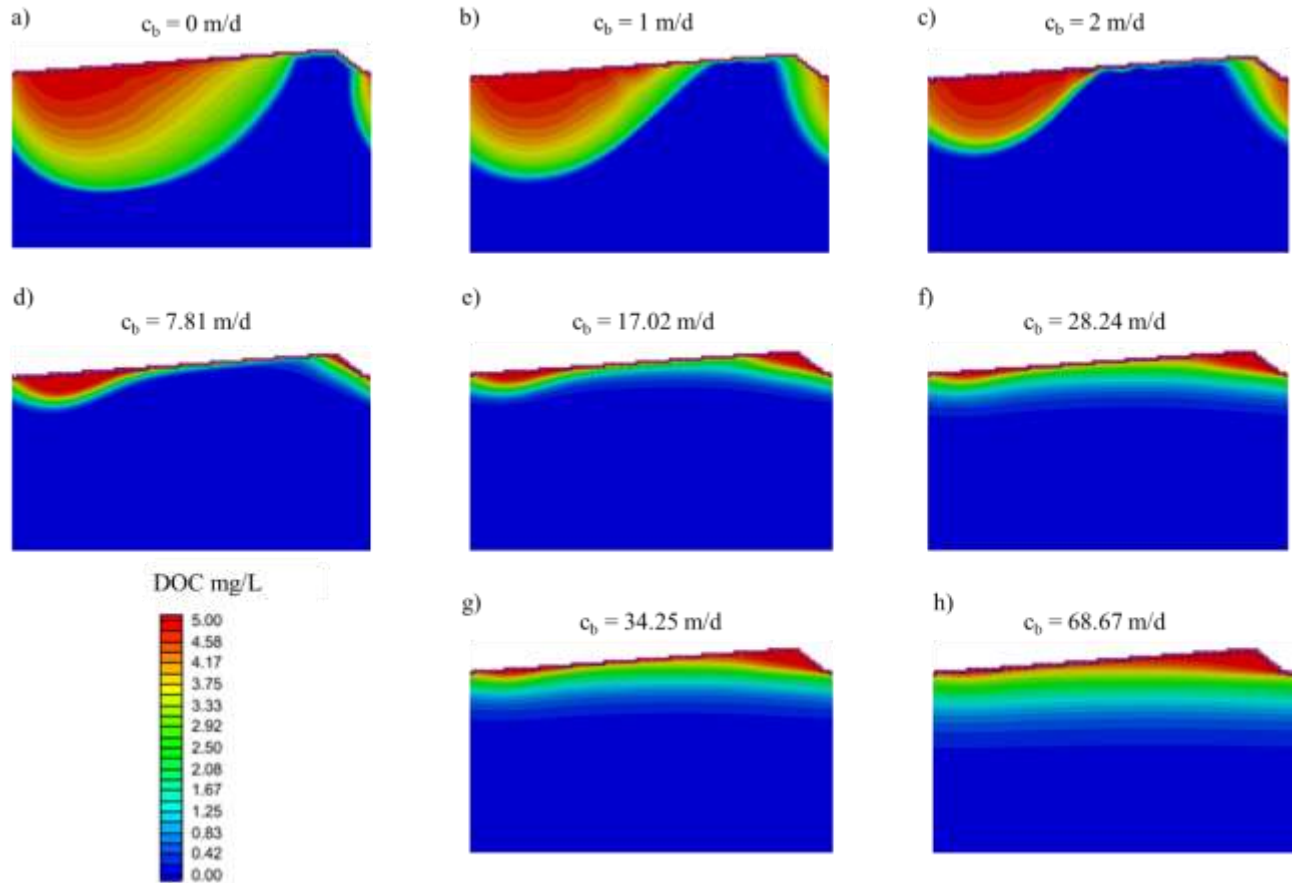


**Figure F5. DOC Concentration maps for all values of celerity, where we held the pressure distribution to value commensurate with  $u_x = 0.75$  m/s,  $d = 1.0$  m. Note, that we do not have  $u_x$  and  $d$  labeled in this graph since we vary  $c_b$  as if it were not a function of these variables (since we held the pressure distribution constant).**

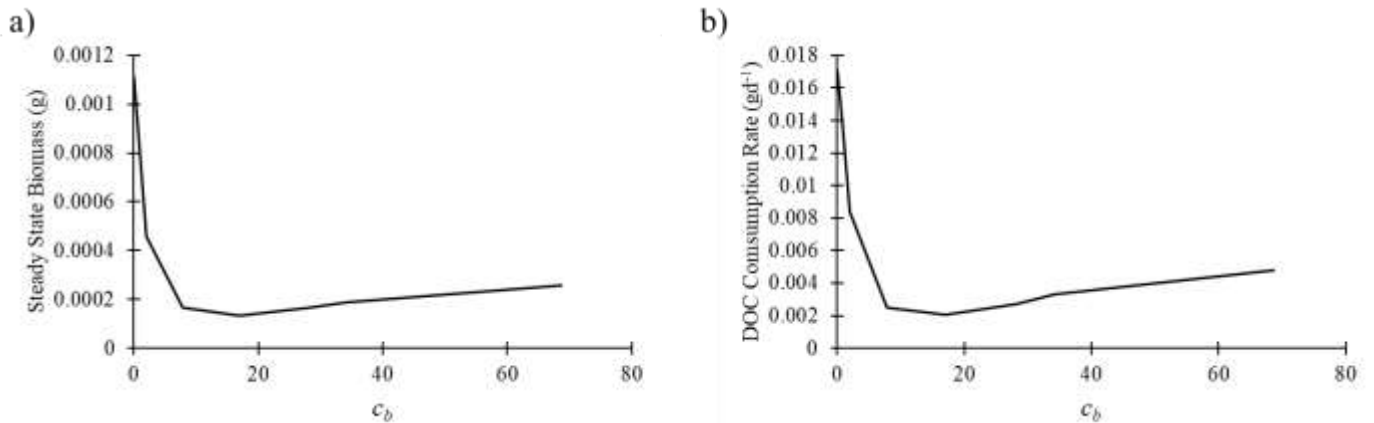


**Figure 6. a) Steady state biomass (g) versus  $c_b$  (m/d). b) DOC consumption rate ( $\text{gd}^{-1}$ ) versus  $c_b$  (m/d).**

## References

- Bardini, L., Boano, F., Cardenas, M.B., Revelli, R. and Ridolfi, L. 2012. Nutrient cycling in bedform induced hyporheic zones. *Geochimica Et Cosmochimica Acta* 84, 47-61.
- Cardenas, M.B. and Wilson, J.L. 2007a. Dunes, turbulent eddies, and interfacial exchange with permeable sediments. *Water Resources Research* 43(8), W08412.
- Cardenas, M.B. and Wilson, J.L. 2007b. Hydrodynamics of coupled flow above and below a sediment-water interface with triangular bedforms. *Advances in Water Resources* 30(3), 301-313.
- Elliott, A.H. and Brooks, N.H. 1997b. Transfer of nonsorbing solutes to a streambed with bed forms: Theory. *Water Resources Research* 33(1), 123-136.
- Hester, E.T., Young, K.I. and Widdowson, M.A. 2013. Mixing of surface and groundwater induced by riverbed dunes: implications for hyporheic zone definitions and pollutant reactions. *Water Resources Research* 49, 5221-5237.
- Hester, E.T., Young, K.I. and Widdowson, M.A. 2014. Controls on mixing-dependent denitrification in hyporheic zones induced by riverbed dunes: A steady state modeling study. *Water Resources Research* 50(11), 9048-9066.
- Marzadri, A., Tonina, D., Bellin, A. and Valli, A. 2016. Mixing interfaces, fluxes, residence times and redox conditions of the hyporheic zones induced by dune-like bedforms and ambient groundwater flow. *Advances in Water Resources* 88, 139-151.

## APPENDIX G: Python code for celerity calculation for CHAPTER 5.

Celerity Calculator (Written by Kyle B. Strom 2021):

### Bedform Celerity Estimator

Based on the van Rijn bedload transport equation. Take the skin component of the bed shear stress and grain size as the primary input. Using an array for the grain size and stress will produce a range of expected celerity values.

```
In [3]: %pylab inline
%config InlineBackend.figure_format='retina' # hig-res plots for a Retina display
```

Populating the interactive namespace from numpy and matplotlib

```
In [5]: # user inputs -----
# variable inputs

# taubs = array([0.217109431,2.466454778]) # input skin friction bed shear stress [Pa or N/m^2]
taubs = array([0.37243156,0.290154716,0.268537772,0.791062353,0.60495182,0.569906318,1.35725644,1.828261497,0.954756688])

# input skin friction bed shear stress [Pa or N/m^2]
dmicron = array([300,300,300,300,300,300,300,300,300]) # sediment size [micron]
theta = 0.3 # bed porosity [fraction of 1]
K = 100/(3600*24) # hydraulic conductivity [m/s?]

# fixed inputs

delta = 0.1 # bedform height [m]
l = 2 # bedform height [m]
```

```
Rs = 1.65 # submerged specific gravity of sand
nu = 1.14e-6 # fluid kinematic viscosity[m/s^2]
rho = 1000. # fluid density [kg/m^3]
g = 9.81 # acc. of gravity [m/s^2]

# calculations -----

# transport calculations

d = dmicron/(1000*1000)
Ds = d*(g*Rs/nu**2)**(1/3)
tauscr = 0.3/(1+1.2*Ds)+0.055*(1-exp(-0.02*Ds))
uscr = sqrt(tauscr*g*Rs*d)

us = sqrt(taubss/rho)
tauss = taubs/(rho*Rs*g*d)

T = zeros(len(tauss))
for i in range(0,len(tauss)):
    if tauss[i] > tauscr[i]:
        T[i] = (tauss[i]-tauscr[i])/tauscr[i]
    else:
        T[i] = 0

qbs = 0.053*T**2.1/Ds**0.3
qb = qbs*d*sqrt(g*Rs*d)

cb = 2*qb/((1-theta)*delta)

# likely bedform type calcs
```

```

bftype=[]
for i in range(0,len(Ds)):
    if Ds[i] > 10:
        if T[i] > 0.4:
            bf = 'dunes'
        elif T[i] > 0:
            bf = 'plane bed'
        else:
            bf = 'no motion'
    else:
        if T[i] > 2:
            bf = 'dunes'
        elif T[i] > 0:
            bf = 'ripples'
        else:
            bf = 'no motion'
    bftype.append(bf)

print('tau* applied / tau*cr =', tauss/tausc)
print('likely bedform types:',bftype)
print('Bedform celerity =',cb,'[m/s]')
print('Bedform celerity / hydraulic conductivity =',cb/K)

tau* applied / tau*cr = [1.95430244 1.52256181 1.40912076 4.15103137 3.17443242 2.99053418
7.12208175 5.39571339 5.01000325]
likely bedform types: ['ripples', 'ripples', 'ripples', 'dunes', 'dunes', 'ripples', 'dunes', 'dunes', 'dunes']
Bedform celerity = [1.60374810e-05 4.5277233e-06 2.70832955e-06 1.97036283e-04
9.04111311e-05 7.50985795e-05 7.94847191e-04 3.96421457e-04
3.26888320e-04] [m/s]
Bedform celerity / hydraulic conductivity = [0.01385638 0.003912 0.00234 0.17023935 0.07811522 0.06488517
0.60674797 0.34250814 0.20243151]

```

In [ ]: